Cummulative dissertation

Functional traits determine biomass dynamics, coexistence and energetics in plankton food webs

Nadja Jeanette Kath

Thesis submitted in fulfilment of the requirements

for the degree of Dr. rer. nat. in Ecology

in the

Working Group for Ecology and Ecological Modelling

Institute for Biochemistry and Biology

Faculty of Science

University Potsdam

Supervisor:

Prof. Dr. Ursula Gaedke

Mentor:

Dr. Hans-Georg Müller

Evaluation:

Prof. Dr. Ursula Gaedke

PD Dr. Birte Matthiessen

Prof. Dr. Ralph Tollrian

January 25, 2022

Published online on the
Publication Server of the University of Potsdam:
https://doi.org/10.25932/publishup-55123
https://nbn-resolving.org/urn:nbn:de:kobv:517-opus4-551239

Acknowledgements

First of all, I would like to warmly thank my supervisor Ursula Gaedke who advised me scientifically during my PhD time, but had also a lot of good private advice. Thanks for always caring for me and for all the nice encouragements like fruits from your garden.

I want to thank my supervisors during my different PhD projects: Christian Guill for the support during our ATN project, for the weekly student meetings and for the linux support. You're able to explain everything in such a great way, although I think I need one more lecture about how to produce a really good paper airplane. Alice Boit for teaching me how to write a manuscript, but also for the huge amount of DynaTrait support, without it my last year would have been much more trouble. Mridul K. Thomas for guiding me through the forest of machine learning. Ellen van Velzen, thank you in so many ways: for all the scientific guidance and the sincere joy about my results not only during our maladaptation project and for all the help with the English language throughout the years. But most of all for all the chats we had in and between our offices which made me feel better and often help to find my motivation again (and maybe sometimes yours).

Thanks to my working group Ecology and Ecosystem Modelling for all the support: Laurie A. Wojcik for a great time together in the office and for commenting on my thesis (so many helpful suggestions!), Ruben Ceulemans, Markus Stark and the other PhD students for helpful exchange on the good and bad sides of PhD life, constructive PhD meetings including comments on my summary and for creating an atmosphere in the building full of humour and support (you were a much better neighbour than the dead plants right now, but also a little more distracting). Janne Hülsemann for cosy office days, especially with the teapot and its warmer. Xenia Fahrentholz for always helping with the organisational stuff for my PhD, my teaching or DynaTrait. I had great moments around the office during kicker matches, at barbecues or during short tea breaks.

Thanks to the DynaTrait community who I met during our terrific conferences. Thanks for answering my annoying coordinator mails ;-)

Vielen Dank an meine Freunde, die immer wieder gefragt haben, wo ich stehe, und an mich geglaubt haben. Danke an Antonia für die Ratschläge, fürs Ertränken der Probleme auf dem Wasser und fürs Vorbild sein. Danke an Robin für lange Spieleabende und die tolle Verköstigung sowie fürs stets offene Ohr.

Ein großes Dankeschön geht an meine Familie, die mich über die Jahre unterstützt und mir am Ende den Raum für diese Arbeit gegeben hat. Danke insbesondere an meine Mutter für all die benötigte Ermunterung und Hilfestellung. Danke für all die liebevollen Nachrichten.

Quiek kch kch an die Schweinels. Ihr bringt mich so oft zum Lächeln. Danke!

Danke, Mario. Ohne Dich wäre das hier niemals möglich gewesen. Danke für all die Zeit, die Du mit Kochen und Kümmern verbracht hast, danke für all die Unterstützung mit Ratschlägen, ehrlichen Meinungen und Knuddeln über die Jahre. Danke, dass Du diese Zeit mit mir gemeinsam gegangen bist. Ich bin gespannt, was noch auf uns wartet, und hoffe und glaube fest, dass wir nun alles gemeinsam schaffen werden.

Content

Summary

Plankton food webs are the basis of marine and limnetic ecosystems. Especially aquatic ecosystems of high biodiversity provide important ecosystem services for humankind as providers of food, coastal protection, climate regulation, and tourism. Understanding the dynamics of biomass and coexistence in these food webs is a first step to understanding the ecosystems. It also lays the foundation for the development of management strategies for the maintenance of the marine and freshwater biodiversity despite anthropogenic influences.

Natural food webs are highly complex, and thus often equally complex methods are needed to analyse and understand them well. Models can help to do so as they depict simplified parts of reality. In the attempt to get a broader understanding of the complex food webs, diverse methods are used to investigate different questions.

In my first project, we compared the energetics of a food chain in two versions of an allometric trophic network model. In particular, we solved the problem of unrealistically high trophic transfer efficiencies (up to 70%) by accounting for both basal respiration and activity respiration, which decreased the trophic transfer efficiency to realistic values of ≤30%. Next in my second project I turned to plankton food webs and especially phytoplankton traits. Investigating a long-term data set from Lake Constance we found evidence for a trade-off between defence and growth rate in this natural phytoplankton community. I continued working with this data set in my third project focusing on ciliates, the main grazer of phytoplankton in spring. Boosted regression trees revealed that temperature and predators have the highest influence on net growth rates of ciliates. We finally investigated in my fourth project a food web model inspired by ciliates to explore the coexistence of plastic competitors and to study the new concept of maladaptive switching, which revealed some drawbacks of plasticity: faster adaptation led to higher maladaptive switching towards undefended phenotypes which reduced autotroph biomass and coexistence and increased consumer biomass.

It became obvious that even well-established models should be critically questioned as it is important not to forget reality on the way to a simplistic

model. The results showed furthermore that long-term data sets are necessary as they can help to disentangle complex natural processes. Last, one should keep in mind that the interplay between models and experiments/ field data can deliver fruitful insights about our complex world.

Zusammenfassung

Plankton-Nahrungsnetze sind die Grundlage mariner und limnischer Ökosysteme. Besonders die aquatischen Ökosysteme mit hoher Biodiversität erbringen wichtige Ökosystemdienstleistungen für uns Menschen wie beispielsweise die Bereitstellung von Nahrung, Küstenschutz, Klimaregulation sowie Tourismus. Die Dynamiken und die Koexistenz der Arten in diesen Ökosystemen zu verstehen, ist ein erster Schritt für die Entwicklung von Möglichkeiten zum Schutz ihrer Biodiversität.

Aufgrund der hohen Komplexität natürlicher Nahrungsnetze braucht es oft ebenso komplexe Methoden um sie zu analysieren und zu verstehen. Modelle können dabei unterstützen, da sie Teile der Realität vereinfacht abbilden. In meiner Dissertation arbeitete ich mit verschiedenen Nahrungsnetzmodellen, um die Dynamiken in Nahrungsnetzen zu verstehen.

In meinem ersten Projekt haben wir die Energieflüsse einer Nahrungskette in zwei Versionen eines allometrisch skalierten Nahrungsnetzmodells untersucht. Wenn nur die klassische basale Respiration einbezogen wird, steigt die trophische Transfereffizienz auf bis zu unrealistische 70 %. Durch die Einbeziehung der aktivitätsbezogenen Respiration sank die trophische Transfereffizienz auf realistische Werte von maximal 30 %. Danach wandte ich mich in meinem zweiten Projekt Plankton-Nahrungsnetzen und den Eigenschaften des Phytoplanktons zu. Bei der Untersuchung eines Langzeitdatensatzes von 21 Jahren aus dem Bodensee fanden wir einen Beweis für einen Trade-off zwischen Verteidigung und Wachstumsrate in einer natürlichen Phytoplankton-gemeinschaft. In diesem Datensatz konzentrierte ich mich anschließend in meinem dritten Projket auf Ciliaten, welche die wichtigsten Fraßfeinde von Phytoplankton im Frühjahr darstellen. Die Methode der *boosted regression trees* zeigte, dass Temperatur und Räuber den größten Einfluss auf die Nettowachstumsraten der Ciliaten haben. Schließlich nutzten wir in meinem vierten Projekt ein von Ciliaten inspiriertes Nahrungsnetzmodell, um die Koexistenz von Konkurrenten mit veränderlichen Eigenschaften und das neue Konzept des *maladaptive switching* zu untersuchen, welches Nachteile der Plastizität zeigt: höhere

Wechselraten zwischen den Phänotypen führten zu höherem *maladaptive switching* in Richtung der unverteidigten Phänotypen, was die Biomasse und Koexistenz der Autotrophen reduziert und die Biomasse des Konsumenten erhöht.

Es wurde offensichtlich, dass auch etablierte Modelle kritisch hinterfragt werden müssen, da es wichtig ist, die Realität auf dem Weg zu einem einfachen Modell nicht zu vergessen. Meine Ergebnisse zeigten des Weiteren, wie wichtig Langzeitdatensätze sind, da sie helfen können, komplexe natürliche Prozesse zu beleuchten. Dieses Wechselspiel zwischen Modellen und Daten aus Experimenten oder Felduntersuchungen kann fruchtbare Ergebnisse liefern und zu einem größeren Verständnis unserer komplexen Welt beitragen.

1. Introduction

An ecosystem is defined as a biological community together with the abiotic environment it is surrounded by (Begon *et al.*, 2011). Ecosystems can differ in size and complexity: their size ranges from the gut biome of a fly to a whole tropical rainforest. They can be characterized by different characteristics such as production, nutrient cycling or biodiversity which depend on the environment, the species living in this ecosystem and their interactions. The net primary production for example varies a lot across ecosystems: 130 g m^{-2} yr^{-1} for a desert grassland, 270 m^{-2} yr^{-1} for lakes, and between 1500 and 3000 m^{-2} yr^{-1} for tropical grasslands and marshes (Woodwell and Whittaker, 1968 and literature cited therein; Lewis Jr., 2011). Another example is the percentage of net primary production allocated to roots which varies from 50% in deserts to only 20% in temperate forests where light competition plays a larger role for the plants (Cain *et al.*, 2011).

Ecosystems often change due to succession, seasonal variability or disturbances. Succession alters habitats over years to centuries, e.g. from open habitats on bare soil on dunes or lava flows into shrublands and forests or after abandonment of agricultural fields (Kamijo *et al.*, 2002; Wang, 2002). The first colonizers on lava flow on the volcanic island Miyake-Jima in Japan changed the soil conditions, including nutrient enrichment, to be beneficial for other plants which then outcompete these first colonizers (Kamijo *et al.*, 2002). Seasonal variability changes the abiotic and biotic conditions in temperate lakes: temperature, the amount of nutrients, and grazing pressure vary a lot during the year (Sommer *et al.*, 2012). Disturbances are either short-term (pulse perturbations) such as a forest fire, a nutrient pulse or removal of seedlings due to heavy rainfall; or they are long-term or permanent (press perturbations) such as climate change consequences, e.g. increasing temperature or a decreased amount of precipitation (Wojcik *et al.*, 2021). These disturbances can have multiple consequences: local extinction of species and changed production were found in a marine phytoplankton community (Bestion *et al.*, 2020 and literature cited therein). Increasing temperature is an important part of the current climate change and will change ecosystems and the food webs they contain. Temperature increase can change the diet breadth and

increase the bacterial–grazer biomass flux within the microbial food web (Petchey *et al.*, 2010; Sarmento *et al.*, 2010). To better understand changes like this, we will thus take a closer look at food webs.

1.1. Food webs

Food webs connect species according to their trophic interactions, depicted by energy fluxes. Energy enters a species as ingestion, which is partly respired and partly assimilated. The assimilated energy is partly put into production of new biomass (either somatic or reproductive growth) and partly excreted; the last contributes to the detritus pool (see Fig. 2.1 in chapter 2).

The species in food webs can be assigned to trophic levels starting from 1 for plants and detritus. The trophic level of its prey plus one is the trophic level of each consumer, resulting in 2 for direct consumers as herbivores and detritivores and 3 or more for carnivores. The trophic position of an omnivore consuming prey of different trophic levels can be a decimal number, e.g. on owl consuming mostly herbivorous mice but also some insectivorous shrews. When the biomasses of all organisms in a food web are grouped according to their trophic level, biomass pyramids can be drawn revealing the biomass distribution.

Most food webs are located within one ecosystem, e.g. in a gall on saltbushes, or a plankton community (Polis, 1991; Boit *et al.*, 2012). They can also reach across ecosystems such as a food web on Bear Island in the Arctic Ocean connecting the marine, the terrestrial and the freshwater realm (Pimm and Lawton, 1980). Sea birds eat marine animals and polar bears hunt seals, while several birds eat invertebrates from the freshwater habitats. These connections between ecosystems can increase the food web complexity.

Food webs can be top-down regulated or bottom-up regulated due to for example predation pressure or nutrient limitations, respectively. It is nowadays accepted that both processes contribute to the regulation of food webs (Wang *et al.*, 2020). Different factors can change these relative contributions. In pitcher plants high temperature led to higher top down control (Hoekman, 2010) and in boreal streams top down control was highest at intermediate temperatures (Kishi *et al.*, 2005). In studies on

habitat fragmentation and predator diet breadth, both processes played a role (Jiang and Morin, 2005; Wang *et al.*, 2020). Data on Daphnia suggest that its reproduction and population growth rates are bottom-up controlled, while their biomasses are top-down controlled (Maciej Gliwicz, 2002).

Trophic cascades arise from the interaction between two trophic levels resulting in a change in species abundance or composition at other trophic levels: a famous study describes how sea otters by feeding on urchins release the kelps from urchin predation (Simenstad *et al.*, 1978). A second example is the overfishing of pelagic predatory fish in the Black Sea leading to an increase in planktivorous fish and phytoplankton and a decrease in zooplankton (Daskalov, 2002). Terrestrial examples are much rarer. In experiments in the tropical rainforest understorey, in absence of carnivorous beetles the number of ants on piper plants increased, reducing the amount of herbivory and increasing the leaf area of the piper plants (Dyer and Letourneau, 1999).

The ratio of production between two adjacent trophic levels is the trophic transfer efficiency (Kath *et al.*, 2018). It depends on the food and metabolism of the organisms, e.g. it is usually larger for carnivores and invertebrates than for herbivores and vertebrates, such as carnivorous beetles or spiders, should have high trophic transfer efficiencies. As trophic cascades change the biomass on different trophic levels, the trophic transfer efficiency is usually affected as well (see chapter 2).

Food webs or parts of them that are well known can be used as model communities to gain knowledge for specific groups or patterns as plankton food webs or intra-guild predation (Diehl and Feissel, 2001; Boit *et al.*, 2012). Phytoplankton and ciliates in aquatic food webs are often used as model communities as they have short generation times due to their small size, they are very diverse and differ in size, defence and thus have a high functional diversity and they are embedded in a large, complex food web (see chapter 3 and 4). Modelling only a part of a food web allows us to understand the species interactions in detail. We can move afterwards to more complex and realistic food webs where we have plenty of interactions.

1.2 Species interactions

Species interactions are diverse and can be categorized e.g. by the impact of one species on the other species. Predation and parasitism are trophic interactions which are beneficial for one of the partners and detrimental to the other partner. Predation is the key interaction in food webs and leads usually to the death of the prey. Parasites usually do not kill their prey (immediately) and the size ratio is different: while predators are usually at least the same size as their prey, parasites are often smaller than their prey. Predation can be counteracted by defences and avoidance strategies, which can be pre- and post-attack (Ehrlich and Gaedke, 2018). Pre-attack defence means to avoid the attack. One way is vertical dial migration, e.g cyclopods migrating to deeper water layers and back to avoid being consumed by backswimmers during the day (Gilbert and Hampton, 2001). Other pre-attack defences are camouflage in toad-headed lizards and inactivity to reduce the chance for predator contact in black-bellied salamanders (Dempsey *et al.*, 2021; Wan *et al.*, 2021). Possible post-attack defences are e.g. toxins in cyanobacteria, size in phytoplankton or spines in rotifers (Jang *et al.*, 2003; Gilbert, 2012; Marañón, 2015).

Non-trophic interactions can be positive for both partners: these mutualisms include e.g. pollination where both partners benefit. It is estimated that 88% of all plant species rely on animals as pollinators which makes pollination an important interaction also in food webs (Ollerton *et al.*, 2011; Hale *et al.*, 2020).

Facilitation is an interaction which is beneficial for one partner and beneficial to neutral to the other one. One example for indirect facilitation are two plants in salt marshes, saltmarsh rush and high-tide bush. The high-tide bush had a lower growth rate when the saltmarsh rush was experimentally removed, probably due to changed abiotic conditions such as more salt and less oxygen, but the saltmarsh rush was not affected by the removal of the high-tide bush (Hacker and Bertness, 1996). Additional complexity was given by aphids feeding on the high-tide bush which also benefitted from the presence of saltmarsh rush. Thus for the high-tide bush, the effects of the saltmarsh rush were mixed, but the positive ones prevailed (Hacker and Bertness, 1996). Another example for indirect effects could be found in a food web in shallow ponds in America: the

marbled salamander larvae consumed zooplankton and spotted salamander larvae which also fed on zooplankton. Experiments have shown that the indirect effect via selection on spotted salamander was larger than the direct feeding link between the marbled salamander and zooplankton: Locally adapted spotted salamander larvae exacerbated the biomass decline in zooplankton, but dampened the negative effect on zooplankton diversity (Urban, 2013).

Competition is an interaction which is negative for both partners. Arctic foxes and snowy owls competing for lemmings represent an example for a trophic and exploitative competition as they compete for the same food resource, despite other interactions connecting both (Duchesne *et al.*, 2021). Barnacles and mussels competing for space at the shore represent an example for a non-trophic competition. Interference competition is defined as two species actively interfering with each other to exclude the other one from the shared habitat or a resource, e.g. house wrens destroying nest sites and removing eggs of other birds (Kennedy and White, 1996).

1.3 Traits and trade-offs

All species interactions are influenced by the species' traits, properties related to their fitness, for example the success of a predator depends on the prey defence. Other traits are growth rate, clutch size, and light or nutrient affinity. These traits are not independent, but are constrained by trade-offs due to energy limitation. Several trade-offs have been found: one between growth and defence in a phytoplankton freshwater community (Ehrlich *et al.*, 2020, see chapter 3), between resistance against a phage and competitive ability in a bacterium (Meaden *et al.*, 2015), between defence against a gape-limited and a gape unconstrained predator in salamanders (Urban, 2008) and a three-way trade-off between cell size and the competitive abilities for nitrogen and phosphorus in phytoplankton (Edwards *et al.*, 2011).

While traits can be genetically fixed, some species have plastic traits, so they can adapt to their variable environment. Plants can adapt their leaves to different amounts of light and increase their root biomass in nutrient-poor soils (Sultan, 2000). Another example are inducible defences which

are only expressed when predation pressure is high, whereby costs are saved when predation pressure is low: rotifers and daphnids form spines, Hokkaido frog tadpoles will be bulgy and red algae release toxins when their predators are present (Kishida and Nishimura, 2004; Boeing *et al.*, 2005; Aránguiz-Acuña *et al.*, 2010; Nylund *et al.*, 2013). A food web of two plastic species experiencing a trade-off between defence and growth rate is investigated in chapter 5. In this chapter, also one drawback of plasticity is studied: maladaptive switching is switching from a higher-fitness phenotype to a lower-fitness one due to the wrong perceptions of kairomones or stochasticity.

Traits, trade-offs and their shape determine how many species can coexist (Ehrlich *et al.*, 2017, 2020, see chapter 3). Traits affect also biomass dynamics, e.g. in a system of green sunfish hunting both salamander larvae and freshwater isopods (Huang and Sih, 1990). Both the isopods and the salamander reduced their activity as a defence and stayed in refuges, but while the isopods always did so, the salamander only showed this behaviour when fish were more active due to isopod presence. Thus the isopod presence increased the survival of salamanders. The salamanders in turn drove the isopods out of their refuges exposing them to a higher predation pressure, thus decreasing the isopod survival. This showed how defence behaviour influences the biomass dynamics which we want to take a closer look at.

1.4 Biomass dynamics and consequences on food webs

There are in principle four types of biomass dynamics: a stable equilibrium, stable oscillations such as found in the shots of red grouse (Martínez-Padilla *et al.*, 2014), unstable oscillations, e.g. in moths or beetles (Hassell *et al.*, 1976 and literature cited therein), and chaotic dynamics which were found e.g. in experiments with flour beetles (Cushing *et al.*, 2001). In complex natural systems, we found often oscillations. There are several types of cycles, two are (regular) predator-prey cycles where the predator biomass follows with a quarter lag behind the prey biomass and antiphase cycles where the maxima of two species are half a cycle apart. Both types have been found in several lab experiments, e.g. for amoebae eating bacteria and rotifers consuming algae (Fussmann *et al.*, 2000; Hiltunen *et al.*, 2014 and literature cited therein). Antiphase cycles results

from eco-evolutionary dynamics or plasticity (Yoshida *et al.*, 2003; Yamamichi *et al.*, 2019, see chapter 5). There are also reversed cycles where the predator peaks are followed by the prey peaks (Cortez and Weitz, 2014; van Velzen and Gaedke, 2018) and intermittent cycles "which are characterized by interruptions where predator-prey cycles are strongly dampened or disappear entirely, after which they re-establish themselves" (van Velzen *et al.*, 2022) found in voles, snowshoe hares and chemostat runs (Krebs *et al.*, 2013; Ecke *et al.*, 2017; Blasius *et al.*, 2020). To differentiate between types of biomass dynamics can help to detect for example trait changes when looking at biomass time series from experiments or field measurements.

1.5 Thesis overview

The broad range of topics led to a high range of methods in my thesis (Fig. 1.1).

For large food webs, usually simple models are used to minimize the amount of parameters that have to be measured or estimated. Allometric trophic network models (ATN) simulate the energy flux in a trophic network assuming allometric relationships for species and their biological rates, i.e. larger species having slower rates. These models are very flexible and are often used to model food webs and study their dynamics, stability, biodiversity and coexistence (Brose *et al.*, 2006; Brose, 2008; Berlow *et al.*, 2009; Heckmann *et al.*, 2012; Schneider *et al.*, 2012, 2016; Kath *et al.*, 2018). In my second chapter, I compared the energetics of the original ATN model and an extended version and found that additionally accounting for the activity respiration decreased the trophic transfer efficiency to realistic values ≤30%. This extended version reflects the energetics of organisms much better and is thus a good basis to further investigate food webs models, e.g. combined with pollination (Hale *et al.*, 2020).

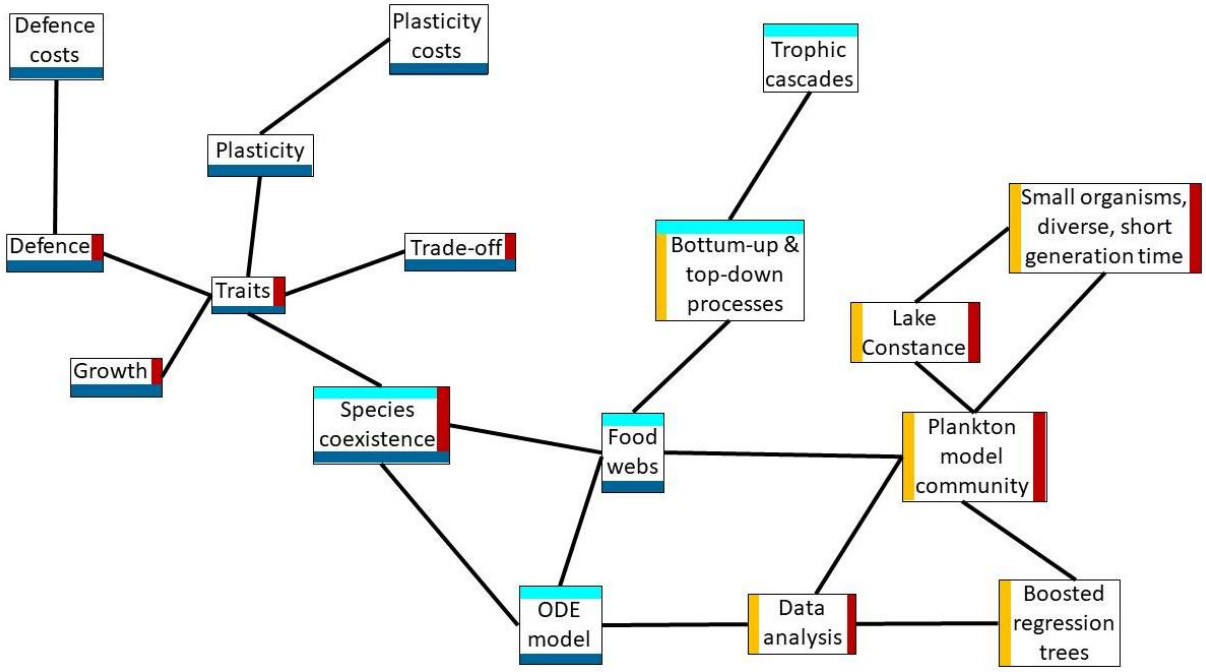

Fig. 1.1: Overview of the topics covered in the chapters 2 to 5 (bright cyan = 2, red = 3, yellow = 4, dark cyan = 5).

After examining the energetics of a food chain, I wanted to explore the species coexistence on one trophic level, so I switched to work on a plankton food web. Long-term, high frequency data sets are laborious to collect, but they can be used to test ecological theories, to parameterize models and to understand and quantify complex ecosystem processes (Lindenmayer *et al.*, 2012). Trade-offs were assumed in many models (Yoshiyama *et al.*, 2009; Kenitz *et al.*, 2017; van Velzen and Gaedke, 2017) but so far have been found mostly in lab experiments (Tessier *et al.*, 2000; Meaden *et al.*, 2015; Burson *et al.*, 2018; but see Edwards *et al.*, 2011). With the trade-off between defence and growth rate in a natural phytoplankton system we provide the first empirical proof from the field within this theory and I showed with the trait-based approach how the coevolved phytoplankton community reacts to different environmental conditions based on their traits (see chapter 3).

While the processes ruling phytoplankton dynamics are studied a lot, the influences of top-down and bottom-up processes on zooplankton are not that well studied: ciliates are the most important grazers of phytoplankton in spring in some lakes and they closely interact with phytoplankton due to trait changes in that time (Tirok and Gaedke, 2007), but what rules their

dynamics is still quite unclear. Ciliates are a very diverse group regarding size, feeding behaviour and mobility making it hard to understand all relevant ecological processes. Simple statistical methods might fail in explaining their dynamics as they cannot take both top-down and bottom-up factors into account. Machine learning techniques can do so and thus process highly complex data sets (Elith *et al.*, 2006; Baltensperger *et al.*, 2020; Pomati *et al.*, 2020). Boosted regression trees aggregate weak predictions from a series of decision trees to generate a stronger prediction model capable to analyse high-dimensional data. In chapter 4, I used boosted regression trees to reveal the importance of environmental predictors in ciliates' net growth rates.

While ciliate dynamics have not been understood in every detail yet, they still inspired models and promoted theory development (Kerimoglu *et al.*, 2014; Våge *et al.*, 2018). Experiments with plastic ciliates feeding on phytoplankton and being consumed by another predatory ciliate have led to the idea to model plasticity. In chapter 5 I used a set of ordinary differential equations to model a food web with one consumer and two plastic, competing prey species to investigate the new concept of maladaptive switching. Additionally, I explored which trade-off parameters matter for the two competing species to coexist or outcompete the other one. These are then worth to be investigated with experiments to close the circle between experiments and models (Flynn, 2005; Heuschele *et al.*, 2017).

Declaration of contributions

Chapter 2:

Nadja J. Kath, Alice Boit, Christian Guill and Ursula Gaedke (2018) Accounting for activity respiration results in realistic trophic transfer efficiencies in allometric trophic network (ATN) models. *Theoretical Ecology*.

NJK, CG and UG designed the study. NJK and CG developed and implemented the model. NJK analysed and interpreted the results with CG and UG. NJK and AB wrote the manuscript to which UG and CG contributed.

Chapter 3:

Elias Ehrlich*, Nadja J. Kath* and Ursula Gaedke (2020) The shape of a defence-growth trade-off governs seasonal trait dynamics in natural phytoplankton. *The ISME Journal*.

*These authors contributed equally.

EE, NJK and UG designed the study. NJK performed the data analysis. EE developed the theory and did the numerical analysis of the model. EE and NJK wrote the manuscript to which UG contributed.

Chapter 4:

Nadja J. Kath, Mridul K. Thomas, Ursula Gaedke (Under review). Mysterious ciliates: seasonally recurrent and yet hard to predict. *Journal of Plankton Research.*

NJK and UG designed the study. NK performed the data analysis with the help of MKT. NJK, MKT and UG interpreted the results. NJK wrote manuscript to which UG and MKT contributed.

Chapter 5:

Nadja J. Kath, Ursula Gaedke and Ellen van Velzen (Submitted). The double-edged sword of inducible defences: costs and benefits of maladaptive switching from the individual to the community level. *Scientific Reports*.

NJK, EVV and UG designed the study. NJK developed and implemented the model with the help of EVV. NJK analysed and interpreted the results with EVV and UG. NJK and EVV wrote the manuscript to which UG contributed.

References

Aránguiz-Acuña, A. *et al.* (2010) Benefits, costs and reactivity of inducible defences: an experimental test with rotifers: Reactivity of inducible defences in rotifers. *Freshw. Biol.*, **55**, 2114–2122.

Baltensperger, A. P. *et al.* (2020) Implications of future climate- and land-change scenarios on grassland bird abundance and biodiversity in the Upper Missouri River Basin. *Landscape Ecol.*, **35**, 1757–1773.

Begon, M. *et al.* (2011) *Ecology: From Individuals to Ecosystems*. 4th ed. Blackwell Publishing Ltd, Oxford, UK.

Berlow, E. L. *et al.* (2009) Simple prediction of interaction strengths in complex food webs. *Proc. Natl. Acad. Sci. U.S.A.*, **106**, 187–191.

Bestion, E. *et al.* (2020) Abrupt declines in marine phytoplankton production driven by warming and biodiversity loss in a microcosm experiment. *Ecol. Lett.*, **23**, 457–466.

Blasius, B. *et al.* (2020) Long-term cyclic persistence in an experimental predator–prey system. *Nature*, **577**, 226–230.

Boeing, W. J. *et al.* (2005) Costs and benefits of Daphnia defense against *Chaoborus* in nature. *Can. J. Fish Aquat. Sci.*, **62**, 9.

Boit, A. *et al.* (2012) Mechanistic theory and modelling of complex food-web dynamics in Lake Constance: Mechanistic modelling of complex food web dynamics. *Ecol. Lett.*, **15**, 594–602.

Brose, U. *et al.* (2006) Allometric scaling enhances stability in complex food webs. *Ecol. Lett.*, **9**, 1228–1236.

Brose, U. (2008) Complex food webs prevent competitive exclusion among producer species. *Proc. R. Soc. B.*, **275**, 2507–2514.

Burson, A. *et al.* (2018) Competition for nutrients and light: testing advances in resource competition with a natural phytoplankton community. *Ecology*, **99**, 1108–1118.

Cain, M. L. *et al.* (2011) *Ecology*. 2nd ed. Sinauer Associates, Inc., Sunderland, USA.

Cortez, M. H. and Weitz, J. S. (2014) Coevolution can reverse predator-prey cycles. *Proc. Natl. Acad. Sci. U.S.A.*, **111**, 7486–7491.

Cushing, J. M. *et al.* (2001) A chaotic attractor in ecology: theory and experimental data. *Chaos, Solitons & Fractals*, **12**, 219–234.

Daskalov, G. M. (2002) Overfishing drives a trophic cascade in the Black Sea. *Mar. Ecol. Prog. Ser.*, **225**, 53–63.

Dempsey, B. L. *et al.* (2021) Predator-avoidance of larval black-bellied salamanders (*Desmognathus quadramaculatus)* in response to cues from native and nonnative salmonids. *Ethol. Ecol. & Evol.*, 1–15.

Diehl, S. and Feissel, M. (2001) Intraguild prey suffer from enrichment of their resources: a microcosm experiment with ciliates. *Ecology*, **82**, 2977–2983.

Duchesne, É. *et al.* (2021) Variable strength of predator-mediated effects on species occurrence in an arctic terrestrial vertebrate community. *Ecography*, **44**, 1236–1248.

Dyer, L. A. and Letourneau, D. K. (1999) Trophic cascades in a complex terrestrial community. *Proc. Natl. Acad. Sci. U.S.A.*, **96**, 5072–5076.

Ecke, F. *et al.* (2017) Dampening of population cycles in voles affects small mammal community structure, decreases diversity, and increases prevalence of a zoonotic disease. *Ecol. Evol.*, **7**, 5331–5342.

Edwards, K. F. *et al.* (2011) Evidence for a three-way trade-off between nitrogen and phosphorus competitive abilities and cell size in phytoplankton. *Ecology*, **92**, 2085–2095.

Ehrlich, E. *et al.* (2020) The shape of a defense-growth trade-off governs seasonal trait dynamics in natural phytoplankton. *ISME J.*, **14**, 1451–1462.

Ehrlich, E. *et al.* (2017) Trait-fitness relationships determine how trade-off shapes affect species coexistence. *Ecology*, **98**, 3188–3198.

Ehrlich, E. and Gaedke, U. (2018) Not attackable or not crackable-How pre- and post-attack defenses with different competition costs affect prey coexistence and population dynamics. *Ecol. Evol.*, **8**, 6625–6637.

Elith, J. *et al.* (2006) Novel methods improve prediction of species' distributions from occurrence data. *Ecography*, **29**, 129–151.

Flynn, K. J. (2005) Castles built on sand: dysfunctionality in plankton models and the inadequacy of dialogue between biologists and modellers. *J. Plankton Res.*, **27**, 1205–1210.

Fussmann, G. F. *et al.* (2000) Crossing the Hopf Bifurcation in a Live Predator-Prey System. *Science*, **290**, 1358–1360.

Gilbert, J. J. (2012) Predator-induced defense in rotifers: developmental lags for morph transformations, and effect on population growth. *Aquat. Ecol.*, **46**, 475–486.

Gilbert, J. J. and Hampton, S. E. (2001) Diel vertical migrations of zooplankton in a shallow, fishless pond: a possible avoidance-response cascade induced by notonectids: Notonectids and zooplankton migrations. *Freshw. Biol.*, **46**, 611–621.

Hacker, S. D. and Bertness, M. D. (1996) Trophic Consequences of a Positive Plant Interaction. *Am. Nat.*, **148**, 559–575.

Hale, K. R. S. *et al.* (2020) Mutualism increases diversity, stability, and function of multiplex networks that integrate pollinators into food webs. *Nat. Commun.*, **11**, 2182.

Hassell, M. P. *et al.* (1976) Patterns of Dynamical Behaviour in Single-Species Populations. *J. Anim. Ecol.*, **45**, 471–486.

Heckmann, L. *et al.* (2012) Interactive effects of body-size structure and adaptive foraging on food-web stability: Body size, adaptivity and food-web stability. *Ecol. Lett.*, **15**, 243–250.

Heuschele, J. *et al.* (2017) On the missing link in ecology: improving communication between modellers and experimentalists. *Oikos*, **126**, 1071–1077.

Hiltunen, T. *et al.* (2014) A newly discovered role of evolution in previously published consumer-resource dynamics. *Ecol. Lett.*, **17**, 915–923.

Hoekman, D. (2010) Turning up the heat: Temperature influences the relative importance of top-down and bottom-up effects. *Ecology*, **91**, 2819–2825.

Huang, C. and Sih, A. (1990) Experimental Studies on Behaviorally Mediated, Indirect Interactions through a Shared Predator. *Ecology*, **71**, 1515–1522.

Jang, M.-H. *et al.* (2003) Toxin production of cyanobacteria is increased by exposure to zooplankton. *Freshw. Biol.*, **48**, 1540–1550.

Jiang, L. and Morin, P. J. (2005) Predator Diet Breadth Influences the Relative Importance of Bottom-Up and Top-Down Control of Prey Biomass and Diversity. *Am. Nat.*, **165**, 350–363.

Kamijo, T. *et al.* (2002) Primary succession of the warm-temperate broad-leaved forest on a volcanic island, Miyake-jima, Japan. *Folia Geobot.*, **37**, 71–91.

Kath, N. J. *et al.* (2018) Accounting for activity respiration results in realistic trophic transfer efficiencies in allometric trophic network (ATN) models. *Theor. Ecol.*, **11**, 453–463.

Kenitz, K. M. *et al.* (2017) Seasonal succession in zooplankton feeding traits reveals trophic trait coupling: Plankton succession and trait coupling. *Limnol. Oceanogr.*, **62**, 1184–1197.

Kennedy, E. D. and White, D. W. (1996) Interference Competition from House Wrens as a Factor in the Decline of Bewick's Wrens. *Conserv. Biol.*, **10**, 281–284.

Kerimoglu, O. *et al.* (2014) Modeling the spring blooms of ciliates in a deep lake. *Hydrobiologia*, **731**, 173–189.

Kishi, D. *et al.* (2005) Water temperature determines strength of top-down control in a stream food web. *Freshw. Biol.*, **50**, 1315–1322.

Kishida, O. and Nishimura, K. (2004) Bulgy tadpoles: inducible defense morph. *Oecologia*, **140**, 414–421.

Krebs, C. J. *et al.* (2013) Synchrony in the snowshoe hare (*Lepus americanus*) cycle in northwestern North America, 1970–2012. *Can. J. Zool.*, **91**, 562–572.

Lewis Jr., W. (2011) Global primary production of lakes: 19th Baldi Memorial Lecture. *IW*, **1**, 1–28.

Lindenmayer, D. B. *et al.* (2012) Value of long-term ecological studies. *Austral. Ecol.*, **37**, 745–757.

Maciej Gliwicz, Z. (2002) On the different nature of top-down and bottom-up effects in pelagic food webs: *Top-down versus bottom-up effects*. *Freshw. Biol.*, **47**, 2296–2312.

Marañón, E. (2015) Cell Size as a Key Determinant of Phytoplankton Metabolism and Community Structure. *Annu. Rev. Mar. Sci.*, **7**, 241–264.

Martínez-Padilla, J. *et al.* (2014) Insights into population ecology from long-term studies of red grouse *Lagopus lagopus scoticus*. *J. Anim. Ecol.*, **83**, 85–98.

Meaden, S. *et al.* (2015) The cost of phage resistance in a plant pathogenic bacterium is context-dependent. *Evolution*, **69**, 1321–1328.

Nylund, G. M. *et al.* (2013) Costs and Benefits of Chemical Defence in the Red Alga Bonnemaisonia hamifera. *PLoS ONE*, **8**, e61291.

Ollerton, J. *et al.* (2011) How many flowering plants are pollinated by animals? *Oikos*, **120**, 321–326.

Petchey, O. L. *et al.* (2010) Predicting the effects of temperature on food web connectance. *Phil. Trans. R. Soc. B*, **365**, 2081–2091.

Pimm, S. L. and Lawton, J. H. (1980) Are Food Webs Divided into Compartments? *J. Anim. Ecol.*, **49**, 879.

Polis, G. A. (1991) Complex Trophic Interactions in Deserts: An Empirical Critique of Food-Web Theory. *Am. Nat.*, **138**, 123–155.

Pomati, F. *et al.* (2020) Interacting Temperature, Nutrients and Zooplankton Grazing Control Phytoplankton Size-Abundance Relationships in Eight Swiss Lakes. *Front. Microbiol.*, **10**, 3155.

Sarmento, H. *et al.* (2010) Warming effects on marine microbial food web processes: how far can we go when it comes to predictions? *Phil. Trans. R. Soc. B*, **365**, 2137–2149.

Schneider, F. D. *et al.* (2016) Animal diversity and ecosystem functioning in dynamic food webs. *Nat. Commun.*, **7**, 12718.

Schneider, F. D. *et al.* (2012) Body mass constraints on feeding rates determine the consequences of predator loss: Allometric predator effects. *Ecol. Lett.*, **15**, 436–443.

Simenstad, C. A. *et al.* (1978) Aleuts, Sea Otters, and Alternate Stable-State Communities. *Science*, **200**, 403–411.

Sommer, U. *et al.* (2012) Beyond the Plankton Ecology Group (PEG) Model: Mechanisms Driving Plankton Succession. *Annu. Rev. Ecol. Evol. Syst.*, **43**, 429–448.

Sultan, S. E. (2000) Phenotypic plasticity for plant development, function and life history. *Trends Plant Sci.*, **5**, 537–542.

Tessier, A. J. *et al.* (2000) A Fundamental Trade-Off in Resource Exploitation by Daphnia and Consequences to Plankton Communities. *Ecology*, **81**, 826–841.

Tirok, K. and Gaedke, U. (2007) Regulation of planktonic ciliate dynamics and functional composition during spring in Lake Constance. *Aquat. Microb. Ecol.*, **49**, 87–100.

Urban, M. C. (2013) Evolution mediates the effects of apex predation on aquatic food webs. *Proc. R. Soc. B.*, **280**, 20130859.

Urban, M. C. (2008) Salamander evolution across a latitudinal cline in gape-limited predation risk. *Oikos*, **117**, 1037–1049.

Våge, S. *et al.* (2018) Simple models combining competition, defence and resource availability have broad implications in pelagic microbial food webs. *Ecol. Lett.*, **21**, 1440–1452.

van Velzen, E. *et al.* (2022) Quantifying the capacity for contemporary trait changes to drive intermittent predator-prey cycles. *Ecol. Monog.*.

van Velzen, E. and Gaedke, U. (2017) Disentangling eco-evolutionary dynamics of predator-prey coevolution: the case of antiphase cycles. *Sci. Rep.*, **7**, 17125.

van Velzen, E. and Gaedke, U. (2018) Reversed predator-prey cycles are driven by the amplitude of prey oscillations. *Ecol. Evol.*, **8**, 6317–6329.

Wan, L. *et al.* (2021) Camouflage versus running performance as strategies against predation in a lizard inhabiting different habitats. *Ecol. Evol.*, **11**, 17409–17416.

Wang, G.-H. (2002) Plant traits and soil chemical variables during a secondary vegetation succession in abandoned fields on the Loess Plateau. *Acta Botanica Sinica*, **44**, 990–998.

Wang, R. *et al.* (2020) Habitat fragmentation changes top-down and bottom-up controls of food webs. *Ecology*, **101**.

Wojcik, L. A. *et al.* (2021) Functional diversity buffers the effects of a pulse perturbation on the dynamics of tritrophic food webs. *Ecol. Evol.*, **11**, 15639–15663.

Woodwell, G. M. and Whittaker, R. H. (1968) Primary Production in Terrestrial Ecosystems. *Am. Zool.*, **8**, 19–30.

Yamamichi, M. *et al.* (2019) Modelling inducible defences in predator–prey interactions: assumptions and dynamical consequences of three distinct approaches. *Ecol. Lett.*, ele.13183.

Yoshida, T. *et al.* (2003) Rapid evolution drives ecological dynamics in a predator–prey system. *Nature*, **424**, 303–306.

Yoshiyama, K. *et al.* (2009) Phytoplankton Competition for Nutrients and Light in a Stratified Water Column. *Am. Nat.*, **174**, 190–203.

Chapter 2

Accounting for activity respiration results in realistic trophic transfer efficiencies in allometric trophic network (ATN) models

Nadja Kath, Alice Boit, Christian Guill, Ursula Gaedke

Manuscript is available at http://link.springer.com/article/10.1007/s12080-018-0378-z.

Abstract

Allometric trophic network (ATN) models offer high flexibility and scalability while minimizing the number of parameters, and have been successfully applied to investigate complex food web dynamics and their influence on food web diversity and stability. However, the realism of ATN model energetics has never been assessed in detail, despite their critical influence on dynamic biomass and production patterns. Here, we compare the energetics of the currently established original ATN model, considering only biomass-dependent basal respiration, to an extended ATN model version, considering both basal and assimilation-dependent activity respiration. The latter is crucial in particular for unicellular and invertebrate organisms which dominate the metabolism of pelagic and soil food webs. Based on metabolic scaling laws, we show that the extended ATN version reflects the energy transfer through a chain of four trophic levels of unicellular and invertebrate organisms more realistically than the original ATN version. Depending on the strength of top-down control, the original ATN model yields trophic transfer efficiencies up to 71% at either the third or the fourth trophic level, which considerably exceeds any realistic values. In contrast, the extended ATN version yields realistic trophic transfer efficiencies ≤ 30% at all trophic levels, in accordance with both physiological considerations and empirical evidence from pelagic

systems. Our results imply that accounting for activity respiration is essential for consistently implementing the metabolic theory of ecology in ATN models and for improving their quantitative predictions, which makes them more powerful tools for investigating the dynamics of complex natural communities.

Key words: food web, trophic transfer efficiency, allometric trophic network model, allometry, energy transfer, activity respiration

Introduction

The metabolic theory of ecology relates biological rates to body size, and serves to predict metabolic activity from the individual to the community level (Brown et al. 2004). Allometrically scaled trophic network (ATN) models implement this theory in a food web context by linking consumers to their resources in food webs. Yodzis and Innes (1992) parameterized the first ATN model which is the theoretical basis of a fruitful series of ATN modelling studies for ecological theory building, e.g. contributing to the diversity-stability debate (Benoît and Rochet 2004; Brose et al. 2006; Heckmann et al. 2012), coexistence theory (Brose 2008), hypotheses on biodiversity-ecosystem functioning (Schneider et al. 2016) and for investigating biodiversity loss (Berlow et al. 2009; Schneider et al. 2012). The main advantage of ATN models is their scalability from small modules to large and complex food webs in a widely applicable approach with only few assumptions.

The ATN approach builds upon the fact that material ingested by a consumer is either excreted or allocated to respiration or production (Fig. 2.1). The assimilation efficiency differs for carnivores and herbivores because of the respective food's quality and stoichiometry. Regarding losses to respiration, all previous studies with ATN models except for Boit et al. (2012) and Kuparinen et al. (2016) considered only respiration proportional to biomass, here called basal respiration, whereas respiratory losses due to activity, hereafter called activity respiration, were not specifically accounted for. This approximation may apply to 27urcate27yte27c

mammals and birds with high maintenance costs. However, it appears less suitable for modelling pelagic and soil food webs, which mostly consist of unicellular and invertebrate organisms with low basal respiration, but high activity respiration, which is proportional to food uptake (Anderson 1992). The study by Boit et al. (2012) on the seasonal plankton succession in Lake Constance already indicated that the ATN model successfully reproduced general community patterns only if the important physiological process of activity respiration was accounted for. In contrast, the original ATN model considerably overestimated heterotrophic production if activity respiration was ignored (Boit et al. 2012). Kuparinen et al. (2016) used the ATN model as extended by Boit et al. (2012) to successfully model the effects of fishing on a food web and the fish life-history traits. These two studies called for the in-depth evaluation of ATN model energetics which we present in this work. To differentiate between the two model versions, we employ the terms "original" (Yodzis and Innes 1992) and "extended" ATN model (Boit et al. 2012).

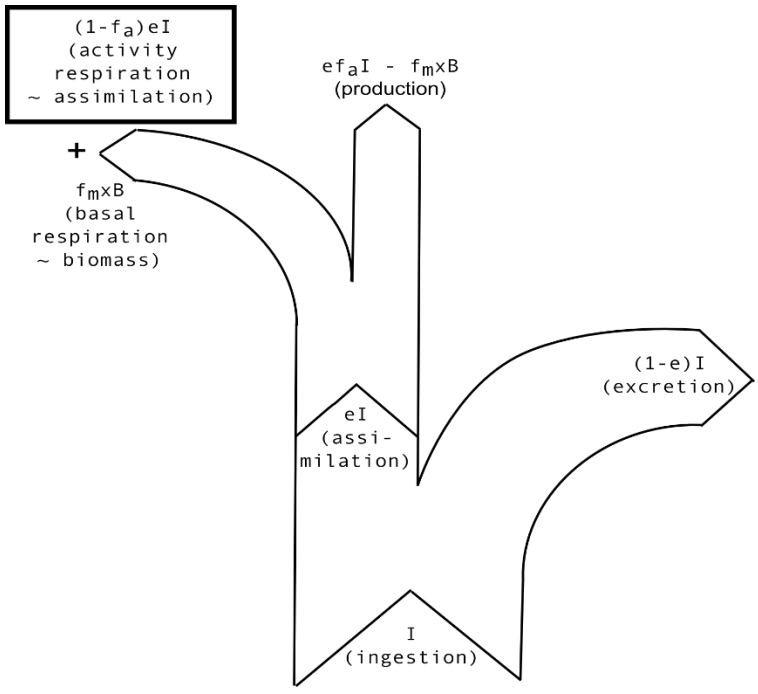

Fig. 2.1: The carbon (surrogate for energy) flow scheme implemented in the ATN model approach. The original version by Yodzis & Innes (1992) does not separate activity from basal respiration, but assumes that all respiration is proportional to biomass. The missing part of activity respiration proportional to assimilation (box) is added to the original ATN model in this study. Model parameters are e: assimilation efficiency, f_a: factor accounting for activity respiration, f_m: factor accounting for basal respiration, x: metabolic rate; B: biomass and I ingestion (for details see Tab. 2.1 and Methods)

To quantify and evaluate model energetics, we determine the trophic transfer efficiency (TTE) between four ascending trophic levels (autotrophs, herbivores, carnivores, and top predators) for both the original and the extended ATN version. We find that only by accounting for activity respiration, the ATN model achieves realistic TTE towards the higher trophic levels. To explain this model 29urcate29y, we additionally compared biomasses, respiration and production of both model versions for different levels of top predator mortality. The latter elucidates the influence of top-down vs. bottom-up control on the TTE and the formation of trophic cascades. We discuss our findings in the context of previous modelling studies and observations from pelagic systems to promote the inclusion of activity respiration in future ATN models. Achieving more realistic energetics and improving quantitative predictions will make ATN models more powerful tools to investigate complex natural food webs in order to better serve their purpose in ecological theory building.

Methods

Allometric trophic network (ATN) models represent consumer-resource relationships based on allometric scaling of key physiological rates (e.g. ingestion) with individual body mass, which achieves minimum data necessity for model parameterization (Yodzis & Innes 1992). Ingested carbon serves as surrogate for energy and is allocated to either excretion, respiration, or production (Fig. 2.1, Begon et al. 2006). The original ATN model formulation does not differentiate between basal respiration proportional to the biomass, and activity respiration proportional to the amount of assimilated food (Fig 2.1).

General ATN model equations and parameters

We applied the ATN model equations to a linear chain of 4 trophic levels from autotrophs (A) and herbivores (H) to carnivores (C) and top predators (T). In order to facilitate comparability between studies, our notation and parameterization closely follows that of previous ATN modelling studies (Brose et al. 2006; Boit et al. 2012). Growth of the autotrophs is modelled by a logistic function (Eq. 2.1), and consumption by all consumers is described by a Holling type II functional response (Eq. 2.1-2.4, Holling 1959) . Together, the rates of change of the biomasses B_i (i = A, H, C, T) at

the four trophic levels are given by the following ordinary differential equations:

$$\frac{dB_A}{dt} = rB_A\left(1 - \frac{B_A}{K}\right) - yx_H \frac{B_A}{B_0 + B_A} B_H \quad (2.1)$$

$$\frac{dB_H}{dt} = f_a e_h y x_H \frac{B_A}{B_0 + B_A} B_H - yx_C \frac{B_H}{B_0 + B_H} B_C - f_m x_H B_H \quad (2.2)$$

$$\frac{dB_C}{dt} = f_a e_c y x_C \frac{B_H}{B_0 + B_H} B_C - yx_T \frac{B_C}{B_0 + B_C} B_T - f_m x_C B_C \quad (2.3)$$

$$\frac{dB_T}{dt} = f_a e_c y x_T \frac{B_C}{B_0 + B_C} B_T - f_m x_T B_T - dB_T{}^2. \quad (2.4)$$

The maximum growth rate of the autotrophs is described by r and their carrying capacity by K. The functional responses for consumption are expressed by the metabolic rate of the respective consumer, x_H, x_C, x_T, the maximum ingestion rate y normalized by the respective metabolic rate, and the half-saturation constant B_0. The assimilation efficiency for herbivores is denoted as e_h, the one for carnivorous predators as e_c, the fraction of assimilated carbon not respired is defined by f_a, i.e. (1- f_a) is the fraction of carbon lost by activity respiration, and the fraction of maintenance respiration linked to biomass is f_m. The metabolic rates x_i scale allometrically with body mass m_i with an allometric exponent of -0.25 (Yodzis and Innes 1992). The autotrophs' body mass is set to 1 and the consumer-resource body-mass ratio is 1000 for all trophic levels. The standard values of all parameters are given in Tab. 2.1. The death rate constant of the top predator is given by d (Eq. 2.4, Tab. 2.1) and it was varied between 0 and 0.05 in steps of 0.0001. The term dB_T represents the top predator's per capita death rate. The case $d = 0$ represents an extreme case as it leads to a massive accumulation of top predator biomass which in nature would attract pathogens, parasites, or another carnivore, which all induce mortality.

Table 2.1: Parameter values. If the original and extended ATN version are differently parameterized, their values are 31urcate31 with ^{orig} and ^{ext}, respectively. Dimensionless units are 31urcate31 as [-].

Parameter name	Abbreviation	Value [dimension]	Literature
Mass-specific maximum growth rate of the autotrophs	r	1 $[\frac{1}{time}]$	(Brose et al. 2006)
Carrying capacity	K	1 $[\frac{mass}{volume}]$	(Brose et al. 2006)
Metabolic rate	x_i	0.314 $mass_i^{-0.25}$ $[\frac{1}{time}]$	(Brose et al. 2006)
Maximum ingestion rate relative to metabolic rate	y	8 [-]	(Brose et al. 2006)
Half – saturation constant	B_0	0.5 $[\frac{mass}{volume}]$	(Brose et al. 2006)
Fraction of assimilated carbon used for production	f_a	1 ^{orig} / 0.4 ^{ext} [-]	(Boit et al. 2012)
Factor for maintenance respiration	f_m	1 ^{orig} / 0.1 ^{ext} [-]	Boit et al. 2012)
Assimilation efficiency for herbivorous species	e_h	0.45 [-]	(Yodzis and Innes 1992)
Assimilation efficiency for carnivorous species	e_c	0.85 [-]	(Yodzis and Innes 1992)
Death rate constant of top predator	d	[0, 0.05] $[\frac{volume}{time\ mass}]$	varied in this study

Calculation of central rates

All central rates, i.e. ingestion, excretion, basal and activity respiration, and production have the same dimension mass · volume^{-1} · time^{-1}. The total ingestion rate I_i of the consumer species on trophic level i with biomass B_i is given by

$$I_i = yx_i \frac{B_{i-1}}{B_0 + B_{i-1}} B_i \quad (2.5).$$

Multiplied with the assimilation constant e_i and the activity respiration factor f_a, the term I_i constitutes the first term in Eq. 2.2-2.4. The total excretion rate E_i of trophic level i is proportional to its ingestion rate and is given by

$$E_i = (1 - e_i)I_i = (1 - e_i)yx_i \frac{B_{i-1}}{B_0 + B_{i-1}} B_i \quad (2.6).$$

The assimilation efficiency e_i describes the fraction of the ingested material that is assimilated and not lost by excretion. It is higher for carnivores than for herbivores (Tab. 2.1) since the former consume high-quality food of similar biochemical composition as themselves, whereas plants often contain nutrient-poor material which is hard to digest.

Basal respiration is the energy lost due to maintenance processes. It is analog to the basal metabolic rate defined for homoiotherms (Gessaman 1973) as measured in the thermoneutral zone where homoiotherms have very low costs for thermoregulation and are most similar to ectotherms in this regard. Basal respiration $R_{b,i}$ is defined as

$$R_{b,i} = f_m x_i B_i \quad (2.7)$$

and is therefore proportional to the standing stock biomass. Activity respiration is the energy spent for processes related to the production of new biomass (including locomotion, foraging, food handling and digestion, ontogenetic processes and reproduction). We call f_a the fraction of energy not lost due to activity processes. Following Boit et al. (2012), the activity respiration $R_{a,i}$ is calculated as

$$R_{a,i} = (1 - f_a)\, e_i\, I_i = (1 - f_a)e_i yx_i \frac{B_{i-1}}{B_0 + B_{i-1}} B_i \quad (2.8).$$

This part is neglected in the original ATN model, i.e. $f_a = 1$.

The production summarizes all processes that lead to creation of new biomass (somatic and reproductive growth). On average, the production at trophic level i compensates for losses by predation, i.e. the ingestion by trophic level $i+1$. If we neglect non-grazing mortality, which typically plays a minor role in pelagic systems (Gaedke et al. 2002), the production P_i can either be calculated as ingestion of the next higher trophic level I_{i+1} or as ingestion at trophic level i minus excretion E_i and total respiration $R_i = R_{a,i} + R_{b,i}$,

$$P_i = I_{i+1} = I_i - E_i - R_{a,i} - R_{b,i} \quad (2.9).$$

For the top predator, the ingestion by a higher trophic level is replaced by its death rate dB_T^2 (Eq. 2.4). These different ways to calculate the production (Eq. 2.9) enable us to infer the trophic transfer efficiencies.

Trophic transfer efficiency

The trophic transfer efficiency (TTE) is defined as the ratio of the production of two adjacent trophic levels and is therefore dimensionless. It is used to quantify the fraction of energy passed on to the next trophic level. To calculate the maximum TTE, it is crucial to remember that ingested carbon can only be excreted, respired or invested into new production (Fig. 2.1). When one of the first two rates increases, the production decreases. Following Yodzis and Innes (1992), carnivores are assumed to have an assimilation efficiency of 85% and herbivores of 45% (Tab. 2.1). From physiological considerations based on a comprehensive data set across different taxonomic groups (Humphreys 1979; Hendriks 1999) it can be estimated that at most half of the assimilated carbon can be allocated to production (Fig. 2.1), which yields an upper limit to the maximum feasible TTE_i between trophic level i and $i+1$:

$$\text{Maximum feasible TTE}_{i\to i+1} \leq 0.5\ \frac{e_{i+1}\, I_{i+1}}{P_i} \quad (2.10).$$

This results in a maximum feasible TTE of at most 42.5% of the ingested carbon for carnivores and of 22.5% for herbivores (cf. Tab. 2.2). Note that this is a very conservative estimation. Most taxa have considerably higher respiratory losses and thus lower production to assimilation ratios, resulting in a lower maximum feasible TTE.

One way to calculate the TTE to the next trophic level in the model is

$$TTE_{i\to i+1} = \frac{P_{i+1}}{P_i} = \frac{e_{i+1} I_{i+1} - (R_{a,i+1} + R_{b,i+1})}{I_{i+1}} = \frac{f_a e_{i+1} y \frac{B_i}{B_h + B_i} - f_m}{y \frac{B_i}{B_h + B_i}} \quad (2.11).$$

This expression has an upper limit that is reached for unlimited food supply $B_i \to \infty$. For this limit, the rightmost part of Eq. 2.11 can be simplified to

$$TTE_{i \to i+1} < \frac{f_a e_{i+1} y - f_m}{y} \quad (2.12)$$

as an expression for the upper bound of the TTE inherent in the ATN model (Eq. 2.1-2.4). When calculating this model inherent maximum TTE from the first to the second trophic level, the autotrophs' maximum biomass is their capacity K and not infinity, and Eq. 2.11 is used for the calculation instead of Eq. 2.12.

To differentiate the inherent TTE (upper bound of the TTE in the ATN model) from the actually obtained TTE during the dynamic simulations, the latter will thereafter be called obtained TTE.

Simulations

Biomasses and resulting values are mean values of the last 50,000 time steps of a 100,000 step time series. All calculations and figures were made using Python 2.7.6. For integration of the ordinary differential equations, the adaptive step-size lsoda solver was used with absolute and relative error tolerances $\varepsilon_{abs} = \varepsilon_{rel} = 10^{-13}$.

Results

We first evaluated the maximum inherent trophic transfer efficiency (TTE) assuming unlimited food supply. We found a value of 32.5% for the herbivores and 72.5% for the carnivores and top predators in the original ATN model, which exceeds by far the maximum feasible TTE of 22.5% for herbivores and 42.5% for carnivores and top predators (Eq. 2.10, 2.12, Tab. 2.2). In the extended ATN version, the maximum inherent TTE was 16.1% for the herbivores and 32.8% for the carnivores and top predators (Eq. 2.12, Tab. 2.2). The maximum inherent TTE was smaller in the extended version as more carbon is respired instead of transported through the food chain to the upper trophic levels.

Tab. 2.2: Three trophic transfer efficiencies (TTE) are given, the maximum feasible TTE according to the given assimilation efficiencies (Tab. 2.1) and assuming that production equals respiration (Humphreys, 1979) (Eq. 2.10), the maximum inherent TTE assuming maximum food concentration (Eq. 2.12), and the maximum TTE obtained from the simulations for both the original and the extended ATN version for the three trophic levels in %.

	Max. feasible TTE	Max. inherent TTE		Max. obtained TTE	
		Original	Extended	Original	Extended
$TTE_{3\rightarrow 4}$	42.5	72.5	32.8	50.5	30.1
$TTE_{2\rightarrow 3}$	42.5	72.5	32.8	44.5	30.2
$TTE_{1\rightarrow 2}$	22.5	26.3	16.1	14.1	13.2

As a second and more practical step, we investigated the TTE obtained in dynamic simulations of a four trophic level food chain using both the original and extended ATN version over a gradient of the top predator's death rate constant *d*. In the extended ATN version, which accounts for activity and basal respiration separately, the maximum obtained TTE at trophic level 3 and 4 never exceeded the maximum feasible TTE (Fig. 2.2, Tab. 2.2, Eq. 2.10). In contrast, in the original ATN model the obtained TTE at trophic level 4 exceeded the maximum feasible TTE of 42.5% for $d > 0.0029$ (Fig. 2.2, maximum observed value 50.5%). At trophic level 3, the TTE of the carnivores in the original ATN model exceeded the maximum feasible TTE for small values of *d* ($d < 0.0006$, Fig. 2.2). The consistently lower obtained TTE in the extended ATN version indicates that this model version represents the energy transfer towards the higher trophic level more realistically than the original ATN model.

With an increasing death rate constant *d* of the top predator, its own as well as the herbivore's obtained TTE increased, whereas the carnivore's obtained TTE decreased (Fig. 2.2). This alternating pattern of increasing and decreasing obtained TTE with increasing *d* resulted from a trophic cascade: Higher values of *d* lowered the top predator's biomass, which in turn lowered its total ingestion. Released from top-down control, the carnivore's biomass and thus its ingestion increased. This pattern

propagated down to the herbivores and autotrophs. Since the TTE is a monotonously increasing function of the biomass on the respective lower trophic level (Eq. 2.11, Appendix A, Fig. A3), this alternating pattern of decreasing and increasing biomasses translates directly to the TTEs on the different trophic levels.

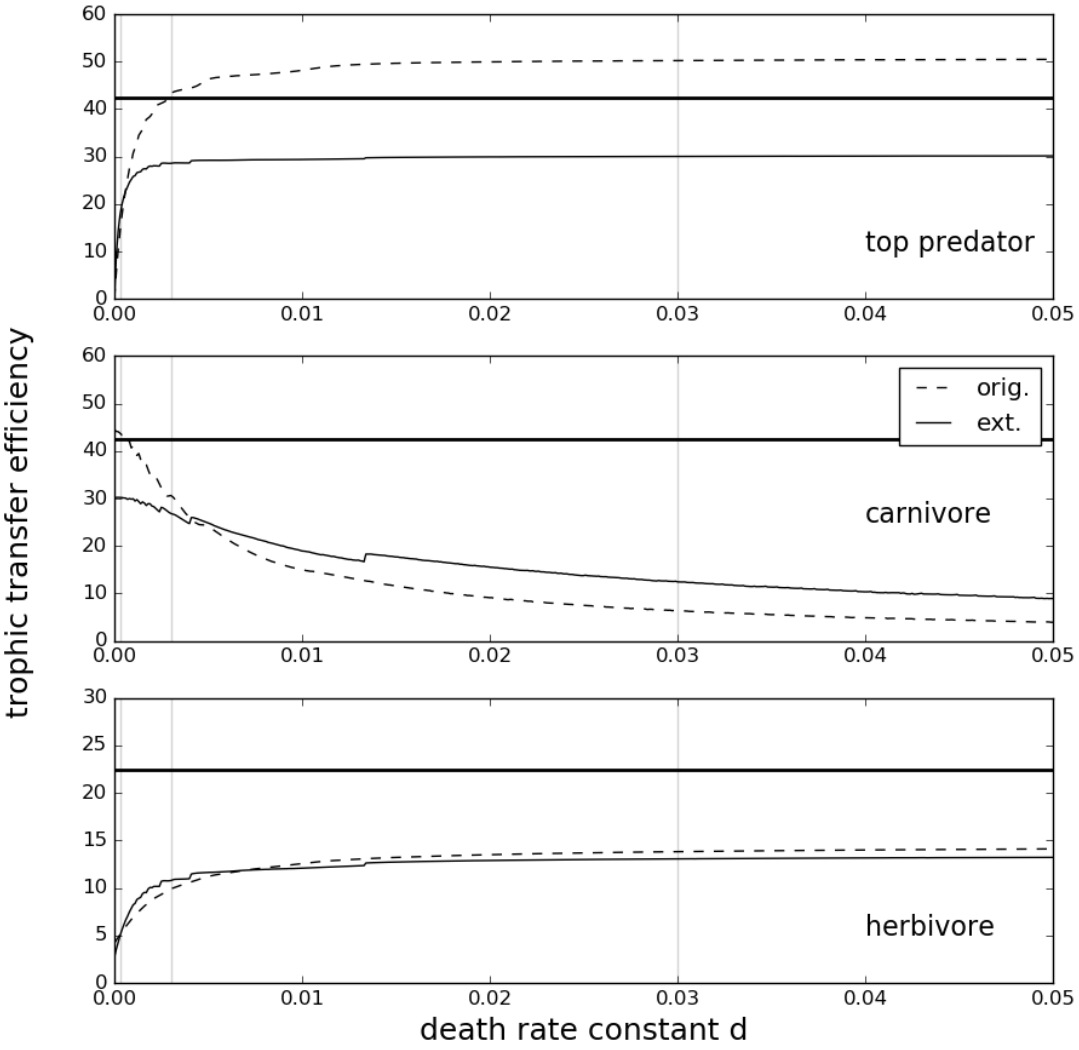

Fig. 2.2: Trophic transfer efficiency (TTE) obtained in simulations (in percent, defined as the production ratio of upper vs. lower trophic level) of the top predator (top panel), carnivore (center) and herbivore (bottom) in the original (dashed lines) and extended (solid lines) ATN version for different top predator's death rate constants d. Grey vertical lines indicate the position of the biomass pyramids provided in Fig. 2.3. The horizontal lines indicate the maximum feasible TTE (see Methods 'Trophic transfer efficiency', Tab. 2.2)

The herbivore's obtained TTE remained below the maximum feasible TTE of 22.5% (Eq. 2.10) in both model versions (Fig. 2.2). The reason is the nonlinear dependence of the autotroph's production on its carrying capacity and its interaction with the nonlinear grazing function of the herbivore. When assuming a chain of three trophic levels where the carnivore as the highest trophic level experiences a quadratic death term, the herbivore was under strong top-down control and exceeded its maximum feasible TTE by up to a factor of 1.1 (Appendix A, Fig. A1, A2).

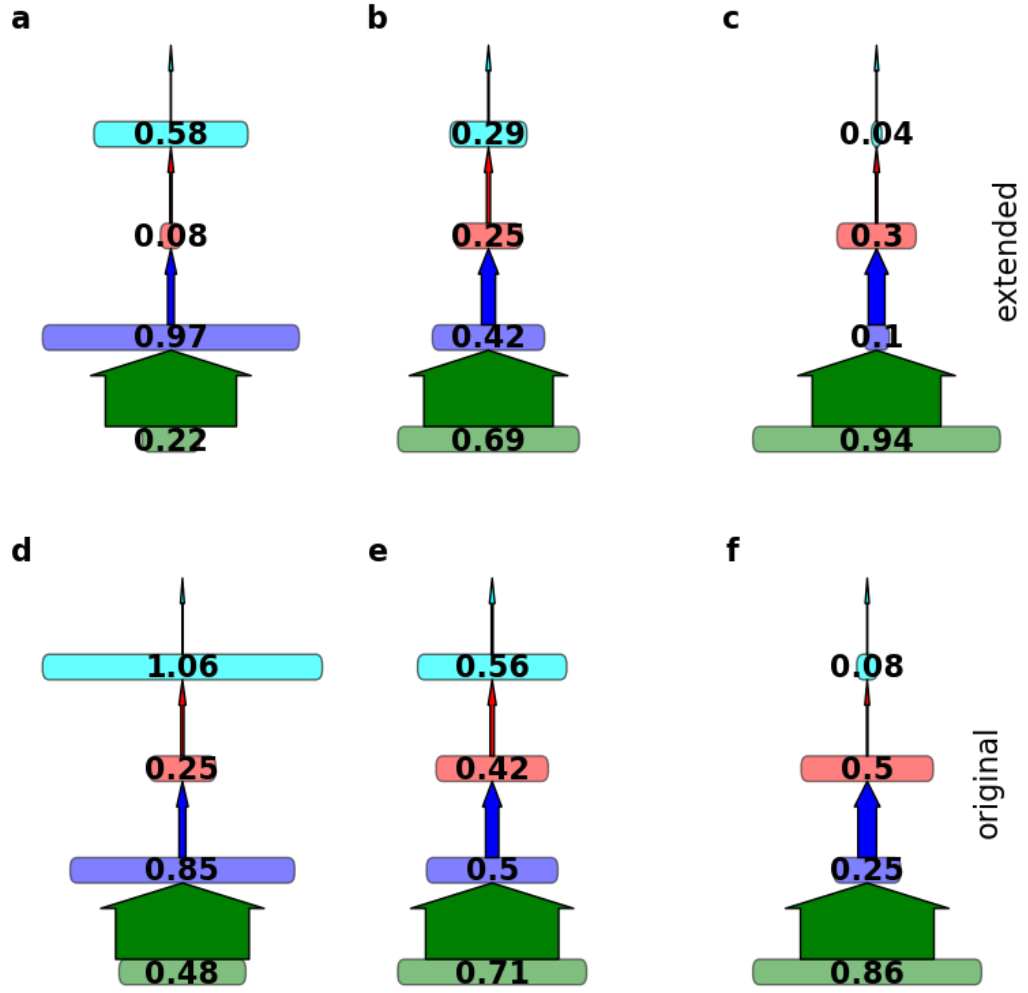

Fig. 2.3: Comparison of the mean biomasses (bold numbers) within the food chain of the extended ATN version including activity respiration (a-c) and the original ATN model (d-f), for different top predator's death rate constants d = 0.0003 (a, d), d = 0.003 (b, e), and d = 0.03 (c, f). Arrows indicate production rates. Their width is scaled to autotroph's production as 100%. Box widths are scaled with the species' biomasses

Depending on the top predator's death rate, the models exhibited different trophic cascade patterns. For small *d* (0.0003), the herbivore and the top predator accumulated high biomasses resulting in a top-heavy trophic cascade (Fig. 2.3a, d). For larger *d* (0.0030), the biomasses resembled roughly a column (Fig. 2.3b, e) and for higher *d*, a bottom-heavy trophic cascade occurred (Fig. 2.3c, f).

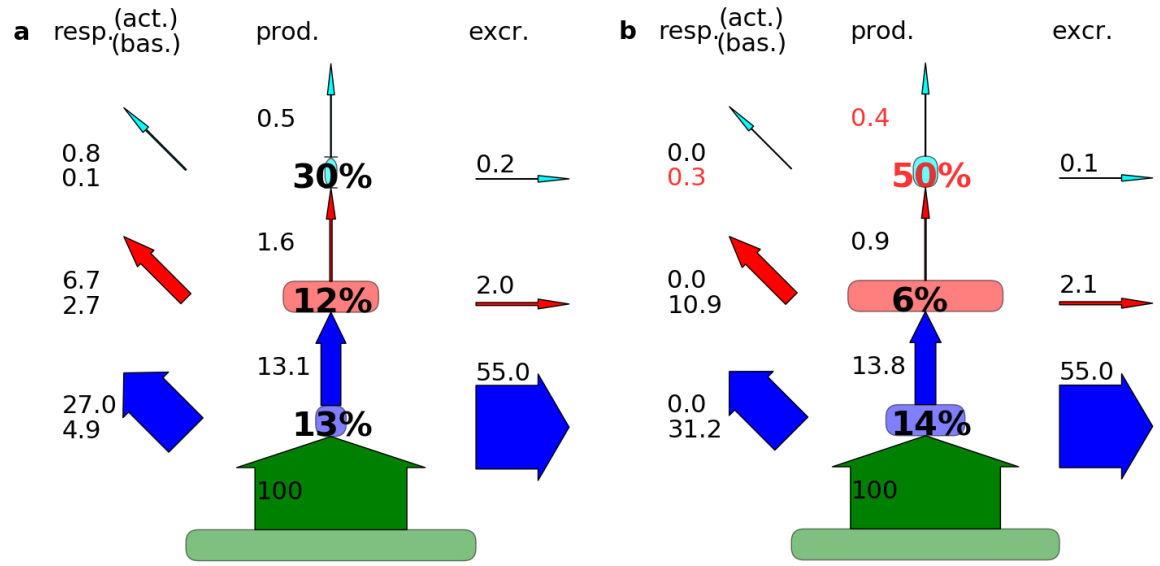

Fig. 2.4: Comparison of the energy transfer within the food chain of the extended ATN version including activity respiration (a), and the original ATN model (b). The biomass pyramids are based on the same data as Fig. 2.3c and 2.3f, i.e. d= 0.03. Included values are basal and activity respiration (numbers on the left, activity above basal respiration), production (numbers in the middle to the left of the upward arrows), trophic transfer efficiency (bold large numbers), and excretion (numbers above the right arrows). All fluxes are standardized to autotroph's production as 100%, so that wider arrows indicate larger values. Box widths are scaled with the species' biomasses. Red values point out inconsistencies with the physiological considerations that respiration is equal to or less than production (Humphreys 1979)

To further elucidate the reason for the inconsistencies between the obtained TTE of the original ATN model and physiological considerations and realistic estimates, we 38urcate38 the carbon fluxes in the bottom-heavy trophic cascade (Fig. 2.3c, f) in more detail (Fig. 2.4, Tab. 2.3). The alternating biomasses indicate where the inconsistencies are most obvious. In the original ATN model, the top predator's respiration was small compared to its ingestion, resulting in a large production per ingested unit of carbon (Tab. 2.3). This led to a production being 33% higher than the

respiration (Fig. 2.4b) and an obtained TTE of 50% (Fig. 2.4b, Tab. 2.3). In contrast, in the extended ATN version the respiration per ingested unit of carbon was higher due to the activity respiration, which resulted in a lower production and an obtained TTE of 30% (Fig. 2.4a).

In the original ATN model, respiration per ingestion and production per ingestion varied considerably more between trophic levels than in the extended ATN version. This was due to the overemphasis of basal respiration and neglecting of the activity respiration: Only a high biomass (here, of the carnivore) resulted in respiration losses of substantially more than 50% of the assimilation and thus, a realistic TTE in the original ATN model. In the extended ATN version, respiration per ingestion and production per ingestion did not vary that much across trophic levels even in the presence of a strong trophic cascade because respiration is not solely coupled to the standing biomass stock, but also to the assimilation. As low biomasses are connected with high per capita rates in the ATN models, a low biomass-related basal respiration is counteracted by high activity respiration and vice versa.

Tab. 2.3: Respiration to ingestion ratio (R/I) and production to ingestion ratio (P/I ≙ obtained TTE since non-grazing mortality was not included in the ATN model for the 1st – 3rd trophic level, thus the production of the trophic level below is ingested entirely, see 'ATN model equations') for both the original (orig.) and extended (ext.) ATN version with the top predator's death rate constant d = 0.03. Autotrophic respiration is already included in the growth rate and therefore not listed here. Values were calculated from the biomass, respiration and production values shown in Fig 2.3f and Fig. 2.4b for the original ATN model, and in Fig. 2.3c and Fig. 2.4a for the extended ATN version, respectively.

	R/I		P/I ≙ TTE	
	orig	ext	orig	ext
Top predator	35%	55%	50%	30%
Carnivore	79%	72%	6%	12%
Herbivore	31%	32%	14%	13%

Discussion

Allometric trophic network models (ATN) are an important tool to 40urcate dynamics of food webs (Boit et al. 2012; Hudson and Reuman 2013; Schuwirth and Reichert 2013; Kuparinen et al. 2016) and their diversity and stability (Brose et al. 2006; Rall et al. 2008; Berlow et al. 2009; Heckmann et al. 2012). Despite their frequent use, the ATN's energetics were not yet explicitly addressed, though they decisively influence dynamic patterns of the model (Boit et al. 2012). Here, we compared the energetics of the original ATN model (Yodzis and Innes 1992; Brose et al. 2006) which considers only basal respiration, and an extended ATN version (Boit et al. 2012) including both basal and activity respiration. We found that the trophic transfer efficiency (TTE) could become unrealistically high in the original ATN model in both static calculations and dynamic simulations, whereas it always fell into a physiologically and ecologically realistic range in the extended ATN version. The reason for the more realistic energy transfer is the inclusion of the activity respiration that depends on the amount of assimilated carbon in the extended ATN version.

The threshold above which we consider a TTE unrealistically high was set very conservatively and follows from the assumption that the energy allocated to production can at most be equal to respiration (Humphreys 1979). This yields a maximum feasible TTE of 22.5% for herbivores and 42.5% for carnivores (Eq. 2.10). These upper theoretical limits are usually not reached in natural communities even when dominated by unicellular organisms or invertebrates, except when a trophic level is under high predation pressure. Empirically established maximum TTE range between 13% and around 30% for both herbivores and carnivores from pelagic systems and including small to large fish (Straile 1997; Jennings et al. 2002; Barnes et al. 2010). The extended ATN version reflects these natural energetic constraints well by keeping the obtained TTE in a realistic range up to 30% (cf. Fig. 2.2). In contrast, the original ATN model led to an obtained TTE up to 51% (cf. Fig 2.2) which overestimates the empirical values of at most 30% by a factor of 1.7.

The metabolic theory of ecology does not differentiate between basal respiration proportional to the standing biomass stock and activity respiration (Brown et al. 2004). Brown et al. (2004) stated that the

metabolic rate generally depends only on biomass and that the field metabolic rate, analog to our activity respiration, is a "fairly constant multiple of the basal rate" and therefore also depends only on the biomass. A similar assumption also served as basis for the ATN models accounting only for basal respiration proportional to the biomass. This assumption is reasonable if resource levels are fairly constant, however, biomasses and ingestion rates vary in nature and dynamic models and so does, ultimately, also the TTE (Appendix A, Fig. A3).

The different patterns of trophic cascades illustrate the problematic consequences of linking respiration only to biomass. The amount of top-down control exerted by the top predator or the carnivore and thus the strength of the trophic cascade were modulated by the death rate constant *d*. For small *d*, the top predator had a high biomass and controlled the carnivore. The carnivore's obtained TTE then became unrealistically high in the original ATN model, and the food web became (too) top heavy. The link between a high TTE and top heavy food webs is also described in a review of 23 food webs (McCauley et al. 2018). For intermediate *d*, the biomasses were approximately equally distributed across different trophic levels which is in line with the flat biomass distribution established for pelagic systems (Gaedke 1992). For higher *d*, the top predator was top-down controlled by its death rate and released the carnivore from grazing pressure, but in this case the top predator's obtained TTE became unrealistically high. In any case, the obtained TTE was too high at one particular trophic level within a pronounced trophic cascade because the top-down controlled trophic levels had a low biomass and thus a low basal respiration. Thus, the assumption of Brown et al. (2004) that activity respiration and field metabolic rate are proportional to a standing biomass stock only holds for equally distributed biomasses, but not for unequally distributed biomasses in trophic cascades.

The link between activity respiration and ingestion as we introduced it here to the ATN model allows for a more flexible reaction to dynamic instead of constant biomasses. This is important when modelling large food webs with rapidly changing dynamics such as pelagic systems. ATN and other food web models are known to form trophic cascades (Carpenter et al. 2016) which are observed in many ecosystems (Carpenter et al. 1985; Pace

et al. 1999; Shurin et al. 2002) and, as we showed here, strongly affects the TTE. Other ATN models dampened the trophic cascades with mechanism such as predator interference or type III functional response which obfuscates this underlying energetic problem to some extent (Rall et al. 2008). However, they do not solve it, as the model inherent TTE is independent of these mechanisms. The ATN approach has also been used to parameterize large-scale ecosystem models such as the Madingley model (Harfoot et al. 2014). In this model, neglecting activity respiration seems to have contributed to unrealistically top heavy biomass distributions as well, underlining the importance of more accurate assumptions regarding basic energetic processes than the original ATN provides. The pronounced trophic cascades as seen in our study are due to the structurally simplistic food chain and would be dampened in natural systems, e.g. by a higher trophic connectance via omnivory.

Other models, like Rosenzweig-MacArthur-type predator-prey-models (Rosenzweig and MacArthur 1963; Weitz and Levin 2006) incorporate respiration losses only by a constant factor named conversion efficiency related to ingestion and production, thus this type of model only accounts for (what we call here) activity respiration. Basal respiration may be implicitly considered in a death rate proportional to the biomass. Anderson (1992) pointed out the difference between basal and activity respiration especially for unicellular organisms and invertebrates whose activity respiration exceeds the basal respiration as they are poikilotherms with low maintenance costs when inactive. In our extended ATN version, we combined both respiration rates and implemented these ideas by introducing the factor f_a in the formulation of assimilation (cf. Eq. 2.8, Methods, Fig. 2.1), thereby making activity respiration proportional to the amount of assimilated carbon.

Following Boit et al. (2012), we set the parameter $f_a = 0.4$ for all consumers assuming that respiration is slightly larger than production (Humphreys 1979). Although this conservative estimate satisfies fundamental energetic constraints, a more differentiated picture may emerge when defining a more empirically grounded value range for f_a for different taxa. In the same way, the parameter $f_m = 0.1$ (following Boit et al. (2012)) may be adapted to fit different taxa. As a recent meta-analysis reveals that the differences in

respiration rates between taxonomic groups are not only due to consumer type (e.g. herbivore or carnivore) (Lang et al. 2017), future research could aim to entangle the influences of taxonomic group, activity, and food availability on respiration rates. Until then due to the scarcity of experimental data on activity vs. basal respiration rates of invertebrates, the parameterization of f_a and f_m in a specific food web context remains a challenge for future modelling studies with ATNs.

The complexity of the model did not increase from a mathematical point of view even though we introduced two additional parameters (f_a and f_m) in the extended ATN version. The number of effective parameters that independently determine model dynamics is the same in the original and the extended ATN version. This becomes obvious when we introduce new parameters for the extended ATN model: $e_{prod,i} = e_i f_a$ as the production efficiency (equivalent to e_i in the original model) and $x_{b,i} = f_m x_i$ (equivalent to x_i in the original model) as the per capita basal metabolic rate. When aiming for a concise mathematical description of the model, we recommend to use these effective parameters. Here, however, we chose not to do so in order to emphasize the underlying biological processes. In the same vein, we argue that we do not merely propose to use different values for some parameters of the ATN model, but stress the conceptual advancement of the ATN model by clearly distinguishing between basal and activity respiration, which is essential for improving quantitative predictions about ecosystem energetics.

To conclude, basal and activity respiration depend on different processes and should both be considered explicitly in models covering metabolic processes. Including activity respiration in the ATN model lowers the obtained TTE to realistic values in comparison to empirically derived values. Especially for food webs mainly based on unicellular organisms and invertebrates or modelling ecosystems prone to trophic cascading, we recommend using the extended ATN version to achieve more realistic energetics. Far more than a mere modelling fix, reflecting the energy flux through food webs in a realistic way is indispensable for upscaling and integrating smaller modules to larger community networks or even large-scale ecosystem models. ATN models will then be ready for quantitatively

linking trophic interactions in biodiverse communities to ecosystem-level biomass dynamics and biogeochemical cycling.

Acknowledgments

We thank P. de Ruiter and an anonymous reviewer for helpful comments on an earlier version of the manuscript. This work was funded by DFG (GA 401/26-1) as part of the Priority Programme 1704 (DynaTrait).

References

Anderson TR (1992) Modelling the influence of food C:N ratio, and respiration on growth and nitrogen excretion in marine zooplankton and bacteria. J Plankton Res 14:1645–1671. doi: 10.1093/plankt/14.12.1645

Barnes C, Maxwell D, Reuman DC, Jennings S (2010) Global patterns in predator-prey size relationships reveal size dependency of trophic transfer efficiency. Ecology 91:222–232. doi: 10.1890/08-2061.1

Begon M, Townsend CR, Harper JL (2006) Ecology - From Individuals to Ecosystems, 4th editio. Blackwell Publishing

Benoît E, Rochet M-J (2004) A continuous model of biomass size spectra governed by predation and the effects of fishing on them. J Theor Biol 226:9–21. doi: 10.1016/S0022-5193(03)00290-X

Berlow EL, Dunne JA, Martinez ND, et al (2009) Simple prediction of interaction strengths in complex food webs. Proc Natl Acad Sci 106:187–191. doi: 10.1073/pnas.0806823106

Boit A, Martinez ND, Williams RJ, Gaedke U (2012) Mechanistic theory and modelling of complex food-web dynamics in Lake Constance. Ecol Lett 15:594–602. doi: 10.1111/j.1461-0248.2012.01777.x

Brose U (2008) Complex food webs prevent competitive exclusion among producer species. Proc Biol Sci 275:2507–2514. doi: 10.1098/rspb.2008.0718

Brose U, Williams RJ, Martinez ND (2006) Allometric scaling enhances stability in complex food webs. Ecol Lett 9:1228–1236. doi: 10.1111/j.1461-0248.2006.00978.x

Brown JH, Gillooly JF, Allen AP, et al (2004) Toward a metabolic theory of ecology. Ecology 85:1771–1789. doi: 10.1890/03-9000

Carpenter SR, Cole JJ, Pace ML, Wilkinson GM (2016) Response of plankton to nutrients, planktivory and terrestrial organic matter: A model analysis of whole-lake experiments. Ecol Lett 19:230–239. doi: 10.1111/ele.12558

Carpenter SR, Kitchell JF, Hodgson JR (1985) Cascading Trophic Interactions and Lake Productivity. Bioscience 35:634–639. doi: 10.1525/bio.2010.60.10.17

Gaedke U (1992) The size distribution of plankton biomass in a large lake and its seasonal variability. Limnol Oceanogr 37:1202–1220.

Gaedke U, Hochstädter S, Straile D (2002) Interplay between energy limitation and nutritional deficiency: Empirical data and food web models. Ecol Monogr 72:251–270. doi: 10.1890/0012-9615(2002)072[0251:IBELAN]2.0.CO;2

Gessaman JA (1973) Methods of estimating the energy cost of free existence. In: Logan UT (ed) Ecological energetics of homeotherms. Utah State University Press, pp 3–31

Harfoot MBJ, Newbold T, Tittensor DP, et al (2014) Emergent Global Patterns of Ecosystem Structure and Function from a Mechanistic General Ecosystem Model. PLoS Biol. doi: 10.1371/journal.pbio.1001841

Heckmann L, Drossel B, Brose U, Guill C (2012) Interactive effects of body-size structure and adaptive foraging on food-web stability. Ecol Lett 15:243–250. doi: 10.1111/j.1461-0248.2011.01733.x

Hendriks AJ (1999) Allometric Scaling of Rate, Age and Density Parameters in Ecological Models. Oikos 86:293–310. doi: 10.2307/3546447

Holling CS (1959) Some Characteristics of Simple Types of Predation and Parasitism. Can Entomol 91:385–398.

Hudson LN, Reuman DC (2013) A cure for the plague of parameters: constraining models of complex population dynamics with allometries. Proc R Soc B Biol Sci 280:20131901. doi: 10.1098/rspb.2013.1901

Humphreys WF (1979) Production and Respiration in Animal Populations. J Anim Ecol 48:427–453. doi: 10.2307/4171

Jennings S, Warr KJ, Mackinson S (2002) Use of size-based production and stable isotope analyses to predict trophic transfer efficiencies and predator-prey body mass ratios in food webs. Mar Ecol Prog Ser 240:11–20. doi: 10.3354/meps240011

Kuparinen A, Boit A, Valdovinos FS, et al (2016) Fishing-induced life-history changes degrade and destabilize harvested ecosystems. Sci Rep 6:1–9. doi: 10.1038/srep22245

Lang B, Ehnes RB, Brose U, Rall BC (2017) Temperature and consumer type dependencies of energy flows in natural communities. Oikos 4:1–9. doi: 10.1111/oik.04419

McCauley DJ, Gellner G, Martinez ND, et al (2018) On the prevalence and dynamics of inverted trophic pyramids and otherwise top-heavy communities. Ecol Lett. doi: 10.1111/ele.12900

Pace ML, Cole JJ, Carpenter SR, Kitchell JF (1999) Trophic cascades revealed in diverse ecosystems. Trends Ecol Evol 14:483–488. doi: 10.1016/S0169-5347(99)01723-1

Rall B, Guill C, Brose U (2008) Food-Web Connectance and Predator Interference Dampen the Paradox of Enrichment. Oikos 117:202–213. doi: 10.1111/j.2007.0030-1299.15491.x

Rosenzweig MI, MacArthur RH (1963) Graphical Representation and Stability Conditions of Predator-Prey Interactions. Am Nat 97:209–223. doi: 10.1086/662677

Schneider FD, Brose U, Rall BC, Guill C (2016) Animal diversity and ecosystem functioning in dynamic food webs. Nat Commun 7:12718. doi: 10.1038/ncomms12718

Schneider FD, Scheu S, Brose U (2012) Body mass constraints on feeding rates determine the consequences of predator loss. Ecol Lett 15:436–443. doi: 10.1111/j.1461-0248.2012.01750.x

Schuwirth N, Reichert P (2013) Bridging the gap between theoretical ecology and real ecosystems: Modeling invertebrate community composition in streams. Ecology 94:368–379. doi: 10.1890/12-0591.1

Shurin JB, Borer ET, Seabloom EW, et al (2002) A cross-ecosystem comparison of the strength of trophic cascades. Ecol Lett 5:785–791. doi: 10.1046/j.1461-0248.2002.00381.x

Straile D (1997) Gross growth efficiencies of protozoan and metazoan zooplankton and their dependence on food concentration, predator-prey weight ratio, and taxonomic group. Limnol Oceanogr 42:1375–1385. doi: 10.4319/lo.1997.42.6.1375

Weitz JS, Levin SA (2006) Size and scaling of predator-prey dynamics. Ecol Lett 9:548–557. doi: 10.1111/j.1461-0248.2006.00900.x

Yodzis P, Innes S (1992) Body Size and Consumer-Resource Dynamics. Am Nat 139:1151–1175. doi: 10.1086/285380

Chapter 3

The shape of a defense-growth trade-off governs seasonal trait dynamics in natural phytoplankton

Elias Ehrlich*, Nadja J. Kath* and Ursula Gaedke

Manuscript is available at https://www.nature.com/articles/s41396-020-0619-1.

* These authors contributed equally to this work

Abstract

Theory predicts that trade-offs, quantifying costs of functional trait adjustments, crucially affect community trait adaption to altered environmental conditions, but empirical verification is scarce. We evaluated trait dynamics (anti-predator defense, maximum growth rate and phosphate affinity) of a lake phytoplankton community in a seasonally changing environment, using literature trait data and 21 years of species-resolved high-frequency biomass measurements. The trait data indicated a concave defense-growth trade-off, promoting fast-growing species with intermediate defense. With seasonally increasing grazing pressure, the community shifted towards higher defense levels at the cost of lower growth rates along the trade-off curve, while phosphate affinity explained some deviations from it. We discuss how low fitness differences of species, inferred from model simulations, in concert with stabilizing mechanisms, e.g. arising from further trait dimensions, may lead to the observed phytoplankton diversity. In conclusion, quantifying trade-offs is key for predictions of community trait adaptation and biodiversity under environmental change.

Introduction

Identifying trade-offs between functional traits of species is central to ecology because it provides a fundamental basis to understand species coexistence and the trait composition of natural communities[1]. Trade-offs emerge through physiological, energetic, behavioural, genetic or resource allocation constraints[2] and can be detected within one species[3,4] as well as on the community level among different species sharing similar individual-level constraints[5,6]. Such interspecific trade-offs promote species diversity and guide the way of community trait changes under altered environmental conditions[7,8].

Box 3.1: Theory on trade-off curves, fitness landscapes, survival of species and trait dynamics.

The survival of species and the trait dynamics within a community depend on the species trade-offs between functional traits, quantifying the costs of trait adjustments, and the environmental conditions that determine the fitness landscape. The **trade-off curve** is defined as the boundary of the set of feasible trait combinations, representing all possible phenotypes of species (Fig. 3.1)[60]. The trade-off curve is fixed by individual-level constraints (e.g. energetic or physiological constraints) and may have different shapes (e.g. concave or convex, Fig. 3.1), reflecting different costs of trait adjustments.

Species fitness is defined as the net per capita growth rate[61]. The fitness landscape within a two-dimensional trait space can be represented by **fitness isoclines** (Fig. 3.1)[62], connecting trait combinations of equal fitness. The slope of these fitness isoclines depends on the abiotic and biotic environmental conditions (e.g. grazing pressure, Fig. 3.1). Trait combinations along the trade-off curve reaching the highest fitness value represent fitness maxima (Fig. 3.1). Species with these trait combinations are positively selected and survive in the long term. Species itself can change the fitness landscape in a way favourable for species with other strategies/niches (a stabilizing mechanism), e.g. high densities of fast-growing, undefended species lead to increased predator abundance favouring defended species (and *vice versa*). In the sense of Chesson's coexistence theory[36], such stabilizing mechanisms may level out fitness differences between species and allow for their stable coexistence.

Given linear fitness isoclines, implying linear trait-fitness relationships[14], theory predicts that concave trade-offs favour species with intermediate trait combinations (Fig. 3.1a-c), while convex trade-offs promote species with extreme trait combinations (Fig. 3.1d-f). Under directionally changing environmental conditions, the fitness maximum moves continuously along a concave trade-off curve driving continued sorting of many different species, which results in changes of the community trait composition. For example, an increasing grazing pressure (e.g. due to a lower mortality of grazers) promotes species with higher defense values at the cost of a decreasing maximum growth rate (Fig. 3.1a-c). In contrast, for convex trade-off curves, fitness is always maximal for only one or two of the extreme trait combinations depending on the environmental conditions (Fig. 3.1d-f).

Theory indicates that it is the shape of the trade-off curve between two traits, reflecting costs of trait adjustments, which determines species coexistence and how trait values change in response to environmental forcing[9–11]. We summarize the theory and specify predictions in Box 3.1 and Fig. 3.1. While theory revealing the importance of the shape of the trade-off curve for coexistence and trait dynamics is well developed[12–14], its empirical verification has been left far behind. Two studies successfully tested the theory in small-scale lab experiments assembling different bacterial strains[15,16]. However, respective approaches from the field are lacking, leaving open the question how the trade-off shape affects the trait composition of natural communities. In this article, we combine theory and long-term field data to provide evidence for the frequently postulated defense-growth trade-off and to show how its shape affects seasonal trait dynamics of phytoplankton in a large European lake.

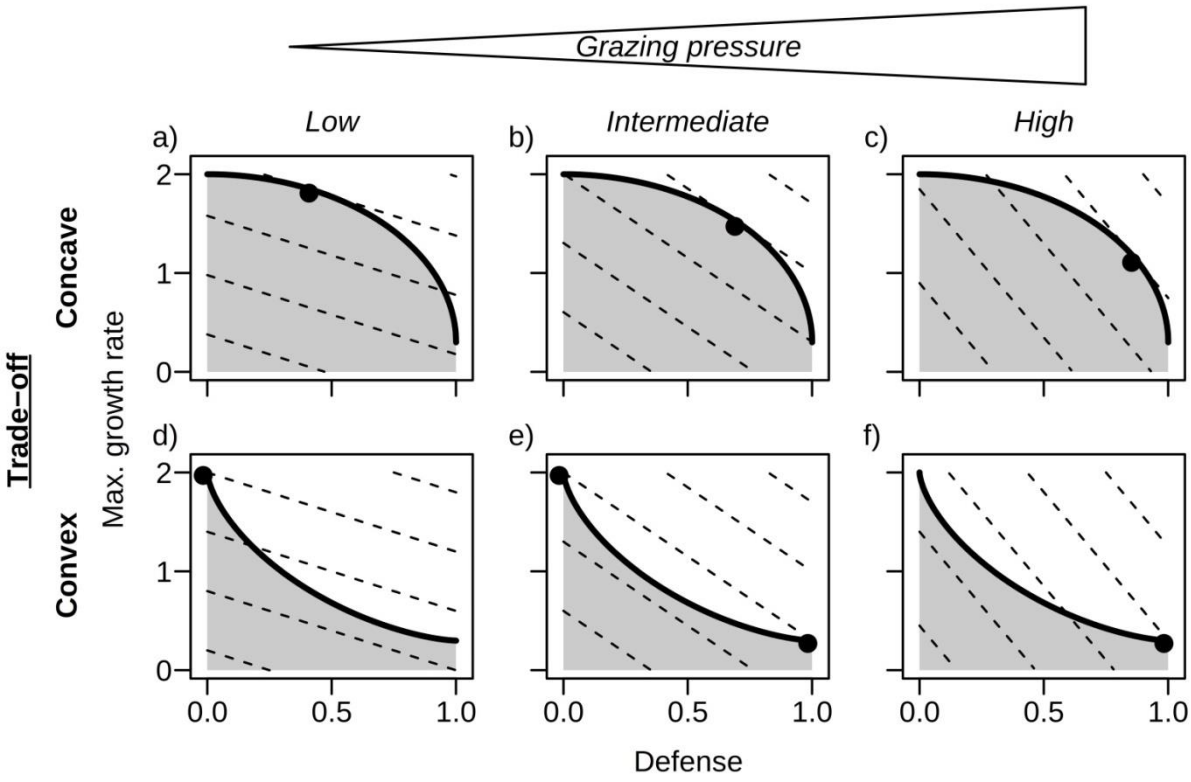

Fig. 3.1: The shape of the trade-off curve in concert with the environment determines the strategies of maximal fitness in a community. Our example considers a trade-off between defense and maximum growth rate (d^{-1}) in a prey community with grazing pressure as a biotic environmental factor. The trade-off curve (thick solid line) represents the boundary of the set of feasible trait combinations (grey area) and may be, for example, (a-c) concave or (d-f) convex. The fitness landscape is shaped by the grazing pressure (low, intermediate or high), resulting in different slopes of the fitness isoclines (dashed lines). The trait combinations reaching the highest fitness isocline are fitness maxima (dots) and are positively selected. If two or more trait combinations are of maximal fitness in the long term, the respective species with these trait combinations coexist I, otherwise only one species survives (a-d, f).

Phytoplankton communities are well-suited for addressing this issue as important functional traits of phytoplankton have been measured in the lab revealing key trade-offs[17,18]. Phytoplankton communities are extremely diverse spanning a large trait space[19,20] indicating that trade-offs play a decisive role in maintaining their biodiversity, although the number of limiting factors allowing for niche differentiation seem to be low compared to the high number of coexisting species (known as Hutchinson's 'Paradox of the Plankton'[21]). Furthermore, phytoplankton species have short generation times allowing for pronounced seasonal succession[22].

This offers the opportunity to observe species sorting in response to recurrently changing environmental conditions driving community trait dynamics.

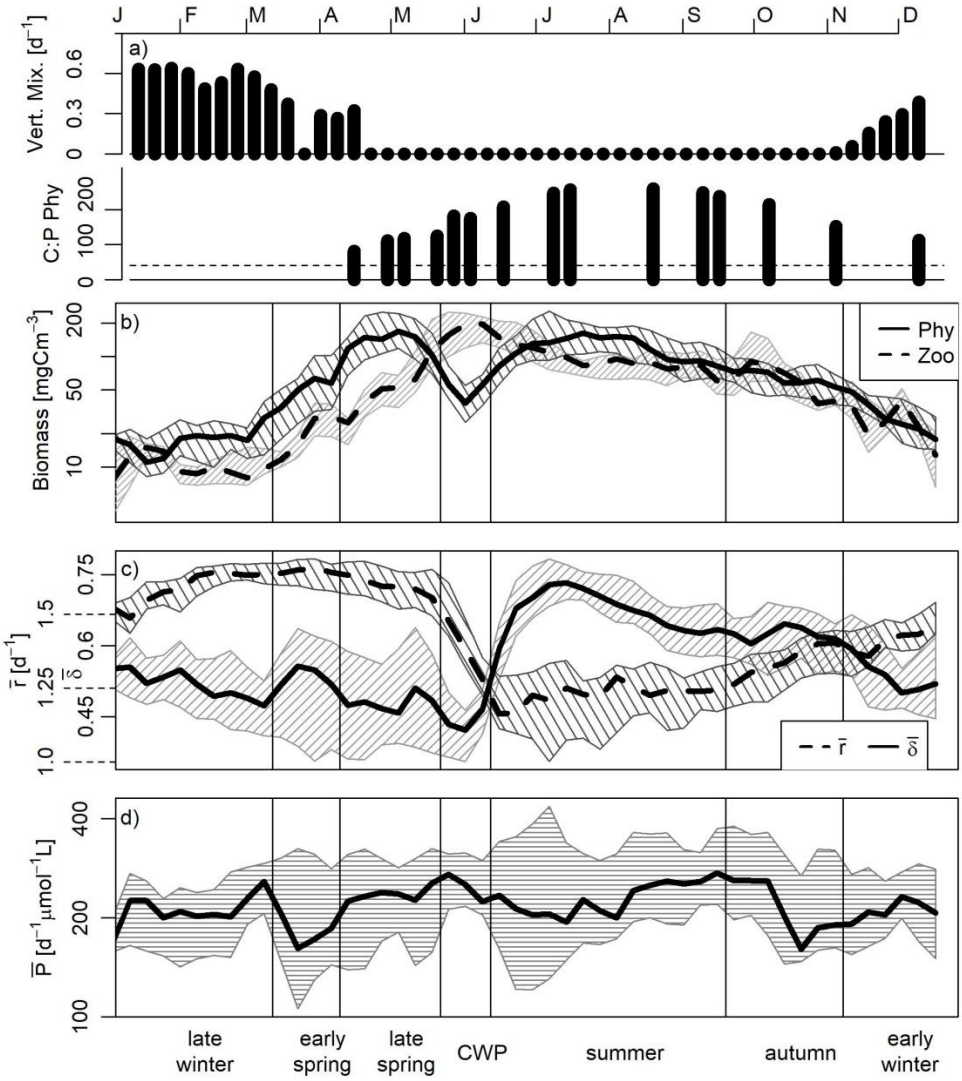

Fig. 3.2: Seasonal dynamics of a) abiotic factors, b) total biomasses of phytoplankton (Phy) and herbivorous zooplankton comprising ciliates, rotifers and herbivorous crustaceans (Zoo), and c, d) phytoplankton community average trait values (maximum growth rate $\bar{r}$, defense $\bar{\delta}$ and phosphate affinity $\bar{P}$) in a standardized year. A) The vertical mixing intensity quantifies the relative amount of phytoplankton exported from the euphotic zone (0-20 m) to larger depths (20-100 m). The carbon to phosphorous (mass) ratio of phytoplankton, C:P Phy, indicates the degree of nutrient depletion (dashed line marks the Redfield ratio). B-d) Interannual medians (lines) and interquartile ranges (shaded areas) are shown for the biomasses and the community average trait values. CWP denotes the clear-water phase. For methodical details see the methods and Appendix B1.

Previous trait-based studies on phytoplankton communities already quantified trade-offs among different resource utilization traits[5] and revealed how the trait composition of phytoplankton communities in different lakes and a marine system depended on light and nutrient conditions[23–26]. However, phytoplankton can also be strongly affected by herbivory selecting for phytoplankton defense, which was not considered in these studies but is likely to have a crucial effect on their seasonal trait dynamics[22]. Defense against predation often comes at a physiological cost[18], like a lower maximum growth rate[27,28] or a lower competitive ability[3]. Competitive ability is used here in the sense of Tilman[6]: a high competitive ability refers to a low equilibrium resource concentration in monoculture (R^*), where growth equals mortality. Hence, the competitive ability of a species is defined by its resource uptake affinity, but may also depend on its maximum growth rate, especially at high rates of background mortality. Trade-offs between defense and competitive ability or maximum growth rate can mediate antagonistic effects of top-down and bottom-up control on the trait composition. A large body of theory assumes such trade-offs between defense and maximum growth rate[29,30] or between defense and competitive ability[31,32]. However, there is no study that empirically quantifies the shape of these trade-offs and uses this information in combination with theoretical insights on trade-off curves (see Box 3.1 and Fig. 3.1) to explain how predation and abiotic conditions drive the trait dynamics and variation of natural communities.

Here, we use 21 years of high-frequency density measurements of a natural lake phytoplankton community (large, deep, mesotrophic Lake Constance) and literature trait data (defense against predation, maximum growth rate and phosphate affinity) in order to identify how potential interspecific trade-offs govern the community trait dynamics under seasonally changing environmental conditions. In the studied lake, zooplankton grazing, vertical mixing and phosphate depletion are important limiting factors of phytoplankton[33,34], which all undergo a highly repetitive seasonal succession (Fig. 3.2a,b). As for the environmental factors, we found distinct seasonal dynamics in the community average values of defense and maximum growth rate, but not for phosphate affinity (Fig. 3.2c,d). The phytoplankton trait values were

taken from Bruggeman, who obtained the trait values from a statistical model fed with lab trait measurements, phylogenetic and allometric relationships[35]. From this data set, we could infer a distinct concave trade-off between defense and maximum growth rate for the Lake Constance phytoplankton community. Phosphate affinity showed no strong relationships to these traits, but we found slight evidence for a multidimensional trade-off. We parameterized a phytoplankton model with the observed concave defense-growth trade-off, which reproduces the seasonal shift in the biomass-trait distribution within the trait space. For comparison, we parameterized the model also with a hypothetical convex trade-off, which fails in reproducing the observed pattern. This reveals the importance of knowing the exact trade-off shape for understanding trait dynamics. Furthermore, in reference to modern coexistence theory[36], we discuss how low fitness differences of species found along the trade-off curve can promote the maintenance of the large diversity in this community, when taking into account stabilizing mechanisms arising from further trait dimensions and environmental fluctuations.

Material and methods

Study site and sampling

Upper Lake Constance (Bodensee) is a large (472 km²), deep (mean depth = 101 m), warm-monomictic, mesotrophic lake bordered by Germany, Switzerland and Austria. It has a well-mixed epilimnion and a large pelagic zone[37]. Lake Constance underwent re-oligotrophication during which the total phosphorous concentration declined 4-fold from 1979 to 1996 leading to an annual phytoplankton biomass and production decline by 50% and 25 %, respectively[34]. The re-oligotrophication did not qualitatively affect the biomass-trait distribution in respect to defense and maximum growth rate (Fig. B5, Appendix B3) and had little impact on phosphate affinity (Fig. 3.2d, Fig. B6). Thus, it is not further considered.

Plankton sampling was conducted weekly during the growing season and approximately fortnightly in winter, culminating in a time series of 853 phytoplankton biomass measurements from 1979 to 1999 (for details see Appendix B1 and https://fred.igb-berlin.de/Lakebase). Phytoplankton counts and cell volume estimates were obtained using Utermöhl[38]

inverted microscopy and were converted into biomass based on a specific carbon to volume relationship[39]. Measurements were taken from the uppermost water layer between 0 and 20 m depth, which roughly corresponds to the epilimnion and the euphotic zone. We aggregated almost all species into 36 morphotypes of phytoplankton comprising individual species or higher taxonomic units that are functionally identical or very similar under the functional classification employed here. This guaranteed a consistent resolution of phytoplankton counts across years and neglects species which were very irregularly encountered. The morphotypes constitute a mean value of 92% and a median value of 96% of total phytoplankton biomass on annual average, with particularly high values from spring to summer. Most of the neglected biomass originates from heterotrophs as *Gymnodinium* spp. And *Ochromonas* spp. Not belonging to the phytoplankton *sensu strictu*. Zooplankton was sampled with the same frequency as phytoplankton. Data for all major herbivorous zooplankton groups (ciliates, rotifers, cladocerans and calanoid copepods) were simultaneously available from 1987 to 1996.

Seasonal patterns

We subdivided the year into seven consecutive phases: late winter, early spring, late spring, clear-water phase (CWP), summer, autumn and early winter. Each phase was characterized by a well-defined combination of abiotic and biotic factors driving the phytoplankton community (Fig. 3.2): Strong vertical mixing implying a high phytoplankton net export from the euphotic zone (0-20 m) to deep water layers (20-100 m) occurred during winter and partly early spring (Appendix B1). Grazing pressure was most important during the CWP and summer, and declined towards autumn. Nutrient depletion was most relevant in summer and autumn when vertical mixing, supplying nutrients from larger depths, was absent.

Trait data and trade-offs

All trait values were consistently taken from Bruggeman[35]. He compiled lab-measurements of traits from the literature for numerous taxa and derived from allometric and phylogenetic relationships a statistical model comprising trait values for these and other taxa. For consistency, we used only the values of this model. We defined defense δ as 1 – edibility.

Bruggeman[35] defined edibility as the rate of prey consumption relative to the rate at which the most commonly reported prey, *Rhodomonas minuta*, was consumed by *Daphnia*, which were both dominant prey and grazers in Lake Constance. *Daphnia* dominated the herbivorous crustaceans from the CWP until autumn[40], and its feeding preferences largely overlap with the other herbivorous groups: The highly diverse ciliate and rotifer communities mainly graze on small, undefended algae, but some specialized species consume also larger morphotypes, which were classified as more defended by Bruggeman[41,42]. The only calanoid copepod, *Eudiaptomus,* shows also large overlap with the prey spectrum of *Daphnia*[43]. Regarding the phytoplankton taxa considered in our study, 93% of the edibility measurements originated from lab cultures of phytoplankton strains from Lake Constance sampled during the first part of our study period[44]. Thus, we consider the edibility values of Bruggeman[35] to be fairly representative for the grazer community in Lake Constance. Phosphate affinity was defined as maximum growth rate divided by the half-saturation coefficient for phosphate, standardized to continuous illumination and a temperature of 20°C. All morphotypes, their assigned trait data and taxonomy are listed in Tab. B1. To detect a potential trade-off, we tested the relationship between traits using the Spearman rank correlation coefficients (not biomass weighted).

Model

We developed a simple food web model to show which phytoplankton trait combinations are favored under low (e.g., during early spring) and high grazing pressure (e.g., during summer). The model included N phytoplankton species, which face a defense-growth trade-off, and one zooplankton group:

$$\frac{dP_i}{dt} = \left(r_i \frac{R}{K+R} - \frac{G\,(1-\delta_i)\,Z}{H+\sum_{i=1}^{N} P_i} - m_P\right) P_i \qquad (3.1)$$

$$\frac{dZ}{dt} = \left(\varepsilon\, \frac{G\, \sum_{i=1}^{N}[(1-\delta_i)P_i]}{H + \sum_{i=1}^{N} P_i} - m_z\right) Z$$

where P_i represents the biomass of phytoplankton species i, Z the zooplankton biomass and R the nutrient concentration limiting phytoplankton growth. Assuming a fixed nutrient pool R_{max}, the available

nutrient concentration can be written as $R = R_{max} - \sum_{i=1}^{N} P_i - \frac{1}{\varepsilon} Z$, i.e. the total amount of nutrients minus the nutrients fixed in biomass of phytoplankton and zooplankton[45]. Note that the nutrients are in units of phytoplankton biomass. r_i denotes the maximum growth rate of phytoplankton species i, δ_i its defense against zooplankton, K the half-saturation constant for nutrient uptake (determined by its nutrient affinity), and m_P the natural mortality of phytoplankton. The latter two are assumed to be equal for all phytoplankton species. G represents the maximum grazing rate of zooplankton, H the half-saturation constant of zooplankton for phytoplankton ingestion, ε the conversion efficiency of phytoplankton biomass into zooplankton biomass and m_z the mortality of zooplankton (for a detailed parameter description see Appendix B4). By changing m_z, we vary the importance of grazing pressure on phytoplankton. We run simulations for two different scenarios with constant conditions, i.e. without periodical forcing: 1. m_z is high, and 2. m_z is low, mimicking distinct seasonal phases of low (1.) and high grazing pressure (2.). From these simulations, we obtain the dominant trait combinations for each phase and the time to extinction of inferior species as a fitness estimate. We assume a concave trade-off curve between r_i and δ_i, similar to the one found in the empirical data (Fig. 3.3), and considered 199 different phytoplankton species with trait values spanning the whole feasible trait space. For details on the justification, parametrization, initialization and numerical integration of the model see Appendix B4.

Results

The results section is divided into four parts: First, we present insights into seasonal dynamics of abiotic conditions, total phyto- and zooplankton biomasses and phytoplankton community average trait values, defined as the biomass-weighted mean of the trait values of all morphotypes. For these total biomasses and community average trait values, we show the interannual medians and the corresponding interquartile ranges at each standardized sampling date in order to provide information on interannual variability. Secondly, we reveal insights on the trade-offs obtained from trait data for the phytoplankton morphotypes encountered in Lake Constance and the mean annual biomass-trait distribution. Thirdly, we show how the biomass-trait distribution changes seasonally in response to

altered environmental conditions. Finally, we compare the observed patterns with our model predictions.

Seasonal dynamics

Abiotic factors and phyto- and zooplankton biomasses showed seasonal patterns typical for a temperate, monomictic lake with winter mixing and phytoplankton spring and summer blooms, the latter under nutrient depletion, and in between the clear-water phase (CWP) when zooplankton biomass comprising ciliates, rotifers, cladocerans and calanoid copepods was maximal (Fig. 3.2a,b). Also the phytoplankton community average values of defense $\bar{\delta}$ and maximum growth rate $\bar{r}$ exhibited a distinct seasonality (Fig. 3.2c). $\bar{\delta}$ was low in late winter and spring with relatively large differences among years. At the end of the CWP, it increased sharply, reached its maximum in summer and declined slowly thereafter. The low interannual variation during this period suggests a high selection pressure on this trait. $\bar{r}$ exhibited the opposite seasonal trend. It was high in late winter and spring and declined sharply during the CWP with a low interannual variability (Fig. 3.2c). In summer, $\bar{r}$ was low and more variable among years and re-increased thereafter. In contrast, the community average phosphate affinity $\bar{P}$ did not show such a clear and recurrent seasonal pattern (Fig. 3.2d). The fluctuations of $\bar{P}$ were small compared to the large trait range (3 -1600 $d^{-1}\mu mol^{-1}L$).

Trade-offs

The 36 dominant morphotypes co-occurring in large, deep Lake Constance covered a large range of values in defense δ and maximum growth rate r (Fig. 3.3a). In general, a low value in δ was accompanied by a high value in r, and *vice versa* (Spearman rank correlation coefficient ρ = -0.61, p = 10^{-4}). We found no morphotype that maximizes both δ and r simultaneously, suggesting a physiological or energetic constraint. Morphotypes with low values in both traits, resulting in low fitness, were not found either, indicating past competitive exclusion. Many morphotypes had an intermediate δ and high r or *vice versa* implying a concave trade-off curve. At distinct defense levels, diatoms and chlorophytes had generally higher maximum growth rates than the other morphotypes suggesting that other trait dimensions may play a role as well.

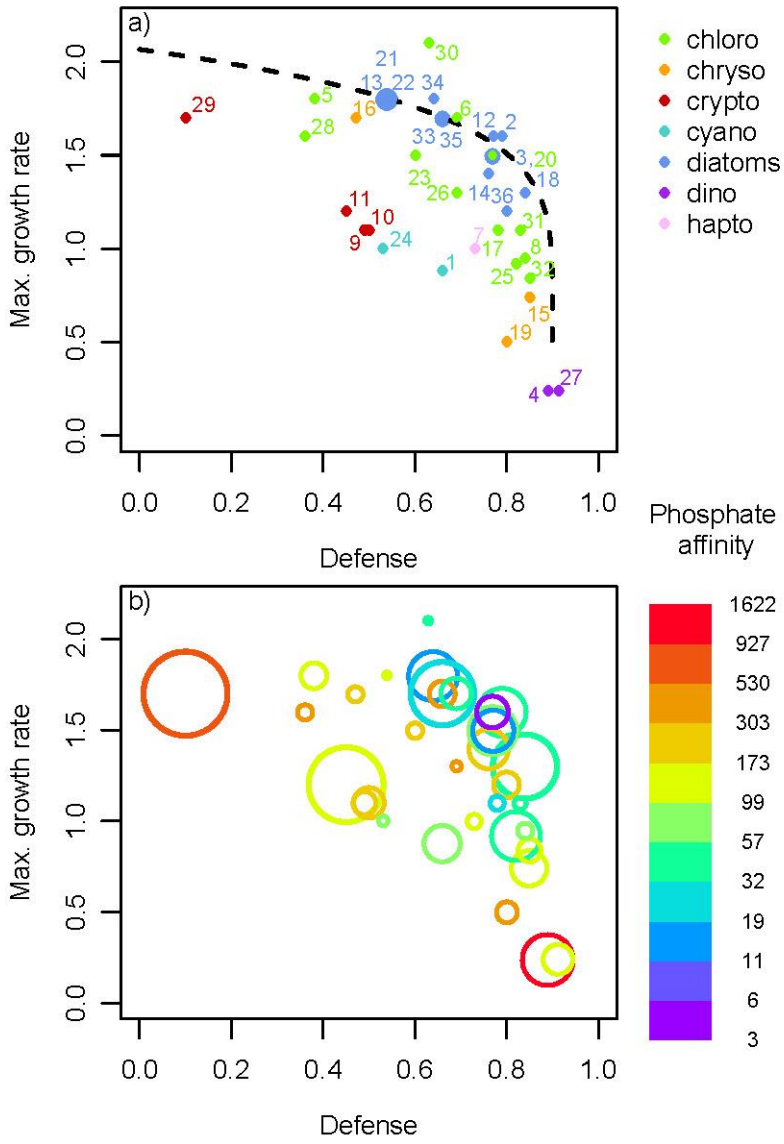

Fig. 3.3: Defense δ and maximum growth rate r (d^{-1}) of the 36 most abundant phytoplankton morphotypes in Lake Constance. (a) Numbers specifiy the morphotypes (see Tab. B1 for further details). The dashed line represents the modelled trade-off curve, used for the numerical simulations presented in Fig. 3.5a, b. Colors indicate different taxonomic groups, i.e., 58urcate58yte, cryptomonads, chrysophytes, haptophytes, cyanobacteria, diatoms and dinophytes. (b) Colors indicate a third trait dimension, phosphate affinity ($d^{-1}\mu mol^{-1}L$), and the area of the circles is scaled by the mean annual relative biomass of the morphotypes.

Mean annual biomass-trait distribution

The mean annual biomass distribution in the δ-r trait space is obtained by weighting the morphotypes with their relative contribution to the total annual phytoplankton biomass (Fig. 3.3b). As expected by theory, the

biomass was concentrated along the trade-off curve (i.e. for a given value of δ, morphotypes with a higher r dominated over those with lower r) and at intermediate δ and rather high r with some remarkable exceptions. A morphotype at one end of the trade-off curve, exhibiting the lowest δ, *Rhodomonas ssp.* (#29, cf. Fig 3.3a and Tab. B1), constituted the highest annual share of biomass of an individual morphotype and occurred in almost every sample although its r did not exceed the values of some more defended morphotypes. Among others (for more details, see discussion), its success may be attributable to its very favourable value along a third trait dimension, phosphate affinity (Fig. 3.3b). We found also substantial biomass at the other end of the δ-r trade-off curve mostly due to a strongly defended morphotype with a very low growth rate, *Ceratium hirundinella* (#4), which had the highest phosphate affinity of all morphotypes. This pattern can be generalized, as mostly morphotypes with trait combinations further away from the trade-off curve showed higher values in phosphate affinity indicating that fitness losses due to lower δ or r may be counteracted by higher phosphate affinity (Fig. 3.3b). For example, a group of diatoms (*Asterionella 59urcate* (#2), *Fragilaria crotonensis* (#18), *Stephanodiscus neoastreae* (#33), *Stephanodiscus ssp.* (#34)) and the chlorophyte *Cyclotella* ssp. (#12), forming the upper part of the concave δ-r trade-off curve, grew fast relative to their rather high level of δ, but had only low to intermediate phosphate affinity. An exception to that was *Cryptomonas* ssp. (#11) which had intermediate values for all traits but the second highest mean annual relative biomass of all morphotypes (for further trait dimensions, see discussion). Overall, the δ-r trade-off was much more clearly expressed than the relationship between P and δ or r, respectively (Fig. B2), but we found some indication for a three-way trade-off among δ, r and P, whereby the trade-off between δ and r dominated (Online Movie).

Seasonal dynamics of the biomass-trait distribution

The biomass distribution within the δ–r trait space varied systematically during the season (Fig. 3.4, Fig. B4) in line with pronounced changes of the major forcing factors of phytoplankton development (Fig. 3.2). For example, in early spring, intensive vertical mixing (resulting in a high export of phytoplankton from the euphotic zone to larger depth) was a dominant

driver of the phytoplankton community in deep Lake Constance, while grazing pressure and nutrient depletion were very low (Fig. 3.2a,b). Accordingly, morphotypes with high r being able to compensate for high losses and to exploit the high nutrient concentrations dominated, whereas morphotypes with low r and high δ were almost absent (Fig. 3.4a). This is reflected in the seasonal phase means of the community average trait values, $\bar{\delta}$ = 0.52 and $\bar{r}$ = 1.57 d^{-1}. In contrast during summer stratification, nutrient depletion and grazing pressure were the dominant drivers of phytoplankton (Fig. 3.2a,b) and the biomass-trait distribution shifted towards morphotypes with intermediate or high δ and accordingly lower r (Fig. 3.4b, $\bar{\delta}$ = 0.69, $\bar{r}$ = 1.18 d^{-1}) (for other seasonal phases see Fig. B4).

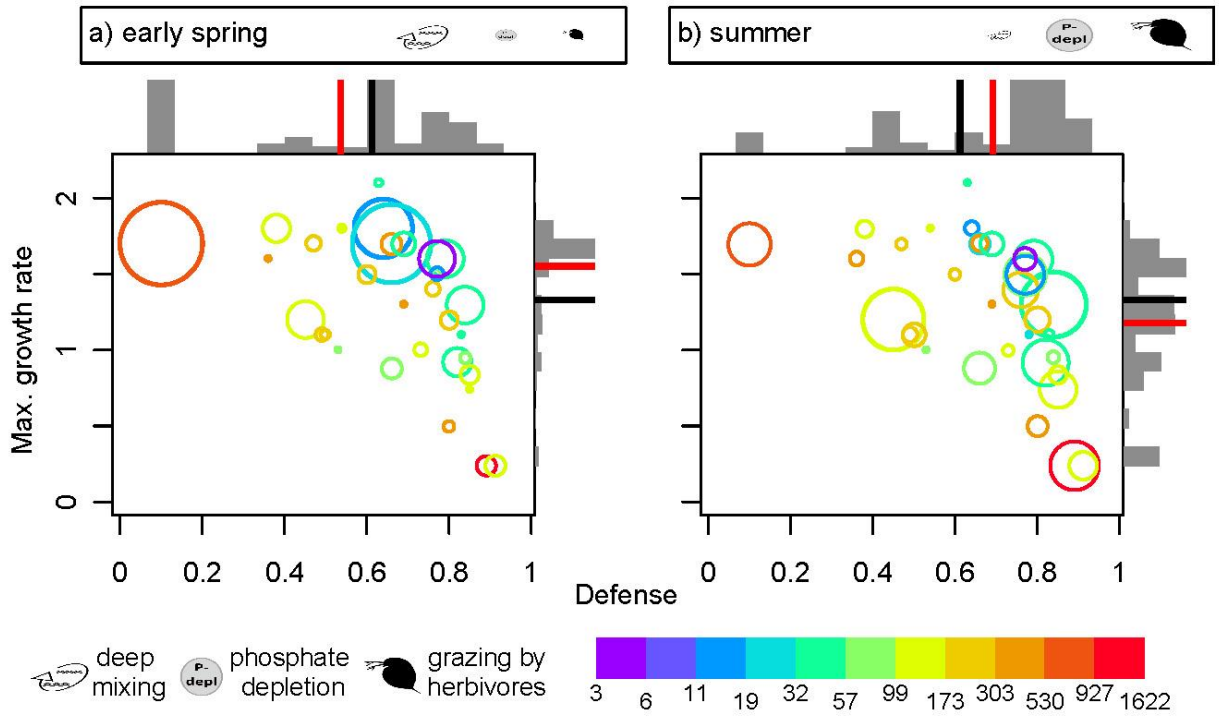

Fig. 3.4: Positions in the trait space of defense δ and maximum growth rate r (d^{-1}) of the 36 most abundant phytoplankton morphotypes in Lake Constance for a) early spring and b) summer. Colors indicate the morphotypes' phosphate affinity ($d^{-1}\mu mol^{-1}L$) and the area of the circles the mean relative biomasses. The bars display the relative biomass distribution along the two trait axes in each phase. The red lines in the bar plots mark the phase mean of the community average trait values and the black lines display the annual mean of the community average trait values as a reference ($\bar{\delta}$ = 0.61, $\bar{r}$ = 1.33). The icons represent the dominant drivers of the phytoplankton community (vertical mixing, phosphate depletion, grazing by herbivores) and their size indicates their relative importance for phytoplankton net growth in each phase.

Model results

A phytoplankton species model, parametrized with the empircally established concave trade-off (Fig. 3.3a, dashed line), reproduced the general pattern in the data, that is, the favorable trait combinations shift from early spring (low grazing pressure) to summer (high grazing pressure) towards higher δ_i at the cost of a lower r_i (Fig. 3.4; 3.5a,b). For the given concave trade-off curve and set of trait combinations, the model predicted that two very similar species with intermediate δ_i but high r_i coexist in the long-term under low grazing pressure (Fig. 3.5a). Under high grazing pressure, the long-term outcome of the model was the survival of one species with a high δ_i but intermediate r_i (Fig. 3.5b, for biomass dynamics see Fig. B7). When considering the short-term results of the model being more in line with the time scale relevant for the data of the different seasons, we found that many species survived along the concave trade-off curve (especially close to the fitness maximum) the first 50 to 100 days (Fig. 3.5a,b), in accordance with the observations (Fig. 3.4). This holds in particular under low grazing pressure (Fig. 3.5a). Overall, the time until extinction was shorter under high grazing pressure due to the high mortality caused by abundant grazers (Fig. 3.5a,b). In general, the rate of extinction increased (i. e. fitness decreased) towards the unfavourable edge of the trait space (low δ_i, low r_i), where the slope of the fitness isoclines depended on the degree of grazing pressure (cf. Fig. 3.1, Fig. 3.5a,b). Under high grazing pressure, fitness increased more strongly in the direction of the defense axis than under low grazing pressure (cf. Fig. 3.1, see color gradient in Fig. 3.5a,b).

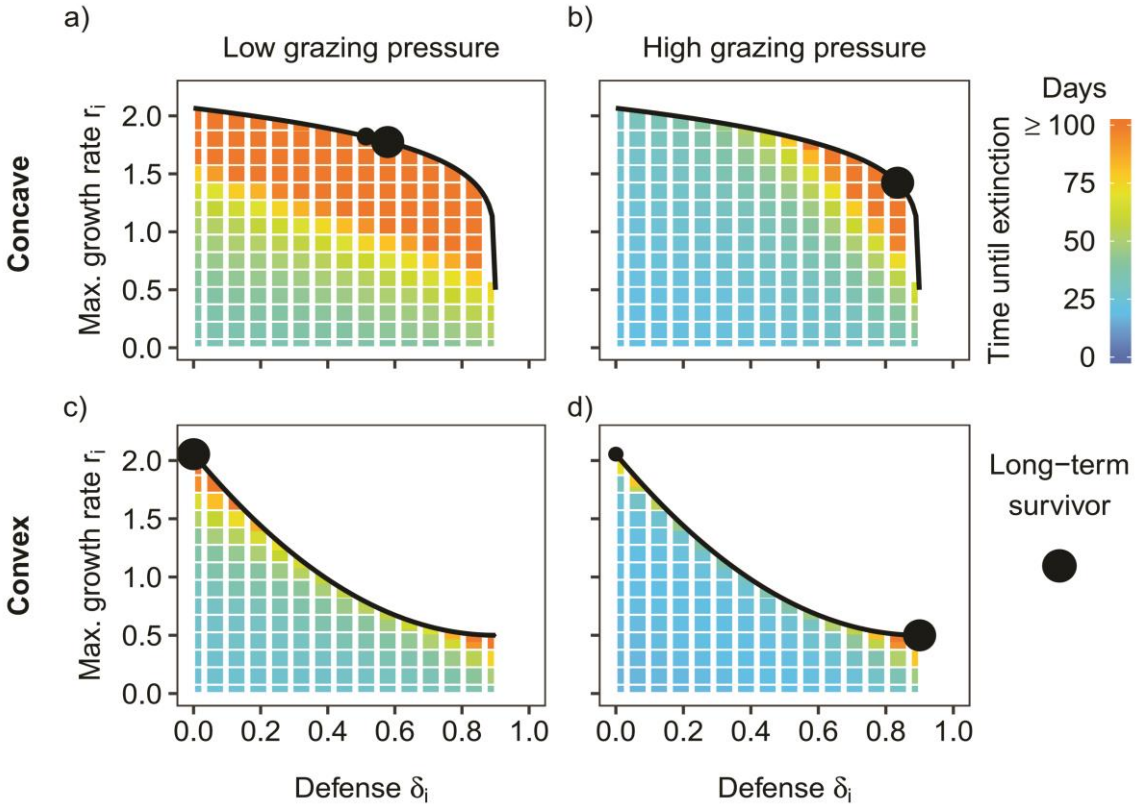

Fig. 3.5: Model predictions for (a, b) a concave or (c, d) a convex trade-off curve between defense δ_i and maximum growth rate r_i (black line) in the scenario of low grazing pressure on phytoplankton ($m_Z = 0.14\ d^{-1}$) mimicking conditions in early spring (a, c), and the scenario of high grazing pressure ($m_z = 0.04\ d^{-1}$) during summer (b, d). The black dots denote the trait combinations of phytoplankton species which survive in the long term (i.e. the fitness maxima), their size marks the mean relative biomass contribution between day 9000 and 10000 averaged among 50 simulations with randomized, different initial conditions (see Appendix B4). The colour grid displays the average time until extinction of the different trait combinations in the short term, that is, within the first 100 days of the simulations.

For a convex trade-off, the model predicted a qualitatively different pattern (Fig. 3.5c,d). Under low grazing pressure, only the undefended species with the highest r_i survived in the long term (Fig. 3.5c). Under high grazing pressure, the undefended prey coexisted with the defended species with a very low r_i, where the biomass of the defended species exceeded the biomass of the undefended species (Fig. 3.5d, for biomass dynamics see Fig. B8). In general, the rate of extinction of inferior species was higher compared to the concave case (Fig. 3.5).

Discussion

The 36 dominating phytoplankton morphotypes in Lake Constance faced a concave trade-off between defense and maximum growth rate. We found that the community average values of defense and maximum growth rate showed opposed seasonal dynamics. We did not observe distinct seasonal dynamics in the community average phosphate affinity, but morphotypes with a rather low growth rate relative to their defense level often had a relatively high phosphate affinity. Theory predicts that concave trade-off curves promote species with intermediate strategies (Box 3.1 and Fig. 3.1). Our data support this prediction as intermediately defended morphotypes with intermediate to high maximum growth rates constituted the largest proportion of total annual phytoplankton biomass. Trait shifts in the phytoplankton community along the concave trade-off curve were exactly in line with seasonal changes of the environmental conditions. The model predicted a shift towards higher defense levels at the cost of lower maximum growth rates with increasing grazing pressure from spring to summer, as found in the data, and revealed low fitness differences of persisting species along the trade-off curve. Assuming a hypothetical convex trade-off in the model, for comparison, produced biomass-trait distributions qualitatively different from the observations. Hence, our model results highlight the importance of quantitative knowledge on the shape of the trade-off.

The quantification of the trade-off was based on trait data provided by Bruggeman[35]. He obtained phytoplankton trait values from a statistical model, fed with a great quantity of lab trait measurements and phylogenetic relationships. He provided also quantitative information on model uncertainties, i.e. the standard errors of the trait estimates[35]. We consider these uncertainties to be minor compared to the measured trait range, not questioning the general pattern of a concave trade-off (Fig. B1b). The defense (edibility) values, used in Bruggeman's statistical model[35], were almost entirely based on measurements of Lake Constance phytoplankton strains, sampled during the first part of our study period[44], and were tested for daphnids, the dominant herbivorous crustaceans in Lake Constance, which have a similar food spectrum as most of the other herbivores (see Methods). Hence, we argue that the concave trade-off

between defense and maximum growth rate obtained from these trait data is adequate for the considered phytoplankton community in Lake Constance. Wirtz and Eckhardt[46] suggested a linear defense-growth trade-off for the same phytoplankton community, but they considered only 7 species, missing several dominant ones. They were able to predict the seasonal dynamics of total phyto- and zooplankton biomass and of the community average trait values[46]. However, they did not consider the biomass distribution in the trait space and thus could not provide predictions on which species/trait combinations may dominate or co-occur. To adequately predict this biomass-trait distribution, the trade-off shape is important. By including trait data on many more than 7 species, we found that the trade-off was concave and hence favoured species with different intermediate defense levels, as observed.

Bruggeman[35] included also data on cell sizes. We found that defense correlated positively and maximum growth rate negatively with cell size (Fig. B3, Appendix B3), providing a potential mechanistic explanation for the existence of the defense-growth trade-off[47,48]. However, other cell size-independent defense strategies are relevant as well, e.g. cell wall thickness, colony formation, toxicity and cell shapes, which introduce substantial scatter into the relationship between defense and size.

Our model showed that, for a concave trade-off curve, two very similar species can stably coexist (Fig. 3.5a, Fig. B7). This is in contradiction with theory predicting the survival of only one species (see Box 3.1 and Fig. 3.1a-c). The two species have intermediate strategies close to the fitness maximum and coexist based on stabilizing mechanisms arising from their slight difference in defense and growth[36]. However, this community is not evolutionary stable[49]. Given gradual evolution, we expect that one species would reach the exact fitness optimum via trait adaptation and outcompete the others for a concave trade-off curve[10,12]. Even without evolution, such a coexistence would not last if a species exactly at the fitness maximum is initially present in the community. In line with our model results, Leibold[50] predicted a similar coexistence pattern based on a graphical approach, although his focus was not on the trade-off structure: Two very similar prey species coexisted in a food web with different prey species sharing one resource and one predator and a continuous transition

occurred in the set of prey species persisting under gradually changing environmental conditions. With increasing system productivity, species with a higher defense level persisted[50], similar to the pattern in our study when increasing the grazing pressure. This indicates that he implicitly assumed a trade-off structure equivalent to the concave trade-off in our study. We argue that the behavior of communities in respect to coexistence (e.g. coexistence of similar intermediate strategies vs. different extreme strategies) and species replacement under environmental change may allow conclusions on the underlying trade-off structure.

The low trait variation maintained in the long-term model simulations is in contradiction with the empirical data showing a large trait variation, including species having intermediate strategies as well as specialized species (highly defended or fast growing). The high number of species in such phytoplankton communities, exceeding the number of limiting factors (i. e. potential niches), is well known as the 'Paradox of the Plankton'[21]. In the absence of stabilizing mechanisms arising from variation of interacting populations or environments in space or time[36], the number of coexisting species cannot exceed the number of limiting factors[51]. In line with that, our simple model, including only two niche dimensions (i.e. being defended or fast-growing), generated coexistence of maximal two species. Nevertheless, low fitness differences allowed for short-term co-occurrence of species in the model along and slightly below the concave trade-off curve (see green/orange region in Fig. 3.5a,b), a similar trait space where species persisted in the natural community (Fig. 3.3b). In contrast, feasible trait combinations well apart from the trade-off curve (low defense and low maximum growth rate) went quickly extinct in the model, implying a high fitness disadvantage. This provides an explanation for their absence in Lake Constance and in the whole data set of Bruggeman[35] (Fig. B1a).

According to modern coexistence theory[36], low fitness differences (as found along the trade-off curve) can form a fundamental basis for long-term maintenance of biodiversity: as then even slight stabilizing mechanisms (i.e. mechanisms slightly increasing negative intraspecific interactions relative to negative interspecific interactions) can lead to stable coexistence of many species. Fitness differences can be very low along a trade-off curve, if its shape is very similar to the shape of fitness isoclines[14,52], e.g. for a

nearly linear trade-off given linear fitness isoclines (Fig. 3.1). Stabilizing mechanisms, which overcome fitness differences and may help to explain the high trait variation observed along the trade-off curve, can be divided into: 1. Niche differentiation along further trait axes, and 2. Fluctuation-dependent mechanisms, like relative non-linearity in competition and the storage effect[36].

Several trait dimensions, not considered in our model, may contribute to the biodiversity in the phytoplankton community, by further reducing fitness differences or by enabling niche differentiation. For instance, a high phosphate affinity is beneficial under strong nutrient depletion during summer and autumn. Although we found no clear increase of this trait on the community level during summer, it may explain the success of certain morphotypes. For example, the defended dinophytes (like *Ceratium hirundinella* and *Peridinium sp.,* taxon number #4 and #27 in Fig. 3.3a) have very high phosphate affinities and constitute substantial biomass, despite their very high defense costs regarding the maximum growth rate (Fig. 3.3b). The undefended *Rhodomonas* ssp. (#29) also had a high phosphate affinity (Fig. 3.3a,b), which sheds light on its observed high biomasses and very regular occurrence in spite of its maximum growth rate not exceeding the one of intermediately defended morphotypes. In fact, we found a weak three-dimensional trade-off among defense, growth rate and phosphate affinity (Online Movie), though the negative correlation between the former two was the most striking pattern in the trait data (Fig. B2, Appendix B3).

Different light spectra and phytoplankton photopigmentation represent another important source for niche differentiation[17,25]. For example, *Rhodomonas* spp. (#29) is able to use additional light spectra, based on the red accessory photopigment phycoerythrin allowing photosynthesis at greater depths, which is relevant year round due to vertical mixing and self-shading. The same holds for *Cryptomonas* spp. (#11) which also reached high biomasses irrespectively of its rather low maximum growth rate relative to its defense level (Fig. 3.3a,b). The cyanobacteria (*Anabaena* spp. And *Oscillatoria* spp., #1 and #24) also produce additional photopigments, which may compensate for their relative low maximum growth rates (Fig. 3.3a,b). Motility, in terms of swimming/floating towards

light, can increase the performance with respect to light harvesting[17], which is relevant for e.g. the cyanobacteria showing buoyance regulation. Furthermore, vertical migration of some phytoplankton morphotypes, like *Ceratium hirundinella* (#4), enable exploiting additional nutrient sources from deeper water layers, when the water column is stratified during summer. Mixotrophy represents another possibility to obtain additional phosphate, which is relevant in Lake Constance[53]. The low phosphate affinities of bacterivorous mixotrophs as *Dinobryon ssp.* (#15) may partly explain the seasonally and interannually invariant signal in the community average phosphate affinity (Fig. 3.2d, Fig. B6) as they predominantly occur during summer and in later years. Diatoms seem to have maximal fitness regarding their defense and maximum growth rate, and are indeed present at high biomasses (Fig. 3.3a,b). However, they face disadvantages due to the production of shells, implying an additional silica demand and causing high sedimentation rates during stratified conditions, which leads to lower net growth rates than expected from their maximum growth rate. This helps to explain their success during early spring (Fig. 3.4a).

Relative non-linearity in competition and the storage effect represent further stabilizing mechanisms, which may be relevant for our system and both depend on fluctuations in populations or environmental conditions (e.g. nutrient concentrations)[36]. Abrams[11] showed for a competition model that stable coexistence of two specialists using two different resources and one generalist is possible under asynchronous resource fluctuations. The species coexisted based on the relative non-linearity in their resource uptake functions[51]. Such relative non-linearity enabling stable coexistence has not been found for the type of predator-prey model considered here, but may be relevant when including additional resources (e.g. silica, light) with seasonally fluctuations. This can lead to coexistence of a high number of phytoplankton species, exceeding the number of limiting resources under non-equilibrium conditions[54,55]. However, we did not include such seasonal forcing in our model simulations, but run different scenarios with constant environmental conditions mimicking distinct seasonal phases. Based on that, we obtained insights on the fitness landscape, that is, which trait combination would be favored during a certain seasonal phase and which

species would be of low fitness (i.e. go quickly extinct in the simulation). The model purpose was not to reproduce the dynamics and the stable coexistence of many species across years in a distinct lake. This would demand a more complex modelling approach implementing, among others, periodical forcing of the abiotic environment (light, vertical mixing intensity, nutrient availability) and details like the overwintering strategies of phytoplankton, which goes beyond the scope of this article.

Lake Constance exhibits a pronounced seasonality (Fig. 3.2a,b). Our data demonstrate that the instantaneous fitness maximum gradually moves along the trade-off curve from fast growing, intermediately defended species in early spring to slowly growing but more defended species in summer and then back in winter (Fig. B4, Appendix B3). Thus, different species along the trade-off curve have maximal fitness at different times of the year. This pattern of gradually moving fitness maxima is specific to concave trade-off curves (Fig. 3.1a-c) and is not expected for convex ones (Fig. 3.1d-f). Phytoplankton species form resting stages under unfavorable conditions, which buffers population losses[56]. This gives rise to storage effects[36], contributing to the maintenance of numerous phytoplankton species along the trade-off curve.

Lake Constance has successfully served as a model system for large open water bodies including marine ones[57]. It exhibits a typical seasonal plankton succession, driven by vertical mixing, grazing and nutrient limitation[22]. These environmental factors are also main drivers of marine phytoplankton, which is ecologically similar to freshwater phytoplankton and may face similar trade-offs[58]. Trade-offs between defense and growth are also relevant in terrestrial plant communities, for example grasslands[59]. Thus, our findings are likely relevant for numerous ecosystems. Furthermore, our results show that the information on trade-off shapes allows for an understanding of ongoing trait changes directly under field conditions.

Overall, the identification of the major trade-off and its shape provided a remarkable key to understand trait shifts and altering species composition in the phytoplankton community under seasonally changing environmental conditions. Although multiple trait dimensions likely play a role, our

results showed that defense and maximum growth rate represent key traits in phytoplankton of Lake Constance, where grazers are known to strongly impact phytoplankton net growth[37]. A high maximum growth rate is beneficial at high resource concentrations, but also at low concentrations, when not coming at substantial costs of a lower nutrient uptake affinity. The maintenance of trait variation was likely promoted by low fitness differences along the concave trade-off curve. Low fitness differences allow coexistence by even slight stabilizing mechanisms arising from niche differentiation along multiple trait axes and fluctuations in environmental conditions, continuously moving favorable trait combinations along the concave trade-off curve. Our study successfully explained major trait dynamics based on a simple model, including only the interspecific defense-growth trade-off, and allowed to verify the theory on trade-off shapes in the field. In conclusion, quantifying trade-off shapes enhances our understanding of trait dynamics and variation in natural communities.

Data availability

The data shown in this paper are available under https://doi.org/10.6084/m9.figshare.11830464.v1.

Acknowledgements

Many thanks to Alexander Wacker, Alice Boit, Guntram Weithoff and the anonymous reviewers for very constructive comments on an earlier version of the manuscript. We thank Michael Raatz for fruitful discussions on the results and Dietmar Straile for providing a more readable version of the Bruggeman (2011) data. This research was funded by the German Research Foundation (DFG, GA 401/26-1/2).

References

1. Tilman D. Causes, consequences and ethics of biodiversity. Nature. 2000 May 11;405(6783):208–11.

2. Stearns SC. Trade-Offs in Life-History Evolution. Funct Ecol. 1989;3(3):259–68.

3. Yoshida T, Hairston NG, Ellner SP. Evolutionary trade-off between defence against grazing and competitive ability in a simple unicellular alga, Chlorella vulgaris. Proc R Soc B Biol Sci. 2004 Sep;271(1551):1947–53.

4. Barry MJ. The costs of crest induction for Daphnia carinata. Oecologia. 1994 Mar;97(2):278–88.

5. Litchman E, Klausmeier CA, Schofield OM, Falkowski PG. The role of functional traits and trade-offs in structuring phytoplankton communities: scaling from cellular to ecosystem level. Ecol Lett. 2007 Dec;10(12):1170–81.

6. Tilman D, Kilham SS, Kilham P. Phytoplankton Community Ecology: The Role of Limiting Nutrients. Annu Rev Ecol Syst. 1982 Nov;13(1982):349–72.

7. Kneitel JM, Chase JM. Trade-offs in community ecology: linking spatial scales and species coexistence. Ecol Lett. 2004 Jan;7(1):69–80.

8. Edwards KF, Klausmeier CA, Litchman E. A Three-Way Trade-Off Maintains Functional Diversity under Variable Resource Supply. Am Nat. 2013 Dec;182(6):786–800.

9. Levins R. Theory of Fitness in a Heterogeneous Environment. I. The Fitness Set and Adaptive Function. Am Nat. 1962;96(891):361–73.

10. Rueffler C, Van Dooren TJM, Metz JAJ. Adaptive walks on changing landscapes: Levins' approach extended. Theor Popul Biol. 2004 Mar;65(2):165–78.

11. Abrams PA. The Prerequisites for and Likelihood of Generalist-Specialist Coexistence. Am Nat. 2006;167(3):329–42.

12. de Mazancourt C, Dieckmann U. Trade-Off Geometries and Frequency-Dependent Selection. Am Nat. 2004 Dec;164(6):765–78.

13. Jones LE, Becks L, Ellner SP, Hairston Jr. NG, Yoshida T, Fussmann GF. Rapid contemporary evolution and clonal food web dynamics. Philos Trans R Soc B Biol Sci. 2009 Jun 12;364(1523):1579–91.

14. Ehrlich E, Becks L, Gaedke U. Trait-fitness relationships determine how trade-off shapes affect species coexistence. Ecology. 2017 Dec 15;98(12):3188–98.

15. Maharjan R, Nilsson S, Sung J, Haynes K, Beardmore RE, Hurst LD, et al. The form of a trade-off determines the response to competition. van Baalen M, editor. Ecol Lett. 2013 Oct;16(10):1267–76.

16. Meyer JR, Gudelj I, Beardmore R. Biophysical mechanisms that maintain biodiversity through trade-offs. Nat Commun. 2015 Dec 19;6(1):6278.

17. Litchman E, Klausmeier CA. Trait-Based Community Ecology of Phytoplankton. Annu Rev Ecol Evol Syst. 2008;39(1):615–39.

18. Pančić M, Kiørboe T. Phytoplankton defence mechanisms: traits and trade-offs. Biol Rev. 2018 May;93(2):1269–303.

19. Smith VH, Foster BL, Grover JP, Holt RD, Leibold MA, DeNoyelles F. Phytoplankton species richness scales consistently from laboratory microcosms to the world's oceans. Proc Natl Acad Sci. 2005 Mar 22;102(12):4393–6.

20. Weithoff G. The concepts of "plant functional types" and "functional diversity" in lake phytoplankton - a new understanding of phytoplankton ecology? Freshw Biol. 2003;48(9):1669–75.

21. Hutchinson GE. The Paradox of the Plankton. Am Nat. 1961;95(882):137–45.

22. Sommer U, Adrian R, De Senerpont Domis L, Elser JJ, Gaedke U, Ibelings B, et al. Beyond the Plankton Ecology Group (PEG) Model: Mechanisms Driving Plankton Succession. Annu Rev Ecol Evol Syst. 2012;43(1):429–48.

23. Edwards KF, Litchman E, Klausmeier CA. Functional traits explain phytoplankton community structure and seasonal dynamics in a marine ecosystem. Elser J, editor. Ecol Lett. 2013 Jan;16(1):56–63.

24. Edwards KF, Litchman E, Klausmeier CA. Functional traits explain phytoplankton responses to environmental gradients accross lakes of the United States. Ecology. 2013;94(7):1626–35.

25. Stomp M, Huisman J, Vörös L, Pick FR, Laamanen M, Haverkamp T, et al. Colourful coexistence of red and green picocyanobacteria in lakes and seas. Ecol Lett. 2007 Apr;10(4):290–8.

26. Smith S, Yamanaka Y, Pahlow M, Oschlies A. Optimal uptake kinetics: physiological acclimation explains the pattern of nitrate uptake by phytoplankton in the ocean. Mar Ecol Prog Ser. 2009 May 29;384:1–12.

27. Agrawal AA. Algal defense, grazers, and their interactions in aquatic trophic cascades. Acta Oecologica. 1998 Jul;19(4):331–7.

28. Kasada M, Yamamichi M, Yoshida T. Form of an evolutionary tradeoff affects eco-evolutionary dynamics in a predator–prey system. Proc Natl Acad Sci. 2014 Nov;111(45):16035–40.

29. Tirok K, Gaedke U. Internally driven alternation of functional traits in a multispecies predator- prey system. Ecology. 2010;91(6):1748–62.

30. Abrams PA. Is predator-mediated coexistence possible in unstable systems? Ecology. 1999;80(2):608–21.

31. Jones LE, Ellner SP. Effects of rapid prey evolution on predator–prey cycles. J Math Biol. 2007 Sep;55(4):541–73.

32. Klausmeier CA, Litchman E. Successional Dynamics in the Seasonally Forced Diamond Food Web. Am Nat. 2012;180(1):1–16.

33. Gaedke U, Ollinger D, Straile D, Bäuerle E. The impact of weather conditions on the seasonal plankton development. Arch fuer Hydrobiol. 1998;53:565–85.

34. Gaedke U. The response of the pelagic food web to re-oligotrophication of a large and deep lake (L. Constance): Evidence for scale-dependent hierarchical patterns? Arch für Hydrobiol. 1998;53:317–33.

35. Bruggeman J. A phylogenetic approach to the estimation of phytoplankton traits. J Phycol. 2011 Feb;47(1):52–65.

36. Chesson P. Mechanisms of Maintenance of Species Diversity. Annu Rev Ecol Syst. 2000 Nov;31(1):343–66.

37. Gaedke U, Hochstädter S, Straile D. Interplay between energy limitation and nutritional deficiency: Empirical data and food web models. Ecol Monogr. 2002;72(2):251–70.

38. Utermöhl H. Zur Vervollkommnung der quantitativen Phytoplankton-Methodik. Mitteilungen der Int Vereinigung der Limnol. 1958;9:1–38.

39. Menden-Deuer S, Lessard EJ. Carbon to volume relationships for dinoflagellates, diatoms, and other protist plankton. Limnol Oceanogr. 2000 May;45(3):569–79.

40. Straile D, Geller W. Crustacean zooplankton in Lake Constance from 1920 to 1995: Response to eutrophication and re-oligotrophication. Arch Hydrobiol Spec Issues Adv Limnol. 1998;53:255–74.

41. Rothhaupt K. Changes of the functional responses of the rotifers Brachionus rubens and Brachionus calyciflorus with particle sizes. Limnol Oceanogr. 1990;35(I):24–32.

42. Gaedke U, Wickham SA. Ciliate dynamics in response to changing biotic and abiotic conditions in a large, deep lake (Lake Constance). Aquat Microb Biol. 2004;34:247–61.

43. Steiner S. Dynamik und Energietransfer einer planktischen Crustaceengesellschaft in der Abhängigkeit von der Nahrungsgrundlage und den Planktivoren. 2002.

44. Knisely K, Geller W. Selective feeding of four zooplankton species on natural lake phytoplankton. Oecologia. 1986 Apr;69(1):86–94.

45. Klauschies T, Gaedke U. Nutrient retention by predators undermines predator coexistence on one prey. Theor Ecol. 2019;535195.

46. Wirtz K-W, Eckhardt B. Effective variables in ecosystem models with an application to phytoplankton succession. Ecol Modell. 1996 Nov;92(1):33–53.

47. Sunda W, Hardison D. Evolutionary tradeoffs among nutrient acquisition, cell size, and grazing defense in marine phytoplankton promote ecosystem stability. Mar Ecol Prog Ser. 2010 Feb 22;401:63–76.

48. Acevedo-Trejos E, Brandt G, Bruggeman J, Merico A. Mechanisms shaping size structure and functional diversity of phytoplankton communities in the ocean. Sci Rep. 2015 Aug;5(1):8918.

49. Edwards KF, Kremer CT, Miller ET, Osmond MM, Litchman E, Klausmeier CA. Evolutionarily stable communities: a framework for understanding the role of trait evolution in the maintenance of diversity. Becks L, editor. Ecol Lett. 2018 Dec 11;21(12):1853–68.

50. Leibold MA. A Graphical Model of Keystone Predators in Food Webs: Trophic Regulation of Abundance, Incidence, and Diversity Patterns in Communities. Am Nat. 1996 May;147(5):784–812.

51. Armstrong RA, McGehee R. Competitive Exclusion. Am Nat. 1980 Aug 5;115(2):151–70.

52. Purves DW, Turnbull LA. Different but equal: the implausible assumption at the heart of neutral theory. J Anim Ecol. 2010 Nov;79(6):1215–25.

53. Kamjunke N, Henrichs T, Gaedke U. Phosphorus gain by bacterivory promotes the mixotrophic flagellate Dinobryon spp. during re-oligotrophication. J Plankton Res. 2006 Oct 4;29(1):39–46.

54. Huisman J, Weissing FJ. Biodiversity of plankton by species oscillations and chaos. Nature. 1999 Nov;402(6760):407–10.

55. Litchman E, Klausmeier CA. Competition of Phytoplankton under Fluctuating Light. Am Nat. 2001 Feb;157(2):170–87.

56. Fryxell GA, America PS of. Survival Strategies of the Algae. New York and London: Cambridge Univ. Press; 1983. 144 p.

57. Gaedke U. The size distribution of plankton biomass in a large lake and its seasonal variability. Limnol Oceanogr. 1992 Sep;37(6):1202–20.

58. Weithoff G, Beisner BE. Measures and Approaches in Trait-Based Phytoplankton Community Ecology – From Freshwater to Marine Ecosystems. Front Mar Sci. 2019 Feb;6(February):1–11.

59. Lind EM, Borer E, Seabloom E, Adler P, Bakker JD, Blumenthal DM, et al. Life-history constraints in grassland plant species: a growth-defence trade-off is the norm. van der Putten W, editor. Ecol Lett. 2013 Apr;16(4):513–21.

60. Rueffler C, Van Dooren TJM, Metz JAJ. The Evolution of Resource Specialization through Frequency-Dependent and Frequency-Independent Mechanisms. Am Nat. 2006 Jan;167(1):81–93.

61. Metz JAJ, Nisbet RM, Geritz SAH. How should we define "fitness" for general ecological scenarios? Trends Ecol Evol. 1992;7(6):198–202.

62. Sibly R, Calow P. An Integrated Approach to Life-Cycle Evolution using Selective Landscapes. J Theor Biol. 1983;102:527–47.

Chapter 4

Mysterious ciliates: seasonally recurrent and yet hard to predict

Nadja J. Kath, Mridul K. Thomas, Ursula Gaedke

Abstract

Ciliates represent a crucial link between phytoplankton and bacteria and mesozooplankton in pelagic food webs, but little is known about the processes influencing the dynamics of individual species. Using long-term, high frequency observations, we compared the diversity and the temporal variability in biomass and species composition of the ciliate community in large, deep, mesotrophic Lake Constance to that of the phytoplankton and rotifer communities in the same lake. Furthermore, we used boosted regression trees to evaluate possible environmental predictors (temperature, three prey groups, three predator/competitor groups) influencing ciliate net growth. The biomass of all ciliate species showed a common, recurrent seasonal pattern, often with peaks in spring and summer. The ciliate community was more diverse than the rotifer community, exhibited highly synchronous dynamics and its species were regularly encountered during the season. The top-down control by copepods likely contributes to the ciliates' synchronized decline prior to the clear water phase when food concentration is still high. The high temporal autocorrelation of the ciliate biomasses together with the inter-annual recurrent seasonal patterns and the low explanatory power of the environmental predictors suggest that the dynamics of individual ciliate species are strictly controlled, yet it remains difficult to determine the responsible factors.

Key words: boosted regression trees, long-term time series, community composition, synchrony

Introduction

Ciliates are an important component in freshwater plankton (Müller *et al.*, 1991; Löder *et al.*, 2012; Lischke *et al.*, 2016). They represent a crucial link between small producers, such as phytoplankton and bacteria, and mesozooplankton and are thus highly relevant for the transfer of matter and energy along the size gradient to large organisms such as fish. Ciliates usually contribute only a moderate fraction to the overall plankton biomass as they are small and often top-down controlled by their predators (Wickham, 1998; Lischke *et al.*, 2016). Nevertheless, they often consume high amounts of the primary production and thus have a large influence on the food web as they are significant grazers of bacteria and small phytoplankton (Gaedke *et al.*, 2002; Sommer *et al.*, 2012). Reasons for this are their high weight-specific grazing rates (Hansen *et al.*, 1997) and their very short life cycles which enables them to react quickly to changes in prey biomass and composition (Tirok and Gaedke, 2007). This may render them the most important grazers in spring (Weisse *et al.*, 1990; Gaedke and Straile, 1994; Gaedke *et al.*, 2002), when the metazoan activity is still hampered by low temperatures (Johansson *et al.*, 2004; Tirok and Gaedke, 2006, 2007). In turn, ciliates are a substantial food source for large zooplankton (Adrian and Schneider-Olt, 1999; Kunzmann *et al.*, 2019).

Freshwater ciliates are a species-rich and ubiquitous group spanning three orders of magnitude in volume, suggesting high functional diversity (Müller, 1991). Due to their differences in size, modes of feeding and locomotion, and defence, a broad range of prey organisms and potential predators exists. Disentangling the complex trophic interactions around the ciliate community remains a crucial challenge in understanding their population dynamics and roles in the plankton food web. A number of feeding trials have been done in the lab, mostly with one prey at a time and for a limited number of ciliate species (e.g. Müller and Schlegel, 1999; Weisse *et al.*, 2001; Chen *et al.*, 2020). Experiments addressing the role of potential predators of ciliates are even more limited, revealing that rotifers may be intra-guild predators on small ciliates (Weisse and Frahm, 2002). Microcosm experiments demonstrated negative effects of copepods and cladocerans on ciliates due to competition and predation (Wickham, 1998; Burns and Schallenberg, 2001; Kunzmann *et al.*, 2019) as they are a preferred food item of copepods (Paffenhöfer *et al.*, 2005; Vargas *et al.*, 2006; Kunzmann *et al.*, 2019). However, trophic relationships expected

from single feeding trials in the lab may not even hold in more species rich microcosms (Flöder *et al.*, 2018), which hampers extrapolation to field conditions. Thus, a number of studies used field data to infer feeding relationships of ciliates (Cleven, 2004; Posch *et al.*, 2015) or the potential impact of ciliate predators or competitors (Wickham, 1998). However, studies integrating simultaneously potential bottom-up and top-down effects from field data are still lacking.

To address this question, we used here temporally highly resolved data from deep, large, monomictic, mesotrophic Lake Constance. The dataset comprises twelve years of taxonomically resolved ciliate measurements, all potential food, predator and competitor groups, and abiotic environmental conditions. The phytoplankton data are taxonomically-resolved which enabled aggregating them into groups according to their presumed edibility for ciliates. Additionally, bacteria and autotrophic picoplankton were investigated as a possible food source. The species-resolved crustacean data enabled a differentiated analysis of their potential role as predators and/or competitors.

In Lake Constance, ciliates contributed about 17% to the total zooplankton biomass (Boit and Gaedke, 2014), and consumed around 50% of the primary production on annual average underlining their high functional importance (Gaedke *et al.*, 2002). The overall ciliate biomass followed a bimodal pattern of a spring and summer bloom interrupted by lower biomass around the clear water phase. The dominant ciliate morphotypes in spring, e.g. *Balanion planctonicum, Urotricha 77urcate,* and *Rimostrobilidium lacustris*, reacted immediately to the onset of the phytoplankton spring bloom which was then dominated by suitable food such as phytoflagellates and *Stephanodiscus* (Müller, 1991; Müller *et al.*, 1991). Most ciliates declined earlier than phytoplankton prior to the clear water phase suggesting that predation by copepods rather than food shortage is the main reason (Ehrlich and Gaedke, 2020). The dynamics in summer are not that easy to explain, but predation and competition seems to be equally or more important than the bottom-up control: Very small and large ciliates correlated negatively with daphnid biomass during summer, and total ciliate biomass and species composition did not respond to the decrease in total phosphorous concentration during winter mixing from 58 to 17 µg P/l during the study period (Gaedke and Wickham, 2004), despite changes in phytoplankton biomass and composition (Gaedke 1998, Kümmerlin 1998).

Ciliate populations were highly synchronized throughout the season compared to the other plankton groups and their temporal variability was typically low according to autoregressive models and spectral time series analysis (Huber and Gaedke, 2006; Vasseur and Gaedke, 2007). Considering only the spring bloom, compensatory dynamics between different functional ciliate groups were found reducing the temporal variability of total ciliate biomass during this period (Tirok and Gaedke, 2007, 2010).

We approached the challenge of disentangling complex trophic interactions for numerous ciliates from observational data using boosted regression trees (BRTs). This machine learning tool uses *boosting* to aggregate weak predictions from a series of decision trees to generate a stronger prediction model capable of analysing high-dimensional data. Machine learning tools as BRTs may be effective tools to describe and predict the complexity of ecological systems (Elith *et al.*, 2006; Baltensperger *et al.*, 2020; Pomati *et al.*, 2020). They do not require strong assumptions which renders them particularly useful for the intended study given the scarcity of reliable information on the ciliates' trophic interactions under natural conditions. Nevertheless, they allow adding information (weak constraints on the model) about the direction of a predictor's effect. They can reveal the relative importance of potentially influential predictors.

Our goal was to better understand the processes driving ciliate morphotypes' dynamics and their role in the plankton food web. Thus, we characterised ciliates in comparison to the equally species rich, fast growing phytoplankton and rotifer communities in respect to the temporal intra- and interannual variability of their individual morphotype biomasses and their regularity of occurrence, their diversity and turn-over in morphotype composition. Furthermore, we investigated in concert the top-down and bottom-up forcing on ciliate morphotypes to infer the most relevant predictors influencing their seasonal occurrence using BRTs revealing the effect of environmental predictors on the net growth rate of 17 ciliate morphotypes. The BRTs suggest that temperature, likely representing different seasonal effects, was overall the most important predictor, followed by *Cyclops* as the most important predator for many ciliate morphotypes, whereas relationships to algal groups were weaker.

The lack of strong relationships between ciliate morphotypes and the environment reveal the difficulty to disentangle causal relationships in natural, complex, highly diverse and presumably highly adaptive food webs even based on 12 years of comprehensive ecosystem data and sophisticated data analysis techniques.

Methods

Overview of approach

We characterized the ciliate community in Lake Constance by comparing its variability, synchrony, diversity, and evenness with that of the phytoplankton and rotifer community. We give an overview of the seasonal dynamics of the ciliate morphotypes and of the environmental predictors influencing them, i.e. their food, predators and competitors, and temperature. We finally use boosted regression trees to evaluate the possible role of seven predictors on ciliate growth: temperature as main abiotic factor, three possible food sources, bacteria plus autotrophic picoplankton and two algae groups (MEA = most edible algae, mainly phytoflagellates, and WEA = well edible algae, including small centric diatoms), and three predators groups: herbivorous cladocerans comprising daphnids and *Bosmina*, the calanoid copepod *Eudiaptomus* and cyclopoid copepods.

Sampling

Upper Lake Constance is a large (volume ca. 50 km^3), deep (mean depth 101 m, maximum depth 252 m), warm-monomictic lake north of the European Alps which was mesotrophic during the study period. Owing to its size (476 km^2), steep shores and a less pronounced stratification than typically found in smaller lakes, Lake Constance has a large pelagic zone and a relatively deep, well-mixed epilimnion.

Plankton sampling was conducted from 1987 to 1998 (bacteria and autotrophic picoplankton sampling until 1997, for details see https://fred.igb-berlin.de/Lakebase). All plankton was sampled weekly during the growing season and approximately every 2 weeks in winter by a large team of scientists. Depth-resolved samples were collected at a central sampling site of 147 m depth, in the north-western part of Upper Lake

Constance (Überlinger See). We use here mean concentrations within the uppermost 0-20 m depth, roughly reflecting the epilimnion and euphotic depth. The abundance of all planktonic organisms was assessed using advanced microscopic techniques.

Ciliates were fixed with Lugol's solution and counted in 56 categories which were grouped into 24 morphotypes (Tab. 4.1, Appendix Tab. C1) following Müller (1989), Müller et al. (1991) and Weisse & Müller (1998). They represent either individual species or higher taxonomic units that could be identified by light microscopy. We did not include unidentified ciliates in our analysis. Their relative share was generally small (mean 2.2 %, median 0.9%, 90th percentile 5.1%, max. 44%) of total ciliate biomass. In 0.2% of the sampling dates, it was higher than 25% which were excluded from further consideration. Ciliate cell volume was established by measuring cell dimensions. It was converted to units of carbon assuming a carbon to fresh-weight ratio of 15.4% (Weisse & Müller 1998).

Phytoplankton counts and cell volume estimates were converted into biomass based on a specific carbon to volume relationship (Menden-Deuer and Lessard, 2000). Phytoplankton was classified into different edibility groups based on lab studies performed with crustaceans (e.g. Knisely and Geller, 1986) and ciliates (Müller and Schlegel, 1999) from Lake Constance. We distinguished two groups of phytoplankton edible for ciliates. One comprised small individual algal cells, mostly phytoflagellates (MEA = most edible algae, 25-2100 μm^3) and the other group consists of small centric diatoms such as *Stephanodiscus hantzschii* and *Cyclotella* spp. And small green algae such as *Chlorella* spp. (WEA = well edible algae, 5-650 μm^3) which are presumably mostly edible for many ciliates. All other phytoplankton species were considered to be less edible and not considered in further analysis.

Bacterioplankton and autotrophic picoplankton (APP) densities were converted to biomass as described by (Weisse, 1991 and literature cited therein, https://fred.igb-berlin.de/Lakebase). The bacterioplankton and APP biomass was summed up.

Crustaceans potentially interacting with ciliates comprised: Cyclopoid copepods, the calanoid copepod *Eudiaptomus gracile* and *Daphnia longispina* (formerly *D. 80urcate), D. galeata, Bosmina* sp. which we combined to 'Daphnia' in our analysis due to their similar feeding range

and *Bosmina* being quantitatively less important. Biomass was calculated from length–dry weight relationships established for Lake Constance and assuming a carbon content of 50% of dry weight (Straile and Geller, 1998).

Water temperature was mostly measured automatically with high spatio-temporal resolution. For the few periods were such data were not available estimates were obtained from the air temperature.

Tab. 4.1: Characterization of the ciliate morphotypes including their names, abbreviation of the name, cell volume [µm³], longest linear dimension (LLD, [µm]) taken as a measure how edible they are for crustaceans (Some ciliate morphotypes comprise different counting categories, thus there are up to 3 measurements for cell volume and longest linear dimension for one ciliate morphotype."-" indicates no measurements for the counting category/morphotype), their feeding type (Gaedke and Wickham 2004), their mean biomass when encountered in a sample [mg C / m²], and the coefficient of variation (CV) of their biomass across the twelve years of sampling when encountered in a sample, the number of net growth rate I measurements and the R^2 for the full net growth rate r model [%] (r and 7 environmental predictors). Abbreviations for the feeding type are picoplankton p, nanoplankton n, microplankton m, interception feeders I and filter feeders F.

Name	Abb.	Cell volume	LLD	Feeding type	Mean biomass	CV	# *r* measure-ments	R^2 for net growth rate model
Askenasia sp.	A	7,200 / 37,000	25.5 / 43.6	n & I	17	1.26	417	4
Balanion planctonicum	Bp	1,300	14.6	n & I	18	2.10	429	3
Histioba-lantium bodanicum	Hb	34,000 / 68,000	45.5 / 73.6	p, n & I	74	1.25	401	3
Limno- and Pelago-strombidium sp.	LP	32,000 / 77,000	45.5 / 57.3	n & F	48	1.65	404	6
Monodinium / Didinium	MD	38,000 / 70,000 / 116,000	44.8 /- /-	n,m & I	9	2.35	141	4

Peritrichs on *Anabaena*	Pa	16,000	35.2	p & F	24	1.52	102	8
Peritrichs on diatoms	Pd	10,000 / 37,000	30 / 43.3	p & F	17	1.86	344	6
Pelagohal-teria viridis	Pv	6,500	-	p & F	10	1.54	116	8
Rimostrom-bidium lacustris	Rl	119,000	68.6	n & F	49	2.37	342	3
Sessile suctoria	ses	7,000 / 30,000 / 40,000	-	n, m & I	10	2.40	174	1
Small oligotrichs	sO	2,700 / 6,500	17.8 / 25.5	p, n & F	45	1.32	433	6
Small suctico-ciliates	suc	1,300	21.5	p & F	3	3.09	259	7
Tintinnids	T	24,000	46.7 / 53.3	n & F	33	1.89	338	5
Urotricha furcata	Uf	1,700	17.4	n & I	6	2.07	423	4
Urotricha sp. 2	U2	9,500	29.3	n & I	7	1.31	292	3
Urotricha sp. 3	U3	24,000 / 81,000 / 500,000	39.6 /- /-	n & I	14	1.81	231	4
Vaginicola sp.	V	3,500	24.5	p & F	2	2.21	108	8

Standardization and smoothing

To reduce variability due to different winter weather conditions we standardized the sampling dates within each year by centring them to the begin of the clear-water phase (CWP) which is defined as week 0 (Ehrlich et al 2020 ISME, Ehrlich and Gaedke 2020).

Net growth rates of ciliates, r, were calculated as the differences in $\log_{10}$-transformed biomass between two adjacent sampling dates divided by the number of days, which were typically 7 (5-21) days apart. In weeks with more than one sample, the date nearest to the sample routine was picked

and the other date(s) omitted. Only the 17 ciliate morphotypes with more than 100 growth rate estimates in all 12 years were taken into account.

Before fitting the boosted regression trees, we smoothed the measured biomass to remove outliers of ecologically unrealistic high growth rates using the function gam of the R package mgcv (smoothing parameter 0.01 and method "REML", Appendix Fig. C1). As the number of measurements where individual ciliate morphotypes were encountered varied, we chose the dimension of the basis used to represent the smooth term as 66% of the samples based on a visual comparison of different amounts of smoothing. The smoothing did not change the results meaningfully (data not shown).

Diversity index and frequency distributions

Diversity and evenness were calculated using the Simpson indices D = 1-$\sum_i^N p_i^2$ and E = $\frac{D}{1-1/N}$ with p_i being the relative biomass of morphotypes i and N being the number of morphotypes. Temporal changes in community composition were quantified using the Pinkham and Pearsson's similarity index. It was calculated as $\sum \frac{min(p_{ia},p_{ib})}{max(p_{ia},p_{ib})}\frac{1}{N}$ with p_{ia} (p_{ib}) being the relative biomass of morphotypes i on sampling dates a and b.

We grouped the ciliate net growth rates into 15 equidistant classes to explore their frequency distributions. To compare the distributions among ciliate morphotypes, we calculated the mean $\bar{x}$, variance v, skewness S, and kurtosis K.

Boosted regression tree models

For each ciliate morphotype boosted regression tree (BRT) models were calculated to understand the influence of 7 environmental predictors on either their biomasses or net growth rates. Additionally, the influence of biomass respective net growth rate one time step before was analyzed as a measure for autocorrelation. We found a high positive first order autocorrelation for biomass and a negative first order autocorrelation for net growth rate (Appendix Tab. C3). The R^2 for all models can be found in the Appendix (Tab. C3). We concentrated on the ciliate net growth rate models to understand their seasonal dynamics.

We used 10-fold cross-validation to estimate the optimal BRT model parameters. For each ciliate morphotype, the data set was divided into ten equal consecutive subsamples of time. At every step, nine subsamples were used to fit the model and to predict *r* for data in the tenth subsample. This was repeated with all ten subsamples and the mean prediction error for each parameter combination was calculated.

Additional information on single predictors can improve model performance. Therefore we enforced a monotonic increasing relationship to the food predictor *most edible algae* which can be consumed by all ciliates, a monotonic decreasing relationship to the predator *Cyclops* which can consume all ciliates, and no relationships to all predictors which may have a negative or positive impact (temperature, bacteria plus APP, well edible algae, *Daphnia*, *Eudiaptomus*). All analyses were done using R (version 4.0.0) and the packages lubridate, mgcv, tidyverse, tictoc, gbm and tseries, (R Core Team, 2020; Grolemund and Wickham, 2011; Wood, 2011; Wickham *et al.*, 2019; Izrailev, 2014; Greenwell *et al.*, 2019; Trapletti and Hornik, 2021). The BRTs were done with the function gbm of the package gbm.

Optimization

The growth rate model was optimized trying different values for four parameters. We did a stepwise optimization, calculating BRTs in a nested loop for three to five values for every of the four parameters and ten subsamples of the data and choosing the combination with the lowest median across the RMSE of all ciliates and refine these values stepwise, until there the improvement in RMSE was below 1%. We chose 1000 (100 – 10,000 tested) trees to fit, a shrinkage rate of 0.001 (0.000275 – 0.2) applied to each tree in the expansion, also known as the learning rate or step-size reduction, an interaction depth of 4 (2-4) implying a model with up to 2-way interactions, and a bag fraction of 0.3 (0.3-0.5) for our final model.

We also used 10-fold cross-validation to quantify the importance of all predictors. We created set of submodels containing all but one of the predictors in the full model. Using the optimal model parameters of the full model, we quantified the mean predictor error for the full model and all

submodels. The change in prediction error, i.e. the difference in prediction error between the full model and a sub-model excluding one distinct predictor, is a measure of the information contributed by the omitted predictor to the full model. This metric allowed us to compare the importance of all predictors in the full model.

Partial dependence

As measurements for the prediction error R^2 and RMSE were used. R^2 is calculated as the explained variance divided by the overall variance: $R^2 = 1 - \frac{mean((predicted\ data - observed\ data)^2)}{var(observed\ data)}$. RMSE is the square root of the mean standard error: $RMSE = \sqrt{mean((observed\ data - predicted\ data)^2)}$.

Partial dependence plots were generated by estimating the effect of each predictor on the target variable net growth rate in the model, after setting other predictors to levels suitable for ciliate growth: high food concentrations, low predator and competitor biomasses and an intermediate temperature.

Results

We first characterize the ciliate community in Lake Constance by comparing its temporal variability and synchronization of the individual morphotypes and the diversity and evenness with that of the phytoplankton and rotifer community. We then give an overview of the seasonal dynamics of the ciliate morphotypes and of environmental predictors potentially influencing them, i.e. their food, predators and competitors, and temperature. We finally use boosted regression trees to evaluate the possible role of these abiotic and biotic predictors on ciliate net growth.

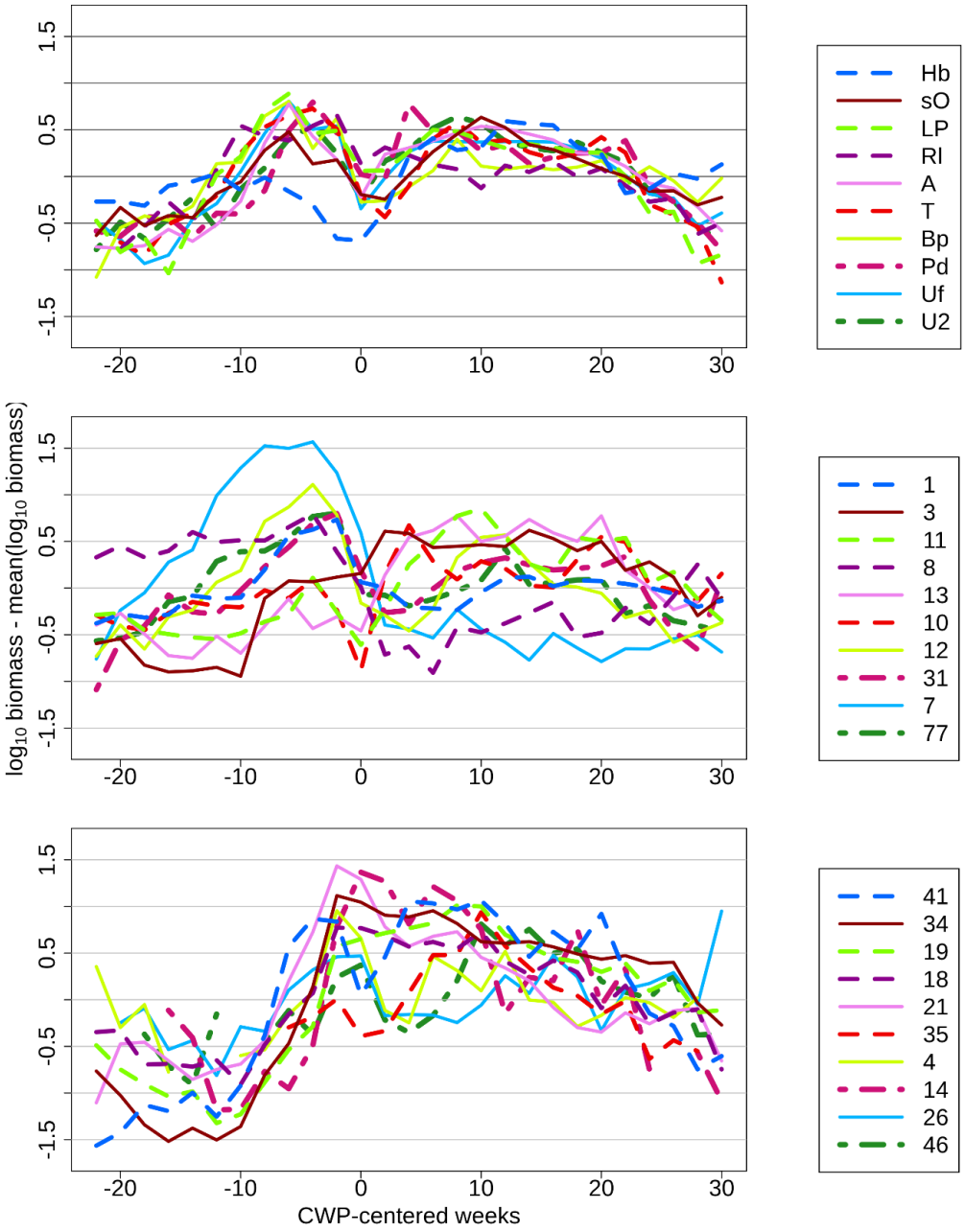

Fig. 4.1: Time series of the 10 quantitatively most important morphotypes (according to their mean biomass) of a) ciliates, b) phytoplankton and c) rotifers. The log10 transformed weekly averages across all years were standardized by subtracting their long-term mean and centred to the beginning of the CWP. Their contribution to total biomass decreases in the given order in the legend (cf. Fig. 4.2). Morphotype numbers and ciliate abbreviations are explained in App. Tab. C1.

The ciliate morphotypes exhibited a high degree of synchrony throughout the annual cycle, except for *Histiobalantium bodamicum* (Hb in Fig 4.1a) during the first half of the year. In contrast, phytoplankton morphotypes

typically reached high values either prior or after the clear-water phase (Fig. 4.1b) implying relatively strong compensatory dynamics between the two groups. Biomasses of rotifer morphotypes were consistently below their annual mean during January to April and varied more independently afterwards (Fig. 4.1c). Thus, similar factors seem to promote and hamper the individual ciliate morphotype growth leading to stronger synchronization than found in the other species-rich plankton communities.

The seasonal amplitude in biomass of ciliate morphotypes was typically lower than for the other plankton groups: In ciliates, maximum values exceeded the long-term mean by a factor of 4 to 8 whereas phytoplankton and rotifer morphotypes exceeded theirs by factors of 4 to 36 (Fig. 4.1). The long-term morphotype variability described by their coefficient of variation varied between 93% and 322% for ciliates, and 69% to 409% for rotifers. These values were significantly lower than for phytoplankton (122-445 %, $p = 0.006$, Appendix Fig. C2) suggesting that ciliate morphotype balance growth and loss processes relatively strongly throughout the annual cycle and thus rather independently from environmental predictors.

Numerous ciliate morphotypes occurred regularly throughout the year and the whole sampling period of twelve years and contributed moderately to total ciliate biomass. Ten out of 24 ciliate morphotypes but only eight out of 36 phytoplankton morphotypes and only five out of 20 rotifer morphotypes were encountered on ≥75% of all sampling dates, i.e. the 25% quantiles of their relative contribution to the total biomass were above the detection level (Fig. 4.2). For the nine most frequent ciliate morphotypes, the median of the relative biomass contribution to the overall ciliate biomass did not exceed 20% but remained consistently above 1%. The contribution of lower ranked morphotypes was temporally more variable and they were increasingly lacking on individual sampling dates (Fig. 4.2a). This suggests that many ciliate morphotypes have broad ecological niches allowing them to thrive under different circumstances but with no morphotype being superior for extended periods of time.

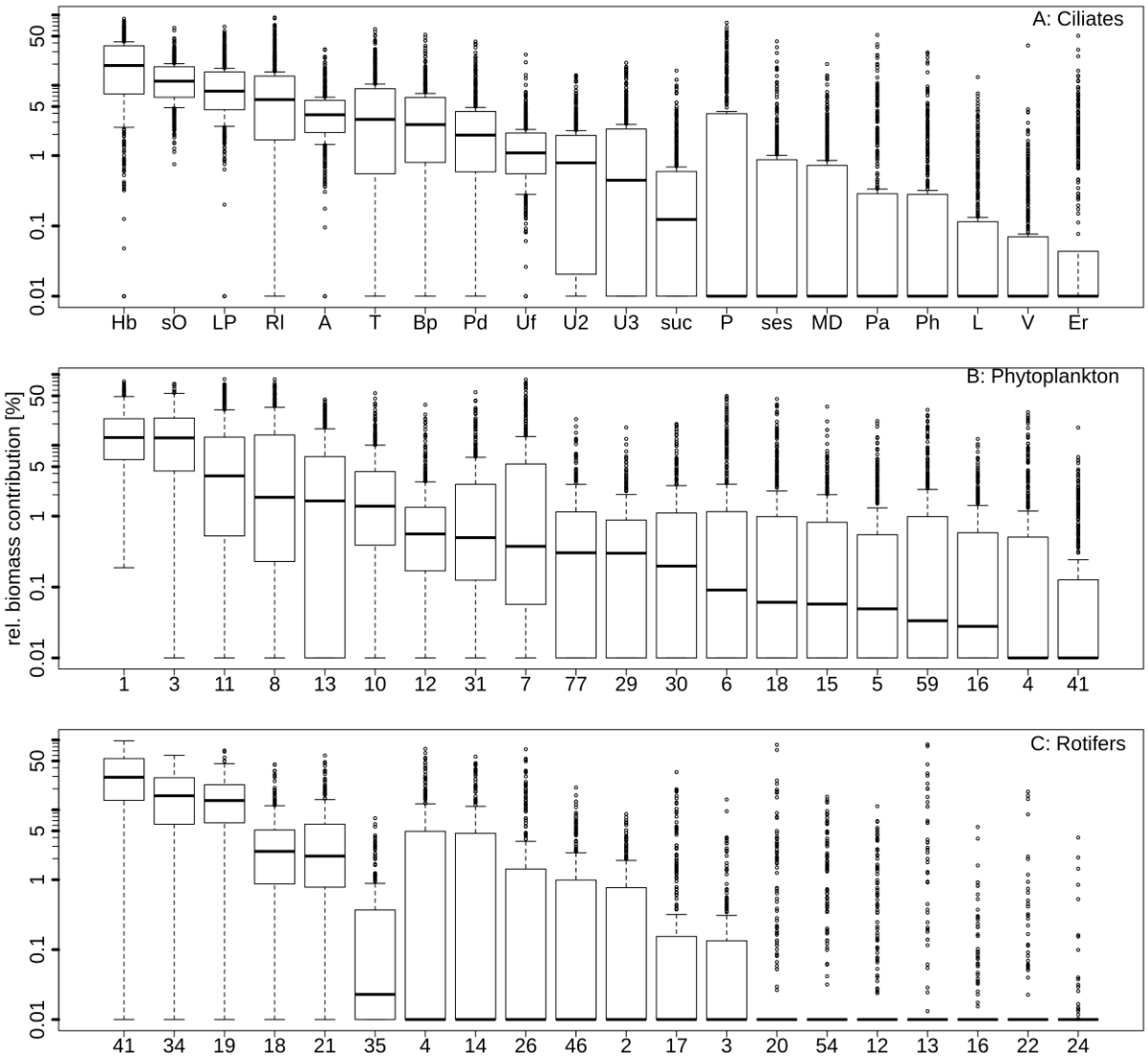

Fig. 4.2: Changes in community composition within a) ciliates, b) phytoplankton and c) rotifers. The relative biomass contributions to total biomass of the 20 most important individual morphotypes of each community are displayed in descending order of their median or 0.75 or 0.9 quantile for ties in the median. Boxes comprise the range from the 25 –75 % quantile. Horizontal bars within boxes represent the median. The whiskers are drawn from the box to the most extreme point within 1.5 interquartile ranges, i. e. the distance between the 25th and the 75th sample quantile. Any value more extreme than this is marked with a dot. If a morphotype was not found in a sample, its relative biomass was set to 10^{-4} which was used as zero replacement value. The box includes this value if a morphotype was not encountered in ≥25 % of the samples. In some instances, morphotypes were not encountered in ≥50 % of the samples which implies that the median is at the bottom line. Morphotype abbreviations and numbers are explained in App. Tab. C1.

An objective way to rate the short- and long-term variability in ciliate composition as high or low is to compare it with the other species-rich plankton communities which have similar generation times and experienced similar forcing by abiotic and biotic processes in the same habitat. In phytoplankton, two very frequent morphotypes occurred in almost every sample and each contributed more than 10 % to the total phytoplankton biomass on more than half of the sampling dates (Fig. 4.2b). As a consequence, the relative share of the subsequent morphotypes declined more rapidly than in ciliates: Only six morphotypes had a median above 1 %, showing a lower evenness within phytoplankton. Individual rotifer morphotypes exhibited the greatest monopolization of biomass of the three plankton communities considered (Fig. 4.2c). Three morphotypes contributed between 10 % and 30 % each to total biomass during at least 50 % of all sampling dates (i.e. had a median higher than 10 %). The majority of the morphotypes were absent in ≥50-75 % of the samples but several of them nevertheless contributed 10 % of the total biomass at other times (see upper whiskers in Fig. 4.2c). This shows that the rotifer community composition changed pronouncedly during at least part of the year (cf. Fig. 4.1). Overall, temporal coherence and regularity of occurrence were higher in ciliates than in phytoplankton and rotifers.

The diversity and evenness in ciliates were significantly higher than in rotifers (Simpson D = 0.75, $p < 2.2*10^{-16}$, Simpson E = 0.71, $p < 2.2*10^{-16}$) and the temporal similarity in morphotype composition (Pinkham and Pearsson P = 0.26) was significantly higher for ciliates than for phytoplankton (P = 0.23, $p < 9.1*10^{-7}$) and rotifers (P = 0.20, $p < 2.6*10^{-16}$) (App. Fig. C4, Fig. C5). These findings suggest that ciliate morphotypes are less specialized on distinct growth conditions and almost balance growth and losses under different environmental conditions. The facts that many ciliate morphotypes were regularly found throughout the season and across years with relatively low temporal variability, and that their biomass was relatively evenly shared by many ciliate morphotypes underpinned this as well.

Seasonal occurrence and inter-annual variability

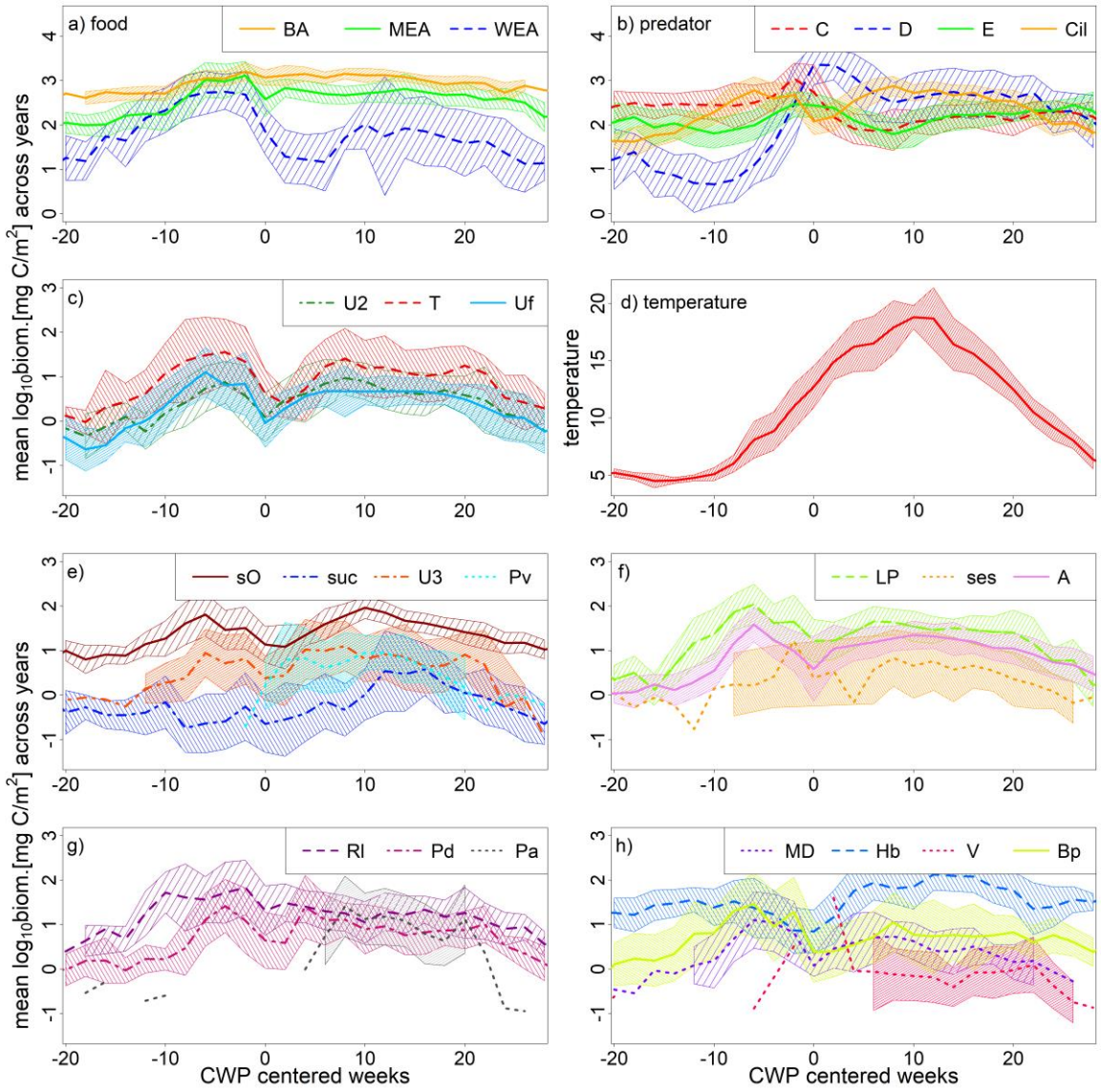

Fig. 4.3: Seasonal course of all ciliate morphotypes and the environmental predictors (three possible food sources MEA = most edible algae, WEA = well edible algae, BA = bacteria plus autotrophic picoplankton, four competitors/predators C = *Cyclops*, D = daphnids, E = *Eudiaptomus*, Cil = sum of all ciliates). Ciliate morphotypes are arranged to be easy distinguishable, see Appendix Tab. C1 for their full names. Data were obtained by taking the mean and standard deviation (plotted only when ≥5 values available) per blocks of two CWP-centred weeks across all years. The y axes always span 4.5 orders of magnitude (except temperature) enabling to compare the inter-annual range among ciliate morphotypes and predictors.

All plankton groups exhibited recurrent seasonal patterns (Fig. 4.3). After a spring bloom, total ciliate and then edible algae biomass declined during the so-called clear-water phase, CWP, a period of algal suppression by

herbivores starting typically between the end of May and the middle of June in Lake Constance. Total ciliate biomass quickly recovered during early summer to a level similar to that in spring until the autumnal decline. It is important to note that ciliate morphotypes started to loose biomass when *Cyclops* and *Eudiaptomus* were at their maximum biomass, while both edible algal groups had still high biomasses (Fig. 4.3a, b). Almost all ciliate morphotypes reached their minimum biomass at the beginning of the CWP and already increased in biomass again when daphnids still had high biomasses (cf. Fig. 4.1, Fig. 4.3). Some ciliate morphotypes reached their maximum biomass in spring (e.g. *Balanion planctonicum* and *Rimostrombidium lacustris*), some during summer (e.g. *Histiobalantium bodamicum*) or only showed up in summer (e.g. *Vaginicola* and sessile suctoria), whereas others had equal biomasses in both seasons (small oligotrichs and peritrichs on diatoms). The ciliate morphotypes which have measurable biomasses only in summer had a higher inter-annual variability than the other ciliate morphotypes (Fig. 4.3c, e-h).

Variability of ciliate net growth rates

The observed net growth rates between adjacent sampling dates r of most ciliate morphotypes were small (Appendix Tab. C2) compared to their high potential growth rates. 66% of the r values of all ciliate morphotypes fell in the range of -0.128 and 0.137 per day, implying a change in biomass between -12% and +15% per day resp. between -59% and +161% over the typical sampling interval of 7 days. No ciliate morphotype showed a skewed distribution of r, while many were more peaked (leptokurtic) than the normal distribution (e.g. *Askenasia* in Fig. 4.4, cf. Appendix Tab. C2, Appendix Fig. C3). Differences in the shapes of the distributions of r may indicate that different ciliate morphotypes follow either a gleaner (peaky distribution) or opportunist strategy (broad distribution with many extreme values or skewed distribution with some extreme positive values); however, we did not find clear differences between morphotype' growth rate distributions.

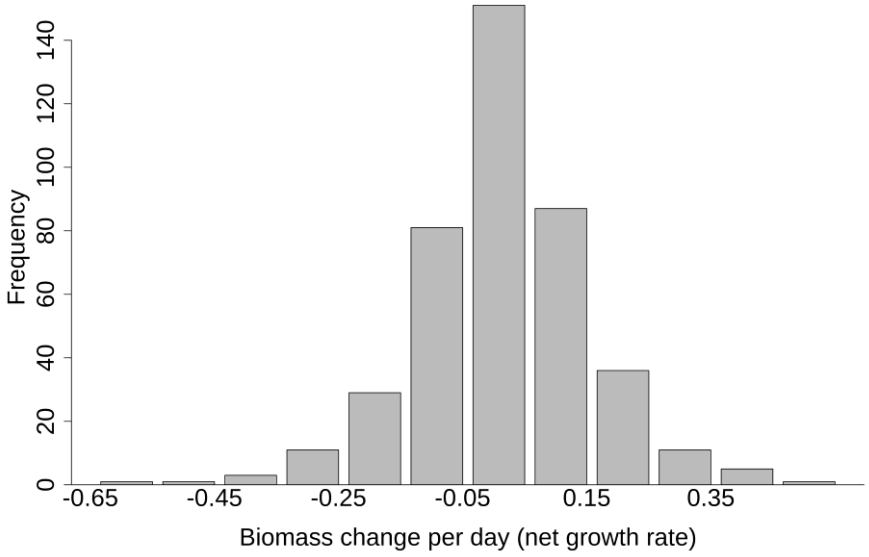

Fig. 4.4: Distribution of the observed net growth rates r of *Askenasia* which is representative for many ciliate morphotypes.

Influence of environmental predictors

We ran boosted regression trees (BRTs) on the smoothed biomasses and net growth rates *r* of individual ciliate morphotypes to determine their dependence on 7 environmental predictors: three possible food sources: most edible algae MEA, well edible algae WEA, and the sum of bacteria and autotrophic picoplankton (for brevity bacteria), three potential predators/competitors *Cyclops*, the calanoid copepod *Eudiaptomus gracilis*, and predominantly herbivorous cladocerans dominated by *Daphnia* and including *Bosmina,* and temperature.

In the models predicting ciliate biomass the ambient growth conditions typically explained only a small amount of the variance (-19% to 35%, mean 6%, App. Tab. C3; values below zero indicate that the prediction is worse than the mean value). In contrast, the biomass of the previous time step accounted on average for 42% of the variance (6-68%, App. Tab. C3). This reveals a high first order positive autocorrelation and suggests that ambient growth conditions had a relatively weak effect on biomass at the time scale of our dataset (App. Fig. C7).

Models predicting the ciliate net growth rate *r* revealed a weak negative first order autocorrelation (accounting for 2-15%, mean 7% of the variance,

App. Tab. C3, App. Fig. C8) and also a low dependence on environmental conditions explaining on average 5% of the variance (1-8%, App. Tab. C3). Less frequently encountered ciliate morphotypes had usually values below average. One to five predictors were important in influencing the *r* of all ciliate morphotypes, with temperature, *Cyclops* and bacteria being the most important predictors followed by *Daphnia* and the well edible algae (Fig. 4.5).

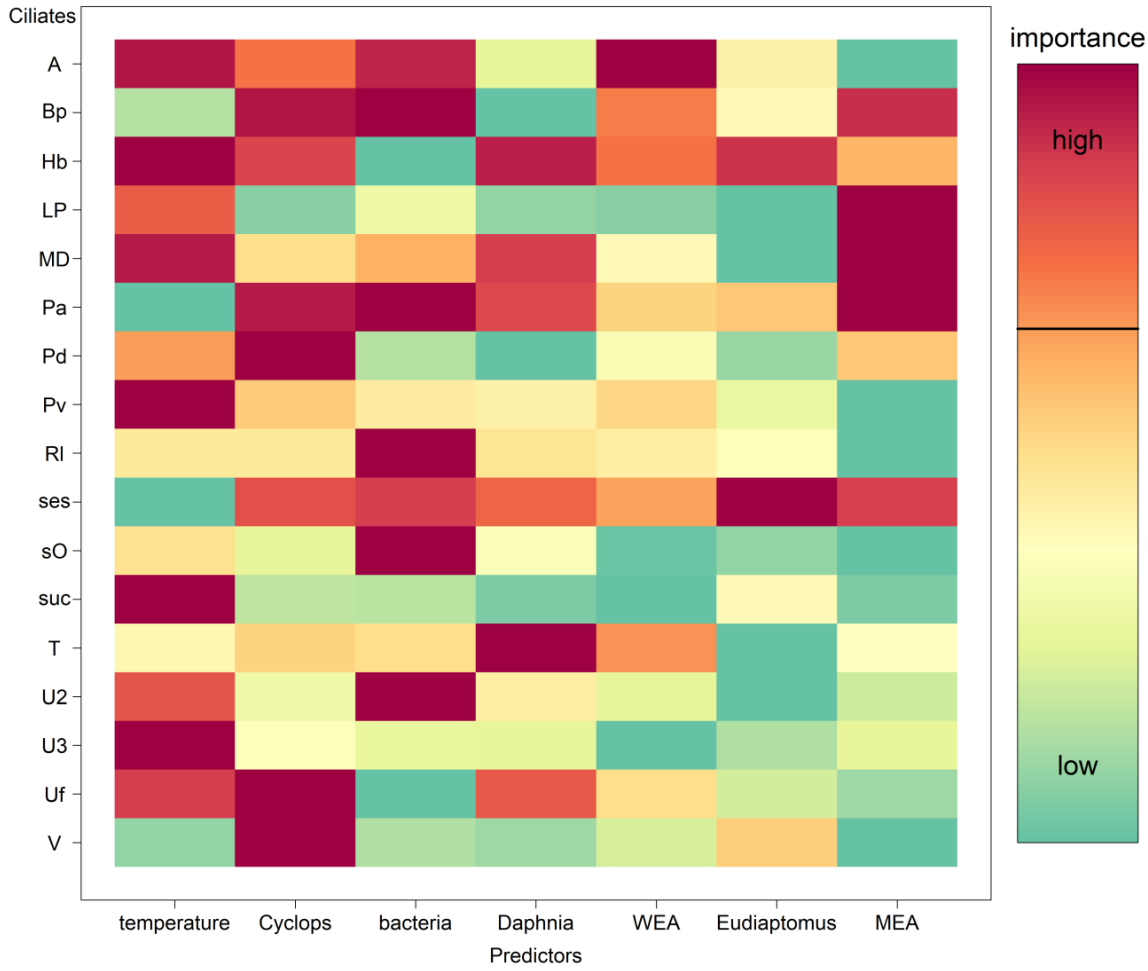

Fig. 4.5: Importance of the predictors based on the R^2 for the r model. Predictors are temperature, bacteria plus autotrophic picoplankton (bacteria), *Cyclops*, *Daphnia*, *Eudiaptomus*, the well edible algae (WEA) and the most edible algae (MEA). Ciliate morphotype abbreviations are explained in Tab. 4.1. Red colours depict higher importance than green ones (scale different for each morphotype).

We present the relationship between *r* and the environmental predictors in groups and in order of decreasing importance in partial dependence plots. They show for each ciliate morphotype the model-estimated response of *r* to

one predictor at a time assuming favourable conditions for all other predictors, i.e. high food concentrations, low predator biomasses and an intermediate temperature.

Influence of temperature

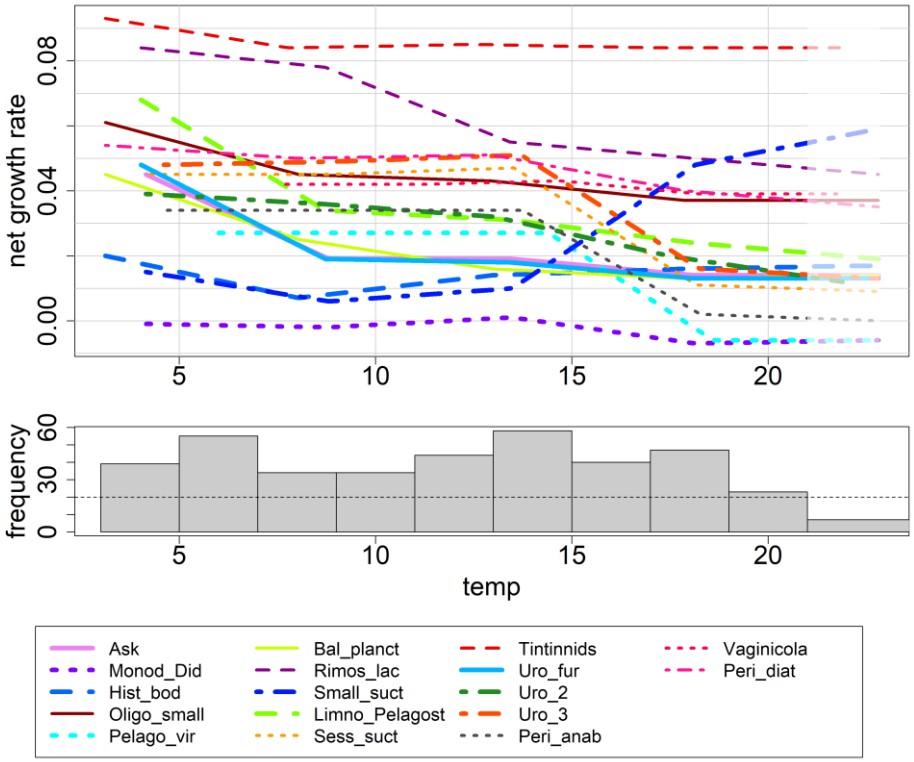

Fig. 4.6: Partial dependence plot for temperature for suitable environmental conditions (high food concentrations and low predator and competitor biomasses). Thicker line widths indicate that temperature is an important predictor for this morphotype (cf. Fig. 4.5). The histogram in the middle provides the number of sampling dates with the respective temperature at which at least one ciliate morphotype was found to inform about the temperature range where reliable predictions are possible. Ranges with low frequencies are presented in lighter shades to indicate the much greater uncertainty in these regions of parameter space.

The models suggested that temperature had the highest importance for most ciliate morphotypes and, counterintuitively, had a negative impact on *r* (Fig. 4.6). Some ciliate morphotypes had their biomass peak in spring, e.g. *Askenasia* and *Urotricha 94urcate*, and they responded all similarly with a sharp decrease in *r* when the temperature increased to about 8°, and remained at this low level. A decrease in *r* at higher temperatures of about 15° was common for other ciliate morphotypes as *Urotricha* 3, which

had their biomass peak in summer. Only the small sucticociliates having their biomass peak in summer were estimated to respond positively to an increasing temperature. Hence, if ciliate morphotypes exhibited a distinct relationship to temperature it was clearly related to their seasonal occurrence.

Influence of potential food

Bacterial biomass (including autotrophic picoplankton) had the highest importance of the three possible food sources (Fig. 4.5). Its seasonal variability was smaller than for the other predictors, changing only by a factor of approximately ten during the season (cf. Fig. 4.3). We found no response at very low biomasses which is in line with expectations. But unexpectedly, despite some ciliate morphotypes feeding on particles in the picoplankton size range, all ciliate morphotypes were negatively associated with high bacterial biomass values, above 1000 mg C/m² (Fig. 4.7a). The negative response did not depend on the feeding size range of the ciliate morphotypes: e.g. picophagous peritrichs on *Anabaena* and nanophagous *Rimostrombidium lacustris* both were predicted to respond negatively to increasing bacterial biomass.

We classified algae as well edible, WEA, which were in the nanoplankton size range (e.g. small *Stephanodiscus* and *Cyclotella* spp., cf. App. Tab. C1) and can be efficiently used as food by some ciliate morphotypes such as *Balanion planctonicum* and *Rimostrombidium lacustris*, whereas others may not digest them (Müller and Schlegel 1999). Some ciliate morphotype such as *Rimostrombidium lacustris* and peritrichs on diatoms responded positively, others such as *Balanion planctonicum* responded negatively to increasing WEA biomass with no systematic differences between the feeding size ranges (Fig. 4.7b).

Algae of good food quality with a longest linear dimension of 7 – 25 µm (e.g. *Rhodomonas minuta*, cf. App. Tab. C1) were defined as most edible algae, MEA, which makes them presumably suitable for all ciliates. Hence, we assumed a positive relationship between r and MEA biomass in our model. The sigmoidal shape of the response curve of some ciliate morphotype is perfectly in line with expectations from theoretical considerations: a first algal biomass increase at very low levels is still insufficient to promote r

and a further increase at already high concentrations suggesting food satiation can hardly further enhance *r* (Fig. 4.7c). While the *r* of some ciliate morphotypes such as the nanophagous tintinnids and the picophagous peritrichs on *Anabaena* responded clearly to the increasing MEA biomass, many other nanophagous ciliate morphotypes did not respond.

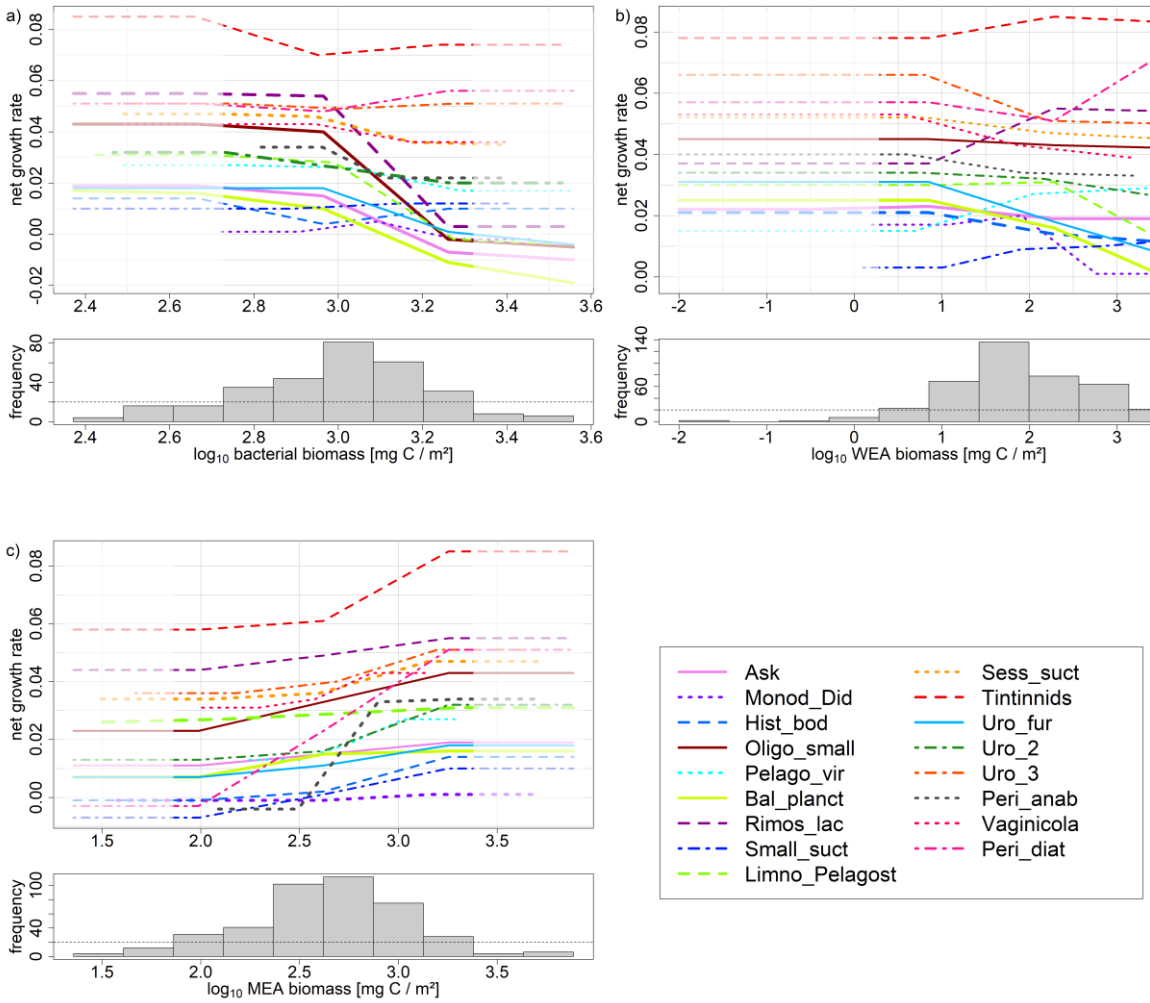

Fig. 4.7: Partial dependence plot for three possible food sources a) bacteria, b) well edible algae and c) most edible algae for suitable environmental conditions (high food concentrations, low predator and competitor biomasses and an intermediate temperature). Thicker line widths indicate that the predictor is important (cf. Fig. 4.5). The histograms below provide the number of sampling dates with the respective biomass to inform about the range where reliable predictions are possible. Ranges with low frequencies are presented in lighter shades to indicate the much greater uncertainty in these regions of parameter space.

Influence of predators and competitors

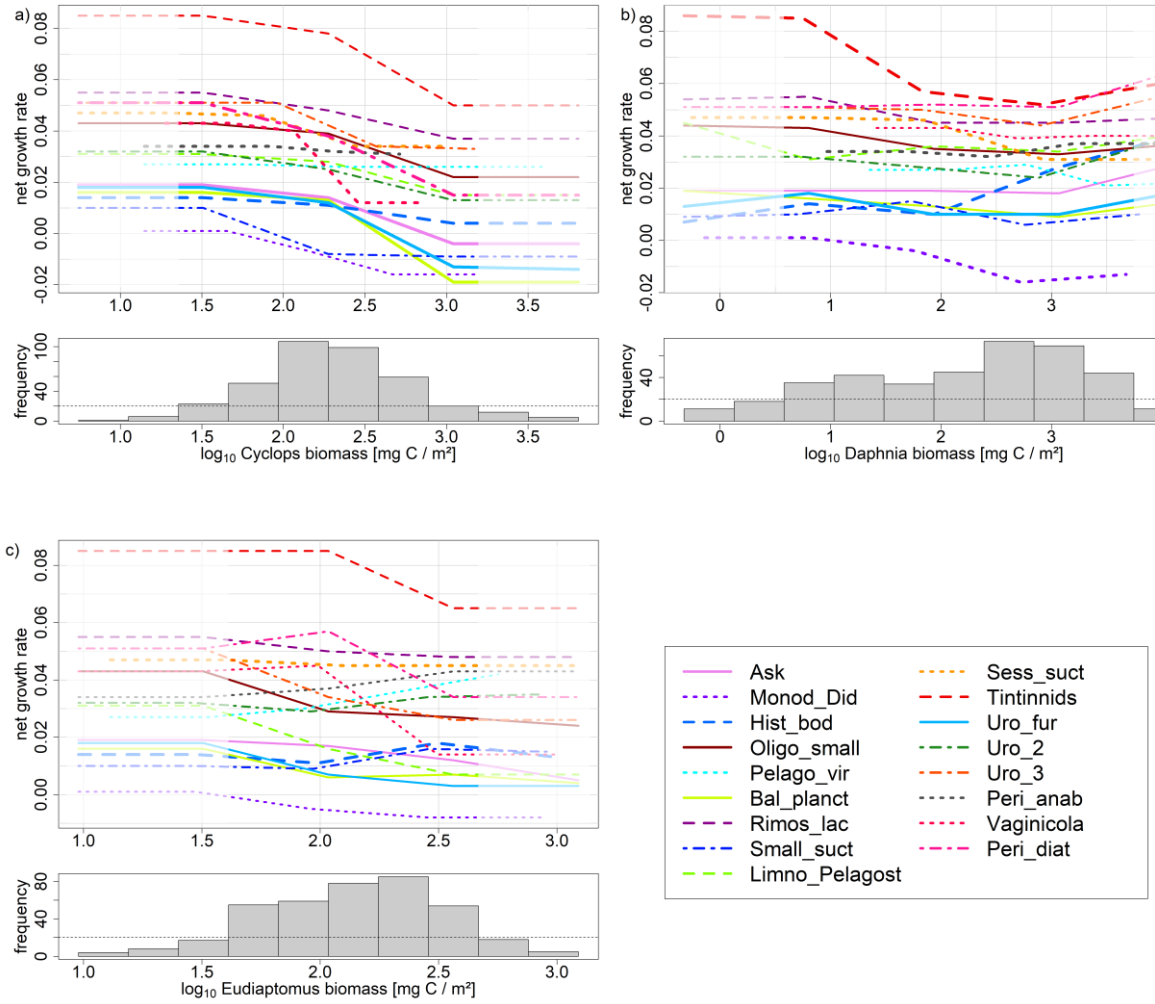

Fig. 4.8: Partial dependence plots for the predators/competitors a) *Cyclops*, b) *Daphnia*, c) *Eudiaptomus* for suitable environmental conditions (high food concentrations, low predator and competitor biomasses and an intermediate temperature). Thicker line widths indicate that the predictor is important (cf. Fig. 4.5). The histograms below provide the number of sampling dates with the respective biomass to inform about the range where reliable predictions are possible. Ranges with low frequencies are presented in lighter shades to indicate the much greater uncertainty in these regions of parameter space.

The cyclopoid copepod *Cyclops* spp. Has a prey range of approximately 2-600 µm which includes all ciliate morphotypes. Therefore, we constrained our model to force a negative association between *Cyclops* biomass and *r*. *Cyclops* was the most important predator (Fig. 4.5). The BRTs suggest a direct negative effect of *Cyclops* spp. On numerous ciliate morphotypes if its biomass exceeded ca. 100 mg C/m² (Fig. 4.8a). The few ciliate

morphotypes which did not respond mostly had their biomass peak in summer when most *Cyclops* species turned into diapause in the sediment to escape their predators (cf. Fig. 4.3). In line with the estimated prey size range of *Cyclops*, we did not find a size-dependent pattern in the responses of the ciliates, ciliate morphotypes of all size classes responded to an increasing *Cyclops* biomass (e.g. *Urotricha 98urcate* (17µm) and peritrichs on diatoms (43 µm), Fig. 4.8a).

The filter-feeding cladocerans dominated by *Daphnia* are omnivorous with a prey size range up to ca. 35 µm. Using similar food items as ciliates, they are more likely competitors than predators for most ciliates. Competition is an indirect effect and was accounted for in the model by including edible algae as predictors. In line, only few ciliate morphotypes responded to *Daphnia*, most of them negatively, including the two ciliate morphotypes feeding on nano- to microplankton, *Monodinium/Didinium* and sessile suctoria (Fig. 4.8b). This is in line with a competition effect as microphytoplankton was not included in the model.

Eudiaptomus is an omnivorous calanoid copepod with a prey range up to 60 µm which suggests that it can function as a predator and a competitor to the ciliates. Most ciliate morphotypes hardly responded to increasing *Eudiaptomus* biomass (Fig. 4.8c). The overall response was weaker than for *Cyclops*. We found no association with ciliate size or feeding behaviour.

Discussion

The biomass of ciliate morphotypes showed a recurrent seasonal pattern, often with peaks in spring and summer separated by a decrease around the CWP. Many ciliate morphotypes exhibited a high synchrony and a low seasonal and inter-annual variability in their biomass compared to phytoplankton and rotifers. The ciliate community had a high diversity, high evenness and numerous morphotypes were regularly encountered during the season revealing a relative constancy in morphotype composition. The high temporal autocorrelation in the biomass together with the inter-annually recurrent seasonal patterns suggest that their dynamics are strictly controlled, yet it remains difficult to determine the factors responsible for it given the low explanatory power of the environmental predictors for both the biomass and net growth rates.

Factors influencing community-level variability and synchrony

Several processes may contribute to the remarkably low variability and high synchrony of the ciliate morphotypes' dynamics. One is the rather similar predation pressure for most ciliates in spring. Furthermore, ciliate species are often widely distributed, not specialized to distinct abiotic conditions, and hibernate more often in the plankton (Finlay *et al.*, 1996). In Lake Constance, they did not respond to the re-oligotrophication during the study period in contrast to phytoplankton (Gaedke 1998, Gaedke and Wickham, 2004). A low responsiveness of protozoans to external forcing was also observed in marine systems (Dolan and Gallegos, 2001) and in experiments with epibenthic ciliates (Wickham *et al.*, 2004). Ciliate species may comprise a high diversity of functionally different clones which may buffer their response to environmental changes (Weisse *et al.*, 2001; Krenek *et al.*, 2012).

Synchronization of the ciliate morphotypes' biomasses may partly originate from the seasonal changes in food supply and the susceptibility to copepod predation in late spring. This yields the bimodal seasonal pattern typical for mesotrophic lakes like Lake Constance with high biomasses in spring and summer and low biomasses in winter and around the clear-water phase (cf. Fig. 4.3, Ehrlich and Gaedke, 2020). Ciliate morphotypes' dynamics were more synchronized than in phytoplankton and rotifers (cf. Vasseur and Gaedke 2007) yielding higher pair-wise correlation coefficients among ciliate than phytoplankton morphotypes (Huber and Gaedke, 2006, cf. Fig. 4.3). In Lake Constance, phytoplankton morphotypes exhibit a trade-off in respect to growth rates, susceptibility to grazing by various grazers and competitive abilities for the most limiting nutrient phosphorous (Ehrlich *et al.*, 2020). This trade-off promotes compensatory dynamics between edible algae (i.e. WEA and MEA) and other algae which are inedible for ciliates and less edible for crustaceans during summer (Vasseur *et al.*, 2005, cf. Appendix Tab. C1). Hence, ciliates may be functionally less diverse than phytoplankton in respect to grazing resistance providing less potential for asynchronous dynamics.

Weak environmental dependence of ciliate growth rates

To investigate the specific role of top-down and bottom-up processes for the ciliate morphotypes' dynamics, we used a series of boosted regression tree models fitted separately to each ciliate morphotype. There are some caveats for boosted regression tree models: first, limited and low-frequency data can be a problem and second, environmental correlations make it hard to disentangle the individual effects properly. This might contribute to the fact that, despite their flexibility and the inclusion of constraints based on mechanistic understanding, these models explained only a small fraction of the variability in net growth rates.

The net growth rate *r* was positive for all ciliate morphotypes at very low temperatures under otherwise suitable growth conditions. In line, unlike the crustaceans, some ciliate morphotypes showed substantial growth below 6° C, e.g. *Limno-/Pelagostrombidium*, *Rimostrombidium lacustris* and *Balanion planctonicum* (cf. Fig. 4.3). This may indicate that ciliates are less temperature-sensitive than their crustacean predators and therefore have a relative advantage in spring. The patterns in temperature response clearly reflect differences in seasonal occurrence of the ciliate morphotypes. As temperature reflects the annual cycle most pronouncedly in our model, temperature may be a surrogate for other seasonal effects which may explain why it was ranked as most important predictor (cf Fig. 4.5).

Potential food sources: We investigated the association between ciliate *r* and bacterial biomass and autotrophic picoplankton. Some of the ciliate morphotypes are presumably able to feed on picoplankton (cf. Tab. 4.1), but unexpectedly, all ciliate morphotypes showed a negative rather than a positive relationship when the picoplankton biomass surpassed 1000 mg C/m². Similar results were obtained when assuming other conditions in the model such as high predator densities or low algal concentrations. A possible explanation for the negative response is a high context dependency, e.g. picoplankton food supply is high around the CWP when the ciliates decline due to the high predation pressure. This prevents them from translating the available food into positive net growth (cf. Fig. 4.3).

As expected, the phytoplankton species considered as most edible for ciliates, MEA, had a distinct positive effect on the *r* of numerous ciliate morphotypes including those considered as solely picoplankton feeders, but the feeding range of the ciliate morphotypes did not play a role. The responses were largely independent of assuming other environmental conditions, but dampened for high predation pressure. Unexpectedly, MEA were overall the least important predictor in the models.

The response of *r* to biomass increases of the well edible algal group, WEA, comprising phytoplankton species considered as potentially usable by numerous but not all of our ciliate morphotypes (Skogstad *et al.*, 1987; Müller and Schlegel, 1999; Hamels *et al.*, 2004) was often less pronounced which is in line with expectations. However, it should be acknowledged that the maximum biomasses of WEA were more than an order of magnitude lower than that of MEA and in a range where we observed that a further increase in MEA still enhanced *r*. The low predictive power of both algal groups may indicate that these two categories are too coarse to reflect the presumably rather species-specific but understudied food spectra of the individual ciliate morphotypes.

Potential predators: Our results suggest that the cyclopoid copepod *Cyclops* spp. Was the most important predator on numerous ciliate morphotypes when its biomass surpassed ca. 100 mg C/m² (cf. Fig. 4.5). This is in line with experimental studies (Wiackowski *et al.*, 1994; Wickham, 1998; Adrian and Schneider-Olt, 1999). Its larger copepodite stages and the adults are considered as omnivorous/carnivorous and all ciliate morphotypes studied here fall into their prey size range. The general results concerning all predators were independent of the other environmental conditions assumed in the model such as low food concentrations or high abundances of the other predators/competitors.

The *r* of most ciliate morphotypes was unrelated to the highly variable cladoceran biomass which included the smaller *Bosmina* but was dominated by the two daphnid species *Daphnia longispina* and *D. galeata* reaching a length of ca. 2.5 mm. This may appear unexpected, as daphnids were often held responsible for the decline of ciliates towards the CWP directly or indirectly via food competition (Müller *et al.*, 1991; Gaedke and

Straile, 1998). However, at least in Lake Constance the decline of ciliates starts already prior to the onset of the CWP and mass development of daphnids (Fig. 4.3, Tirok and Gaedke, 2006, 2007; Ehrlich and Gaedke, 2020). An inter-annual comparison of daphnid biomasses in Lake Constance during summer with that of ciliates of different size classes revealed a size-dependent positive or negative effect (Gaedke and Wickham, 2004). This was not supported by our model, presumably because it accounts separately for the prey biomasses and thus the indirect effects of competition. Thus, our results suggest that the daphnids do not exert a strong predation pressure in contrast to *Cyclops*.

The calanoid copepod *Eudiaptomus* had little effect on the r of most ciliate morphotypes. Its functional role in plankton food webs has been debated for a long time. It has been considered as more algivorous than *Cyclops* but there is also evidence for carnivory (Kunzmann *et al.*, 2019) which we cannot support given the variable and weak response of r to the biomass of *Eudiaptomus*. When comparing its impact with *Cyclops* it should be noted that its maximum biomasses remained a factor of 3 lower than that of *Cyclops* in Lake Constance.

Overall, the changes in r with increasing food concentration or predator biomasses were of similar magnitude. This suggests that ciliate morphotypes are typically affected by both, bottom-up and top-down effects.

Model and sampling uncertainties

The ciliate morphotypes differ in feeding modes and food particle size ranges and each ciliate morphotype consumes only a small part of the plankton resulting in reduced competition and a complex food web with many weak interactions. Weak interactions stabilize food web dynamics, especially when omnivores are involved (McCann *et al.*, 1998; Emmerson and Yearsley, 2004; Li *et al.*, 2021). The resulting high number of mutually entwined interactions bears a high potential to adjust to altered conditions (Tirok and Gaedke, 2007). One mechanism may be fast predator-prey interactions between individual ciliate morphotypes and their specific prey species during extended spring peaks when ciliates are the dominant herbivores (Tirok and Gaedke, 2007). These weak interactions may be a

reason for our low model predictability and may also explain why we found using simpler approaches no significant relationships between e.g. the biomass of ciliates grouped according to their feeding type or size and the biomass of their presumed prey or predators, the predator – prey weight ratio or between biomass and size in ciliates (data not shown).

Another factor that needs to be acknowledged are limitations in the data such as the number of data points (102 – 429 for our data set), sampling frequency relative to the short generation time of ciliates, and measurement precision and accuracy (Elith *et al.*, 2008). Furthermore, next to the usual patchiness in plankton biomass internal seiches occur during thermal stratification at the sampling site with a period of 4-6 days. The seiches change the thickness of the warm epilimnion and, thus, also the areal abundance of planktonic organisms we measured in a fix water depth of 20 m (Gaedke and Schimmele, 1991). This process may alter the ciliate biomass by a factor of up to circa 2 within 2 days imposing noise on the biological processes. In line, we found a negative first order autocorrelation of r (App. Fig. C8) and average values of r were higher when the sampling interval was shorter than a week (data not shown and used). Our data set with almost weekly sampling at 2-4 depth intervals for 12 consecutive years is at the upper limit of what is operationally feasible using manually sampling and microscope counting which delivers a taxonomically detailed picture of the community. Higher spatio-temporal resolution requires automatic probing and image analysis systems which are increasingly becoming available (Thomas *et al.*, 2018) but at least so far at the cost of taxonomical resolution as far as ciliates are concerned..

Conclusions

The total ciliate biomass and individual ciliate morphotypes exhibited relatively recurrent seasonal patterns with low inter-annual variability. Many ciliate morphotypes occurred during extended periods of the year under different growth conditions and had a low temporal variability, i.e. the net growth rates were low compared to the maximum growth rates observed in the lab. This leads to the conclusion that ciliate dynamics are very well controlled: the clear and pronounced response to the onset of the phytoplankton spring bloom and their decline prior to the CWP, i.e. before

their dominant prey substantially declines, probably due to top-down control by copepods, but not daphnids which have lower biomasses, but afterwards they are only moderately related to distinct environmental conditions.

Despite using twelve years of high frequency sampling and a model approach considering all known processes simultaneously, we could only explain a limited amount of the observed variability. Potential reasons include many weak interactions influencing ciliate dynamics which would call for more species-specific predictors. Furthermore, the impact of regulating factors may be highly context dependent and that even moderate noise in the net growth rate may overlay small signals. The ciliate dynamics point to a consistently tight balance between growth and losses but the multifactorial regulating processes are far from being understood under natural conditions.

Acknowledgements

We thank Guntram Weithoff for helpful comments on the manuscript. The research of NJK is funded by the DFG (DynaTrait: GA 401/26-1/2).

References

Adrian, R. and Schneider-Olt, B. (1999) Top-down effects of crustacean zooplankton on pelagic microorganisms in a mesotrophic lake. *Journal of Plankton Research*, **21**, 2175–2190.

Baltensperger, A. P. *et al.* (2020) Implications of future climate- and land-change scenarios on grassland bird abundance and biodiversity in the Upper Missouri River Basin. *Landscape Ecol*, **35**, 1757–1773.

Boit, A. and Gaedke, U. (2014) Benchmarking Successional Progress in a Quantitative Food Web. *PLoS ONE*, **9**, e90404.

Burns, C. W. and Schallenberg, M. (2001) Calanoid copepods versus cladocerans: Consumer effects on protozoa in lakes of different trophic status. *Limnol. Oceanogr.*, **46**, 1558–1565.

Chen, W.-L. *et al.* (2020) Neglect of Presence of Bacteria Leads to Inaccurate Growth Parameters of the Oligotrich Ciliate Strombidium sp. During Grazing Experiments on Nanoflagellates. *Front. Mar. Sci.*, **7**, 569309.

Cleven, E.-J. (2004) Pelagic Ciliates in a Large Mesotrophic Lake: Seasonal Succession and Taxon-Specific Bacterivory in Lake Constance. *Internat. Rev. Hydrobiol.*, **89**, 289–304.

Dolan, J. R. and Gallegos, C. L. (2001) Estuarine diversity of tintinnids (planktonic ciliates). *Journal of Plankton Research*, **23**, 1009–1027.

Ehrlich, E. *et al.* (2020) The shape of a defense-growth trade-off governs seasonal trait dynamics in natural phytoplankton. *ISME J*, **14**, 1451–1462.

Ehrlich, E. and Gaedke, U. (2020) Coupled changes in traits and biomasses cascading through a tritrophic plankton food web. *Limnol Oceanogr*, **65**, 2502–2514.

Elith, J. *et al.* (2008) A working guide to boosted regression trees. *J Anim Ecology*, **77**, 802–813.

Elith, J. *et al.* (2006) Novel methods improve prediction of species' distributions from occurrence data. *Ecography*, **29**, 129–151.

Emmerson, M. and Yearsley, J. M. (2004) Weak interactions, omnivory and emergent food-web properties. *Proc. R. Soc. Lond. B*, **271**, 397–405.

Finlay, B. J. *et al.* (1996) Biodiversity at the Microbial Level: The Number of Free-Living Ciliates in the Biosphere. *The Quarterly Review of Biology*, **71**, 221–237.

Flöder, S. *et al.* (2018) Inter- and intraspecific consumer trait variations determine consumer diversity effects in multispecies predator-prey systems. *Aquat. Microb. Ecol.*, **81**, 243–256.

Gaedke, U. *et al.* (2002) Interplay between energy limitation and nutritional deficiency: empirical data and food web models. *Ecological Monographs*, **72**, 251–270.

Gaedke, U. and Klauschies, T. (2017) Analyzing the shape of observed trait distributions enables a data-based moment closure of aggregate models: Trait distributions and aggregate models. *Limnol. Oceanogr. Methods*, **15**, 979–994.

Gaedke, U. and Schimmele, M. (1991) Internal seiches in Lake Constance: influence on plankton abundance at a fixed sampling site. *J Plankton Res*, **13**, 743–754.

Gaedke, U. and Straile, D. (1998) Daphnids: Keystone species for the pelagic food web structure and energy flow. - A body size-related analysis linking seasonal changes at the population and ecosystem levels. *Arch. Hydrobiol. Spec. Issues Advanc. Limnol.*, **53**, 587–610.

Gaedke, U. and Straile, D. (1994) Seasonal changes of the quantitative importance of protozoans in a large lake : an ecosystem approach using mass-balanced carbon flow diagrams. *Marine Microbial Food Webs*, **8**, 163–188.

Gaedke, U. and Wickham, S. A. (2004) Ciliate dynamics in response to changing biotic and abiotic conditions in a large, deep lake (Lake Constance). *Aquatic Microbial Ecology*, **34**, 247–261.

Greenwell, B. *et al.* (2019) *gbm: Generalized Boosted Regression Models. R package version 2.1.5*.

Grolemund, G. and Wickham, H. (2011) Dates and Times Made Easy with lubridate. *Journal of Statistical Software*, **40**, 1–25.

Hamels, I. *et al.* (2004) Evidence for constant and highly specific active food selection by benthic ciliates in mixed diatoms assemblages. *Limnol. Oceanogr.*, **49**, 58–68.

Hansen, P. J. *et al.* (1997) Zooplankton grazing and growth: Scaling within the 2-2,-µm body size range. *Limnol. Oceanogr.*, **42**, 687–704.

Huber, V. and Gaedke, U. (2006) The role of predation for seasonal variability patterns among phytoplankton and ciliates. *Oikos*, **114**, 265–276.

Izrailev, S. (2014) *tictoc: Functions for timing R scripts, as well as implementations of Stack and List structures.. R package version 1.0.*

Johansson, M. *et al.* (2004) Annual variability in ciliate community structure, potential prey and predators in the open northern Baltic Sea proper. *Journal of Plankton Research*, **26**, 67–80.

Knisely, K. and Geller, W. (1986) Selective Feeding of Four Zooplankton Species on Natural Lake Phytoplankton. *Oecologia*, **69**, 86–94.

Krenek, S. *et al.* (2012) Coping with Temperature at the Warm Edge – Patterns of Thermal Adaptation in the Microbial Eukaryote Paramecium caudatum. *PLoS ONE*, **7**, e30598.

Kunzmann, A. J. *et al.* (2019) Calanoid copepod grazing affects plankton size structure and composition in a deep, large lake. *Journal of Plankton Research*, **41**, 955–966.

Li, X. *et al.* (2021) Energetic constraints imposed on trophic interaction strengths enhance resilience in empirical and model food webs. *J Anim Ecol*, 1365-2656.13499.

Lischke, B. *et al.* (2016) Large biomass of small feeders: ciliates may dominate herbivory in eutrophic lakes. *J. Plankton Res.*, **38**, 2–15.

Löder, M. G. J. *et al.* (2012) Dinoflagellates and ciliates at Helgoland Roads, North Sea. *Helgol Mar Res*, **66**, 11–23.

McCann, K. *et al.* (1998) Weak trophic interactions and the balance of nature. *Nature*, **395**, 794–798.

Menden-Deuer, S. and Lessard, E. J. (2000) Carbon to volume relationships for dinoflagellates, diatoms, and other protist plankton. *Limnol. Oceanogr.*, **45**, 569–579.

Müller, H. (1991) *Pseudobalanion planctonicum* (Ciliophora, Prostomatida): ecological significance of an algivorous nanociliate in a deep meso-eutrophic lake. *J Plankton Res*, **13**, 247–262.

Müller, H. *et al.* (1991) Seasonal succession of ciliates in lake constance. *Microbial Ecology*, **21**, 119–138.

Müller, H. (1989) The relative importance of different ciliate taxa in the pelagic food web of lake constance. *Microb Ecol*, **18**, 261–273.

Müller, H. and Schlegel, A. (1999) Responses of three freshwater planktonic ciliates with different feeding modes to cryptophyte and diatom prey. *Aquatic Microbial Ecology*, **17**, 49–60.

Paffenhöfer, G. *et al.* (2005) Colloquium on diatom-copepod interactions. *Mar. Ecol. Prog. Ser.*, **286**, 293–305.

Pomati, F. *et al.* (2020) Interacting Temperature, Nutrients and Zooplankton Grazing Control Phytoplankton Size-Abundance Relationships in Eight Swiss Lakes. *Front. Microbiol.*, **10**, 3155.

Posch, T. *et al.* (2015) Network of Interactions Between Ciliates and Phytoplankton During Spring. *Front. Microbiol.*, **6**.

R Core Team (2020) *R: A language and environment for statistical computing. R Foundation for Statistical Computing, Vienna, Austria.*

Skogstad, A. *et al.* (1987) Growth of freshwater ciliates offered planktonic algae as food. *J Plankton Res*, **9**, 503–512.

Sommer, U. *et al.* (2012) Beyond the Plankton Ecology Group (PEG) Model: Mechanisms Driving Plankton Succession. *Annu. Rev. Ecol. Evol. Syst.*, **43**, 429–448.

Straile, D. and Geller, W. (1998) Crustacean zooplankton in Lake Constance from 1920 to 1995 : response to eutrophication and re-oligotrophication. *Advances in Limnology*, **53**, 255–274.

Thomas, M. K. *et al.* (2018) The predictability of a lake phytoplankton community, over time-scales of hours to years. *Ecol Lett*, **21**, 619–628.

Tirok, K. and Gaedke, U. (2010) Internally driven alternation of functional traits in a multispecies predator–prey system. *Ecology*, **91**, 1748–1762.

Tirok, K. and Gaedke, U. (2007) Regulation of planktonic ciliate dynamics and functional composition during spring in Lake Constance. *Aquat. Microb. Ecol.*, **49**, 87–100.

Tirok, K. and Gaedke, U. (2006) Spring weather determines the relative importance of ciliates, rotifers and crustaceans for the initiation of the clear-water phase in a large, deep lake. *Journal of Plankton Research*, **28**, 361–373.

Trapletti, A. and Hornik, K. (2021) *tseries: Time Series Analysis and Computational Finance. R package version 0.10-49*.

Vargas, C. A. *et al.* (2006) Phytoplankton food quality determines time windows for successful zooplankton reproductive pulses. *Ecology*, **87**, 2992–2999.

Vasseur, D. A. *et al.* (2005) A seasonal alternation of coherent and compensatory dynamics occurs in phytoplankton. *Oikos*, **110**, 507–514.

Vasseur, D. A. and Gaedke, U. (2007) Spectral Analysis Unmasks Synchronous and Compensatory Dynamics in Plankton Communities. *Ecology*, **88**, 2058–2071.

Weisse, T. *et al.* (2001) Niche separation in common prostome freshwater ciliates: the effect of food and temperature. *Aquat. Microb. Ecol.*, **26**, 167–179.

Weisse, T. *et al.* (1990) Response of the microbial loop to the phytoplankton spring bloom in a large prealpine lake. *Limnol. Oceanogr.*, **35**, 781–794.

Weisse, T. (1991) The annual cycle of heterotrophic freshwater nanoflagellates: role of bottom-up versus top-down control. *J Plankton Res*, **13**, 167–185.

Weisse, T. and Frahm, A. (2002) Direct and indirect impact of two common rotifer species (*Keratella* spp.) on two abundant ciliate species (*Urotricha furcata* , *Balanion planctonicum*): Rotifer impact on ciliates. *Freshwater Biology*, **47**, 53–64.

Wiackowski, K. *et al.* (1994) Differential effects of zooplankton species on ciliate community structure. *Limnol. Oceanogr.*, **39**, 486–492.

Wickham, H. *et al.* (2019) Welcome to the tidyverse. *Journal of Open Source Software*, **4**, 1686.

Wickham, S. A. *et al.* (2004) Control of epibenthic ciliate communities by grazers and nutrients. *Aquat. Microb. Ecol.*, **35**, 153–162.

Wickham, S. A. (1998) The direct and indirect impact of *Daphnia* and *Cyclops* on a freshwater microbial food web. *J Plankton Res*, **20**, 739–755.

Wood, S. N. (2011) Fast stable restricted maximum likelihood and marginal likelihood estimation of semiparametric generalized linear models. *Journal of the Royal Statistical Society (B)*, **73**, 3–36.

Chapter 5

The double-edged sword of inducible defences: costs and benefits of maladaptive switching from the individual to the community level

Nadja J. Kath, Ursula Gaedke, Ellen van Velzen

Abstract

Phenotypic plasticity can increase individual fitness when environmental conditions change over time. Inducible defences are a striking example, allowing species to react to fluctuating predation pressure by only expressing their costly defended phenotype under high predation risk. Previous theoretical investigations have focused on how this affects predator-prey dynamics, but the impact on competitive outcomes and broader community dynamics has received less attention. Here we use a small food web model, consisting of two competing plastic autotrophic species exploited by a shared consumer, to study how the speed of inducible defences across three trade-off constellations affect autotroph coexistence, biomasses across trophic levels, and temporal variability. Contrary to the intuitive idea that faster adaptation increases autotroph fitness, we found that higher switching rates reduced individual fitness as it consistently provoked more maladaptive switching towards undefended phenotypes under high predation pressure. This had an unexpected positive impact on the consumer, increasing consumer biomass and lowering total autotroph biomass. Additionally, maladaptive switching strongly reduced autotroph coexistence through an emerging source-sink dynamic between defended and undefended phenotypes. The striking impact of maladaptive switching on species and food web dynamics indicates that this mechanism may be of more critical importance than previously recognized.

Key words: inducible defence, food web, maladaptive switching, coexistence, source-sink dynamics

Introduction

Under variable environments, species with fixed trait values cannot always be well-adapted, since traits that are adaptive in certain environmental conditions are likely maladaptive in other conditions. Many species can overcome this problem by phenotypic plasticity, which allows them to adapt their trait values by behavioural, morphological or biochemical changes to different environmental conditions. This optimization of their trait values can increase the species' fitness[1,2] and stabilize their population dynamics which decreases their risk of extinction[3–5].

Inducible defences are a striking example of phenotypic plasticity. They allow species to react to a changing predation pressure by only expressing the defended phenotype when predation pressure is high[6,7]. Inducible defences can be behavioural, e.g. vertical migration in zooplankton[8,9], morphological, e.g. algae growing spines or tadpoles enlarging their body size[10,11], or biochemical mechanisms, e.g. toxin production[12]. As defence mechanisms incur costs depending on the extent and type of the defence[13–15], inducible defences economize these defence costs by allowing individuals to express the phenotype that is most suited to the current environmental conditions (undefended and fast-growing when predators are scarce, and well-defended when predators are abundant), thereby increasing the species' fitness[7].

However, there may be costs associated with plasticity which can arise in different ways. Plasticity costs are a reduction in a fitness-related trait, e.g. growth rate, for both the undefended and the defended phenotype of a species due to a high plasticity in expressing a range of defence, e.g. genetic information for toxicity that has to be carried along whether the phenotype produces the toxins or not[16] (Fig. 5.1a). But while it makes sense to assume such costs, they were rarely found even in studies that specifically looked for them[17]. A less obvious type of cost is the possibility of maladaptive phenotype expression or maladaptive switching. Species with inducible defences need the information of the surrounding predation risk

or type of predator from their environment to judge whether and which defence they need to express[18,19]. Different cues such as kairomones can be used for this decision[20]. Maladaptive switching is the risk of individuals switching from a higher-fitness phenotype to a lower-fitness one. This can happen if the cues are misinterpreted, e.g. if they are hampered by environmental influences such as CO_2[21], by lag times between the recognition of cues and the realization of the defence[22], or through simple stochasticity. This may mean that individuals fail to accurately estimate current predator density, and thus make the wrong choice on whether they should display defence. As maladaptive switching is typically neglected in theoretical investigations of the consequences of inducible defences, we aim to investigate under which circumstances maladaptive switching arises, and what its consequences are for the species itself and for the other species in the food web.

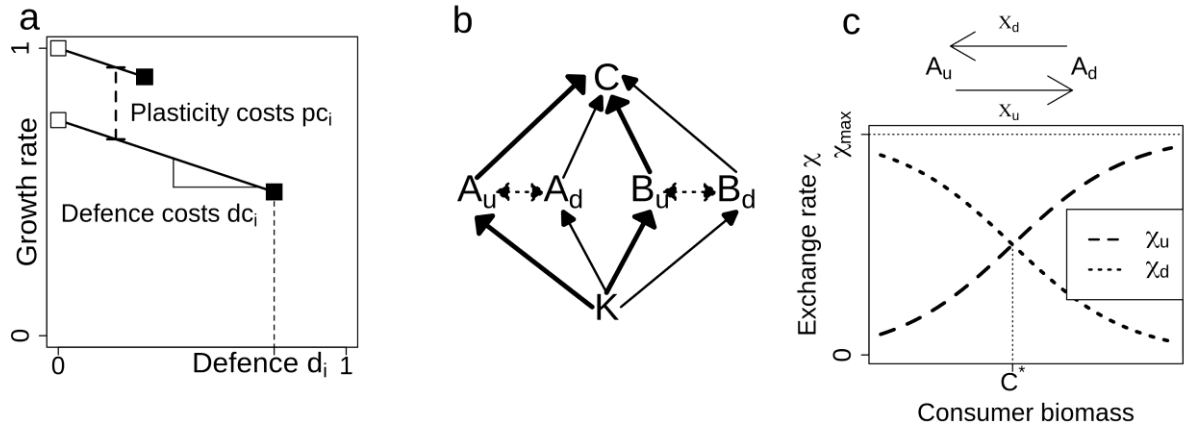

Fig. 5.1: Growth rate – defence trade-off, food web structure, and exchange rates. (a) Trait space of defence and growth rate including the plasticity costs pc_i and defence costs dc_i for a hypothetical species. White squares denote the undefended phenotypes, black squares the defended phenotypes of the same species. Solid lines link phenotypes of the same species. (b) Food web of two plastic, autotrophic species *A* and *B* sharing a carrying capacity *K* and a consumer *C*. Both autotrophic species have an undefended, u, and a defended, d, phenotype. Solid arrows represent biomass fluxes and their width indicates their relative importance. Dotted arrows indicate plastic exchange between phenotypes. (c) Exchange rate χ between both phenotypes and its dependence on the consumer biomass (see eqs. 5.9 and 5.10 in the Methods).

A critical component of inducible defences is the speed of adaptation, which can vary depending on their defence mechanism. Behavioural strategies

can be very fast, while morphological defences are rather slow, and chemical defences are somewhere in between. Differences in speed of adaptation of the prey can make the difference between the predator going extinct or not, and between stasis or oscillations[2]. A higher speed of adaptation is commonly seen as positive for the plastic organism, as either the defence is reached fast or the costs of the defence can be reduced quickly; but this depends on the assumption that switching is always adaptive, i.e. that low-fitness phenotypes switch to high-fitness phenotypes. If this assumption does not hold, faster switching may indeed be detrimental to plastic organisms implying that individuals switch more often from high to low fitness. This indicates the importance of studying whether, and under what conditions, maladaptive switching occurs.

The possibility of maladaptive switching may have consequences beyond directly lowering the fitness of the plastic species: it may impact the growth of their consumers, or lower their competitive ability compared to other prey species. Most studies take only one plastic species into account[12,21] and therefore lack the possibility to investigate the effect of switching speed on competition between two plastic species. Here we investigate the effects of phenotypic plasticity from a community perspective, considering a small food web of two plastic autotroph species A and B having each a defended and an undefended phenotype with a joint consumer C and a shared carrying capacity (Fig. 5.1b). As species cannot optimize all their traits, i.e. defence and growth rate, simultaneously, both autotrophs face a growth-defence trade-off (Fig. 5.1a, see Methods for details). Plasticity is modelled as a switching function[23] connecting both phenotypes of a species with an exchange rate χ_i, which depends on the consumer biomass to represent grazing pressure (Fig. 5.1c, see Methods for details). While individuals will mostly express their defended phenotype when consumer biomass is high, and their undefended phenotype when consumer biomass is low, there is a risk of maladaptive switching[23]. We indeed found a substantial amount of maladaptive switching towards undefended phenotypes, resulting in a source-sink dynamic between phenotypes which reduced autotroph coexistence. These patterns were exacerbated by higher switching rates, which consistently provoked more maladaptive switching. Thus, counterintuitively, a higher speed of

adaptation typically reduced individual fitness, lowering total autotroph biomass and increasing consumer biomass.

Results

In our simulations for the autotrophs, we varied two of the three trade-off properties (level of defence, defence costs and plasticity costs; see Fig. 5.1a) at a time and kept the third one constant, leading to three constellations which are named *parallel*, *crossing*, and *angle* according to their trade-off lines (Tab. 5.1). In all three, the autotrophic species B spanned the entire defence range, i.e. it had a completely undefended phenotype B_u and a maximally defended phenotype B_d. A either had a more limited defence range (in constellations *parallel* and *angle*) or spanned the entire range as well (in constellation *crossing*), representing three distinct ways that the trade-off between defence, growth rate, and plasticity range may play out. For each constellation, to investigate the effect of plasticity we varied the maximum switching rate χ_{max} over 5 orders of magnitude (Tab. 5.1, middle row). These results were also compared with a non-plastic baseline scenario where $\chi_{max} = 0$ (Tab. 5.1, upper row), as well as a rigid scenario where the species have only a single phenotype (Tab. 5.1, bottom row). All parameters and their values can be found in Appendix Tab. D1.

In the following, we give a detailed description of the results for constellation *parallel*, where the autotroph species A and B have the same defence costs resulting in parallel trade-off lines between defence and growth rate, while varying the level of defence for A and varying the plasticity costs for B (Tab. 5.1, left column). We start with examining patterns for the phenotype biomasses, coexistence and community stability in the non-plastic baseline scenario "*parallel 0*", and then compare the corresponding scenarios with a low exchange rate ("*parallel 0.01*") and a high exchange rate ("*parallel 1*"). We next discuss the other two constellations (*crossing* and *angle*, Tab. 5.1) more briefly. Finally, we generalize across all scenarios and focus on the coexistence, the degree of maladaptive switching, and the consumer and total autotroph biomasses.

Non-plastic baseline dynamics: scenario *parallel 0*

Tab. 5.1: Description of the three constellations *parallel*, *crossing*, and *angle* defining the position of the four phenotypes in the trait space of defence and growth rate. The defence and growth rate resp. the properties they depend on are listed for all autotrophs. Autotrophs are denoted by symbols (open triangle undefended phenotype of species A, A_u, filled triangle defended phenotype of species A, A_d, open circle undefended phenotype of species B, B_u, filled circle defended phenotype of species B, B_d, shaded triangle rigid *A*, shaded circle rigid *B*), the arrows describe the properties being varied in the simulations and the lines connect both phenotypes of a species, whereby only solid lines express actual switching between phenotypes.

	Parallel	*crossing*	*angle*
Property kept constant	defence costs (slope of trade-off): 0.3	defence levels: 0 for A_u / B_u and 0.9 for A_d / B_d	plasticity costs (overall growth reduction): 0
Non-plastic, i.e. no plasticity but four single phenotypes ("0")	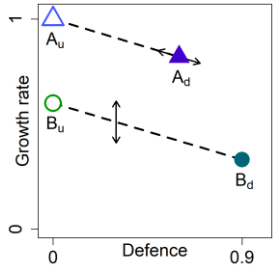	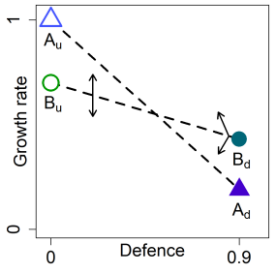	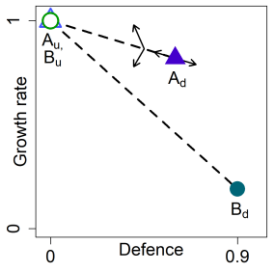
Exchange rate χ_{max} between 10^{-4} and 10^{1} enabling plasticity	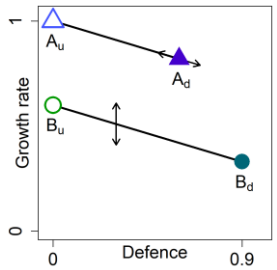	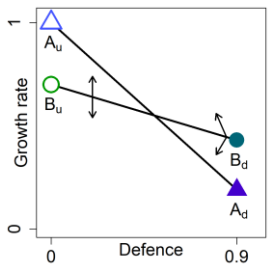	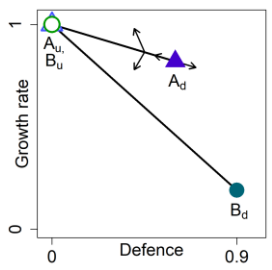
Rigid: one phenotype per species, with mean trait values of its two phenotypes ("*")	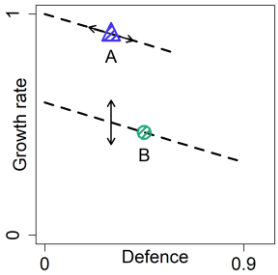	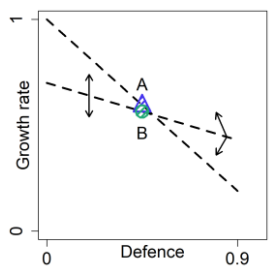	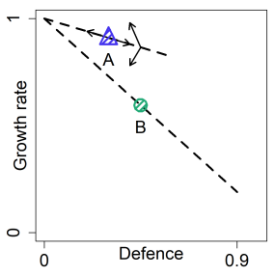

In this scenario, four single phenotypes unconnected by exchange compete with each other. Thus, species coexistence here depends entirely on phenotype coexistence: the trade-offs have to be such that for each species, at least one phenotype is a good enough competitor to survive. Which

phenotypes survive depend on the two trade-off parameters, defence of the defended phenotype of species A (d_{Au}) and plasticity costs for species B (pc_B), which thus determine whether coexistence is possible.

The defence costs were kept constant at an intermediate value of -0.3 for both species, resulting in parallel trade-off lines (Tab. 5.1, scenario "*parallel 0*"). The undefended phenotype of A, A_u, is a growth-specialist with the highest growth rate of all phenotypes. The defended phenotype of the same species, A_d, has a defence between 0 and 0.9 and a relatively high growth rate, and can be viewed as a generalist. Species B has variable plasticity costs which lower the growth rate of both phenotypes. The defended phenotype of species B, B_d, has the lowest growth rate of all phenotypes but is very well-defended, and thus a defence-specialist. Its undefended phenotype, B_u, is as undefended as A_u but has a lower growth rate; it is thus always an inferior competitor and inevitably goes extinct (Fig. 5.2c).

As B_u never survives, coexistence of the autotroph species requires the survival of defence-specialist B_d. B_d can only survive if A_d is not too defended, because A_d has a higher growth rate than B_d and will outcompete B_d in the "defended" niche otherwise (region Ib; Fig. 5.2d, h). A second criterion is that the plasticity costs for B must not be too high, because then the benefits of the defence of B_d no longer outweigh the costs, and it will go extinct even if there are no other highly defended phenotypes around (region Ia; Fig. 5.2d, g). In the regions where B_d goes extinct, species coexistence is not possible (Fig. 5.2e). The generalist A_d either survives by itself (region Ia in Fig. 5.2b, g) if its defence is low to intermediate, or together with the growth-specialist A_u if its defence is high (region Ib in Fig. 5.2a, b, h). In the regions II and III where B_d survives, it never survives on its own, but always together with one of the phenotypes of A. It coexists with the growth-specialist A_u if the plasticity costs are very low (region II in Fig. 5.2), and together with A_d if they are low to intermediate (region III in Fig. 5.2). These two regions do support species coexistence (Fig. 5.2e).

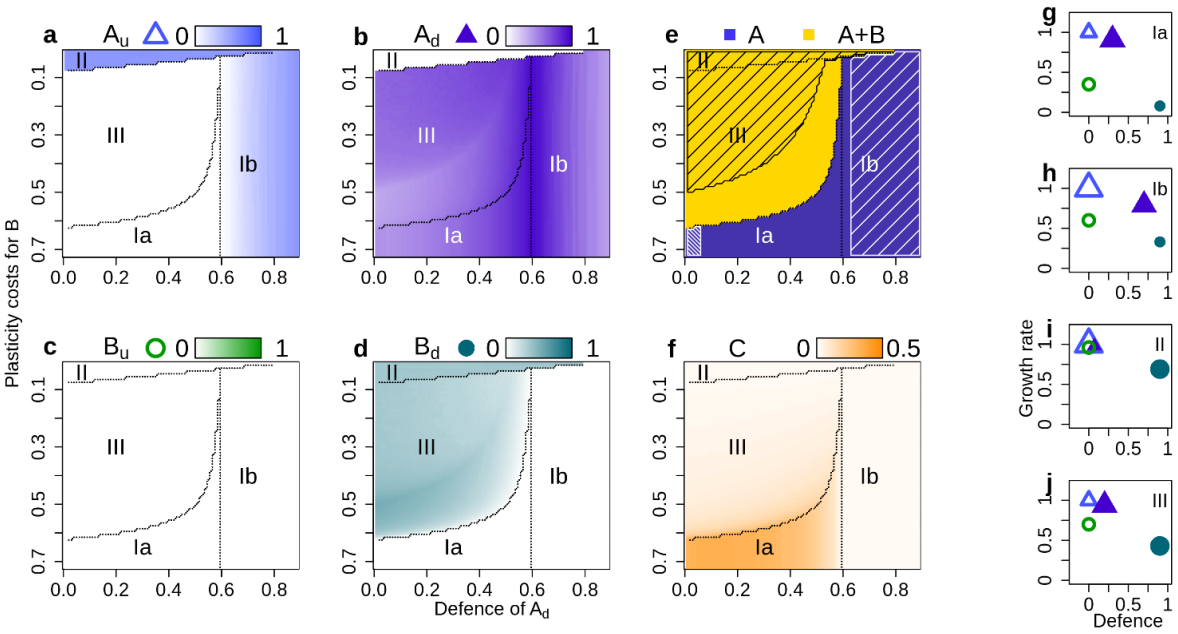

Fig. 5.2: Biomasses, coexistence and trait space for scenario *parallel 0*. Biomasses of the four autotrophic phenotypes (a-d), their coexistence patterns I, the consumer biomass (f) and the autotrophs' trait values (g-j) for scenario "*parallel 0*" (higher biomasses are shown by darker colours). Lines in a-f separate the regions I-III of different coexistence patterns. An exemplary trait combination for every region is shown in g-j; larger symbols indicate the surviving phenotypes. Shaded areas in e depict oscillating systems (quarter-lag predator-prey cycles in dense shading, antiphase cycles in loose shading).

In three of the four regions (Ib, II and III in Fig. 5.2f), consumer biomass is low, because the final community always contains a well-defended phenotype (A_d in region Ib, and B_d in regions II and III); the overall level of defence of the community is relatively high in these regions (Appendix D1a). Conversely, consumer biomass is relatively high in region Ia, because the only surviving autotroph phenotype is relatively fast-growing and fairly undefended (Fig. 5.2f). The regions where a well-defended phenotype survives often show antiphase cycles (Ib, II and III in Fig. 5.2e). These cycles do not occur in the region where only A_d survives (Ia in Fig. 5.2e); but regular quarter-lag predator-prey cycles can be found here if A_d is almost entirely undefended.

While the community defence (i.e. mean defence of the autotroph community) depends strongly on the coexisting phenotypes, the community growth rate is roughly constant because over the entire trait space, at least one phenotype with a high growth rate always survives (Appendix Fig. D1).

The standing variance of the community defence was high when two phenotypes coexist as they occupy different niches along the defence axis (Fig. 5.2h-j). In contrast, the variance of the community growth rate was very low and almost constant across all regions.

Effect of phenotypic plasticity

Even a little bit of plasticity in the scenario *parallel 0.01* (χ_{max} = 0.01) can change the above patterns for coexistence, stability, and average consumer biomass (Fig. 5.3a-h). While the autotrophs are intuitively expected to benefit from being plastic, the effect of plasticity on consumer biomass always turned out to be positive (Fig. 5.3h). This may be explained by the fact that switching was always, on average, maladaptive (Fig. 5.3e, f): the adaptation index φ determining whether the net effect of switching is adaptive or maladaptive (see eq. 5.11-5.13 in the Methods) can approach zero, but is always negative at equilibrium (see Appendix D2), indicating maladaptive switching.

The most striking effect of plasticity was on coexistence, which was affected both positively and negatively by plasticity in different regions of the parameter space (Fig. 5.3a-d,g). A negative effect on coexistence is seen in region II, where the autotroph species previously coexisted (Fig. 5.2e), while with plasticity, B outcompeted A (Fig. 5.3g). Without plasticity, coexistence was possible in this region because A_u and B_d survived; importantly, A_u outcompeted B_u due to its higher growth rate, even though the difference between their growth rates is very small in this region (Fig. 5.2i). Plasticity reverses the competitive exclusion pattern between the two undefended phenotypes: B_u receives a constant flow of biomass from the well-defended B_d, which compensates for its slightly lower growth rate and allows it to outcompete A_u. Thus, coexistence is reduced as a direct consequence of maladaptive switching.

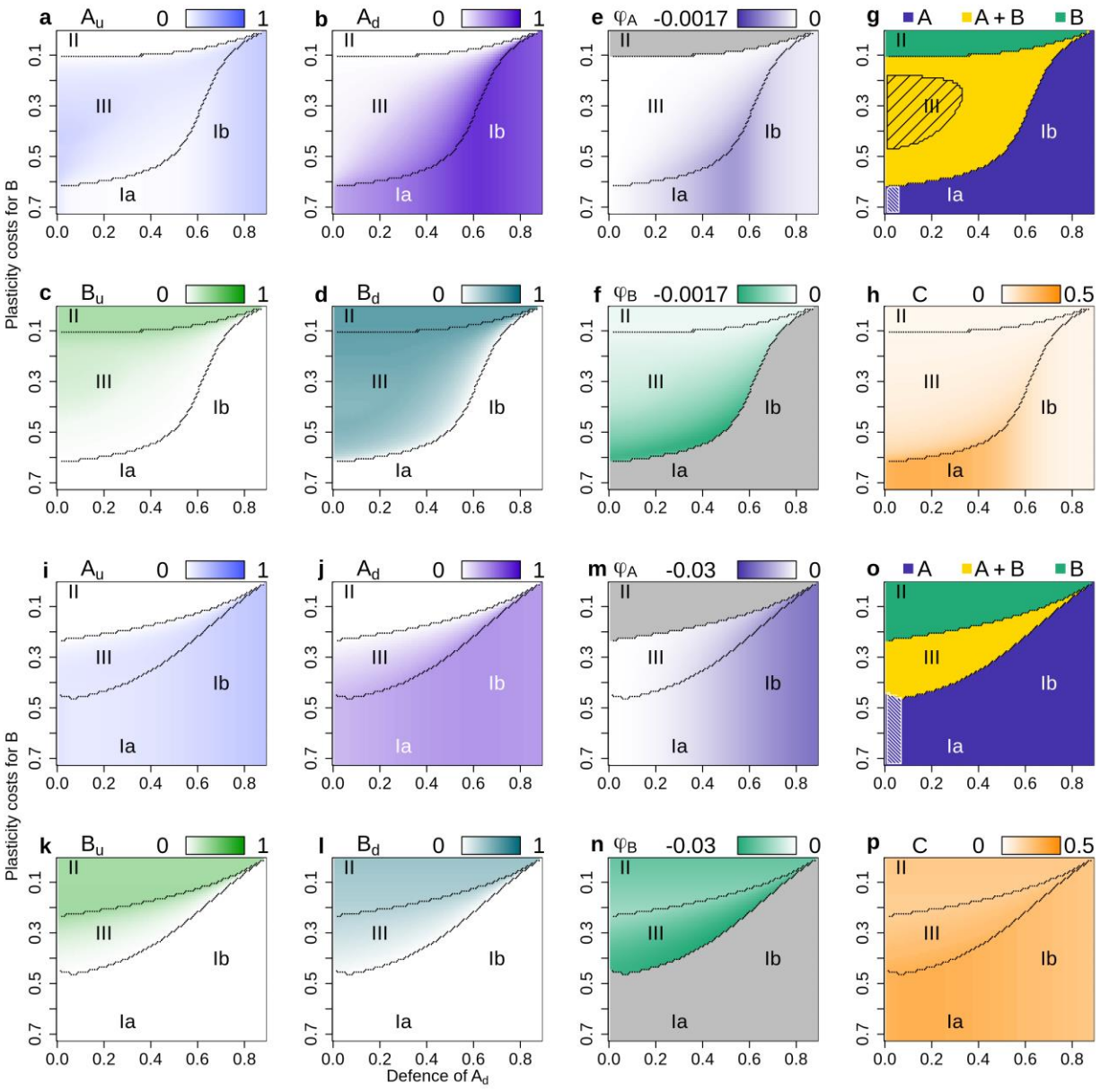

Fig. 5.3: Biomasses and coexistence for the scenarios *parallel 0.01* (a-h) and *parallel 1* (i-p). Biomasses of the four autotrophic phenotypes (a-d, i-l), the autotrophs' maladaptive switching of A (e, m) and B (f, n), the autotroph coexistence patterns (g, o) and the consumer biomass (h, p). Higher biomasses or higher maladaptive switching are shown by darker colours. Lines separate the regions I-III of different autotroph coexistence. Grey areas in e, f, m, n depict areas where the species was extinct. Shaded areas in g and o depict oscillating systems (quarter-lag predator-prey cycles in dense shading, antiphase cycles in loose shading).

Plasticity can also promote coexistence, as the coexistence region now extends into former region Ib where the generalist A_d is highly defended (Fig. 5.2b, Fig. 5.3b). This is also an effect of maladaptive switching, though in this case the effect is indirect, mediated through the effect of

plasticity on consumer biomass. Without plasticity, coexistence was impossible in region Ib because B_d was always outcompeted by A_d: even though the latter had a slightly lower level of defence, this was outweighed by its higher growth rate, making A_d the superior competitor over B_d. However, plasticity changes this because maladaptive switching increases the consumer biomass, which in turn alters the cost/ benefit balance of defence: B_d derives a stronger benefit from its high level of defence, which now outweighs the cost and allows it to survive. Coexistence through this mechanism is not possible when the plasticity costs for B are too high or when A_d is too well-defended, explaining the narrowing of the coexistence "tail" for high defence of A_d (Fig. 5.3g).

While the patterns of coexistence changed when allowing for plasticity, the patterns in the trait values were nearly indistinguishable from the previous scenario (Appendix Fig. D1, D2). Finally, plasticity had a strong impact on the community dynamics, as most of the antiphase cycles were stabilized (Ib, II, III in Fig. 5.3g). Their area decreased sharply as these cycles were characterized by asynchronous dynamics between the two prey phenotypes, which were reduced by plasticity. In contrast, the area of the quarter-lag predator-prey cycles remained unaffected by plasticity.

All the above patterns were found to a far stronger degree with a higher amount of plasticity (χ_{max} = 1; Fig. 5.3i-p). Consumer biomass increased strongly everywhere (cf. Fig. 5.3h, p), reflecting the strong increase in the degree of maladaptive switching (cf. Fig. 5.3e, f, m, n). The higher exchange rates led to more synchronization between the phenotypes, extinguishing the antiphase cycles completely (Fig. 5.3p). It also decreased the biomass of both defended phenotypes (cf. Fig. 5.3b, d, j, l). This in turn led to a lower community defence and a higher community growth rate (Appendix Fig. D3) both contributing to a higher consumer biomass. Finally, there was a sharp decrease in the coexistence region for high plasticity (Fig. 5.3o). Region II, where B outcompetes A through maladaptive switching, doubled in size due to the much higher degree of maladaptive switching (Fig. 5.3m, n). Region I, where A outcompetes B, now also increased, when the level of defence of A_d is relatively low (Fig. 5.3o). This is again an indirect effect of maladaptive switching causing a strong increase in consumer biomass, affecting the cost/ benefit balance of defence: while B_d derives a strong

benefit from its high level of defence, B_u is completely undefended, and is at an extra disadvantage because of its low growth rate. Thus, while B_d would have been able to survive by itself, the high exchange rate causes a strong source-sink dynamic which drives *B* extinct.

Effect of plasticity in constellations *crossing* and *angle*

In constellation *crossing* the trade-off lines of both species cross in the trait space, as the level of defence is the same for both defended phenotypes; species B has a lower growth rate for its undefended phenotype than species *A* due to plasticity costs, while its defence costs are low and thus the growth rate of its defended phenotype is higher than for species A (Tab. 5.1, Appendix Fig. D4). Without plasticity the crossing trade-off lines lead to coexistence of both species in all simulations as A_u and B_d were always the only survivors, mostly showing antiphase oscillations (Appendix Fig. D4).

Allowing for phenotypic plasticity has the same results as were observed for constellation *parallel*: consumer biomass sharply increases (Fig. 5.4a, e); antiphase cycles are dampened or absent; and the area of coexistence decreases (Fig. 5.4b, f). All these changes are more pronounced for higher exchange rates (cf. Fig. 5.4a, b, e, f). Again, the biomass of the defended phenotypes decreased for high exchange rates (Appendix Fig. D5). Switching was always maladaptive for high exchange rates (Fig. 5.4g, h), and mostly maladaptive for low exchange rates (Fig. 5.4c, d). As was seen for constellation *parallel*, maladaptive switching was the reason for the decrease in coexistence. *B* can outcompete *A* when *B* has low plasticity costs. B_d has a much higher growth rate than A_d, while the undefended phenotypes have similar growth rates. The direction of competitive exclusion between A_u and B_u is thus easily reversed by B_d donating biomass to the sink B_u, allowing *B* to occupy both niches and outcompete *A* (region II in Fig. 5.4b, f). The same mechanism happens in reverse for high plasticity and defence costs of *B*: the differences in growth rate for the undefended phenotypes are high, while the defended phenotypes have very similar growth rates. A_u can support A_d, and *A* outcompetes *B* (region III in Fig. 5.4b, f).

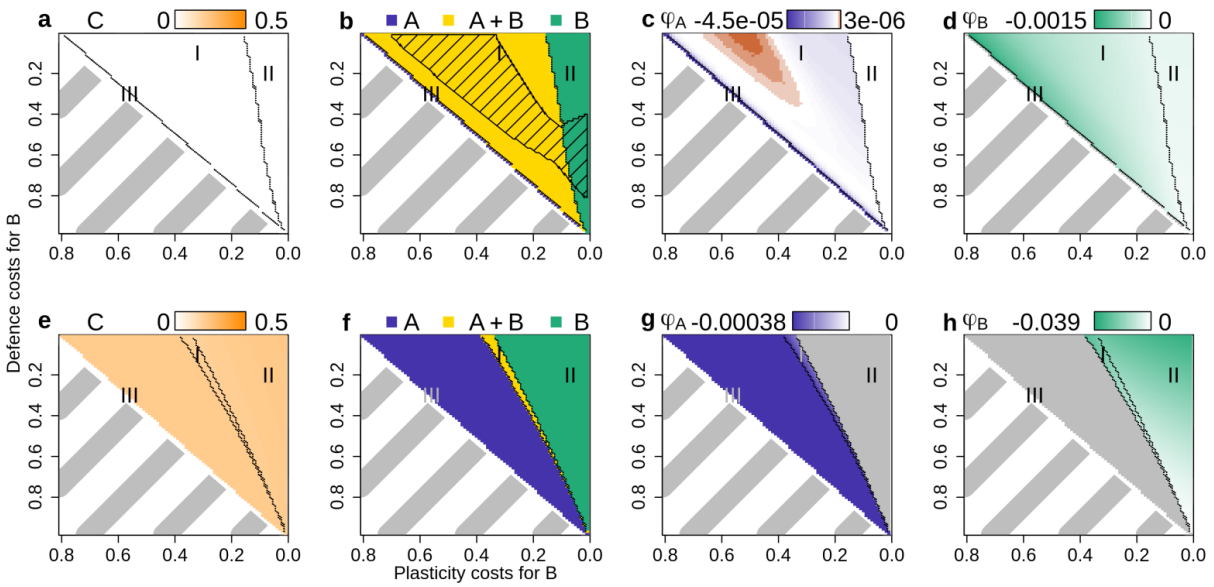

Fig. 5.4: Coexistence and maladaptive switching for scenario *crossing 0.01* (a-d) and *crossing 1* (e-h). Consumer biomass (a, e), the autotroph coexistence patterns (b, f), and the autotrophs' maladaptive switching (c, d, g, h) (higher biomasses or more intensive maladaptive switching are shown by darker colours). Lines separate the regions I-III of different autotroph coexistence. Shaded areas in b depict antiphase cycles. Grey areas in c, d, g, h depict areas where the species was extinct. Shaded grey areas depict areas without simulations (cf. methods). Note that c, d, g, h have each a different colour scale.

In constellation *angle* there are no plasticity costs, and thus the undefended phenotypes A_u and B_u have identical growth rates. The defended phenotypes take the same places in trait space as in the *parallel* constellation: A_d is a generalist, with a lower level of defence and a relatively high growth rate due to low defence costs, whereas B_d is a defence-specialist with a high level of defence but a low growth rate. This leads to the trade-off lines forming an angle (see Tab. 5.1). Without phenotypic plasticity, the coexistence patterns are the same as in constellation *parallel*, except that no competitive exclusion occurs between the undefended phenotypes; instead, they neutrally coexist in regions Ib, II and III (Appendix Fig. D6; cf. Fig. 5.2).

With plasticity, neutral coexistence vanished: the defended phenotype that survived (A_d in region Ib, B_d in region III) could support the undefended phenotype of its own species, driving the other species extinct (Fig. 5.5b, f). As in the other constellations, the area of coexistence and the biomasses of the defended phenotypes decreased and antiphase cycles vanished with

increasing χ_{max} (Fig. 5.5b, f, Appendix Fig. D7), while maladaptive switching and the consumer biomass increased (Fig. 5.5).

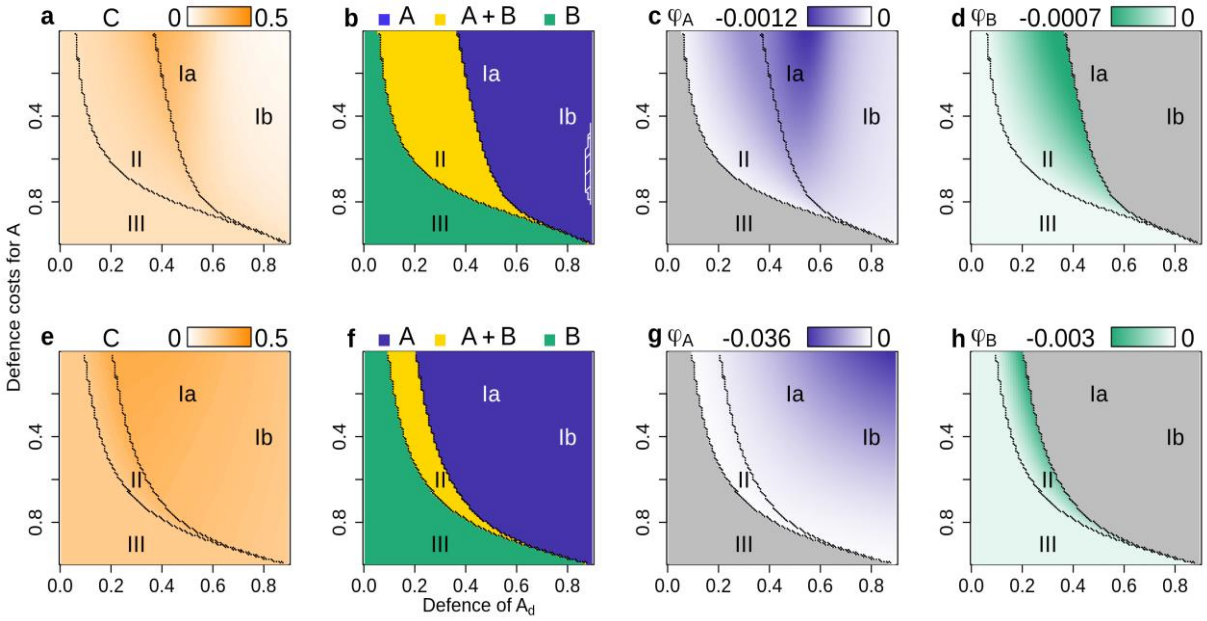

Fig. 5.5: Coexistence and maladaptive switching for scenario *angle 0.01* (a-d) and *angle 1* (e-h). Consumer biomass (a, e), the autotroph coexistence patterns (b, f), and the autotrophs' maladaptive switching (c, d, g, h) (higher biomasses or more intensive maladaptive switching are shown by darker colours). Lines separate the regions I-III of different autotroph coexistence. Shaded areas in b depict antiphase cycles. Grey areas in c, d, g, h depict areas where the species was extinct. Note that c, d, g, h have each a different colour scale.

General results

As plasticity had very similar effects across all three constellations, we here generalize our results: we compare the three constellations for exchange rates over 5 orders of magnitude, as well as the non-plastic scenario and the rigid scenario (Tab. 5.1).

For all constellations, the fraction of simulation runs in the trait space leading to coexistence was highest in the non-plastic scenario and decreased with increasing χ_{max} (Fig. 5.6a-c). In constellation *parallel* the share of coexistence for increasing χ_{max} continuously decreased from 51% to 3% (Fig. 5.6a). In *crossing*, the share decreased from full to no coexistence (Fig. 5.6b). In *angle*, the share of coexistence was 88% in the non-plastic scenario when taking also neutral coexistence into account (Fig. 5.6c). Its

share decreased to 9% for a χ_{max} of 10 and increased again to 25% for the rigid scenario. Maladaptive switching increased for both species and all constellations for increasing χ_{max} (Fig. 5.6d-f). The increased plasticity led to a lower total autotroph biomass and a lower share of defended phenotypes (Fig. 5.6g-i), which resulted in higher consumer biomass (Fig. 5.6g-i).

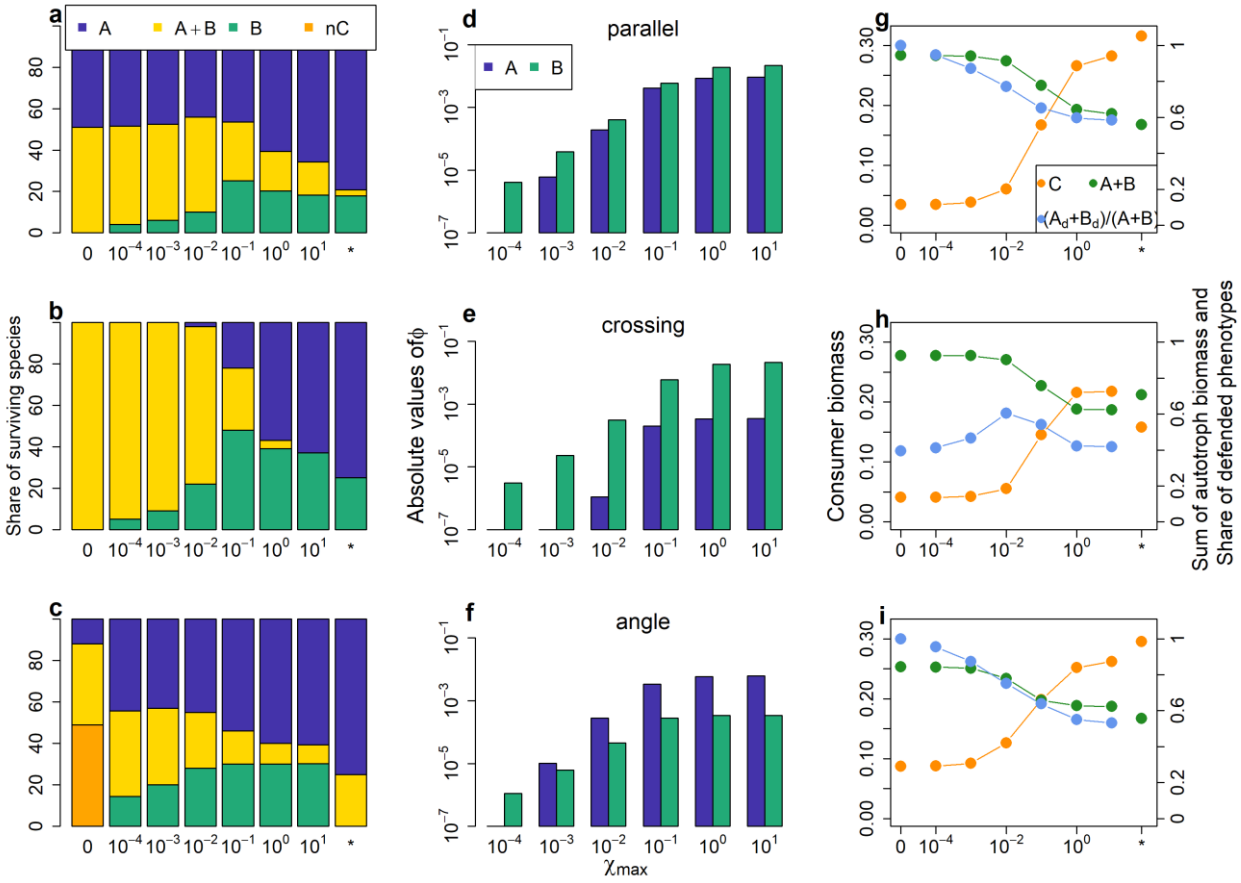

Fig. 5.6: General patterns for coexistence, maladapative switching and biomasses. Share of surviving species in percent (*A*, *B*, coexistence or neutral coexistence) (a-c), median absolute value of maladaptive switching φ (d-f) and median of total autotroph biomass (*A* + *B*), median consumer biomass and share of defended phenotypes ($(A_d+B_d)/(A+B)$) (g-i) for the three constellations and increasing maximum exchange rates χ_{max}. χ_{max} = 0 denotes the non-plastic scenario; * denotes the rigid scenarios. Maladaptive switching and the share of defended phenotypes do not apply for the rigid scenarios.

Interestingly, and counterintuitively, the above patterns show that increasing the speed of plasticity (by increasing χ_{max}) makes the system behave more like the rigid system. The coexistence patterns in scenarios with high χ_{max} approach those of the rigid scenarios in two of the

constellations (Fig. 5.6a, b). Similarly, the total autotroph and consumer biomasses approach the ones in the rigid scenarios (Fig. 5.6g-i). Thus, we found the higher χ_{max} make the autotrophs not more adaptive, but behave more like non-adaptive species.

Discussion

To understand the consequences of phenotypic plasticity, including the consequences of maladaptive switching, we investigated three trade-off constellations in a small food web of two plastic autotrophs and a shared consumer across different levels of plasticity. All constellations showed very consistent patterns: a higher speed of adaptation stabilized the dynamics, decreased the area of autotroph coexistence, increased the degree of maladaptive switching, and thus lowered total autotroph biomass and increased consumer biomass. It is well established that plasticity leads to stabilization[2–5,24], but the other patterns are more surprising. Most importantly, contrary to the intuitive expectation that plasticity in the defence of its prey is disadvantageous for a predator, as the prey can switch between undefended and defended phenotypes, we find it is beneficial for the predator as maladaptive switching enhances the biomass of its undefended prey.

Most of the patterns we found depend strongly on the result that, in the long term, plasticity results in maladaptive switching between phenotypes. To explain why this is such a common result, we started by considering a simplified non-plastic scenario: one autotroph with an undefended and defended phenotype A_u and A_d and one consumer. In this case, eventually A_u and A_d may settle at an equilibrium state where they have equal fitness[25] (provided that the balance between costs and benefits of defence enables their stable coexistence). At e.g. low defence costs, the equilibrium biomass of the defended phenotypes will be high while those of the undefended phenotypes and the consumer will be low. But if the autotrophs can switch, this picture changes: due to the low predation pressure, the switching rate from the defended towards the undefended phenotypes χ_d is high (cf. Fig. 5.1). Together with the higher biomass of A_d this results in a net biomass flow towards the undefended phenotypes. This pushes the phenotypes off their original equilibrium biomasses: A_u increases and A_d decreases, which in turn results in an increased consumer

biomass. This increases the benefit of defence for A_d, causing selection to push for an increase in the relative share of A_d while plastic switching continues to push in the opposite direction. Eventually A_u and A_d reach a new equilibrium where selection and switching balance each other out. Since selection is always adaptive (i.e. increasing the frequency of the high-fitness phenotype), and switching always acts to oppose selection at this equilibrium, switching is maladaptive (see Appendix D2). Higher switching rates exacerbate this process, and the phenotypes are pushed further away from their original equilibrium leading to a higher degree of maladaptive switching. As the switching rates increase, the shares of defended and undefended phenotypes approach 50:50 (Fig. 5.6g-i), and the system behaves more and more like the "rigid" baseline where each species has only a single phenotype and thus cannot adapt at all. Thus, counterintuitively, high switching rates appear to make the autotrophs less adaptive rather than more adaptive, resulting in a higher biomass for undefended phenotypes and thus a higher consumer biomass.

Plasticity also has consequences for competition, and thereby for coexistence of the two autotroph species. Without plasticity, species coexistence is determined by which phenotypes can coexist, which is determined by their locations in trait space[25] (see Appendix Fig. D8). Plasticity can change these coexistence patterns, allowing phenotypes to survive where they would have gone extinct without plasticity, or vice versa. A clear example is the survival of A_u and the extinction of B_u without plasticity (region II in Fig. 5.2), a pattern which was reversed by even a small amount of plasticity (region II in Fig. 5.3) through the source-sink dynamics generated by maladaptive switching. Such effects on survival are particularly likely to happen when the fitness difference between two competing phenotypes is small, as was the case between A_u and B_u in region II (Fig. 5.2I). Without plasticity A_u could always outcompete B_u, but because its growth rate was only slightly higher than that of B_u and B_d is a good competitor with high defence and only low plasticity costs, the biomass flow caused by plasticity could easily overwhelm this and allow B_u to survive instead. This allows one of the autotroph species to completely outcompete the other one under conditions when two non-plastic species coexisted. This result is very similar to the

effect of dispersal in metacommunities, where source-sink dynamics between patches can change coexistence and lead to the extinction of the locally superior competitor[26,27].

Plasticity can also affect coexistence indirectly: it causes an increase in consumer biomass, which affects the fitness of all phenotypes (increasing the fitness of well-defended ones and decreasing the fitness of undefended ones), which can in turn alter coexistence, sometimes increasing the coexistence range (Fig. 5.3g vs. Fig. 5.2e), but more often decreasing it (Fig. 5.3o vs. Fig. 5.2e). Thus, the combined effect of inducible defences on coexistence is highly complex, but overall it reduces the potential for competitive coexistence, and more strongly so for faster switching. While the notion that phenotypic plasticity may hinder coexistence is quite well established[28], current theory focuses on traits that are directly involved in competition and resource uptake, whereas in our system the effects of phenotypic plasticity are also mediated through the interaction between autotrophs and their consumer. Despite this difference, our conclusions are largely the same: inducible defences impact coexistence through their effect on niche differences and fitness differences[28]. Niche differences are reduced because the species can occupy broader niches through switching, while fitness differences are affected (sometimes increased and sometimes decreased) by maladaptive switching, as well as by the impact on consumer biomass. In addition, the source-sink dynamic arising from maladaptive switching equalizes phenotype biomasses at high switching rates, similar to how dispersal in metacommunities decreases inter-patch diversity due to homogenization[29], which reduces niche differences between the competing species further and further until their coexistence becomes impossible.

To represent inducible defences in our model, we used switching functions, which are commonly used for binary defence mechanisms where individuals can switch between discrete undefended and defended phenotypes[23]. Alternatively inducible defences can be modelled using the fitness gradient approach or the optimal gradient approach. Since the dynamical consequences of inducible defences can depend on the approach used[23], the impact on maladaptive switching, consumer biomass and coexistence may depend on the modelling approach as well. However,

directly measuring maladaptive switching as a consequence of plasticity is only possible with the switching function approach, since only this approach explicitly incorporates individual switching decisions. In contrast, the fitness gradient and optimal trait are phenomenological approaches, which consider the average trait in the population instead of modelling individual behaviour, thus making it impossible to measure maladaptive switching. The commonness of these approaches[23], and their underlying assumption that plastic decisions increase fitness, may have contributed to the way that maladaptive switching has long been unnoticed in theoretical studies on the ecological consequences of inducible defences.

Although our results show that switching is almost always maladaptive in the long run, it is important to note that plastic species most likely still have an advantage in the short term: as long as the environment is still variable, they can quickly defend against predators when predation pressure is high and save these costs for their defence when predation pressure is low. On the long term, however, plasticity stabilizes the predator-prey dynamics[2,24], and thus plastic species remove their own advantage of a variable environment in which they have a competitive advantage[2]. As natural food web dynamics are complex and include many species and are subject to temporal variation in abiotic conditions, the stabilizing impact of plasticity may be less strong under natural conditions. Although predator oscillations have been shown to be dampened by inducible defences[3], they may not disappear entirely, and the degree of maladaptive switching may therefore be less severe in nature than found in our model.

Overall, our results show very consistent patterns: a higher switching rate stabilized the dynamics, decreased the area of coexistence for both autotrophic species and increased the degree of maladaptive switching and the consumer biomass. Thus, we conclude that inducible defences can be a double-edged sword: a plastic species may outcompete its competitors via source-sink dynamics, but the negative impact of maladaptive switching can also lower its biomass or even drive it extinct. Plasticity can also have both negative and positive impacts on the food web level: when species are outcompeted, the food web diversity decreases; but the system is stabilized which may prevent further species loss due to strong oscillations.

Moreover, energy transfer to higher trophic levels is enhanced as more undefended prey are available to the consumer due to maladaptive switching. Maladaptive switching may also prevent plastic species from becoming Darwinian Demons counteracting the extinction of other species. Finally, maladaptive switching may also contribute to the fact that plasticity is not universal, despite its seemingly obvious advantages in rapidly changing environments prevailing almost everywhere. Overall, the striking impact of maladaptive switching on species and food web dynamics indicates that this mechanism may be of critical importance for large-scale effects of inducible defences. To what extent these effects can be generalized to more trophic levels and larger food webs under externally forced environmental conditions will be an important subject for future investigations.

Methods

Food web structure

We consider a food web with two plastic autotroph species A and B, having each an undefended (A_u resp. B_u) and a defended (A_d resp. B_d) phenotype. The autotrophs compete for the same resources (modelled as a shared carrying capacity) and are predated on by a joint consumer C (Fig. 5.1b).

Phenotype j of autotroph species i grows logistically with a growth rate r_{ij} and a carrying capacity K_{ij} (equations 5.1-5.4). It is grazed by the consumer following a Holling type II functional response with attack rate a_{ij} and handling time h. Switching between two phenotypes of the same species is represented by the exchange rates χ_i. The consumer C converts the captured biomass with a conversion efficiency ε into own biomass, and dies with a death rate δ (equation 5.5).

Defence is modelled as a binary trait: a species expresses either an undefended or a defended phenotype, e.g. either it grows spines or does not. A second parameter is the defence value, analogous to the spine length of an algal species protecting algae less or more against their predators. The undefended phenotypes have a defence value of 0, (i.e. no defence), while the defended ones have a defence value d_{ij} between 0.01 and 0.9, meaning 1 to 90% of the biomass cannot be consumed by the consumer.

Defence is modelled as a pre-attack defence against the consumer as it scales the maximum attack rate a[30] (Equation 5.7).

per capita growth mortality exchange

$$\dot{A}_u = r_{Au}\left(1 - \frac{A_u + A_d + B_u + B_d}{K_{Au}}\right)A_u - \frac{a_{Au}A_uC}{1 + h(a_{Au}A_u + a_{AD}A_d + a_{Bu}B_u + a_{Bd}B_d)} - \chi_u A_u + \chi_d A_d \quad (5.1)$$

$$\dot{A}_d = r_{Ad}\left(1 - \frac{A_u + A_d + B_u + B_d}{K_{Ad}}\right)A_d - \frac{a_{Ad}A_dC}{1 + h(a_{Au}A_u + a_{AD}A_d + a_{Bu}B_u + a_{Bd}B_d)} + \chi_u A_u - \chi_d A_d \quad (5.2)$$

$$\dot{B}_u = r_{Bu}\left(1 - \frac{A_u + A_d + B_u + B_d}{K_{Bu}}\right)B_u - \frac{a_{Bu}B_uC}{1 + h(a_{Au}A_u + a_{AD}A_d + a_{Bu}B_u + a_{Bd}B_d)} - \chi_u B_u + \chi_d B_d \quad (5.3)$$

$$\dot{B}_d = r_{Bd}\left(1 - \frac{A_u + A_d + B_u + B_d}{K_{Bd}}\right)B_d - \frac{a_{Bd}B_dC}{1 + h(a_{Au}A_u + a_{AD}A_d + a_{Bu}B_u + a_{Bd}B_d)} + \chi_u B_u - \chi_d B_d \quad (5.4)$$

$$\acute{C} = \left(\frac{\varepsilon(a_{Au}A_u + a_{AD}A_d + a_{Bu}B_u + a_{Bd}B_d)}{1 + h(a_{Au}A_u + a_{AD}A_d + a_{Bu}B_u + a_{Bd}B_d)} - \delta\right)C \quad (5.5)$$

$$r_{ij} = r\,(1 - pc_i - dc_i\,d_{ij}), i \in \{A, B\}, j \in \{u, d\} \quad (5.6)$$

$$a_{ij} = a\,(1 - d_{ij}), i \in \{A, B\}, j \in \{u, d\} \quad (5.7)$$

$$K_{ij} = K\,(1 - 0.1pc_i - 0.1dc_i\,d_{ij}), i \in \{A, B\}, j \in \{u, d\} \quad (5.8)$$

$$\chi_u = \frac{\chi_{max}}{1 + e^{b(C^* - C)}} \quad (5.9)$$

$$\chi_d = \chi_{max}\left(1 - \frac{1}{1 + e^{b(C^* - C)}}\right) \quad (5.10)$$

Trade-offs

Trade-offs define the possible combinations of trait values a species can have under the given biological and energetic constraints, i.e. a species cannot optimize all its traits (defence d_{ij} and maximum growth rate r_{ij}) simultaneously. An illustration of the possible trait combinations is shown in Fig. 5.1a. The phenotypes' positions in the trait space of r_{ij} and d_{ij} are defined by three trade-off properties, their defence d_{ij}, defence costs dc_i and plasticity costs pc_i. These define the phenotypes' location along the growth

rate axis and multiplied with the maximum growth rate r they define the growth rate r_{ij} (equation 5.6).

We assume that defended phenotypes always have a lower growth rate than their undefended counterparts of the same species due to resources needed to express the defence. The defence costs dc_i define the slope of the trade-off line between the growth rate r_{ij} and the defence d_{ij}, (Fig. 5.1a, equation 5.6). The plasticity costs are a reduction in growth rate for both phenotypes of a species, due to a high plasticity in expressing a range of defence, e.g. genetic information to sense predator abundance and put the defence into praxis that has to be carried along whether the phenotype produces the toxins or not (Fig. 5.1a, equation 5.6). As plasticity costs are only rarely found in experiments, we model also one constellation without plasticity costs (see Tab. 5.1).

The autotrophs face an additional trade-off between d_i and the capacity K_{ij} (equation 5.8). This trade-off is implemented in the same way as the one between d_{ij} and r_{ij}, but with only 10% of the strength. This second trade-off represents the costs of defence that manifest when resources are scarce (see e.g. [14,31–33]), e.g. a thick cell wall as defence which reduces the nutrient uptake, while the trade-off between r_{ij} and d_{ij} is the dominant one under rich resource conditions.

Exchange rates

Inducible defences with binary traits are well represented by switching functions[23] defining the exchange rate χ_j between the two phenotypes, which depends on the consumer biomass to represent grazing pressure. The exchange rate χ_u defines the switching from the undefended to the defended phenotypes, which increases with increasing consumer biomass as the defence is needed, while the exchange rate towards the undefended phenotype χ_d decreases with consumer biomass (Equations 5.9 – 5.10, Fig. 5.1c). The maximum exchange rate χ_{max} scales the exchange rates, and the steepness of the switching function is determined by b. The inflection point C^* denotes the point at which both exchange rates are equal (Fig. 5.1c). To ensure the inflection point has an ecologically reasonable value, we set it to half of the maximum consumer density in a simulation in which b is set to

zero, thus having a constant exchange rate of $\chi_{max}/2$. Other model parameters can be found in Appendix Tab. D1.

Scenarios

Varying two of the three trade-off properties (defence, defence costs and plasticity costs) and keeping the third one constant leads to three constellations *parallel*, *crossing*, and *angle* (Tab. 5.1). In all three, the autotrophic species B spans the entire defence range, i.e. it has a completely undefended phenotype B_u and a maximally defended phenotype B_d. Species A either has a more limited defence range (in constellations *parallel* and *angle*) or spans the entire range as well (in constellation *crossing*), representing three distinct ways that the trade-off between defence and growth may play out.

In constellation *parallel* both species have the same defence costs leading to parallel trade-off lines between defence and growth rate; A has a higher growth rate, but a lower plasticity range, whereas B has a lower growth rate due to plasticity costs, but a highly defended phenotype (Tab. 5.1, left column). Such a constellation was observed for *Daphnia pulex* clones[34] and for *Brachionus* species[35].

In constellation *crossing* the level of defence is the same for both defended phenotypes. The growth rate of B_u is lower than that of A_u due to plasticity costs, while the defence costs of B are low and thus the growth rate of B_d is relatively high. In contrast, A has a fast-growing undefended phenotype and high defence costs leading to a slow-growing defended phenotype. The trade-off lines of both species thus cross in the trait space (Tab. 5.1, middle column).

In constellation *angle* there are no plasticity costs[17], and thus the undefended phenotypes have identical growth rates. A_d has a high growth rate due to low defence costs but a smaller plasticity range, whereas B has high defence costs for its highly defended phenotype leading to a slow-growing but well defended phenotype. Due to the identical growth rate of the undefended phenotypes, both trade-off lines form an angle (Tab. 5.1, right column).

To investigate the effect of the speed of adaptation, we varied the maximum exchange rate χ_{max} between 10^{-4} and 10^{1} in 6 logarithmic steps. These simulations were also compared to a non-plastic baseline scenario where the exchange rates were set to zero, as well as to a completely non-adaptive scenario where each autotrophic species had only one intermediate phenotype (Tab. 5.1). This yielded 24 scenarios (three constellations *parallel*, *crossing*, *angle* with eight levels of adaptiveness

For each simulation run, the traits of all phenotypes were fixed. Phenotypic plasticity via the exchange rate was thus the only possibility for the species to adapt. For each constellation, two of the three properties were varied in 89 or 99 steps leading to 7921 or 8811 simulation runs per scenario to ensure a wide trait range being simulated. In constellation *crossing*, the combination of high plasticity and defence costs for B reduces the growth rate of its defended phenotype below zero; these simulations were excluded from the analysis (shaded grey areas in Fig. 5.4).

Modelling details and analysis

Each simulation was run for 100,000 time steps. The time series of the last 10,000 time steps were used for all calculations. For each simulation, we calculated the mean biomasses of each autotrophic phenotype and the consumer, their extinction status (a phenotype was regarded as extinct if its mean biomass was below 10^{-6}), autotroph coexistence, and the stability of community dynamics. The two autotrophs coexist if at least one phenotype of each species persists at the end of the simulation. The system was regarded as stable if the coefficient of variation, calculated for the always persistent consumer, was below 0.1. In addition to regular quarter-lag predator-prey cycles, we also found antiphase cycles[32,36] due to phenotype sorting. R (version 4.0.0) and the package deSolve was used for all simulations and the analysis.

Maladaptive switching

Whether switching is adaptive or maladaptive at any given point in time depends on whether more individuals switch from the lower-fitness phenotype to the higher-fitness phenotype (adaptive) or the reverse (maladaptive). A measure for adaptiveness or maladaptiveness in

switching thus needs to contain two elements: the net flow between the phenotypes, and the fitness difference between them. The relative net flow can, exemplary here for species A, be defined as:

$$\Delta_{\chi_A} = \frac{A_u \chi_u - A_d \chi_d}{A_u + A_d} \tag{5.11}$$

Note that $\Delta_{\chi A}$ measures the fraction of the autotroph species A that switches from the undefended to the defended state. When the undefended phenotype is dominant (and χ_u is not too low due to very low consumer biomasses), $\Delta_{\chi A}$ is positive and there is a relative net flow to the defended phenotype. In contrast, when the defended phenotype dominates (and χ_d is not too low due to very high consumer biomasses), $\Delta_{\chi A}$ is negative resulting in a relative net flow to the undefended phenotype.

The fitness difference is defined as:

$$\Delta_{F_A} = F_{Ad} - F_{Au}, \tag{5.12}$$

where F_{Au} and F_{Ad} represent the per capita net growth rates of the undefended and defended phenotypes, respectively (that is, the difference between their per capita growth and mortality terms; see equations 5.1-5.4).

If Δ_{χ_A} and Δ_{F_A} are both positive, there is net flow from undefended to defended phenotypes and defended phenotypes have higher fitness; switching is thus adaptive. The same is true if both terms are negative. On the other hand, if one of these two terms is positive and the other is negative, however, there is maladaptive switching: more individuals switch from the higher-fitness phenotype to the lower-fitness one than vice versa. Thus measuring adaptiveness can be done by multiplying these two terms together:

$$\varphi_A = \Delta_{\chi_A} \cdot \Delta_{F_A} \tag{5.13}$$

The interpretation of this measure is straightforward: switching is adaptive when $\varphi > 0$ and maladaptive when $\varphi < 0$, and more strongly so for larger absolute values of φ.

Author contributions

EVV and UG designed the study, NJK did the simulations, NJK, UG and EVV analysed the results and wrote the manuscript.

Acknowledgements

We thank Ralph Tollrian for profound stimulating ideas to design this study and Linda Weiss and Verena Bamberger for helpful comments on the manuscript. The research of NJK and EV is funded by the DFG (DynaTrait: GA 401/26-1/2).

References

1. Ghalambor, C. K., McKay, J. K., Carroll, S. P. & Reznick, D. N. Adaptive versus non-adaptive phenotypic plasticity and the potential for contemporary adaptation in new environments. *Funct Ecology* **21**, 394–407 (2007).

2. Yamamichi, M., Yoshida, T. & Sasaki, A. Comparing the Effects of Rapid Evolution and Phenotypic Plasticity on Predator-Prey Dynamics. *The American Naturalist* **178**, 287–304 (2011).

3. Verschoor, A. M., Vos, M. & van der Stap, I. Inducible defences prevent strong population fluctuations in bi- and tritrophic food chains. *Ecol Letters* **7**, 1143–1148 (2004).

4. Mougi, A. & Kishida, O. Reciprocal phenotypic plasticity can lead to stable predator-prey interaction. *Journal of Animal Ecology* **78**, 1172–1181 (2009).

5. van der Stap, I. *et al.* Algal defenses, population stability, and the risk of herbivore extinctions: a chemostat model and experiment. *Ecol Res* **24**, 1145–1153 (2009).

6. Tollrian, R. & Harvell, C. D. *The ecology and evolution of inducible defenses*. (Princeton University Press, 1999).

7. Lass, S. & Spaak, P. Chemically induced anti-predator defences in plankton: a review. *Hydrobiologia* **491**, 221–239 (2003).

8. Meester, L. D., Weider, L. J. & Tollrian, R. Alternative antipredator defences and genetic polymorphism in a pelagic predator–prey system. *Nature* **378**, 483–485 (1995).

9. Gilbert, J. J. & Hampton, S. E. Diel vertical migrations of zooplankton in a shallow, fishless pond: a possible avoidance-response cascade induced by notonectids: Notonectids and zooplankton migrations. *Freshwater Biology* **46**, 611–621 (2001).

10. Hessen, D. O. & van Donk, E. Morphological changes in Scenedesmus induced by substances released from Daphnia. *Arch. Hydrobiol.* **127**, 129–140 (1993).

11. Fyda, J. & Wiąckowski, K. Benefits and costs of predator-induced morphological changes in the ciliate Colpidium kleini (Protozoa, Ciliophora). *European Journal of Protistology* **34**, 118–123 (1998).

12. Jang, M.-H., Ha, K., Joo, G.-J. & Takamura, N. Toxin production of cyanobacteria is increased by exposure to zooplankton. *Freshwater Biology* **48**, 1540–1550 (2003).

13. Decaestecker, E., De Meester, L. & Ebert, D. In deep trouble: Habitat selection constrained by multiple enemies in zooplankton. *Proceedings of the National Academy of Sciences* **99**, 5481–5485 (2002).

14. Sampedro, L., Moreira, X. & Zas, R. Costs of constitutive and herbivore-induced chemical defences in pine trees emerge only under low nutrient availability: Costs of constitutive and induced pine tree defences. *Journal of Ecology* **99**, 818–827 (2011).

15. Pančić, M. & Kiørboe, T. Phytoplankton defence mechanisms: traits and trade-offs: Defensive traits and trade-offs. *Biol Rev* **93**, 1269–1303 (2018).

16. Nylund, G. M., Enge, S. & Pavia, H. Costs and Benefits of Chemical Defence in the Red Alga Bonnemaisonia hamifera. *PLoS ONE* **8**, e61291 (2013).

17. Relyea, R. A. Costs of Phenotypic Plasticity. *The American Naturalist* **159**, 272–282 (2002).

18. Herzog, Q., Tittgen, C. & Laforsch, C. Predator-specific reversibility of morphological defenses in Daphnia barbata. *J. Plankton Res.* **38**, 771–780 (2016).

19. Tollrian, R., Duggen, S., Weiss, L. C., Laforsch, C. & Kopp, M. Density-dependent adjustment of inducible defenses. *Sci Rep* **5**, 12736 (2015).

20. Kats, L. B. & Dill, L. M. The scent of death: Chemosensory assessment of predation risk by prey animals. *Écoscience* **5**, 361–394 (1998).

21. Weiss, L. C. *et al.* Rising pCO2 in Freshwater Ecosystems Has the Potential to Negatively Affect Predator-Induced Defenses in Daphnia. *Current Biology* **28**, 327-332.e3 (2018).

22. Scheiner, S. M. The genetics of phenotypic plasticity. XII. Temporal and spatial heterogeneity. *Ecol Evol* **3**, 4596–4609 (2013).

23. Yamamichi, M., Klauschies, T., Miner, B. E. & Velzen, E. Modelling inducible defences in predator–prey interactions: assumptions and dynamical consequences of three distinct approaches. *Ecol Lett* ele.13183 (2019) doi:10.1111/ele.13183.

24. Cortez, M. H. Comparing the qualitatively different effects rapidly evolving and rapidly induced defences have on predator-prey interactions: Rapidly evolved and induced defences. *Ecology Letters* **14**, 202–209 (2011).

25. Ehrlich, E., Becks, L. & Gaedke, U. Trait-fitness relationships determine how trade-off shapes affect species coexistence. *Ecology* **98**, 3188–3198 (2017).

26. Amarasekare, P. & Nisbet, R. M. Spatial Heterogeneity, Source-Sink Dynamics, and the Local Coexistence of Competing Species. *The American Naturalist* **158**, 572–584 (2001).

27. Engel, F. G. *et al.* Dispersal mitigates bacterial dominance over microalgal competitor in metacommunities. *Oecologia* **193**, 677–687 (2020).

28. Turcotte, M. M. & Levine, J. M. Phenotypic Plasticity and Species Coexistence. *Trends in Ecology & Evolution* **31**, 803–813 (2016).

29. Grainger, T. N. & Gilbert, B. Dispersal and diversity in experimental metacommunities: linking theory and practice. *Oikos* **125**, 1213–1223 (2016).

30. Ehrlich, E. & Gaedke, U. Not attackable or not crackable-How pre- and post-attack defenses with different competition costs affect prey coexistence and population dynamics. *Ecol Evol* **8**, 6625–6637 (2018).

31. Kraaijeveld, A. R. & Godfray, H. C. J. Trade-off between parasitoid resistance and larval competitive ability in Drosophila melanogaster. *Nature* **389**, 278–280 (1997).

32. Yoshida, T., Hairston, N. G. & Ellner, S. P. Evolutionary trade–off between defence against grazing and competitive ability in a simple unicellular alga, *Chlorella vulgaris*. *Proc. R. Soc. Lond. B* **271**, 1947–1953 (2004).

33. Meaden, S., Paszkiewicz, K. & Koskella, B. The cost of phage resistance in a plant pathogenic bacterium is context-dependent. *Evolution* **69**, 1321–1328 (2015).

34. Riessen, H. P. Costs of predator-induced morphological defences in Daphnia. *Freshwater Biology* **57**, 1422–1433 (2012).

35. Aránguiz-Acuña, A. *et al.* Benefits, costs and reactivity of inducible defences: an experimental test with rotifers: Reactivity of inducible defences in rotifers. *Freshwater Biology* **55**, 2114–2122 (2010).

36. Becks, L., Ellner, S. P., Jones, L. E. & Hairston Jr, N. G. Reduction of adaptive genetic diversity radically alters eco-evolutionary community dynamic. *Ecology Letters* **13**, 989–997 (2010).

6. Discussion

The previous four chapters each presented a research project on food webs and, with the exception of chapter 2, the way traits influence the species within. Different aspects of this topic were covered using a large variety of methods. First I modelled a food chain without traits investigating the impacts of respiration on the trophic transfer efficiency in the food chain. Then I analysed a long-term phytoplankton data set to validate the assumption of interspecific defence - growth trade-offs in natural systems. I moved on to a ciliate data set from the same lake to investigate which factors affect their net growth rate. Finally I studied the defence - growth trade-off in a small food web model investigating the influence of maladaptive switching on the coexistence of two competitors. I now link these chapters closer to build a more complete picture, starting with the food web theme they all belong to.

6.1 Planktonic food webs

I showed in my second chapter the importance of including both biomass-dependent basal respiration and assimilation-dependent activity respiration in allometric trophic network (ATN) models for depicting realistic trophic transfer efficiencies within a food chain. This is especially important for unicellular organisms and invertebrates which have partly low activity respiration (Simon, 1987) and are thus not well represented in the original ATN model compared to the extended model (Kath *et al.*, 2018). Food webs comprising many unicellular and invertebrate organisms are most affected, these are for example aquatic and soil food webs (de Ruiter *et al.*, 1998; Kalinkat *et al.*, 2013). There are several reasons why pelagic food webs are a good example for the food web modelled with the updated ATN model in chapter 2. First, several lower trophic levels in aquatic food webs consist mostly of unicellular organisms and invertebrates for which the extended version of ATN model including activity respiration makes a huge difference (Schuwirth and Reichert, 2013; Boit and Gaedke, 2014; Kath *et al.*, 2018). Second, four trophic levels are often reached in pelagic food webs which fits to the food chain presented in chapter 2 (Gaedke and Kamjunke, 2006; Boit and Gaedke, 2014; Kammerlander *et al.*, 2016). Third, the lower trophic levels in pelagic food webs usually consist of small, fast-growing organisms which

experience high amplitudes in their food concentrations, e.g. due to seasonal fluctuations. The organisms are adapted to these fluctuations and especially in starvation periods when the food concentration is low, basal respiration is important to describe their metabolism. Finally, as pelagic food webs are located in a three-dimensional habitat, the predators have no possibility to put down their captured prey, but have to swallow it immediately. This leads to a gape limitation as the largest prey an animal can hunt is one that fits into its mouth. As a consequence, organisms at higher trophic levels are larger than organisms at the lower trophic levels, fitting very well with the allometric parameterisation of ATN models. The high number of small invertebrates in pelagic food webs with their short generation times, and thus many generations within one season, makes pelagic food webs also a good system to study biomass-trait feedbacks theoretically and in natural systems. We want to take a closer look at the food web in Lake Constance.

6.2 Lake Constance

The datasets for chapter 3 and 4 originated from Lake Constance. Lake Constance is a large, monomictic, mesoeutrophic, deep lake in the North of the Alps. Because of its size of 472 km² and a mean depth of 101 m, some insights into processes in this lake might be also relevant for marine systems, e.g. vertical mixing into deeper water layers is a problem for phytoplankton being removed from the euphotic zone (Ehrlich *et al.*, 2020). The long-term data sets contain (bi-) weekly measurements for phytoplankton (1979-1999) and ciliates (1987-1998) as well as other zooplankton (rotifers 1987-1992, 1995-1996, daphnids and copepods 1979-1998), bacteria and autotrophic picoplankton (1987-1997), nutrients (1989-1997) and temperature (1979-1999). The data set stimulated a huge amount of research investigating e.g. the seasonal dynamics and variability of phytoplankton and ciliates, predator-prey relationships for ciliates and the calanoid copepod *Eudiaptomus*, the interplay of functional traits between phytoplankton and ciliates in spring, the carbon flow within the food web and seasonal changes of C:P ratios (Müller *et al.*, 1991; Gaedke, 1992; Gaedke *et al.*, 1996; Müller and Schlegel, 1999; Hochstädter, 2000; Tirok and Gaedke, 2007; Kunzmann *et al.*, 2019). Both the phytoplankton and the ciliate community are diverse and consist of small

organisms with short generation times and a high functional diversity. Phytoplankton is a well-studied group: a lot of research has been done on the relationship to their resources (Litchman and Klausmeier, 2001; Yoshiyama *et al.*, 2009; Schwaderer *et al.*, 2011; Burson *et al.*, 2018) and their predators, either the whole zooplankton community or the different effects of ciliates, rotifers, and daphnids (Knisely and Geller, 1986; Sommer *et al.*, 2003; Huber and Gaedke, 2006; Pomati *et al.*, 2020). This knowledge helped us to explain the defence-growth trade-off we found in Lake Constance: in spring, when losses due to mixing are high, fast-growing species dominate, while in summer grazing pressure is dominating and thus defended species gain in biomass (chapter 3). Phosphate affinity as a third trait is one factor explaining the differences between species with similar defence: species with high phosphate affinity such as *Rhodomonas* can have lower maximum growth rates and still high biomasses due to their advantage under nutrient-limited conditions in summer. Ciliates on the other hand are less studied and the few studies mainly investigated the ingestion rates and diet preferences or the potential predators of single species (Müller and Schlegel, 1999; Kunzmann *et al.*, 2019), so there is less knowledge about the ciliate community. Therefore, in chapter 4 we concentrated on the effects of both top-down and bottom-up processes on their net growth rates to know more about their role in the food web. While predation and competition seemed to be more important than food (Fig. 4.5 in chapter 4), temperature was the most important predictor of ciliate net growth rate, implying seasonal effects which calls for further investigations of the processes that change during the season next to temperature.

6.3 Methodical diversity

My chapters show a high methodical diversity: I used data analysis to prove the defence – growth rate trade-off in a phytoplankton community in chapter 3 and three different types of models in the chapters 2, 4 and 5. By choosing a model, modellers themselves experience a trade-off: models cannot maximise three traits simultaneously: realism, precision, and generality (Gross, 2013). Realism assumes that all model parameters and variables can be estimated from observations (Fig. 6.1). Precision means

that the model gives quantitative, accurate descriptions of the system. Generality means that the model can be applied to different systems.

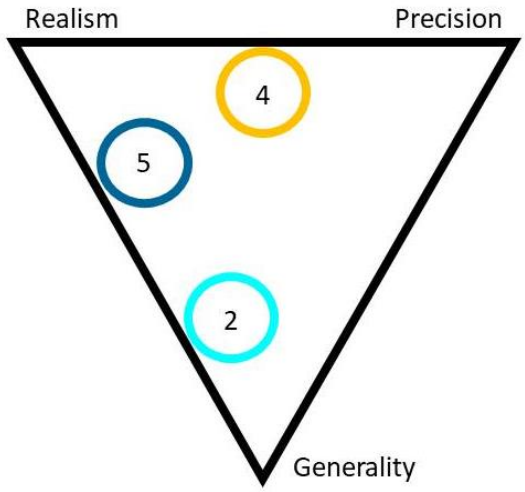

Fig. 6.1: Trait-offs for models and the position of the models from chapter 2, 4 and 5 within this model trait frame.

The allometric trophic network model from chapter 2 combined a high generality with an intermediate realism (Fig. 6.1). It can be parameterised with measurements e.g. for the conversion efficiency between trophic levels and many different food web processes can be investigated with these models because they are not tailored to a specific system, but rather general: allometric trophic network models were used to study theoretical coexistence, specific recent and Pleistocene food webs and pollination (Brose, 2008; Boit *et al.*, 2012; Di Giacomo and Fariña, 2017; Hale *et al.*, 2020). No precise predictions can be made with this model though, e.g. the specific production of a top predator barn owl depends on many factors and could thus not be well predicted with a general allometric trophic network model.

The boosted regression trees in chapter 4 combine an intermediate precision and realism (Fig. 6.1). They predict the net growth rates of ciliate morphotypes depending on environmental conditions as specific food concentrations, predator and competitor biomasses and temperature. As they are lined with observational data, they are tailored to a specific system, the ciliate morphotypes in Lake Constance. On the other hand, the predictions cannot be transferred easily to other conditions, e.g. zooplankton species in a tropical lake.

The small food web model on plasticity from chapter 5 has a high realism and an intermediate generality (Fig. 6.1). The parameters are based on an aquatic system and the concept of maladaptive switching could be investigated in detail and its general implications can be transferred to other systems, but no precise predictions, e.g. the biomass of an undefended alga in a lake can be made.

6.4 Trade-off details determine coexistence of two plastic species

Chapter 3 showed the first evidence for the defence-growth trade-off in a natural community and highlights the importance of the shape of the trade-off. When we developed the food web of two coexisting plastic autotrophs experiencing a defence-growth rate trade-off for chapter 5, we thought about the shape of this trade-off. Due to the lack of experimental data on this trade-off between plastic species, we decided for the simplest trade-off curve, a linear line. While we focused on the mechanisms for coexistence of the two plastic species as the maladaptive switching, a broader picture of the role of the trade-off properties is missing.

When we look at the difference between the defence values of the defended phenotypes of species A and B (for details concerning the food web and traits, see chapter 5), we can see differences between the simulations depending on which species are surviving (Fig. 6.2a). Species A won most often if its defence was only a little lower than the one of species B. Species B won most often if its defence was a lot higher than species A. When the difference of their defence values was intermediate both species most often coexisted.

When we look at the difference of defence costs between the species A and B, the pattern looks different (Fig. 6.2b). Species A won most often if its defence costs are lower than the defence costs of species B. Species B only won if the defence costs were close to equal, while both species coexist if species A had the higher defence costs.

When we look at the differences in plasticity costs between the species A and B, species B always have lower frequencies than survival of species A or coexistence (Fig. 6.2c). Both species coexisted if the plasticity costs of species B were a lot higher or very similar to the ones of species A. If the difference was intermediate, species A mostly won.

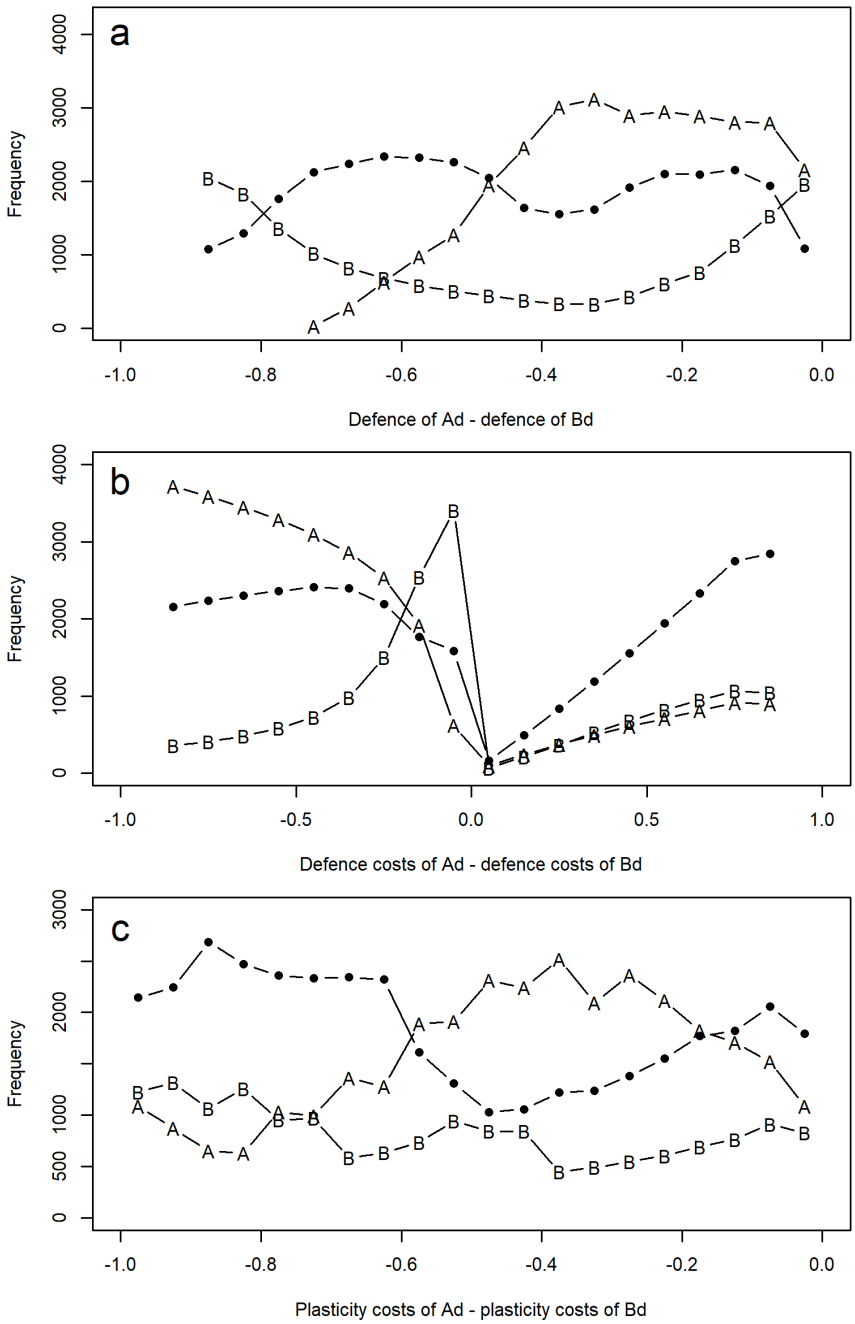

Fig. 6.2: Frequency distributions comprising all scenarios (non-plastic and plastic, not rigid one) depending on the difference in a) defence values of defended phenotypes, b) of absolute values of defence costs, c) plasticity costs between species A and B. A denotes simulations runs in which only phenotype(s) of species A survive(s), B denotes simulation runs in which only phenotype(s) of species B survive(s) and points denote simulation runs in which phenotypes of both species coexist. Constellation crossing is not included in panel a, parallel is not included in panel b, angle is not included in panel c as the respective property is the same for both species.

6.5 Comparison plasticity model with experimental data

The idea for the model on maladaptive switching in chapter 5 came from an experimental system with the autotroph algae *Chlorogonium* spec., the ciliate *Euplotes* feeding on the algae and the predatory flatworm *Stenostomum* feeding on *Euplotes*. *Euplotes* shows inducible defences, they can skip cell division and instead grow lateral wings (Trogant, personal communication).

Combining both experimental and model data in one project could lead to a better understanding of the system and higher citations, but it is not always possible due to delays in experiments or model setup, different communication styles, or time constraints especially for younger scientists (Heuschele *et al.*, 2017). I now compare the defence, growth and the trade-off between them between experimental data from the system mentioned above and our model from chapter 5 to link both. To focus on the interaction between the plastic prey and the non-plastic consumer, we modelled a food web with two trophic levels in which the plastic autotroph growth relies on a carrying capacity instead of explicitly modelled nutrients.

The growth rate of our modelled consumer is 0.21 per day (equal to its death rate). This is between the measured values for *Euplotes* and *Stenostomum* (Fig. 6.5a). As we explored different trade-off scenarios, our growth rates for the plastic autotrophs vary largely between 0.01 and 1 per day depending on the scenario (see chapter 5 for details).

The defence of *Euplotes* is measured as width [µm] standardised to the whole range of measured widths for all *Euplotes* cells. The mean defence averaged across all clones is similar for the undefended and the defended *Euplotes* indicating that the differences between clones are higher than the difference between defended and undefended phenotypes (Fig. 6.3b). In our model, we set the defence of our undefended autotrophs always to 0, while we vary the defence of the defended autotrophs between 0.01 and 1 in different scenarios (Fig. 6.3b). For both the experiments and the model, defence is a binary trait, so either the phenotypes express their defence or not. While in the experiments, all *Euplotes* express their defences as soon as they sense the predator-released kairomone in the water, the probability

to change to the defended phenotype is a smooth transition depending on the consumer biomass in the model (see chapter 5, Fig. 5.1). While we have modelled a pre-attack defence, the experiments seem to hint towards a post-attack defence (Trogant, personal communication).

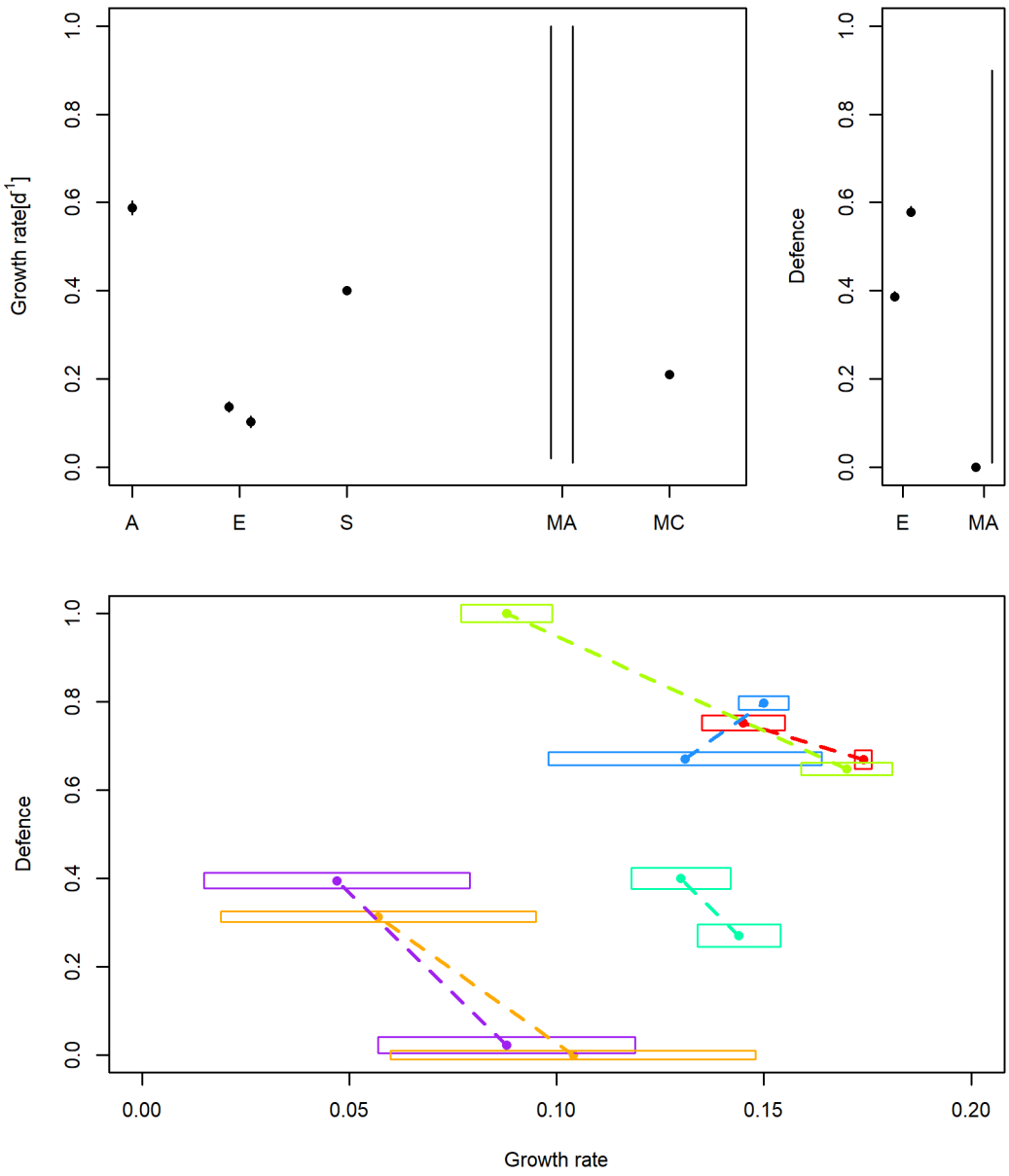

Figure 6.3: Growth rate, defence and trade-off between them for an experimental system (Trogant, personal communication) and model (chapter 5). For experiments, the standard error is plotted as lines/boxes, colours depict different clones. Abbreviations are A algae, E *Euplotes*, S *Stenostomum*, MA modelled algae, MC modelled consumer.

The trade-off lines between growth rate and defence form one of three clearly distinct constellations in our model, they are either parallel, crossing or form an angle. In contrast, the trade-off lines of the different

Euplotes clones overlap and do not show a clear pattern in the experiments (Fig. 6.3c).

The comparison of our model and the underlying experiments show that a model has to be adapted very closely to the data to deliver comparable results. We decided instead to explore the maladaptive switching which cannot be easily measured in experiments. Therefore we changed some properties of our model.

6.6. Perspective

The interplay between models and experiments is important for new ideas and theory building. Models can stimulate new ideas for experiments and field research (Fussmann *et al.*, 2000; van der Stap *et al.*, 2009), test ideas stimulated by experiments or field data (Ehrlich *et al.*, 2020) and build up new theories (Yamamichi *et al.*, 2019) and most of them rely on experimental data for their parameterisation or ideas for hypotheses to test.

It would be interesting to adapt the plasticity model from chapter 5 to an experimental system to test if the results on competition can be confirmed in experiments. To display some of the trade-off constellations of the two plastic species, very variable organisms would be needed. Different clones of small organisms as the ciliate *Euplotes* could be taken for that. Adding one consumer feeding on the *Euplotes* results in a small food web similar to the model. It would be interesting to test if the same trait combinations of the plastic species results in coexistence or competitive exclusion, respectively.

I would also like to try to better predict the ciliates' net growth rate from the Lake Constance data set from chapter 4. Probably more specific predictors have to be taken into account, e.g. different phytoplankton species for each ciliate. As it remained still unclear for many freshwater ciliates which phytoplankton species they consume, I would start with the few species for which some feeding links are known due to lab experiments as *Balanion planctonicum* (Müller, 1991; Müller and Schlegel, 1999; Weisse and Frahm, 2002). Additional feeding experiments with a variety of phytoplankton offered as food and a variety of zooplankton as possible predators for few ciliates which are important for the dynamics in Lake

Constance could help to understand food preferences and thus the tropic links around these ciliates.

The trade-off found in chapter 3 was already a basis for another paper (Ehrlich and Gaedke, 2020). I would like to investigate if this or other trade-offs can be found also in other lake communities. Next to defence and growth rate, nutrient and light traits would be interesting, as trade-offs between these are known (Litchman *et al.*, 2007; Edwards *et al.*, 2013) and we could also prove phosphate affinity played a role as a third trade-off axis (Ehrlich *et al.*, 2020).

References

Boit, A. *et al.* (2012) Mechanistic theory and modelling of complex food-web dynamics in Lake Constance: Mechanistic modelling of complex food web dynamics. *Ecol. Lett.*, **15**, 594–602.

Boit, A. and Gaedke, U. (2014) Benchmarking Successional Progress in a Quantitative Food Web. *PLoS ONE*, **9**, e90404.

Brose, U. (2008) Complex food webs prevent competitive exclusion among producer species. *Proc. R. Soc. B.*, **275**, 2507–2514.

Burson, A. *et al.* (2018) Competition for nutrients and light: testing advances in resource competition with a natural phytoplankton community. *Ecology*, **99**, 1108–1118.

Di Giacomo, M. and Fariña, R. A. (2017) Allometric models in paleoecology: Trophic relationships among Pleistocene mammals. *Palaeogeogr. Palaeoclimatol. Palaeoecol.*, **471**, 15–30.

Edwards, K. F. *et al.* (2013) Functional traits explain phytoplankton community structure and seasonal dynamics in a marine ecosystem. *Ecol. Lett.*, **16**, 56–63.

Ehrlich, E. *et al.* (2020) The shape of a defense-growth trade-off governs seasonal trait dynamics in natural phytoplankton. *ISME J.*, **14**, 1451–1462.

Ehrlich, E. and Gaedke, U. (2020) Coupled changes in traits and biomasses cascading through a tritrophic plankton food web. *Limnol. Oceanogr.*, **65**, 2502–2514.

Fussmann, G. F. *et al.* (2000) Crossing the Hopf Bifurcation in a Live Predator-Prey System. *Science*, **290**, 1358–1360.

Gaedke, U. (1992) The size distribution of plankton biomass in a large lake and its seasonal variability. *Limnol. Oceanogr.*, **37**, 1202–1220.

Gaedke, U. *et al.* (1996) Trophic structure and carbon flow dynamics in the pelagic community of a large lake. In Polis, G. A. and Winemiller, K. O. (eds), *Food Webs*. Springer, Boston, MA, pp. 60–71.

Gaedke, U. and Kamjunke, N. (2006) Structural and functional properties of low- and high-diversity planktonic food webs. *J. Plankton Res.*, **28**, 707–718.

Gross, L. J. (2013) Use of computer systems and models. In Levin, S. A. (ed), *Encyclopedia of Biodiversity*. Elsevier Inc., pp. 213–220.

Hale, K. R. S. *et al.* (2020) Mutualism increases diversity, stability, and function of multiplex networks that integrate pollinators into food webs. *Nat. Commun.*, **11**, 2182.

Heuschele, J. *et al.* (2017) On the missing link in ecology: improving communication between modellers and experimentalists. *Oikos*, **126**, 1071–1077.

Hochstädter, S. (2000) Seasonal changes of C:P ratios of seston, bacteria, phytoplankton and zooplankton in a deep, mesotrophic lake. *Freshw. Biol.*, **44**, 453–463.

Huber, V. and Gaedke, U. (2006) The role of predation for seasonal variability patterns among phytoplankton and ciliates. *Oikos*, **114**, 265–276.

Kalinkat, G. *et al.* (2013) Body masses, functional responses and predator-prey stability. *Ecol. Lett.*, **16**, 1126–1134.

Kammerlander, B. *et al.* (2016) Ciliate community structure and interactions within the planktonic food web in two alpine lakes of contrasting transparency. *Freshw. Biol.*, **61**, 1950–1965.

Kath, N. J. *et al.* (2018) Accounting for activity respiration results in realistic trophic transfer efficiencies in allometric trophic network (ATN) models. *Theor. Ecol.*, **11**, 453–463.

Knisely, K. and Geller, W. (1986) Selective Feeding of Four Zooplankton Species on Natural Lake Phytoplankton. *Oecologia*, **69**, 86–94.

Kunzmann, A. J. *et al.* (2019) Calanoid copepod grazing affects plankton size structure and composition in a deep, large lake. *J. Plankton Res.*, **41**, 955–966.

Litchman, E. *et al.* (2007) The role of functional traits and trade-offs in structuring phytoplankton communities: scaling from cellular to ecosystem level. *Ecol. Lett.*, **10**, 1170–1181.

Litchman, E. and Klausmeier, C. A. (2001) Competition of Phytoplankton under Fluctuating Light. *Am. Nat.*, **157**, 170–187.

Müller, H. (1991) *Pseudobalanion planctonicum* (Ciliophora, Prostomatida): ecological significance of an algivorous nanociliate in a deep meso-eutrophic lake. *J. Plankton Res.*, **13**, 247–262.

Müller, H. *et al.* (1991) Seasonal succession of ciliates in lake constance. *Microb. Ecol.*, **21**, 119–138.

Müller, H. and Schlegel, A. (1999) Responses of three freshwater planktonic ciliates with different feeding modes to cryptophyte and diatom prey. *Aquat. Microb. Ecol.*, **17**, 49–60.

Pomati, F. *et al.* (2020) Interacting Temperature, Nutrients and Zooplankton Grazing Control Phytoplankton Size-Abundance Relationships in Eight Swiss Lakes. *Front. Microbiol.*, **10**, 3155.

de Ruiter, P. C. *et al.* (1998) Biodiversity in soil ecosystems: the role of energy ¯ow and community stability. *Appl. Soil Ecol.*, **10**, 217–228.

Schuwirth, N. and Reichert, P. (2013) Bridging the gap between theoretical ecology and real ecosystems: modeling invertebrate community composition in streams. *Ecology*, **94**, 368–379.

Schwaderer, A. S. *et al.* (2011) Eco-evolutionary differences in light utilization traits and distributions of freshwater phytoplankton. *Limnol. Oceanogr.*, **56**, 589–598.

Simon, M. (1987) Biomass and production of small and large free-living and attached bacteria in Lake Constance. *Limnol. Oceanogr.*, **32**, 591–607.

Sommer, U. *et al.* (2003) Daphnia versus copepod impact on summer phytoplankton: functional compensation at both trophic levels. *Oecologia*, **135**, 639–647.

van der Stap, I. *et al.* (2009) Algal defenses, population stability, and the risk of herbivore extinctions: a chemostat model and experiment. *Ecol. Res.*, **24**, 1145–1153.

Tirok, K. and Gaedke, U. (2007) Regulation of planktonic ciliate dynamics and functional composition during spring in Lake Constance. *Aquat. Microb. Ecol.*, **49**, 87–100.

Weisse, T. and Frahm, A. (2002) Direct and indirect impact of two common rotifer species (*Keratella* spp.) on two abundant ciliate species (*Urotricha furcata* , *Balanion planctonicum*): Rotifer impact on ciliates. *Freshw. Biol.*, **47**, 53–64.

Yamamichi, M. *et al.* (2019) Modelling inducible defences in predator–prey interactions: assumptions and dynamical consequences of three distinct approaches. *Ecol. Lett.*, ele.13183.

Yoshiyama, K. *et al.* (2009) Phytoplankton Competition for Nutrients and Light in a Stratified Water Column. *Am. Nat.*, **174**, 190–203.

Appendix A: Supplementary information for chapter 2

Manuscript is available at http://link.springer.com/article/10.1007/s12080-018-0378-z.

We also modelled a three trophic level food chain in which the carnivore has a density dependent death rate equivalent to the top predator in the chain of four trophic level (Eq. 2.4). With this model setup, we examined the herbivore's obtained TTE when being released from top-down control due to increasing the carnivore's death rate.

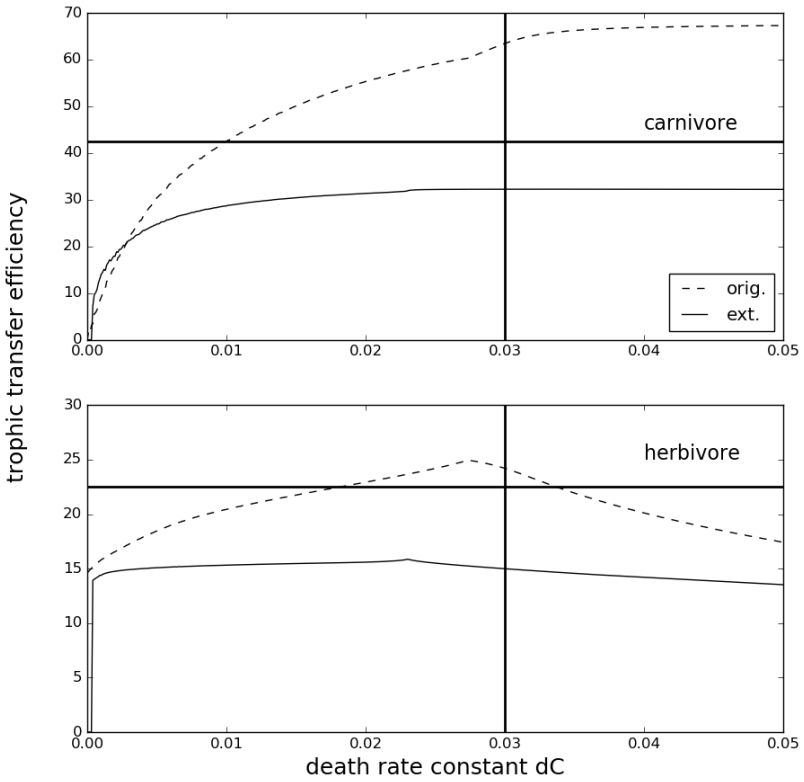

Fig. A1: Trophic transfer efficiency (obtained TTE, defined as the production ratio of upper vs. lower trophic level) of the carnivore (upper panel) and herbivore (bottom) in the original (dashed lines) and extended (solid lines) ATN version for different carnivore's death rate constants d. For one parameter value (vertical line), the biomass pyramids are provided in Fig. A2. The horizontal lines indicate the maximum feasible TTE (Eq. 2.10, Tab. 2.2)

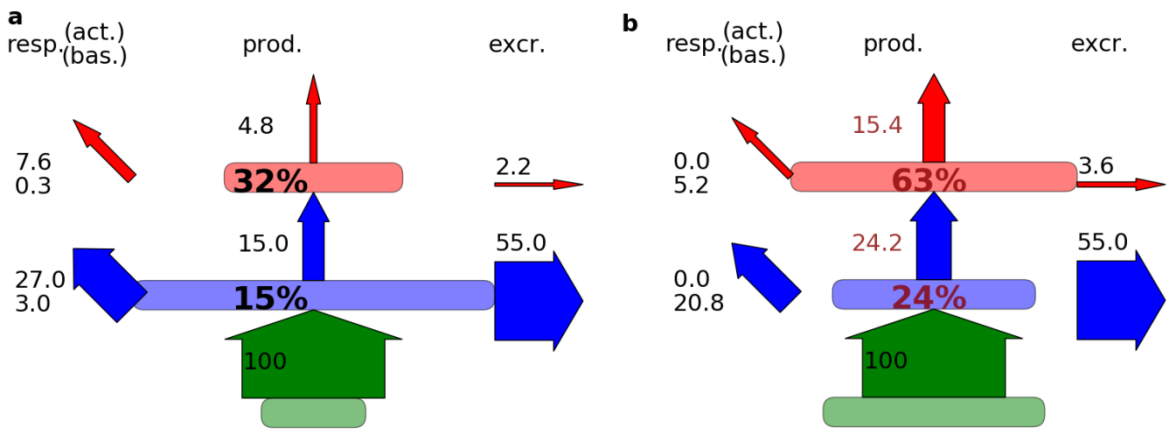

Fig. A2: Comparison of the energy transfer within a three trophic level food chain of the extended ATN version including activity respiration (a), and the original ATN model (b). The biomass pyramids are based on the parameter indicated in Fig. A1, i.e. d= 0.03. Included values are basal and activity respiration (numbers on the left, activity above basal respiration), production (numbers in the middle to the left of the upward arrows), trophic transfer efficiency (bold large numbers), and excretion (numbers above the right arrows). All fluxes are standardized to autotroph's production as 100%, so that wider arrows indicate larger values. Box widths are scaled with the species' biomasses. Red values point out inconsistencies with the physiological considerations that respiration is equal to or less than production (Humphreys 1979)

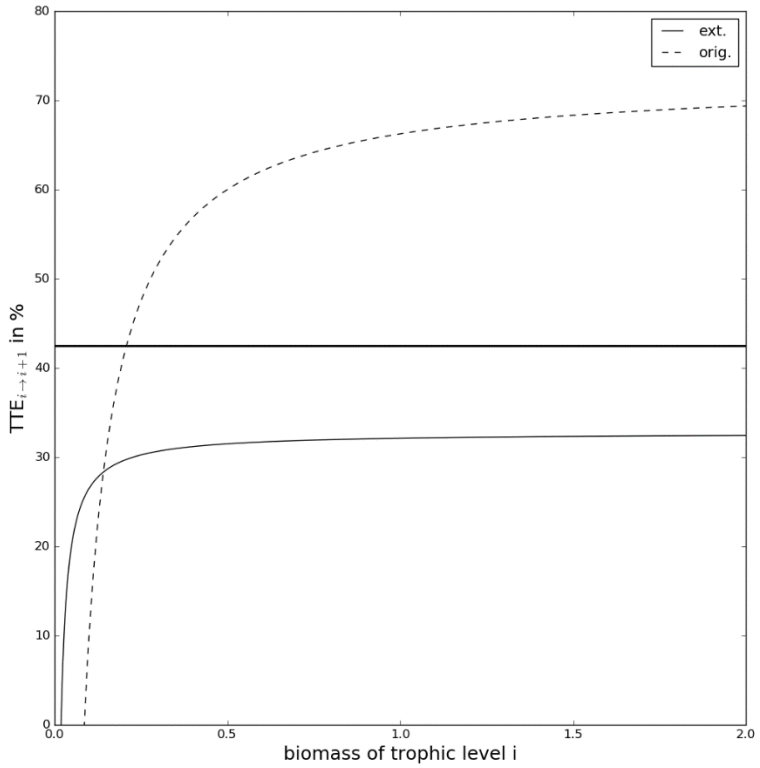

Fig. A3: Trophic transfer efficiency (obtained TTE in %, defined as the production ratio of upper vs. lower trophic level) of a trophic level $i+1$ (here parameterized for both the carnivore and the top predator as they have the same assimilation efficiency) in the original (dashed line) and extended (solid line) ATN version for different food quantities (biomass of the lower trophic level i). The horizontal line indicates the maximum feasible TTE (Eq. 2.10, Tab. 2.2)

Appendix B: Supplementary information for chapter 3

The manuscript is available at https://www.nature.com/articles/s41396-020-0619-1.

The supplement includes five appendices. The first appendix contains information about sampling and data processing. The second appendix provides details on the trait data. The third appendix describes supporting results (trait correlations with phosphate affinity and size, and re-oligotrophication patterns). The fourth and fifth appendix include model details and results.

Appendix B1: Methodical details

Classification of seasonal phases

We subdivided the year into 7 consecutive phases to minimize inter-annual variability due to different climatic conditions. These phases are late winter, early spring, late spring, clear water phase, summer, autumn and early winter (Fig. 3.2). The start and end of each phase was mostly not a fixed calendar date but was determined for each year based upon threshold values of independent physical (vertical mixing, temperature, water transparency), chemical (soluble reactive phosphorous concentration) and/or biological parameters (phytoplankton and zooplankton biomass, chlorophyll concentration and species composition)[1–3]. For example, early spring is defined to start when the chlorophyll concentration and algal biomass start to increase, and the clear-water phase when the chlorophyll concentration and algal biovolume fall below a certain value and the Secchi depth surpasses a distinct level.

Each period is associated with a different well-defined forcing regime. (i) First, during late winter deep mixing and low irradiance lead to a decrease of plankton biomass to the annual minimum level. (ii) Early spring is characterized by unstable stratification, variable underwater light climate, low grazing pressure and high, non-limiting nutrient concentrations, which enables the first growth of algae and some grazers interrupted by mixing events. (iii) During late spring algal biomass further increases with the onset of thermal stratification which reduces nutrient concentrations. The high biomass of mostly small, edible algae promotes growth of different

groups of micro- and meso-zooplankton. Grazing pressure mostly by ciliates increases. (iv) As a consequence, phytoplankton biomass strongly declines, resulting in the clear water phase, which is characterized by the strongest grazing pressure throughout the year, mainly caused by meso-zooplankton as daphnids. Nutrient concentrations re-increase during the clear water phase due to remineralization and with decreased grazing pressure, the summer phytoplankton bloom starts. (v) Summer is marked by severe nutrient depletion leading to strong competition within the phytoplankton community, and the relevance of different zooplankton groups (ciliates, rotifers, cladocerans and copepods) with different feeding strategies and grazing on different groups of phytoplankton. (vi) An increase of the mixing depth as autumn begins leads to a minor reduction of algal biomass and replenishing of nutrients from deeper water. The increase in nutrients may give rise to an autumn phytoplankton and crustacean maximum, paralleled by shifts in algal species composition. (vii) Early winter starts in mid of November and is characterized by an increasing intensity of deep mixing and low irradiance.

Standardized time

The duration of the seasonal phases varied among years. To account for this meteorological year-to-year variation, we aligned the sampling dates to a standardized time axis. First, each sampling date (e.g., day 25 in phase 2 in 1986) was scaled relative to the duration of the respective phase in that year (e.g. phase 2 lasts 50 days in 1986) resulting in the relative sampling day (e.g. 25/50). Multiplying the relative sampling day with the inter-annual mean duration of the respective phase (e.g. 46 days) yields the standardized day number of that sampling date (e.g. 25/50*46=23). Based on this method each sampling date can be assigned to a certain week in a standardized year (data see https://doi.org/10.6084/m9.figshare.11830464.v1). To display the seasonal biomass dynamics (shown in Fig. 3.2), we took the inter-annual median and quartiles of the biomass data for every standardized week and then smoothed the data by averaging the medians/quartiles of two adjacent weeks (moving average).

Aggregation of species into morphotypes

We used an intermediate level of taxonomic resolution distinguishing 36 morphotypes to achieve taxonomic consistency across the long sampling period. Each of these morphotypes contributed at least 5% to the biovolume of total phytoplankton at an individual sampling date during 1979-1982, i.e. the information about rare species got lost for the years 1979-1982. Considering the years 1979-1999, these 36 morphotypes comprise about 92% of total phytoplankton biomass. We omitted counts of morphotypes which could either not be identified, were very rare or encountered only during individual sampling events or short periods. Given its improved reliability for long-term studies we used this dataset in previous studies as well[1,4–6]. Details can also be found in LakeBase (https://fred.igb-berlin.de/Lakebase).

Mean relative biomasses

To evaluate the relative importance of a phytoplankton morphotype over the 21 years of sampling, we derived its mean annual relative biomass as follows: First, we calculated the relative biomass of each morphotype for every sampling date. Second, we averaged these relative biomasses among all dates within each year which yields the corresponding annual relative biomass of each morphotype. Finally, we derived the mean of these annual relative biomasses across years. This procedure reduces the influence of outliers at single dates, and gives equal weight to all sampling dates per year and all years, which partly differed in their total biomass and sampling resolution. The relative importance of each morphotype during distinct seasonal phases (e.g., early spring) were computed accordingly by considering only the relative biomasses of the dates within that phase (data see https://doi.org/10.6084/m9.figshare.11830464.v1). The calculated mean relative biomasses allowed to infer the respective biomass-trait distributions since each morphotype represented a specific trait combination.

C:P ratio

We used the cellular carbon to phosphate mass ratio of phytoplankton (C:P) as an indicator for nutrient depletion which was measured at the standard sampling site in 1995 (data see https://doi.org/10.6084/m9.figshare.11830464.v1)[7]. The cellular C:P is

more informative than the ambient phosphorous concentration in the water as phytoplankton can store phosphorous. Furthermore, most phytoplankton species can take up substantial amounts of phosphorous even at concentrations below the detection limit as they prevail in Lake Constance throughout summer.

Vertical mixing intensity

Given the large depth of the lake, most biological activity and thus sampling effort was concentrated on the upper 0-20 m depth. Thus, we report here the mean biomasses averaged across this water layer. As the surface phytoplankton concentration is usually much higher than in deep strata, deep vertical mixing (i.e. down to 60 or 100m depth) implies a net export from the surface to larger depths. To quantify this phytoplankton export, the vertical mixing intensity was inferred from a one-dimensional hydrodynamic K - ε turbulent exchange model[8,9] and expressed as net exchange rate from the uppermost layer (0-8 m) to the deepest layer (20-100 m). Its temporal dynamics is closely related to the net exchange rate from 0-20 m to 20-100 m and to the observed phytoplankton net growth during spring (data see https://doi.org/10.6084/m9.figshare.11830464.v1).

Appendix B2: Trait data

Tab. B1: Morphotype number and name, its assigned trait values of defense δ, maximum growth rate r (d^{-1}) and phosphate affinity ($d^{-1}\mu mol^{-1}L$) according to Bruggeman[10] and the taxonomic group of all 36 dominant phytoplankton morphotypes in Lake Constance. Bruggeman established a statistical model based on measured trait data and known phylogenetic relationships and trait correlations. We throughout used the values of the statistical model for consistency, although measurements for a few taxa deviated from them. Two morphotypes (*Navicula* spp. and *Cymbella ventricosa* & *C. prostrata*) were not listed by Bruggeman[10]. Hence, we used trait values of the nearest genus for them (*Nitzschia* ssp. for both) having a similar longest linear dimension, cell volume and colony formation.

Morphotype number	Morphotype name	Defense	r	Phosphate affinity	Cell volume	Taxonomic group
1	*Anabaena* spp.	0.66	0.88	94	170	cyanobacteria
2	*Asterionella formosa*	0.79	1.6	56	810	diatoms
3	*Aulacoseira* spp.	0.77	1.5	18	870	diatoms
4	*Ceratium hirundinella*	0.89	0.24	1600	40,000	dinophytes

5	*Chlamydomonas* spp.	0.38	1.8	170	210	chlorophyta
6	*Chlorella* spp	0.69	1.7	45	28	chlorophyta
7	*Chrysochromulina parva*	0.73	1.0	160	250	haptophytes
8	*Cosmarium* spp.	0.84	0.95	72	5,700	chlorophyta
9	*Cryptomonas marssonii*	0.49	1.1	190	1,800	cryptomonads
10	*Cryptomonas rostratiformis*	0.5	1.1	200	3,200	cryptomonads
11	*Cryptomonas* spp.	0.45	1.2	140	1,700	cryptomonads
12	*Cyclotella* spp.	0.77	1.6	3.6	420	diatoms
13	*Cymbella ventricosa* & *C. prostrata*	0.54	1.8	150	320	diatoms
14	*Diatoma* spp.	0.76	1.4	210	1,400	diatoms
15	*Dinobryon* spp.	0.85	0.74	110	360	chrysophytes
16	*Erkenia subaequiciliata*	0.47	1.7	220	100	chrysophytes
17	*Eudorina elegans*	0.78	1.1	32	1,300	chlorophyta
18	*Fragilaria crotonensis*	0.84	1.3	50	1,200	diatoms
19	*Mallomonas* spp.	0.8	0.5	340	2,700	chrysophytes
20	*Mougeotia* spp.	0.77	1.5	87	1,200	chlorophyta
21	*Navicula* spp.	0.54	1.8	150	320	diatoms
22	*Nitzschia* spp.	0.54	1.8	150	320	diatoms
23	*Oocystis* spp.	0.6	1.5	190	510	chlorophyta
24	*Oscillatoria* spp.	0.53	1.0	99	23	cyanobacteria
25	*Pandorina morum*	0.82	0.92	46	2,300	chlorophyta
26	*Pediastrum* spp.	0.69	1.3	310	790	chlorophyta
27	*Peridinium* spp.	0.912	0.24	130	15,000	dinophytes
28	*Phacotus* spp.	0.34	1.6	430	400	chlorophyta
29	*Rhodomonas* spp.	0.1	1.7	550	250	cryptomonads
30	*Scenedesmus* spp.	0.63	2.1	45	160	chlorophyta
31	*Sphaerocystis schroeteri*	0.83	1.1	57	720	chlorophyta
32	*Staurastrum* spp.	0.85	0.84	150	12,000	chlorophyta
33	*Stephanodiscus neoastraea*	0.66	1.7	22	1,500	diatoms
34	*Stephanodiscus* spp.	0.64	1.8	13	580	diatoms
35	*Synedra* spp.	0.66	1.7	420	1,300	diatoms
36	*Tabellaria fenestrata*	0.8	1.2	210	2,700	diatoms

The concave trade-off between δ and r can be also found when including all trait data from Bruggeman[10] (Fig. B1a) or when the standard errors for the 36 morphotyptes are included (Fig. B1b).

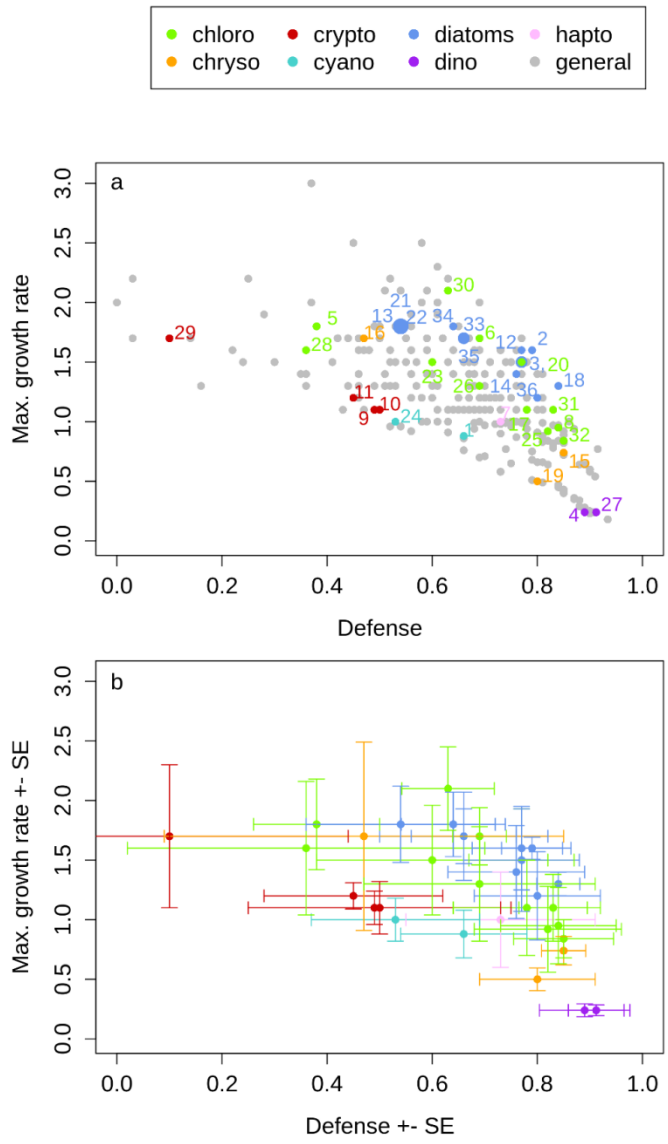

Fig. B1: Defense δ and maximum growth rate r (d^{-1}) of the 36 most abundant phytoplankton morphotypes in Lake Constance (colored dots). Colors indicate different taxonomic groups, i.e., chlorophyta, cryptomonads, chrysophytes, haptophytes, cyanobacteria, diatoms and dinophytes. (a) Including all other phytoplankton morphotypes/species available in Bruggeman[10] (grey dots). The numbers refer to the morphotype names listed in Table B1. Larger dots indicate that two or more morphotypes share the same trait combination. (b) The bars indicate the standard error of the derived trait values of the 36 morphotypes according to Bruggeman[10].

Appendix B3: Supporting results

We describe supporting results here, (1) the trade-offs between phosphate affinity P and defence δ resp. maximum growth rate r, (2) the relationship of all three traits to cell volume, (3) the seasonal trait distribution considering all seven phases, the influence of re-oligotrophication on (4) the seasonal δ-r trait distribution and (5) the phosphate affinity.

(1) A concave trade-off curve was most obvious for the trade-off between δ and r (Fig. 3.3). In the trait space of δ and P, a similar pattern might be seen albeit with more scatter and one exception, *Ceratium hirundinella* being very defended and highly phosphate affine (Fig. B2a, ρ = -0.28, p = 0.09, Spearman rank correlation coefficient never biomass-weighted). The pattern for P and r is even more scattered (Fig. B2b, ρ = -0.12, p = 0.5).

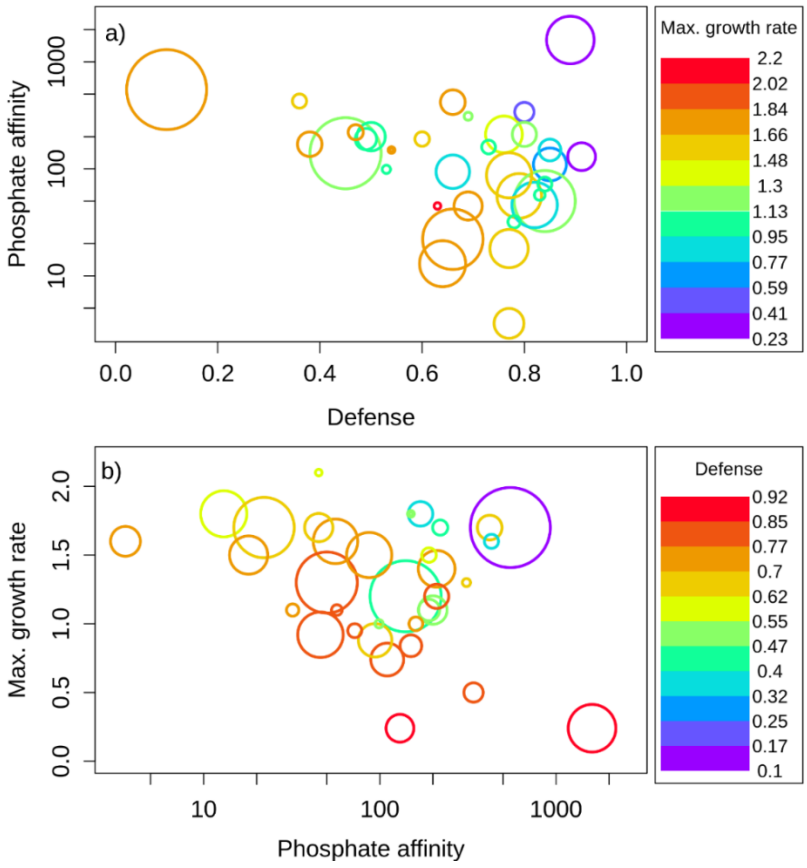

Fig. B2: Trait space of the 36 most abundant phytoplankton morphotypes in Lake Constance. Colors indicate third trait dimension. The area of the circles is scaled by the mean annual relative biomass of the morphotypes. (a) Defense δ and phosphate affinity ($d^{-1}\mu mol^{-1}L$), color represents maximum growth rate r (d^{-1}). (b) Phosphate affinity ($d^{-1}\mu mol^{-1}L$) and maximum growth rate r (d^{-1}), color represents defense δ.

(2) The correlation between each trait and cell volume as a master trait was tested (Fig. B3). Maximum growth rate r was negatively correlated to cell volume (ρ = -0.59, p = 10^{-4}), defense was positively correlated to cell volume (ρ = 0.49, p = 10^{-3}), while we found no correlation for phosphate affinity (ρ = 0.22, p = 0.19). Thus, the trade-off between δ and r may partially arise from the weak correlations of both traits with cell size. However, the large scatter in the relationship between δ and cell size (Fig. B3b) shows that other defense mechanism are important as well, e.g. cell shape, formation of filaments. Hence we used trait data instead of the approximation cell size.

Furthermore, cell size as a functional trait is harder to link directly to a certain environmental driver being sensitive to multiple factors as a 'master trait', compared to, e.g. defense being selected by high grazing pressure, or phosphate affinity being selected by phosphate depletion. Therefore, we do not include cell size in our main consideration of how the community trait composition responds to seasonal environmental changes, but we use cell size more as a 'master trait' providing to some extent a potential mechanism for the observed trade-off between defense and maximum growth rate.

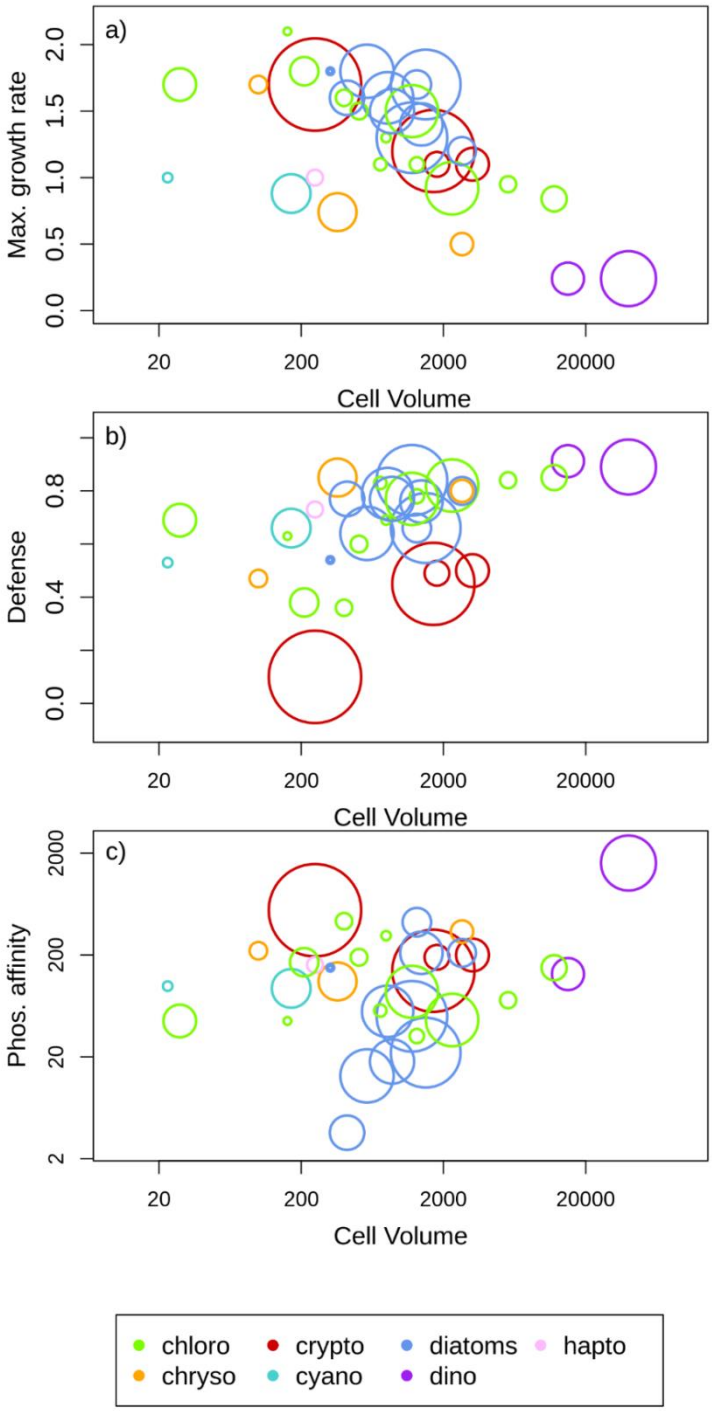

Fig. B3: Relationship between cell volume (µm³) and a) maximum growth rate r (d^{-1}), b) defense δ and c) phosphate affinity ($d^{-1}\mu mol^{-1}L$) for the 36 most abundant phytoplankton morphotypes in Lake Constance (colored circles). Colors indicate different taxonomic groups, i.e., chlorophyta, chrysophytes, cryptomonads, cyanobacteria, diatoms, dinophytes, and haptophytes and the area of the circles scales with mean annual relative biomasses.

(3) The biomass distribution in the δ-r trait space responded to the seasonally changing environment in a remarkably gradual and consistent way (Fig. 3.2). In late winter and early spring, vertical mixing and the resulting high export of phytoplankton from the euphotic zone to deep water layers was a dominant driver of the phytoplankton community in deep Lake Constance while grazing pressure and nutrient depletion were very low. Morphotypes with high r being able to compensate for high losses and to exploit the high nutrient concentrations dominated, whereas morphotypes with low r and high δ were almost absent (Fig. B4a, b). This is reflected in the community average trait values (late winter: $\bar{\delta}$ = 0.51, $\bar{r}$ = 1.56 d^{-1}; early spring: $\bar{\delta}$ = 0.52, $\bar{r}$ = 1.57 d^{-1}). Morphotypes with low or high phosphate affinities had high biomasses, indicating the absence of a selection pressure on this trait. During late spring, grazing pressure increased mostly by ciliates (Fig. 3.2) but did not initiate a shift of the overall biomass distribution towards higher δ ($\bar{\delta}$ = 0.48, $\bar{r}$ = 1.55 d^{-1}) (Fig. B4c). During the clear-water phase (CWP), the grazing pressure was at its annual maximum (Fig. 3.2). The community average maximum growth rate decreased slightly ($\bar{r}$ = 1.35 d^{-1}) while the mean defense level did not change ($\bar{\delta}$ = 0.48) despite the high grazing pressure (Fig. B4d), probably due to a delayed numerical response of highly defended but slowly growing morphotypes. In summer, nutrient depletion and grazing pressure were the dominant drivers of phytoplankton (Fig. 3.2). The biomass shifted towards morphotypes with intermediate or high δ and accordingly low r (Fig B4e, $\bar{\delta}$ = 0.69, $\bar{r}$ = 1.18 d^{-1}). Morphotypes with intermediate to high phosphate affinities gained in importance in line with nutrient depletion. In autumn, nutrient depletion and grazing were still mainly driving the phytoplankton community but declined compared to summer (Fig. 3.2). This resulted in a slight increase of morphotypes with lower δ and higher r ($\bar{\delta}$ = 0.62, $\bar{r}$ = 1.28 d^{-1}) (Fig. B4f). In early winter, vertical mixing again represented the most important driver and nutrient concentrations were high. Morphotypes with high r, intermediate δ and no clear signal in phosphate affinity contributed again a high share to the total phytoplankton biomass (Fig. B4g, $\bar{\delta}$ = 0.56, $\bar{r}$ = 1.40 d^{-1}).

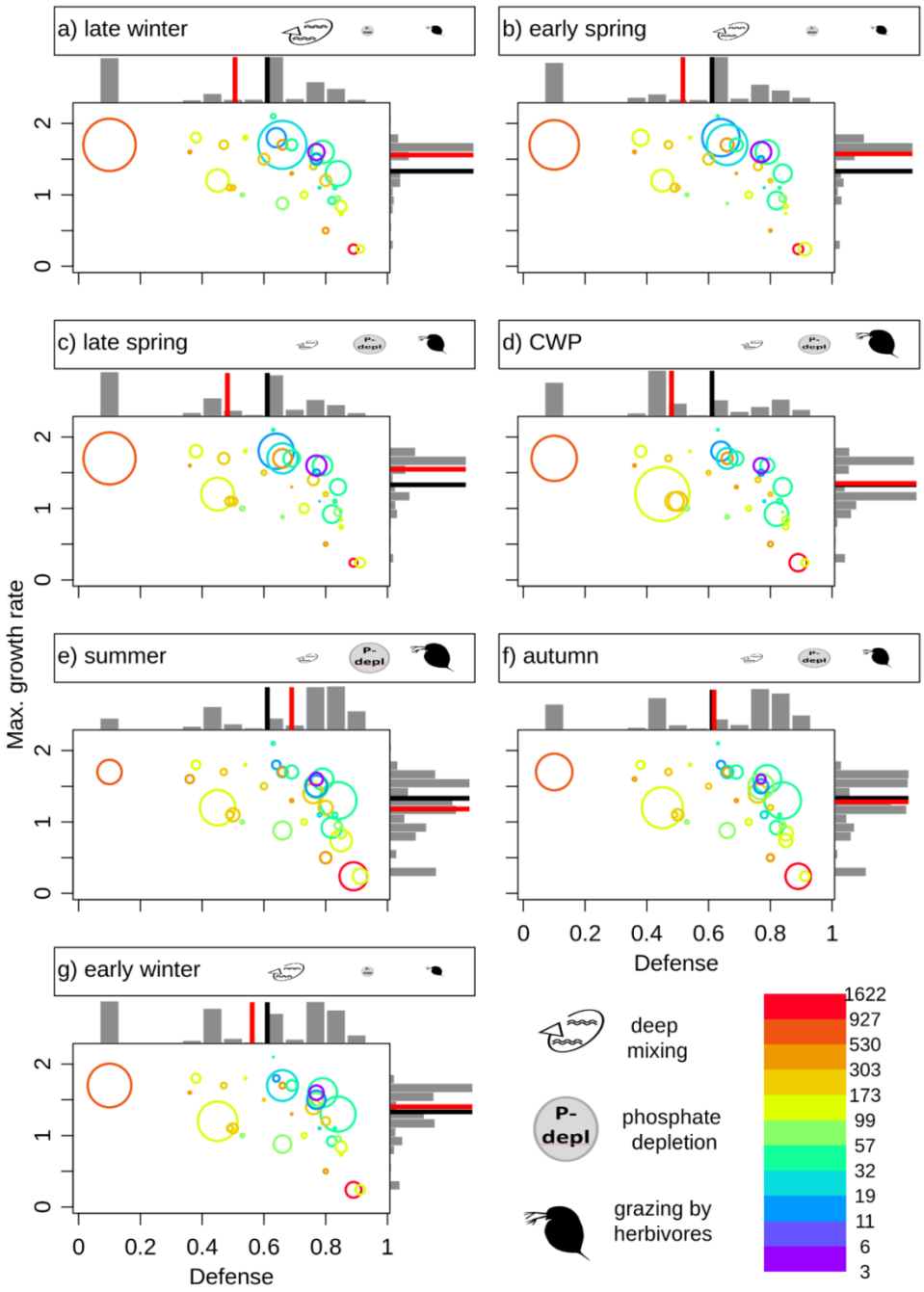

Fig. B4: Positions of the 36 most abundant phytoplankton morphotypes in Lake Constance in the trait space of defense δ and maximum growth rate r (d^{-1}) for seven seasonal phases. Colors indicate the morphotypes' phosphate affinity and the area of the circles the mean relative biomasses of each phase. The bars display the relative biomass distribution along the two trait axes in each phase. The red lines in the bar plots mark the phase means of the community average trait values and the black lines display the annual means of the community average trait values as a reference ($\bar{\delta}$ = 0.61, $\bar{r}$ = 1.33). The icons represent the dominant drivers of the phytoplankton community (vertical mixing, phosphate depletion, grazing by herbivores) and their size indicates their relative importance for phytoplankton net growth in each phase.

(4) Concurrent to the re-oligotrophication of the lake during the study period, the pattern of the seasonal biomass-trait distribution only marginally changed (Fig. B5). In early spring in 1979 – 1988, the morphotypes were on average slightly less defended than on average in 1989-1999 due to *Rhodomonas spp.* being more abundant, while intermediately defended diatoms were less common. These changes did not alter the average maximum growth rate. In summer in 1979-1988, the average maximum growth rate was higher than in 1989-1999, e.g. due to a higher share of the relative fast- growing *Fragilaria crotonensis*, whereas in 1989-1999 slow-growing *Ceratium hirundinella* was relatively more abundant. These changes did not affect the average level of defense. To conclude, the changes in the species composition observed during the re-oligotrophication did not change the overall seasonal pattern with a dominance of fast growing, undefended morphotypes in early spring and of slow growing, highly defended morphotypes in summer.

Our explanation for the lack of a clear responsiveness of the defence-growth rate trait distribution is that the grazing pressure likely changed little during most of the investigation period lasting from 1979-1999. We know that from 1987-1998 neither total ciliate biomass nor species composition changed significantly[11]. The crustaceans, i.e. the other important group of herbivores, had lower abundances in 1997-1998 than in 1979-1996 during July to September. These fairly constant biomasses of herbivores fit with the measurements of 14C primary production from 1980-1996. During this time primary production declined (only) during summer by only 25%[12]. We presume that potential effects on the trait distribution are too small to be clearly visible. On the other hand, the persistence of the trait distribution and its seasonal dynamics suggest that trophic interactions played a major role in this lake during the whole study period, as supported by numerous other studies[13].

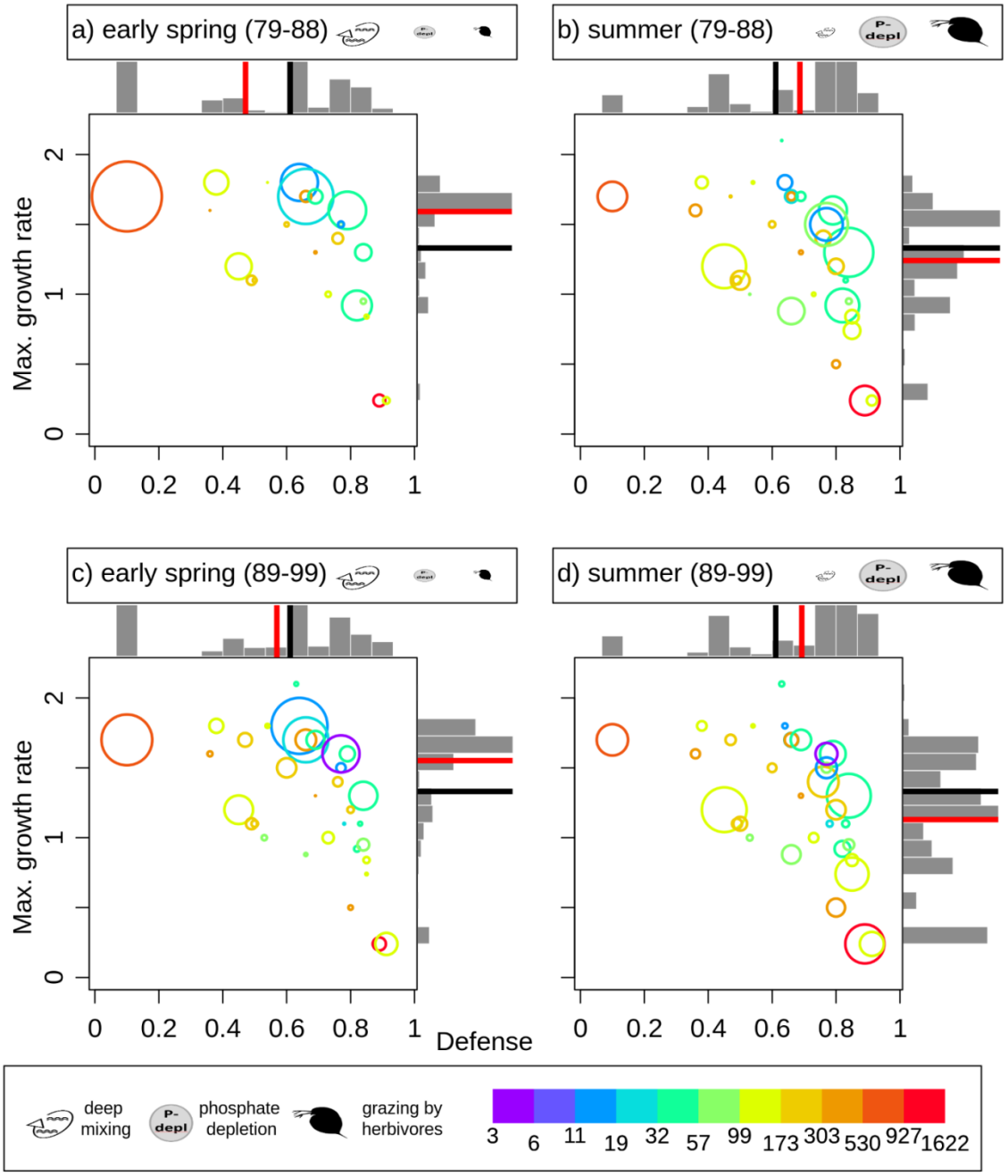

Fig. B5: Positions in the trait space of defense δ and maximum growth rate r (d^{-1}) and mean relative biomasses (scaling the area of the circles) of the 36 most abundant phytoplankton morphotypes in Lake Constance for two seasonal phases (early spring and summer) in 1979-1988 (a,b) and 1989-1999 (c,d). Colors indicate the morphotypes' phosphate affinity. The icons represent the dominant drivers of the phytoplankton community (vertical mixing, phosphate depletion, grazing by herbivores) and their size indicates their relative importance for phytoplankton net growth in each phase. The bars display the relative biomass distribution along the two trait axes in each phase. The red lines in the bar plots mark the phase mean of thecommunity average trait values and the black lines display the annual means of the community average trait values as a reference.

(5) In summer, SRP dropped always below 2 µg P/l in the surface layer and we measured a strong increase in the cellular phytoplankton C:P ratio in summer 1995. Nevertheless we found no distinct seasonal pattern in community average phosphate affinity when considering all years together or the years 1979-1988 (Fig. B6a,b). For the years 1989-1999 we see a slight increase in phosphate affinity during the season, which results in somewhat higher values in summer and autumn compared to 1979-1988. The overall changes of the community average trait values are small relative to the entire trait range (3 -1600 $d^{-1}\mu mol^{-1}L$).

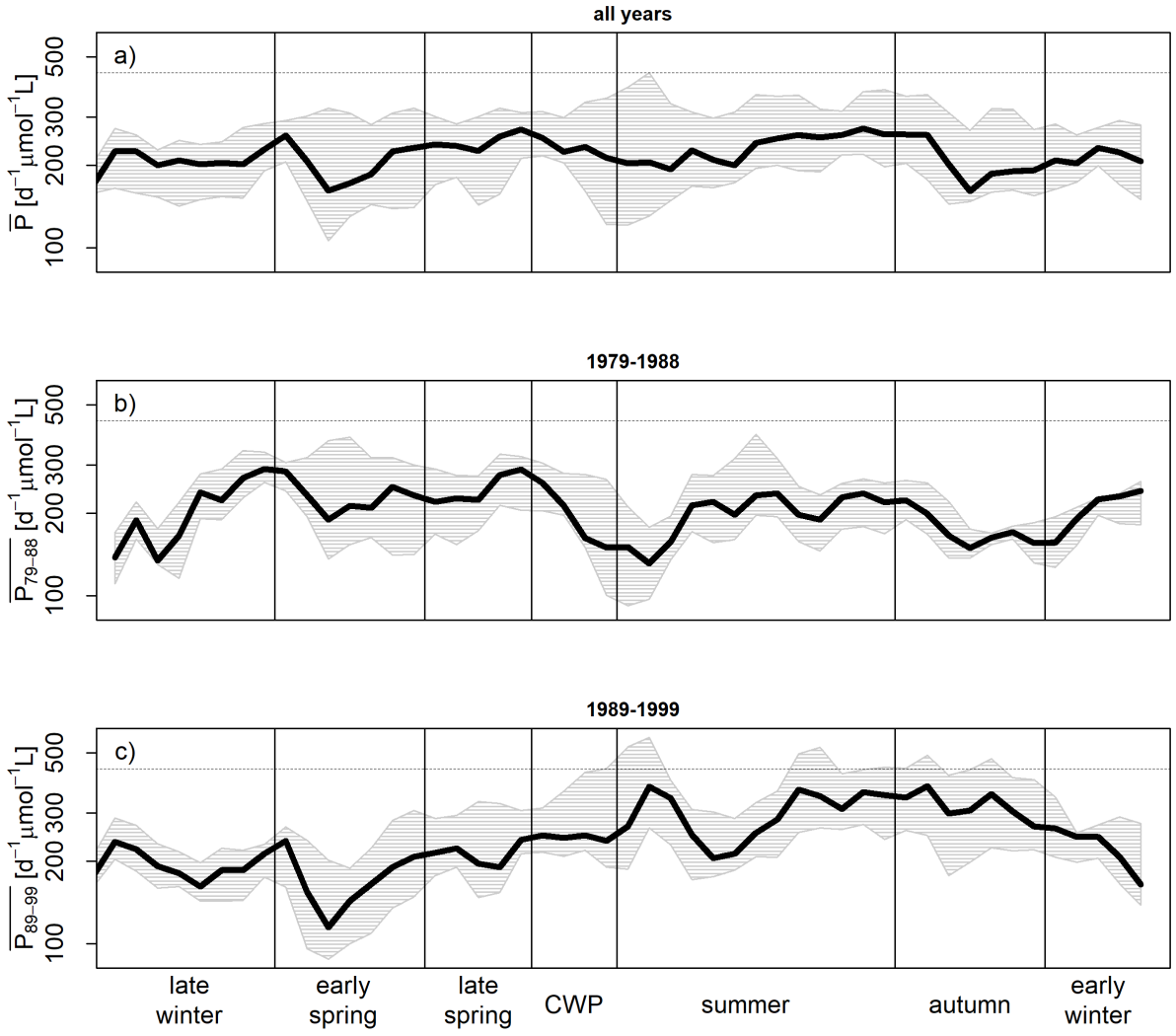

Fig. B6: Seasonal dynamics of the interannual median (black lines) and quartiles (shaded areas) of the phytoplankton community average phosphate affinity $\bar{P}$ in a standardized year of a) all years, b) 1979-1988 and c)1989-1999. CWP denotes the clear-water phase. The dashed line represents maximum of the upper quartile for all years.

Appendix B4: Model description

The model

The following model equations describe the biomass dynamics of N phytoplankton species P_i and one zooplankton group Z:

$$\frac{dP_i}{dt} = \left(r_i \frac{R}{K+R} - \frac{G\,(1-\delta_i)\,Z}{H+\sum_{i=1}^{N} P_i} - m_P\right) P_i \qquad (3.1)$$

$$\frac{dZ}{dt} = \left(\varepsilon \frac{G\ \sum_{i=1}^{N}[(1-\delta_i)P_i]}{H\ +\ \sum_{i=1}^{N} P_i} - m_z\right) Z$$

The phytoplankton growth is limited by nutrients, described by a Monod term. By assuming a fixed pool of nutrients, we can write the available (dissolved) nutrient concentration as $R = R_{max} - \sum_{i=1}^{N} P_i - \frac{1}{\varepsilon} Z$, that is, the total amount of nutrients R_{max} subtracted by the nutrients fixed in biomass of phytoplankton and zooplankton[14]. The nutrient concentration is written in units of phytoplankton biomass, i.e. R_{max} represents the maximum phytoplankton biomass obtainable from the nutrient pool in the absence of mortality. The phytoplankton species differ in their maximum growth rates r_i, but share the same half-saturation constant for nutrient uptake K (in units of phytoplankton biomass, see above) and natural mortality m_P. Hence, the species with the highest r_i, performing well at high resource availability, is also the superior competitor under strong resource depletion (i.e. it has the lowest R^*) in the model. The grazing of zooplankton on phytoplankton is described by a Holling type II function with the maximum grazing rate G and the half-saturation constant H. Phytoplankton species have different values of defense δ_i against zooplankton. We assume that defended phytoplankton cells also demand handling time of the predator equal to that of undefended phytoplankton but without energy gain because unselective feeders, which dominate in Lake Constance, are probably not able to discriminate between them and attack both[15]. Accordingly, δ_i gives the probability of not being consumed (i.e., not ingested or digested) and surviving when attacked with values ranging between 0 (undefended) and 1 (completely defended). The probability of being consumed is then given by $1 - \delta_i$, which scales the maximum grazing rate (see Eq. 3.1) and corresponds to the 'edibility', typically used in a limnetic context[10]. The conversion efficiency of

consumed phytoplankton into zooplankton biomass ε is assumed to be equal among the phytoplankton species. m_z represents the zooplankton mortality.

Trade-off curve

The trade-off curve between defense and maximum growth rate is given by the function

$$r_i = b\,(0.9 - \delta_i)^a + c \qquad (3.2)$$

where a denotes the shape parameter, b the slope parameter and c the maximum growth rate of a most defended species ($\delta_i = 0.9$). If $a < 1$, the trade-off curve is concave. $a > 1$ gives a convex trade-off curve and $a = 1$ a linear one. We assume a concave trade-off curve with $a = 0.2$, $b = 1.6\,d^{-1}$ and $c = 0.5\,d^{-1}$ approximately reflecting the trade-off curve found in the trait data (Fig. 3.3a). For comparison, we consider also a convex trade-off curve with $a = 2$, $b = 1.92\,d^{-1}$ and $c = 0.5\,d^{-1}$, that crosses the concave trade-off curve at minimal and maximal defense levels (i.e. shares the same endpoints).

Parametrization and initialization

We considered different phytoplankton species with trait values spanning the whole feasible trait space. We determined the species trait values according to the following procedure: First, we defined a 15x15 grid of trait combinations covering the whole trait space (δ_i between 0 and 0.9, r_i between 0.0 and $2.1\,d^{-1}$). Second, we extracted only the feasible trait combinations below the trade-off curve. Third, we added 15 trait combinations exactly on the trade-off curve, equally spaced along the whole defense axis, which resulted in a total number of 199 trait combinations representing different phytoplankton species ($N = 199$).

Based on measurements conducted at Lake Constance[13,16,17], we parametrized the model as follows:
$R_{max} = 500\,mg\,C\,m^{-3}, K = 50\,mg\,C\,m^{-3}, G = 1.3\,d^{-1}$, $H = 80\,mg\,C\,m^{-3}$, $\varepsilon = 0.3$, $m_P = 0.2\,d^{-1}$, and $m_Z = 0.14\,d^{-1}$ (spring scenario, low grazing pressure) or $m_Z = 0.04\,d^{-1}$ (summer scenario, high grazing pressure). We initialized the model with random values from a uniform distribution

between 0.1 and 4 $mg\ C\ m^{-3}$ for each P_i and between 1 and 20 $mg\ C\ m^{-3}$ for Z.

Numerical integration

The numerical integrations of the model were done with the ode45 solver of the deSolve package in R[18]. We run the simulations for 10,000 days and calculated the mean biomasses of the last 1000 days to detect the phytoplankton species dominating in the long term. Furthermore, we checked which species survive in the short term, that is, within the first 100 days. The extinction threshold was set to $10^{-4}\ mg\ C\ m^{-3}$. We performed 50 simulations with different random initial conditions and averaged the mean biomasses and the time until extinction among all simulations.

Appendix B5: Phytoplankton biomass dynamics

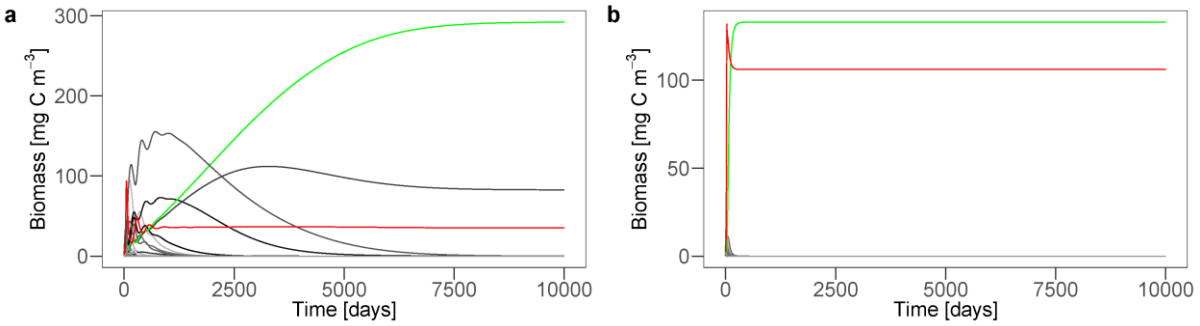

Fig. B7: Simulated long-term biomass dynamics for a concave trade-off curve under (a) low and (b) high grazing pressure (one sample of randomized initial conditions). Grey and green lines represent phytoplankton species with different trait combinations, where the green line marks the most dominant one. The red line corresponds to herbivorous zooplankton. (a) At low grazing pressure, two phytoplankton species with slightly different intermediate defense levels coexist. Their biomasses and the biomass of the herbivorous zooplankton reach a steady-state. (b) At high grazing pressure, only one species, with a higher defense level compared to the species coexisting in (a), survives in the phytoplankton. Its biomass and the biomass of the zooplankton are again in equilibrium.

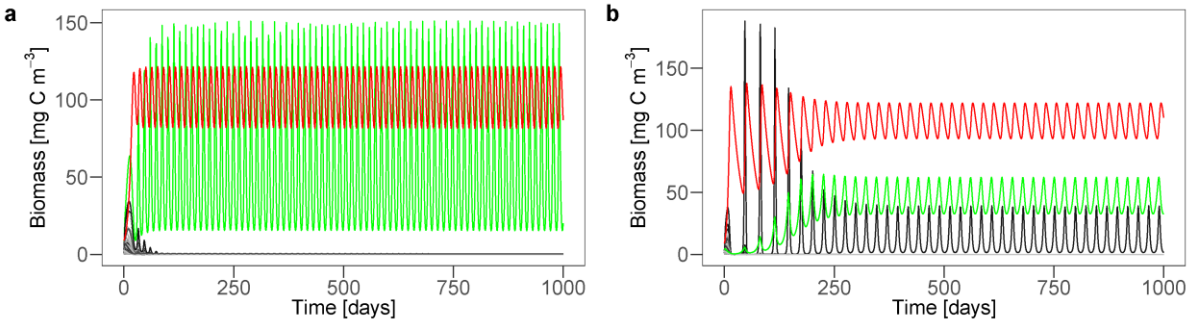

Fig. B8: Biomass dynamics in the first 1000 days of the simulation for a convex trade-off curve under (a) low and (b) high grazing pressure (one sample of randomized initial conditions). Grey and green lines represent phytoplankton species with different trait combinations, where the green line marks the most dominant one. The red line corresponds to herbivorous zooplankton. (a) At low grazing pressure, only a completely undefended phytoplankton species survives and the biomasses of that species and the zooplankton cycle. (b) At high grazing pressure, a completely undefended and a completely defended phytoplankton species (i.e. both extremes) coexist. Their biomasses and the biomass of the predator cycle.

References

1. Rocha MR, Vasseur DA, Gaedke U. Seasonal Variations Alter the Impact of Functional Traits on Plankton Dynamics. Swenson NG, editor. PLoS One. 2012 Dec 12;7(12):e51257.

2. Straile D. Biomass allocation and carbon flow in the pelagic food web of Lake Constance. Arch Hydrobiol Spec Issues Adv Limnol. 1998;53:545–63.

3. Boit A, Gaedke U. Benchmarking successional progress in a quantitative food web. PLoS One. 2014;9(2).

4. Gaedke U, Klauschies T. Analyzing the shape of observed trait distributions enables a data-based moment closure of aggregate models. Limnol Oceanogr Methods. 2017;15(12):979–94.

5. Weithoff G, Gaedke U. Mean functional traits of lake phytoplankton reflect seasonal and inter-annual changes in nutrients, climate and herbivory. J Plankton Res. 2017;39(3):509–17.

6. Weithoff G, Rocha MR, Gaedke U. Comparing seasonal dynamics of functional and taxonomic diversity reveals the driving forces underlying phytoplankton community structure. Freshw Biol. 2015 Apr;60(4):758–67.

7. Hochstädter S. Seasonal changes of C:P ratios of seston, bacteria, phytoplankton and zooplankton in a deep, mesotrophic lake. Freshw Biol. 2000 Jul;44(3):453–63.

8. Bäuerle E, Ollinger D, Ilmberger J. Some meteorological, hydrological and hydrodynamical aspects of Upper Lake Constance. Arch Hydrobiol Spec Issues Adv Limnol. 1998;53:31–83.

9. Gaedke U, Ollinger D, Straile D, Bäuerle E. The impact of weather conditions on the seasonal plankton development. Arch fuer Hydrobiol. 1998;53:565–85.

10. Bruggeman J. A phylogenetic approach to the estimation of phytoplankton traits. J Phycol. 2011 Feb;47(1):52–65.

11. Gaedke U, Wickham SA. Ciliate dynamics in response to changing biotic and abiotic conditions in a large, deep lake (Lake Constance). Aquat Microb Biol. 2004;34:247–61.

12. Häse C, Gaedke U, Seifried A, Beese B, Tilzer MM. Phytoplankton response to re-oligotrophication in large and deep Lake Constance: Photosynthetic rates and chlorophyll concentrations. Arch Hydrobiol Spec Issues Adv Limnol. 1998;53:159–78.

13. Gaedke U, Hochstädter S, Straile D. Interplay between energy limitation and nutritional deficiency: Empirical data and food web models. Ecol Monogr. 2002;72(2):251–70.

14. Klauschies T, Gaedke U. Nutrient retention by predators undermines predator coexistence on one prey. Theor Ecol. 2019 Oct 19;535195.

15. Ehrlich E, Gaedke U. Not attackable or not crackable-How pre- and post-attack defenses with different competition costs affect prey coexistence and population dynamics. Ecol Evol. 2018 Jul;8(13):6625–37.

16. Gaedke U, Straile D. Seasonal changes of trophic transfer efficiencies in a plankton food web derived from biomass size distributions and network analysis. Ecol Modell. 1994 Sep;75–76:435–45.

17. Gaedke U. Functional and taxonomical properties of the phytoplankton community: Interannual variability and response to re-oligotrophication. Arch fuer Hydrobiol. 1998;53:119–41.

18. Soetaert K, Petzoldt T, Setzer RW. Package deSolve: Solving Initial Value Differential Equations in R. J Stat Softw. 2010;33(9):1–25.

Appendix C: Supplementary information for chapter 4

Morphotypes

The morphotype numbers, names and abbreviations for the ciliate, phytoplankton and rotifer community sampled in the Lake Constance data set can be found in Tab. C1.

Tab. C1: Ciliate, phytoplankton and rotifer morphotype numbers, names, abbreviations (for ciliates) and edibility (for phytoplankton). Classification for edibility is based on literature (Vasseur et al., 2005; Boit and Gaedke, 2014; Ehrlich and Gaedke, 2020). Morphotypes are classified as most edible algae (MEA), well edible algae (WEA) or less edible algae (LE, not included in our analysis, as ciliates cannot consume these algae).

Ciliate community		Phytoplankton community			Rotifer community	
Abbrevi-ation	Name	Number	Name	Edi-bility	Number	Name
A	*Askenasia* sp.	1	*Rhodomonas* spp.	MEA	2	*Ascomorpha ovalis*
Bp	*Balanion planctonicum*	3	*Cryptomonas* spp.	MEA	3	*Ascomorpha* spp.
D	*Dileptus* sp.	4	*Cryptomonas marssonii*	MEA	4	*Asplanchna priodonta*
Er	*Epistilis rotans*	5	*Cryptomonas rostratiformis*	LE	12	*Collotheca* spp.
Hb	*Histiobalantium bodamicum*	6	*Dinobryon* spp.	LE	13	*Conochilus hippocrepis*
L	*Lagynophrya*	7	*Stephanodiscus* spp.	WEA	14	*Conochilus unicornis*
Lac	*Lacrymaria* sp.	8	*Stephanodiscus neoastraea*	LE	16	*Filinia* spp.
LP	*Limno-/ Pelago-strombidium* spp.	10	*Asterionella formosa*	LE	17	*Gastropus* ssp.
MD	*Monodinium /Didinium* spp.	11	*Fragilaria crotonensis*	LE	18	*Kellicottia longispina*
P	*Paradileptus* sp.	12	*Synedra* spp.	LE	19	*Keratella cochlearis*

Pa	Peritrichs on Anabaena	13	*Ceratium hirundinella*	LE	20	*Keratella hiemalis*
Pd	Peritrichs on diatoms	14	*Peridinium* spp.	LE	21	*Keratella quadrata*
Ph	*Pelagohalteria viridis*	15	*Pandorina morum*	LE	22	*Lecane* spp.
Rl	*Rimostrombidium lacustris*	16	*Staurastrum* spp.	LE	24	*Lepadella* spp.
S	*Stentor* sp.	18	*Diatoma* spp.	LE	26	*Notholca* spp.
ses	Sessile suctoria	19	*Phacotus* spp.	MEA	34	*Polyarthra* spp.
sO	Oligotrichs < 35µm	20	*Oocystis* spp.	LE	35	*Pompholyx sulcata*
St	*Staurophyra* sp.	21	*Mougeotia* spp.	LE	41	*Synchaeta* spp.
Suc	Small sucticociliates	24	*Anabaena* spp.	LE	46	*Trichocerca* spp.
T	Tintinnids	29	*Chrysochromulina parva*	MEA	54	*Brachionus* spp.
U2	*Urotricha* sp. 2	30	*Chlamydomonas* spp.	MEA		
U3	*Urotricha* sp. 3	31	*Chlorella* and *Microcystis* spp.	WEA		
Uf	*Urotricha furcata*	36	*Mallomonas* spp.	LE		
V	*Vaginicola* spp.	37	*Pediastrum* spp.	LE		
		38	*Scenedesmus* spp.	MEA		
		41	*Cosmarium* spp.	LE		
		43	*Nitzschia* spp.	LE		
		51	*Navicula* spp.	LE		
		55	*Tabellaria fenestrata*	LE		
		56	*Sphaerocystis schroeteri*	LE		
		58	*Eudorina elegans*	LE		
		59	*Aulacoseira* spp.	LE		
		75	*Cymbella*	LE		

		ventricosa and *C. prostrata*		
	77	*Erkenia subaequiciliata*	ME A	
	78	*Oscillatoria* spp.	LE	
	138	*Cyclotella* spp.	WE A	

Time series and temporal variability of biomasses and net growth rates

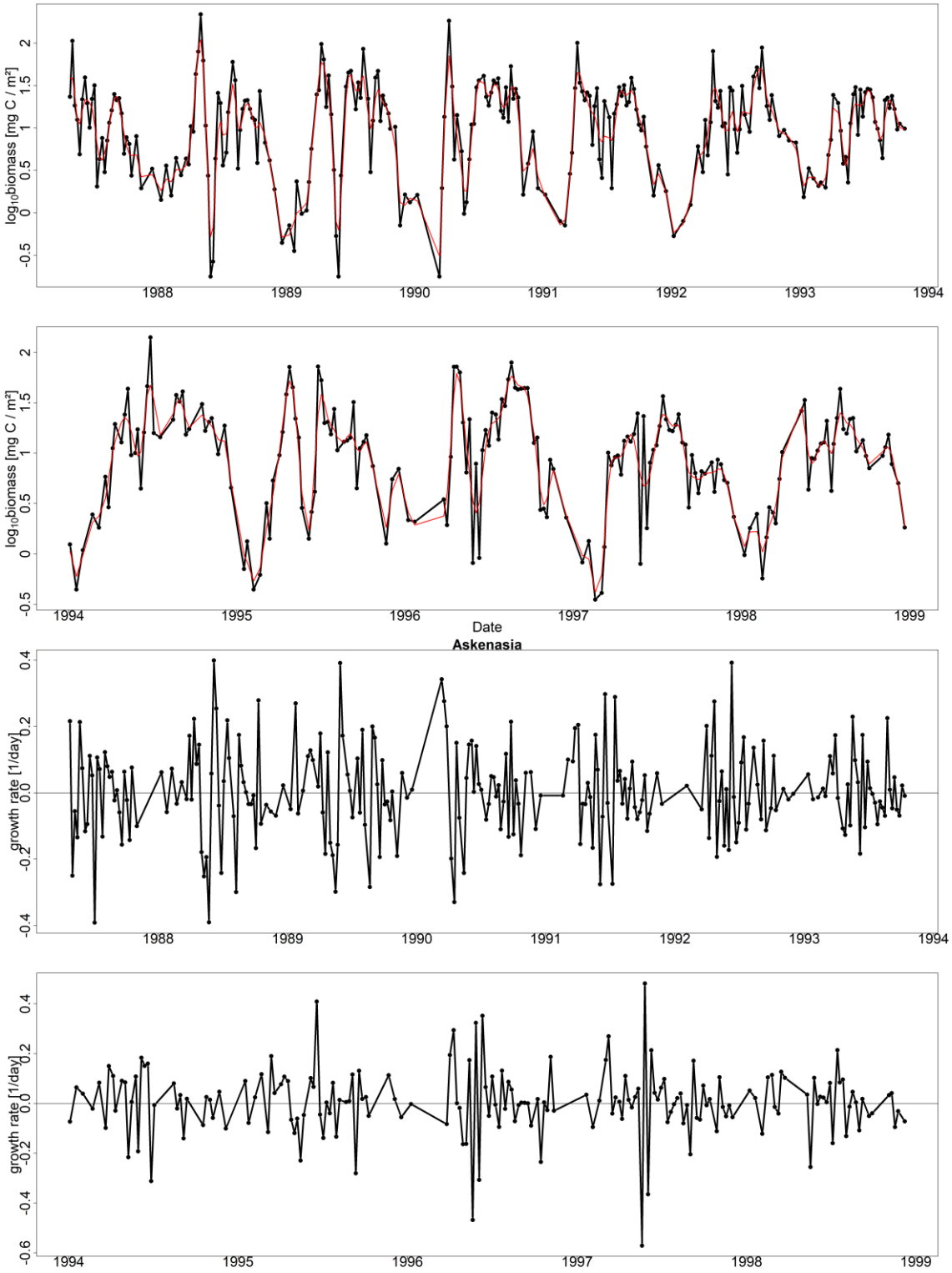

Fig. C1: Time series of $\log_{10}$ biomass and net growth rate, here of Askenasia. The red line shows the smoothed $\log_{10}$ biomass used for boosted regression trees.

The net growth rate of Askenasia is shown as an example time series for original and smoothed data (used for the boosted regression trees) (Fig. C1). The coefficient of variation is smaller within the ciliate community than in the phytoplankton community (Fig. C2).

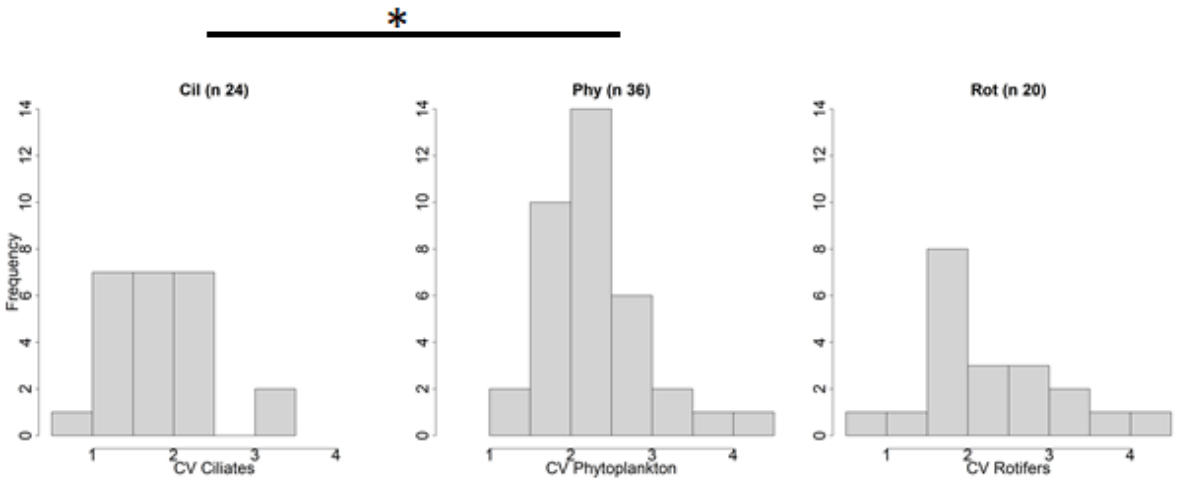

Fig. C2: Coefficient of variation of ciliate, phytoplankton and rotifer morphotypes. The coefficient of variation of the ciliate community is significantly smaller than of the phytoplankton community ($p = 0.0058$). n is the number of morphotypes in that community.

The mean, variance, skewness, and kurtosis of the ciliate morphotype net growth rate distributions are provided in Tab. C2.

Tab. C2: Net growth rates r and their distributions of ciliate morphotypes including the number of measurements for r, the mean, variance, skewness and kurtosis [>3 = leptokurtic = peaky].

Name	Number of *r* measure-ments	Mean *r*	Variance of *r*	Skewness of *r*	Kurtosis of *r*
Askenasia sp.	417	0.005	0.020	-0.13	4.5
Monodinium/Didinium	141	-0.008	0.031	-0.20	4.1
Histiobalantium bodamicum	401	0.003	0.017	0.02	4.0
Small oligotrichs	433	0.001	0.014	-0.06	4.0
Pelagohalteria viridis	116	0.000	0.038	-0.17	3.4
Balanion planctonium	429	0.000	0.033	-0.25	5.1
Rimostrombidium lacustris	342	0.004	0.032	-0.29	3.6
Small sucticociliates	259	0.000	0.024	0.41	5.3
Limno- and	404	0.001	0.028	-0.29	5.4

Pelagostrombidium sp.					
Sessile suctoria	174	0.003	0.024	0.40	3.7
Tintinnids	338	0.005	0.029	-0.05	5.3
Urotricha furcata	423	0.004	0.022	0.02	5.6
Urotricha 2	292	0.005	0.028	0.15	4.8
Urotricha 3	231	0.014	0.040	0.34	3.5
Peritrichs on *Anabaena*	102	0.009	0.049	0.16	3.7
Vaginicola	108	0.009	0.034	-0.32	3.3
Peritrichs on diatoms	344	0.006	0.032	0.26	3.9

Using 15 equidistant classes of the observed ciliate net growth rates, we calculated three indices describing their distribution beyond the skewness S and the kurtosis K (Gaedke and Klauschies, 2017). $C_1 = S^2 + ((K-3)/2)^2$ determines whether the distribution differs from a normal distribution which holds for values $C_1 > 0.36$. $C_2 = S^2 - (K-3)$ determines whether the distribution is bimodal which holds for values $C_2 > 1.2$, $C_3 = (S^2+1)^2/K$ determines whether the deviation from normality is due to skewness ($C_3 > 0.62$) or because the distribution is substantially more peaked than the normal distribution ($C_3 < 0.62$). The classification of the ciliate net growth rate distributions according to skewness and kurtosis show that most of them are peaked and not bimodal or skewed (Fig. C3).

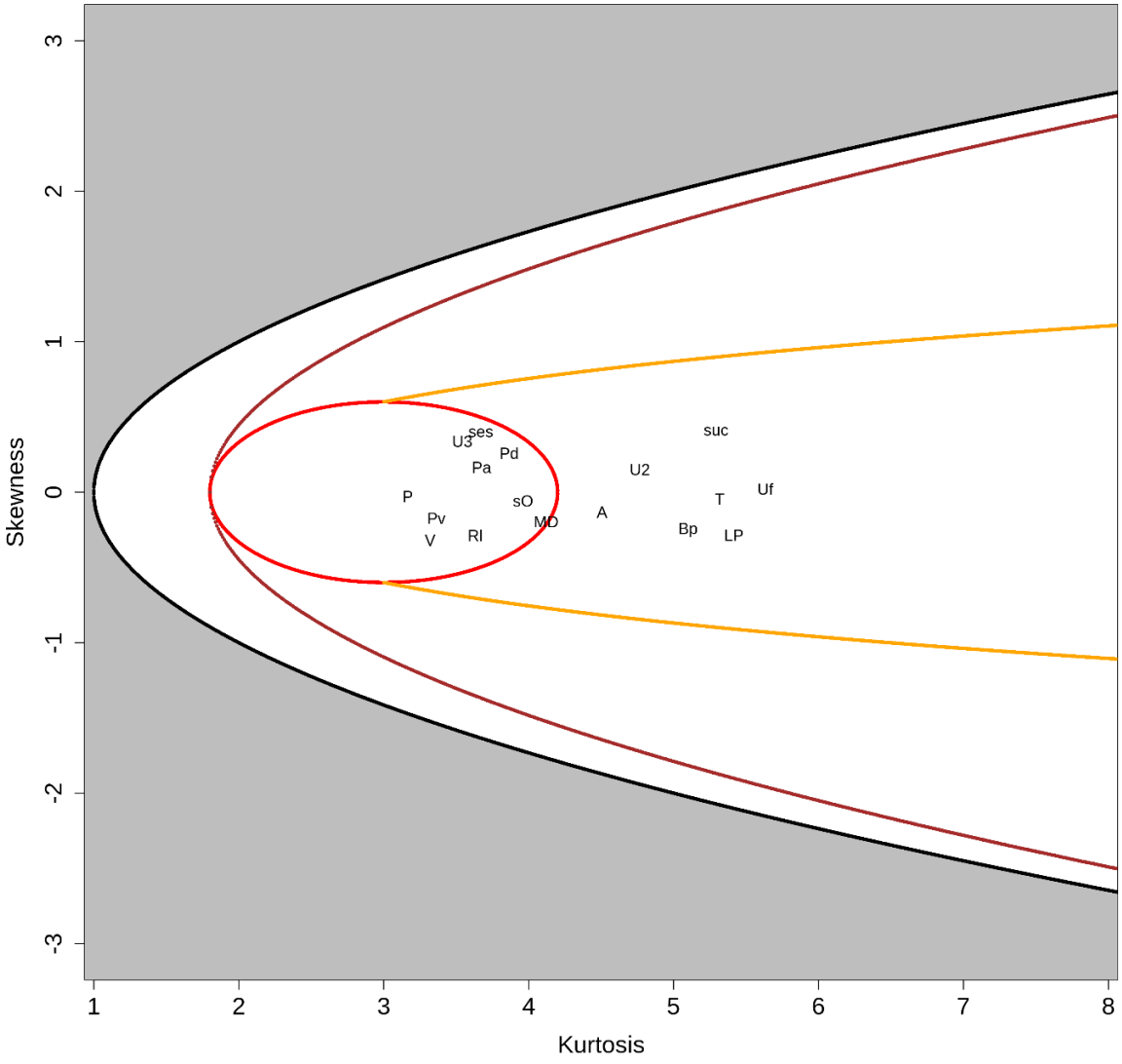

Fig. C3: Characterization of the distributions of ciliate net growth rates r according to their skewness and kurtosis. The outer black line includes the mathematically feasible range of S–K values, the inner red circle the range for normal distributions following the index C1, S–K combinations more extreme than the brown line are classified as bimodal (index C2) and values falling within the inner orange line as peaked (index C3). S–K combinations falling between the C2 (brown) and C3 (orange) isoclines are considered as skewed. Ciliates abbreviations can be found in Tab. C1.

Diversity and similarity

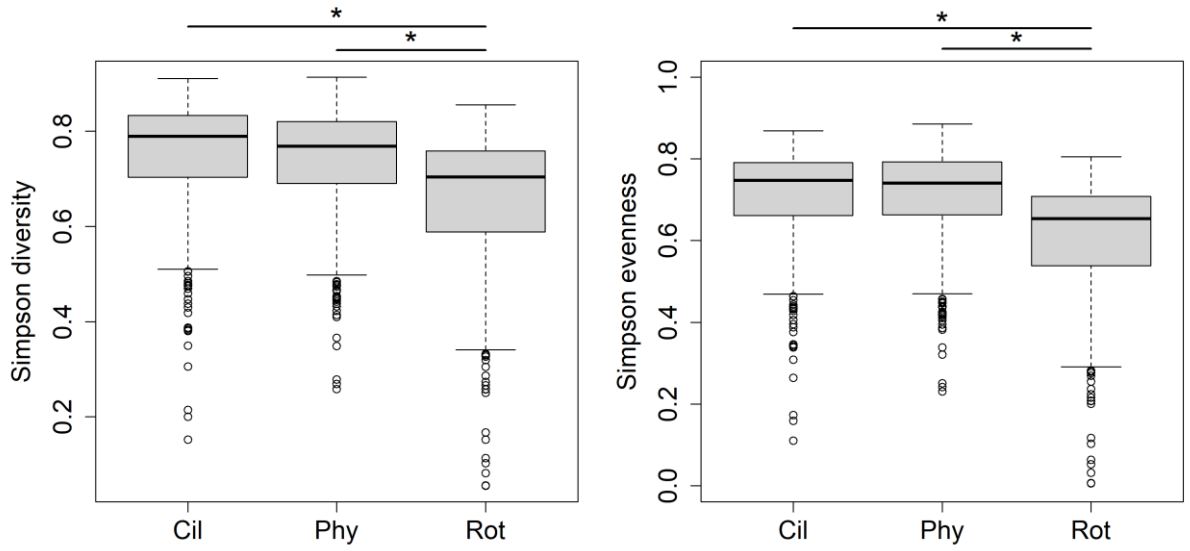

Fig. C4: Diversity (on the left) and evenness (on the right) according to Simpson for ciliates, phytoplankton, rotifers. Simpson diversity D = 1-$\sum_i^N p_i^2$, Simpson evenness E = $\frac{D}{1-1/N}$,.

The ciliate and phytoplankton community has a higher diversity and evenness than the rotifer community (Fig. C4). The similarity of the ciliate community is highest, followed by the phytoplankton community (Fig. C5).

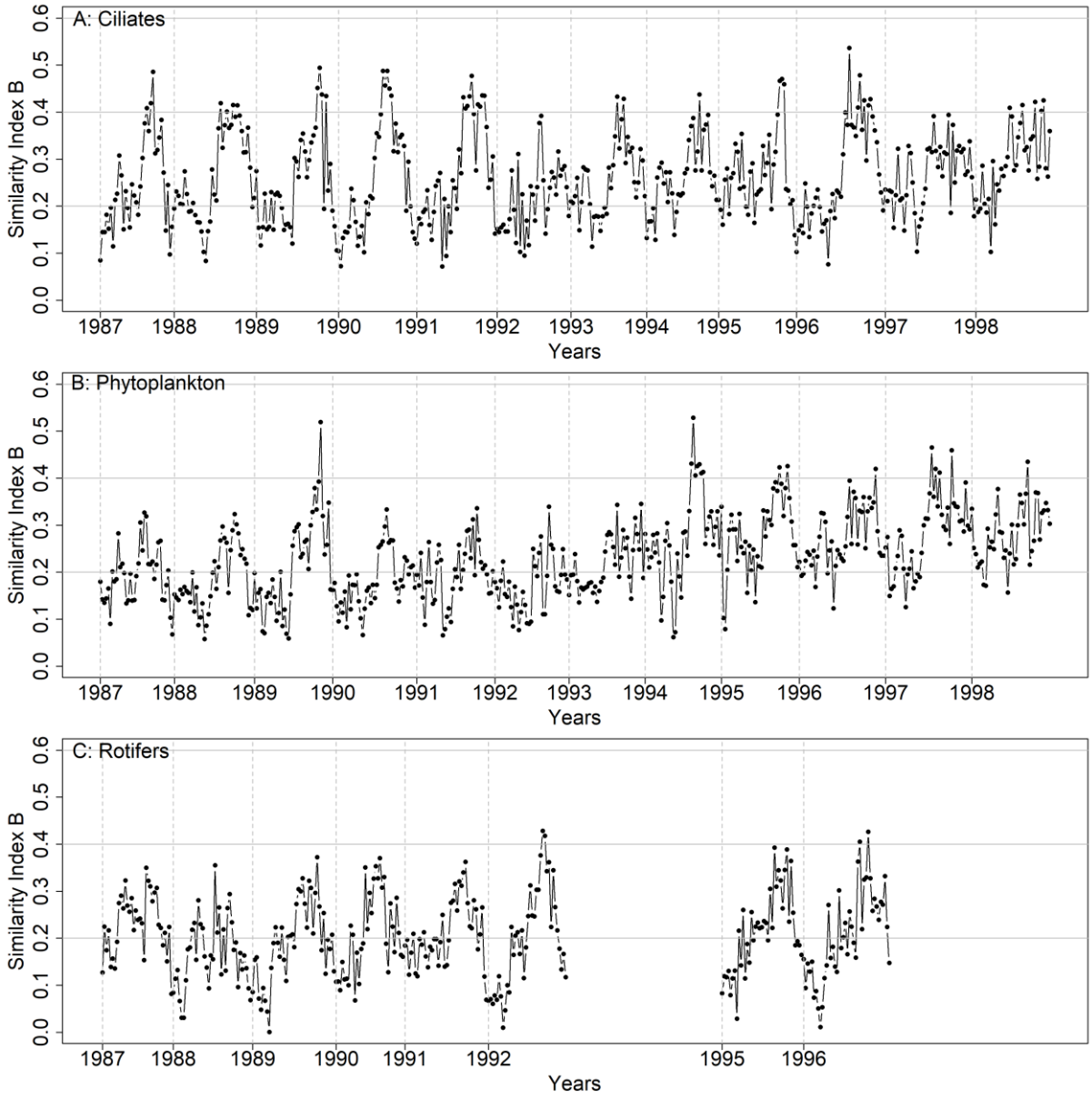

Fig. C5: Time series of the similarity index B $\sum_i^N \frac{min(pia,pib)}{max(pia,pib)} \frac{1}{N}$ (morphotype i, number of morphoptyes N, a and b consecutive days; Pinkham and Pearsson) for the relative morphotype composition of ciliates, phytoplankton, rotifers.

Comparison of different machine learning models

Correlations of predictors used in the BRT model (Fig. C6) can help us to understand how reliable the estimated ciliate responses are likely to be, and whether correlations between predictors may lead to erroneous inferences. In general, it appears that multicollinearity is not a large problem in our dataset. Temperature is perhaps most susceptible to misleading inferences because of the magnitude of its correlations with

multiple other predictors, especially Daphnia. This is unfortunately inescapable, as it essentially captures seasonality.

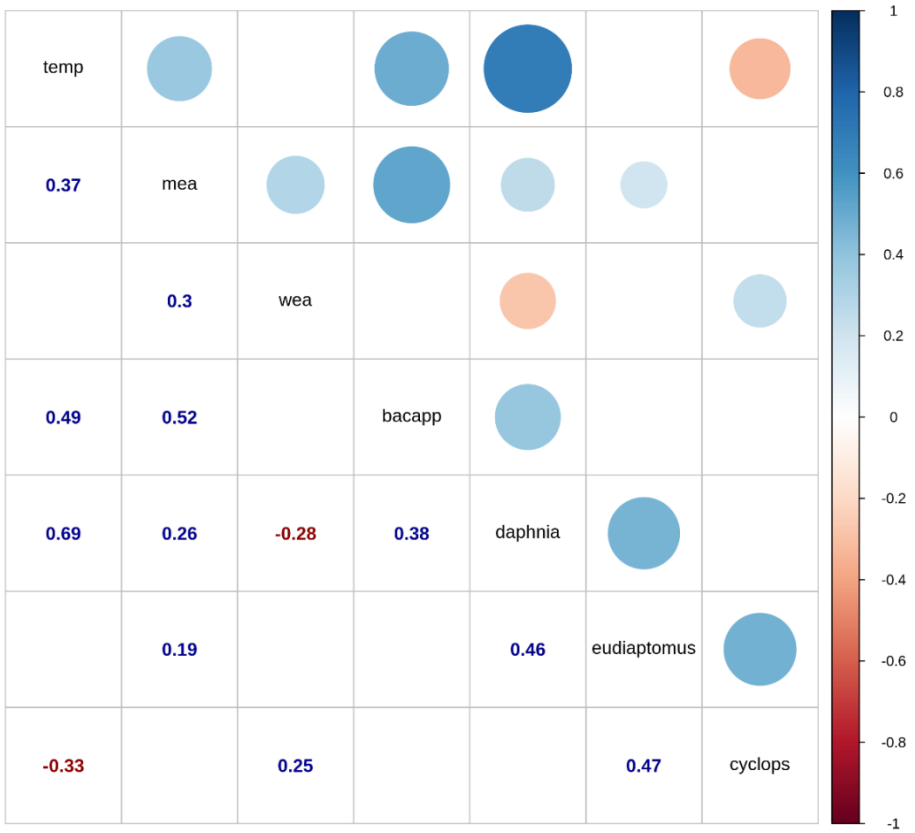

Fig. C6: Correlation matrix of all predictors (only significant correlations are shown using a threshold of 1/420 according to Bonferroni. The size of the circles corresponds to the correlation coefficient.

Different BRTs are provided predicting either the biomass or the net growth rate r (Tab. C3). For both types, four models were calculated by accounting for first only for the environmental predictors (E), second only auto-correlation, i.e. only for the biomass/ net growth rate one sampling date before (Bio_{-1}/ r_{-1}), third both the environmental predictors and the biomass/ net growth rate one time step before (Bio_{-1} + E / r_{-1} + E) and fourth the environmental predictors and the biomass/ net growth rate one and two time steps before (Bio_{-1} + Bio_{-2} + E / r_{-1} + r_{-2} + E).

Tab. C3: For all ciliate morphotypes the number of their r measurements and the R^2 [%] for the BRTs is shown. BRTs predicting either the biomass (bio) or the net growth rate (r) and taking into account either the environmental predictors (E), the biomass/ net growth rate one time step before (Bio_{-1}/ r_{-1}), both the environmental predictors and the biomass/ net growth rate one time step before (Bio_{-1} + E / r_{-1} + E) or the environmental predictors and the biomass/ net growth rate one and two time steps before (Bio_{-1} + Bio_{-2} + E / r_{-1} + r_{-2} + E). The highest R^2 per ciliate morphotype and model type (bio and r) is marked in bold.

Name	# *r*	R^2							
		Models predicting bio				Models predicting *r*			
		E	Bio_{-1}	Bio_{-1} + E	Bio_{-1} + Bio_{-2} + E	E	r_{-1}	r_{-1} + E	r_{-1} + r_{-2} + E
Askenasia sp.	417	35	62	62	**63**	4	6	**9**	**7**
Balanion planctonium	429	-19	**51**	50	50	3	4	9	**14**
Histiobalantium bodamicum	401	22	**64**	**64**	**64**	3	**6**	3	3
Limno- and Pelagostrom-bidium sp.	404	16	49	49	**50**	6	9	13	**14**
Monodinium/ Didinium	141	-9	11	**13**	12	4	**9**	3	5
Peritrichs on Anabaena	102	-5	**19**	13	12	8	**15**	13	12
Peritrichs on diatoms	344	16	**48**	46	47	6	6	6	**9**
Pelagohalteria viridis	116	-3	**18**	15	14	8	**10**	**10**	9
Rimostrombi-dium lacustris	342	7	47	**49**	**49**	3	11	11	**12**
Sessile suctoria	174	-11	**20**	**20**	19	1	**2**	1	1
Small oligotrichs	433	28	**68**	67	**68**	6	3	**9**	8
Small sucticociliates	259	11	**53**	**53**	**53**	7	3	**7**	**8**
Tintinnids	338	-4	**54**	**54**	**54**	5	3	**7**	**7**
Urotricha furcate	423	12	**40**	39	39	4	4	**7**	**7**
Urotricha 2	292	-6	**48**	46	46	3	11	13	**15**

Urotricha 3	231	18	**59**	58	58	4	4	7	**9**
Vaginicola sp.	108	0	**7**	3	4	8	7	**10**	9
Median	338	7	**49**	**49**	**49**	4	6	**9**	**9**
Mean	291	6	**42**	41	41	5	7	8	**9**

We found a high positive first order auto-correlation for the biomasses (Fig. C7) and a negative first order auto-correlation for the net growth rates of the ciliates (Fig. C8).

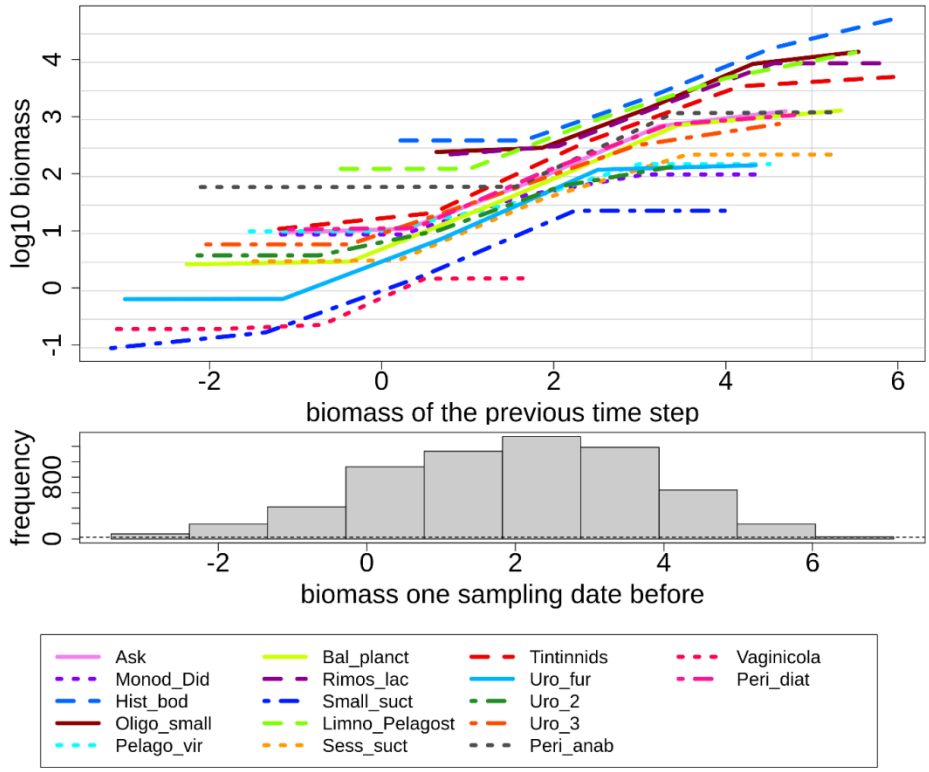

Fig. C7: Partial dependence plot for biomass of the previous time step.

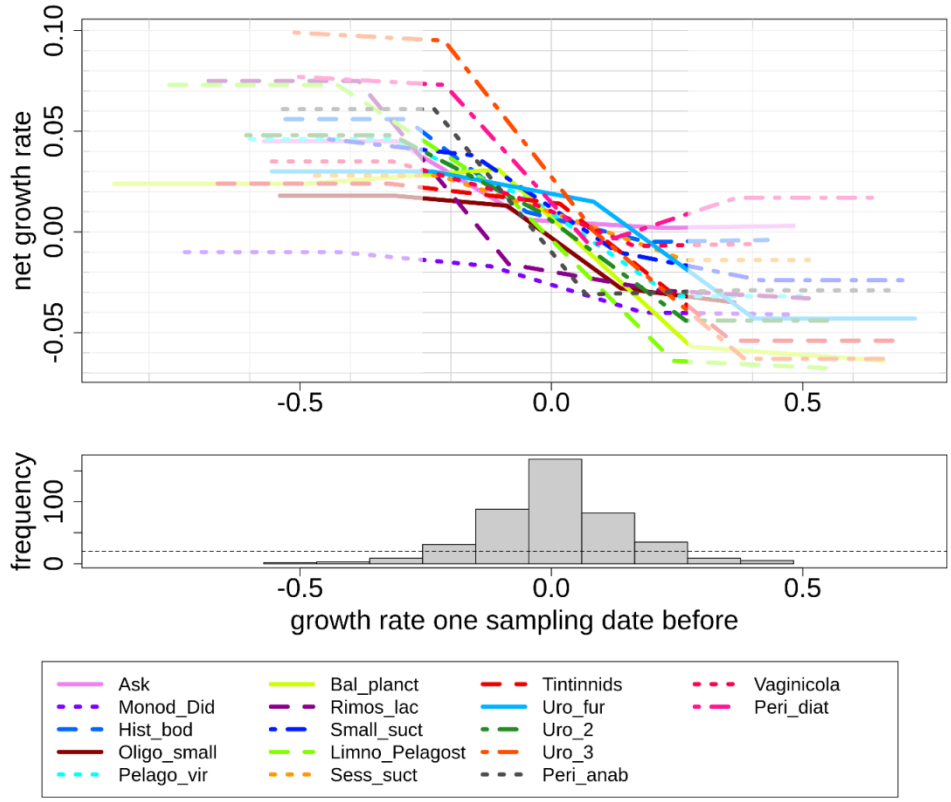

Fig. C8: Partial dependence plot for net growth rate of the previous time step.

Appendix D: Supplementary information for chapter 5

Appendix D1: supporting table and figures

Parameter

Tab. D1: Model parameters. Standard parameters in the model, their abbreviation, unit, value, and reference.

Name	Unit	Range	Meaning
r	$[\frac{1}{d}]$	1	Maximum growth rate of autotrophs
pc_i	[-]	0.01-1	Plasticity costs
K	$[\frac{mg\ C}{l}]$	1	Maximum carrying capacity
dc_i	[-]	0.01-1	Defence costs
a	$[\frac{1}{d}\frac{l}{mg\ C}]$	6	Maximum attack rate
d_{ij}	[-]	0-0.9	Defence, i.e. reduction of attack rate of consumer on A_{ij}
h	[d]	1	Handling time
χ_{max}	$[\frac{1}{d}]$	0-10 across 5 orders of magnitude	Maximum exchange rate between undefended and defended phenotype of a species
b	$[\frac{l}{mg\ C}]$	10	Shape parameter for the exchange function
C^*	$[\frac{mg\ C}{l}]$	0.251	Half of maximum consumer density when b=0
ε	[-]	0.3	Conversion efficiency
δ	$[\frac{1}{d}]$	0.21	Consumer death rate

Traits

We measured the community traits by calculating the weighted mean and weighted variance of the growth rate and the defence. The mean community trait $\bar{\tau}$ was defined as the biomass weighted mean of the trait values of the individual phenotypes τ_{ij}: $\bar{\tau} = \frac{1}{(A_u+A_d+B_u+B_d)}(A_u\tau_{Au} + A_d\tau_{Ad} + B_u\tau_{Bu} + B_d\tau_{Bd})$. The community variance was defined as weighted variance $var(\tau) = \frac{1}{3(A_u+A_d+B_u+B_d)}(A_u(\tau_{Au} - \bar{\tau})^2 + A_d(\tau_{Ad} - \bar{\tau})^2 + B_u(\tau_{Bu} - \bar{\tau})^2 + B_d(\tau_{Bd} - \bar{\tau})^2)$.

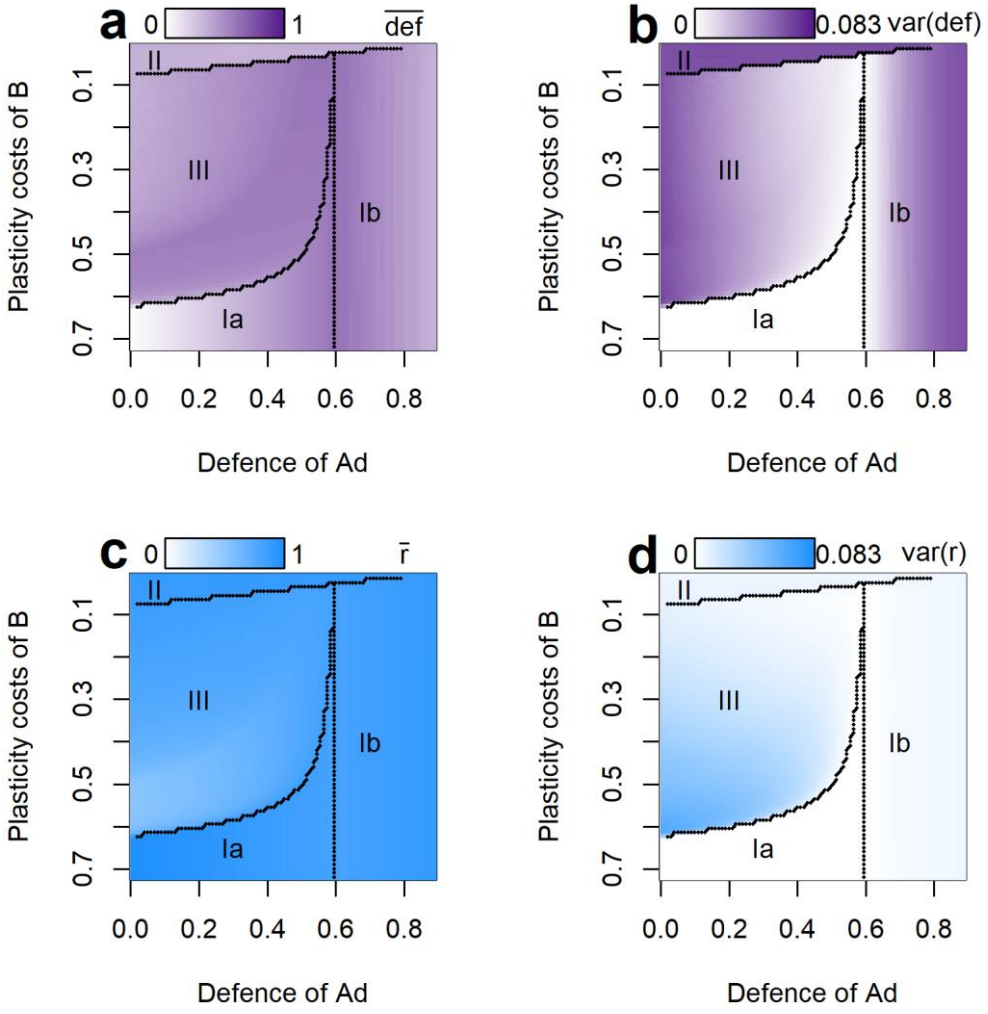

Fig. D1: Trait values of the autotroph community for scenario *parallel 0*. Community mean defence (a), variance of the defence (b), community mean growth rate (c) and variance of the growth rate (d). Lines separate the regions I-III of different autotroph coexistence.

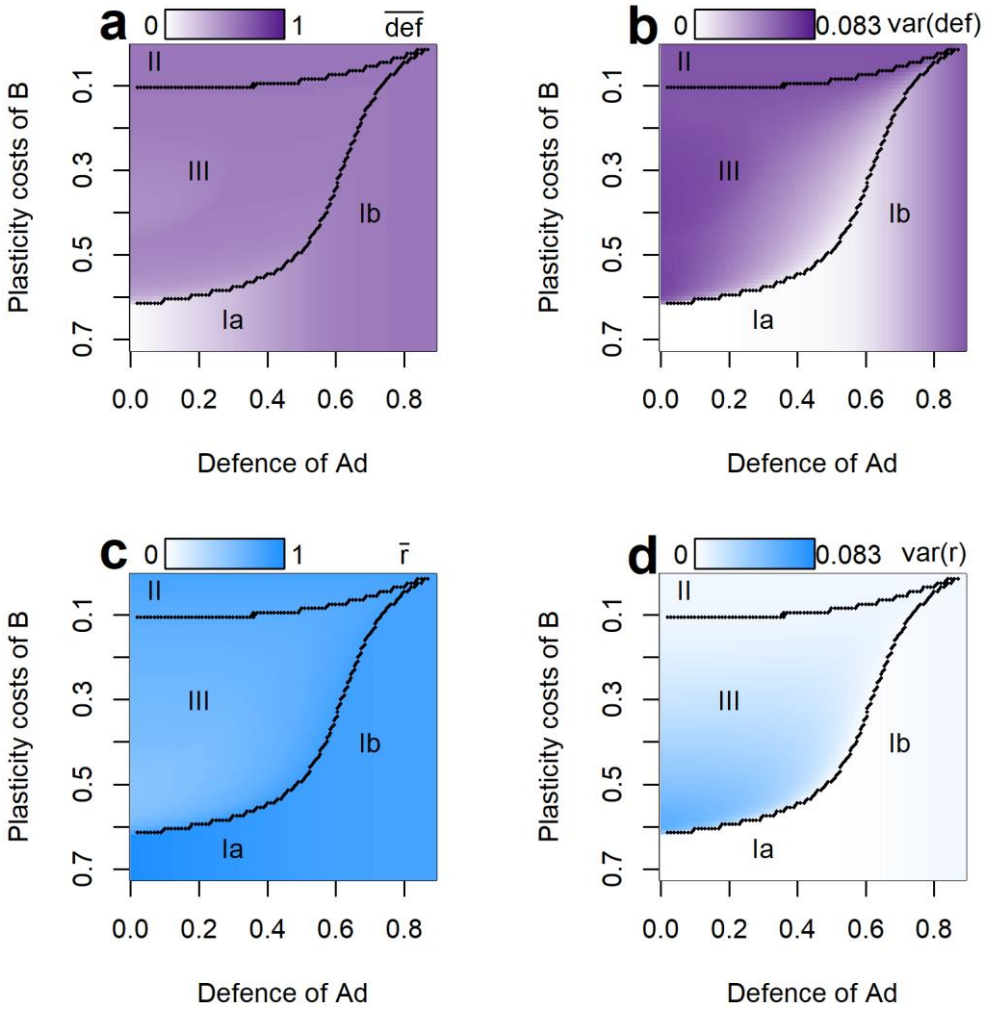

Fig. D2: Trait values of the autotroph community *for scenario parallel 0.01*. Community mean defence (a), variance of the defence (b), community mean growth rate (c) and variance of the growth rate (d). Lines separate the regions I-III of different autotroph coexistence.

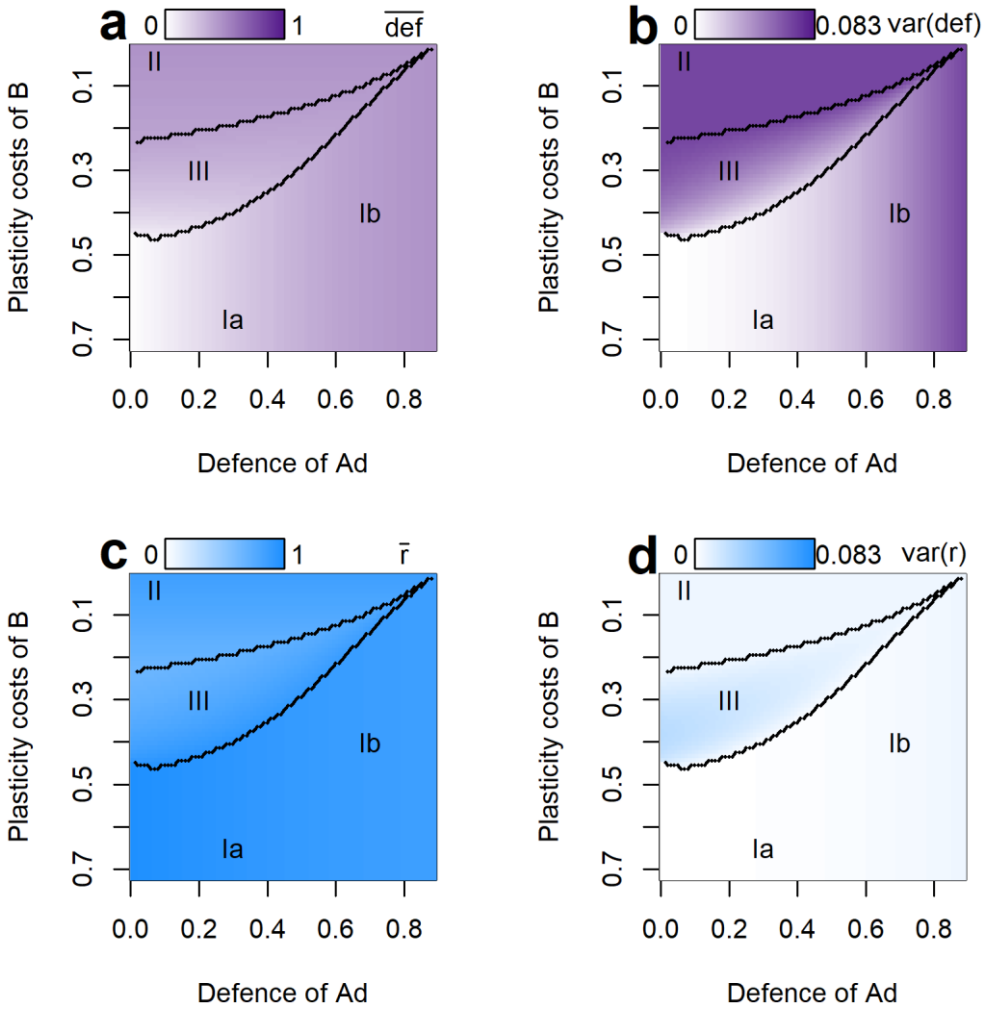

Fig. D3: Trait values of the autotroph community for scenario *parallel 1*. Community mean defence (a), variance of the defence (b), community mean growth rate (c) and variance of the growth rate (d). Lines in separate the regions I-III of different autotroph coexistence.

Constellation *crossing*

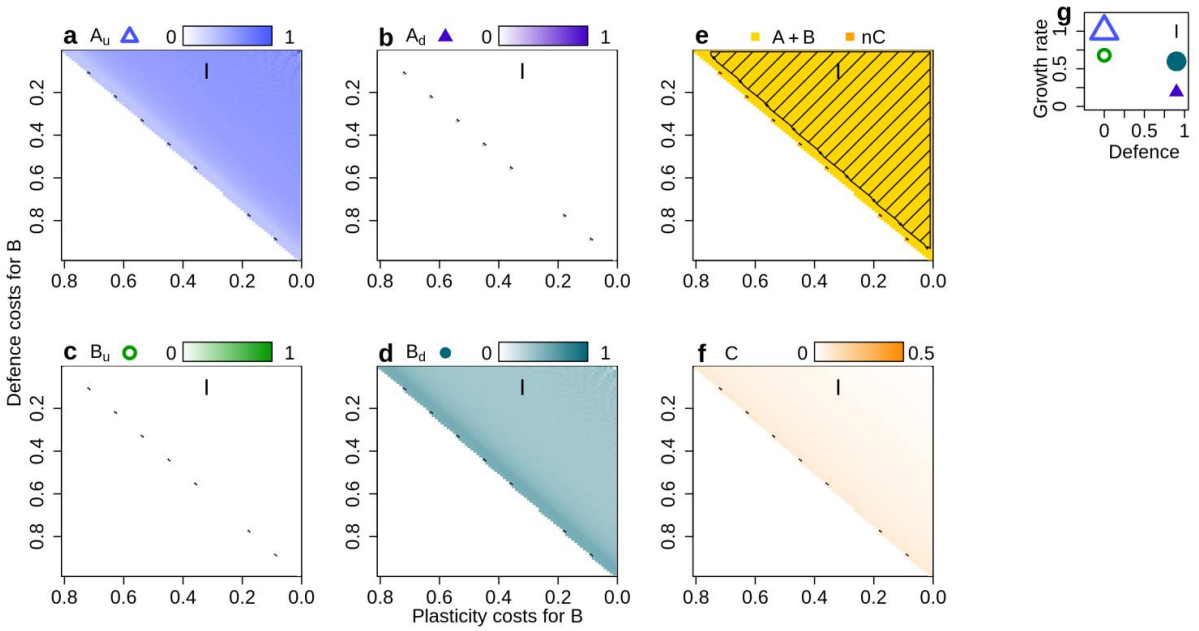

Fig. D4: Biomasses and coexistence for scenario *crossing 0*. Biomasses of the four autotrophic phenotypes (a-d), their coexistence patterns (e), the consumer biomass (f) and an exemplary of the autotrophs' trait values (g) (higher biomasses are shown by darker colours). Larger symbols in g indicate the surviving phenotypes. Shaded areas in e depict oscillating systems (antiphase cycles in loose shading).

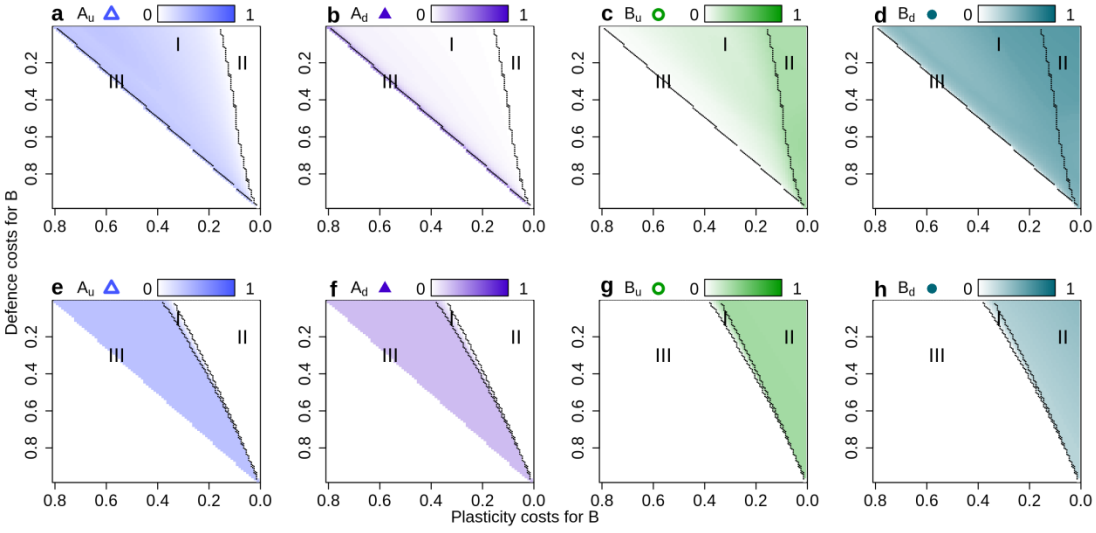

Fig. D5: Biomasses for scenario *crossing 0.01* and *crossing 1*. Biomasses of the four autotrophic phenotypes for scenarios *crossing 0.01* (a-d) and *crossing 1* (e-h) (higher biomasses are shown by darker colours). Lines separate the regions I-III of different autotroph coexistence.

Constellation *angle*

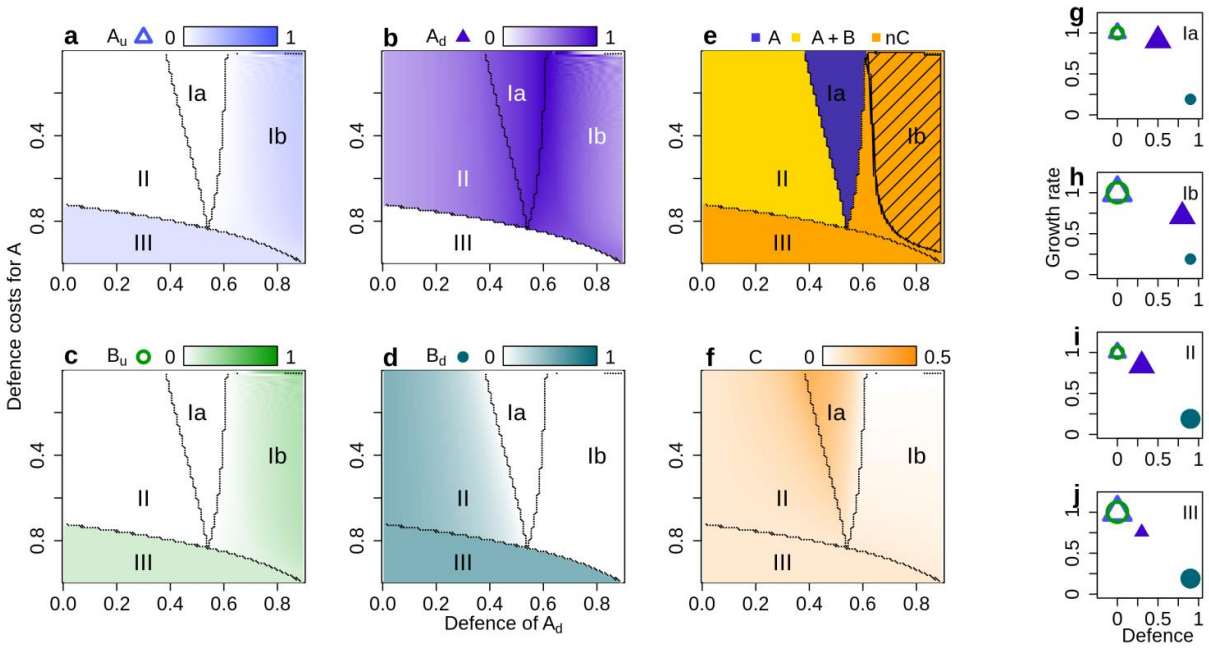

Fig. D6: Biomasses and coexistence for *angle 0*. Biomasses of the four autotrophic phenotypes (a-d), their coexistence patterns (e), the consumer biomass (f) and the autotrophs' trait values (g-j) (higher biomasses are shown by darker colours). Lines in a-f separate the regions I-III of different autotroph coexistence. An exemplary trait combination for every region is shown in g-j; larger symbols indicate the surviving phenotypes. Shaded areas in e depict antiphase cycles.

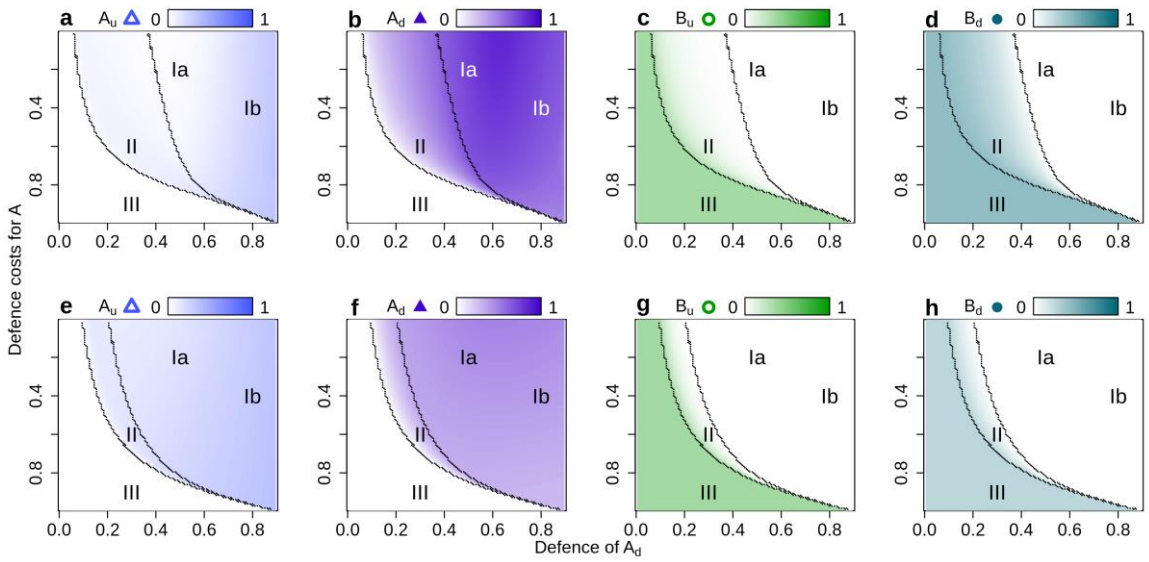

Fig. D7: Biomasses for scenario *angle 0.01* and *angle 1*. Biomasses of the four autotrophic phenotypes for scenarios *angle 0.01* (a-d) and *angle 1* (e-h) (higher biomasses are shown by darker colours). Lines separate the regions I-III of different autotroph coexistence.

Impact of the shape of trade-off lines on coexistence

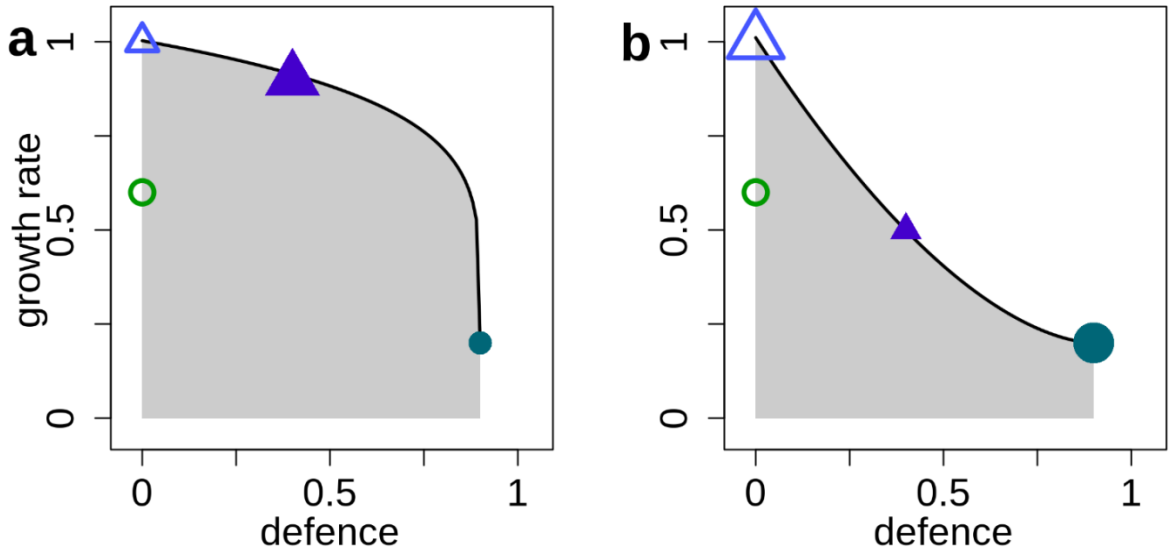

Fig. D8: Concave (a) and convex (b) trade-off curves and the resulting surviving phenotypes. The trade-off curve (solid line) represents the boundary of the set of feasible trait combinations (gray area). The trait combinations with the highest fitness survive. If two or more trait combinations are of maximal fitness in the long term, the respective species with these trait combinations coexist (b), otherwise only one species survives (a). The shown trait combinations are examples, symbols denote different phenotypes. They are based on the scenario *parallel 0*, but with these parameters: defence of A_d = 0.4, defence costs dc_A = -0.25 for the concave and dc_A = -1.25 for the convex trade-off line, dc_B = -0.44, plasticity costs pc_B = 0.4.

Appendix D2: Derivation of maladaptive switching

Our results show that, in the long run, phenotypically plastic switching between phenotypes is nearly always maladaptive. In this appendix we show why this result must hold true if the system is at a stable equilibrium: if there is any switching at this equilibrium, this is always maladaptive, resulting in a source-sink dynamic between the two phenotypes. If there are ongoing oscillations, on the other hand, switching can in the long run still be adaptive (cf. Fig. 5.7C); however, given the strongly stabilizing effect of inducible defences, we rarely found this as a long-term outcome.

To explain why maladaptive switching inevitably arises at a stable equilibrium, we use here a simplified version of the model, with only a single autotroph A, which can express an undefended phenotype A_u and a defended phenotype A_d. In the two-autotroph food web we use in the main text, the mechanism underlying maladaptive switching is the same. We start by showing the equilibrium conditions in a model without switching, and then show how this is modified by phenotypic plasticity.

Single-autotroph model without switching

Without specifying the exact details of growth and consumption terms, a model with two autotroph phenotypes A_u and A_d and a single consumer C can be represented as follows:

$$\begin{aligned} \frac{dA_u}{dt} &= F_u \cdot A_u \\ \frac{dA_d}{dt} &= F_d \cdot A_d \\ \frac{dC}{dt} &= F_c \cdot C \end{aligned} \qquad \text{(D1)}$$

where F_u, F_d and F_c represent the fitness (i.e. the net per capita growth rate) of the undefended autotrophs A_u, defended autotrophs A_d, and consumers C, respectively. This system is at an equilibrium when all three equations are zero; if both autotroph phenotypes and the consumer all survive, this implies that $F_u = F_d = F_c = 0$.

To understand the effect of switching in the next section, it is helpful to rewrite the first two equations to represent the change in total autotroph biomass ($A = A_u + A_d$) and the change in the frequency of the undefended phenotype ($f = A_u/(A_u + A_d)$):

$$\begin{aligned}\frac{dA}{dt} &= \left(f \cdot F_u + (1-f)\cdot F_d\right)A \\ \frac{df}{dt} &= f\cdot(1-f)\cdot\left(F_u - F_d\right) \\ \frac{dC}{dt} &= F_c \cdot C\end{aligned} \qquad \text{(D2)}$$

In equation (D2), the meaning of F_u, F_d and F_c is the same as in the original equation (D1). f is the frequency of undefended phenotypes in the autotroph population, and $(1 - f)$ is the frequency of defended phenotypes. The second equation of D2 shows how fitness differences between the phenotypes will translate into changes in the frequency f: if $F_u > F_d$, undefended phenotypes grow and reproduce faster than defended ones, and the share of undefended phenotypes will increase ($df/dt > 0$). Conversely, if $F_d > F_u$, selection favours defended phenotypes, which will then increase in frequency (i.e. $df/dt < 0$).

The above equations are mathematically completely equivalent to those in equation (D1), and a stable equilibrium is again found when all equations are zero. From the second equation, we can see that coexistence of the two phenotypes (i.e. $f \neq 0$ and $f \neq 1$) implies that, at equilibrium, $F_u = F_d$ (i.e. the two phenotypes must have equal fitness); combined with the first equation, this implies that $F_u = F_d = 0$.

Single-autotroph model with switching

When we include the switching rates χ_u (switching from undefended to defended) and χ_d (from defended to undefended) in the model, the equations in (D2) now become:

$$\begin{aligned}\frac{dA}{dt} &= \left(f \cdot F_u + (1-f)\cdot F_d\right)A \\ \frac{df}{dt} &= \underbrace{f\cdot(1-f)\cdot\left(F_u - F_d\right)}_{selection} \underbrace{- f\cdot\chi_u + (1-f)\cdot\chi_d}_{switching}\end{aligned} \qquad \text{(D3)}$$

(The equation for the consumer C does not change, and is not included from this point.)

It can be seen that the switching rates do not directly affect the change in the total autotroph biomass A, since undefended and defended individuals are counted there as a single population. Instead, they affect the frequencies: χ_u lowers the frequency of undefended phenotypes f (since it represents the switching from undefended to defended phenotypes), while χ_d increases f (since it represents switching from defended to undefended phenotypes).

In the above equations (D3), just as before, the system is at a stable equilibrium when all equations are zero. Without switching, this always means that $F_u = F_d = 0$ (see previous section); but here, this is modified by the switching rates to:

$$\underbrace{f \cdot (1-f) \cdot (F_u - F_d)}_{selection} = \underbrace{f \cdot \chi_u - (1-f) \cdot \chi_d}_{switching} \qquad \text{(D4)}$$

In more intuitive terms: the frequency of undefended phenotypes (second line in equation (D3)) does not change when the effects of selection and of switching balance each other out.

By definition, selection is always adaptive, i.e. it results in an increase in the frequency of whichever phenotype has a higher fitness; this must be true, since selection directly responds to the fitness differences between the phenotypes (equation (D2-D4)). Equation (D4) therefore implies that, in equilibrium, switching must always be maladaptive, since it acts in the opposite direction to selection. In other words, if undefended phenotypes have a higher fitness ($F_u > F_d$), selection will "push" for an increase in the frequency of undefended phenotypes. Hence, for the equilibrium to remain stable, there must be net switching from undefended to defended phenotypes (i.e. from the high-fitness to the low-fitness phenotype) to maintain a stable frequency. Thus, if any switching is occurring at a stable equilibrium, it will always be maladaptive.

The only possibility for no maladaptive switching is no switching at equilibrium at all. In this case, the "selection" and "switching" parts of equation (D3-D4) are both zero. While this is not strictly impossible, it is

very unlikely, and in our simulations, we always found a net flow between the phenotypes at equilibrium (Appendix Fig. D4-D6, left panels).

The above derivation shows that, when the system is at a stable equilibrium, any switching must always be maladaptive. When there are ongoing oscillations, this does not apply, and in this case switching can on average still be adaptive in the long run (cf. Fig. 5.7C).

Declaration of Authorship

I, Nadja J. Kath, declare that this dissertation titled, "Functional traits determine biomass dynamics, coexistence and energetics in plankton food webs" and the work presented in it are my own. I confirm that:

- This work was done wholly while in candidature for a research degree at this University.
- No part of this thesis has previously been submitted for a degree or any other qualification at this University or any other institution.
- Where I have consulted the published work of others, this is always clearly attributed.
- Where I have quoted from the work of others, the source is always given. With the exception of such quotations, this thesis is entirely my own work.
- I have acknowledged all main sources of help.
- Where the thesis is based on work done by myself jointly with others, I have made clear exactly what was done by others and what I have contributed myself.

Signed:

Date: